Enantioselective and Chemoselective Acylation of (*R*,*S*)-Propranolol Catalyzed by *Candida antarctica* Lipase B: A Theoretical and Experimental Approach

Presented by:

Andrés Mauricio Escorcia Cabrera

UNIVERSIDAD INDUSTRIAL DE SANTANDER

FACULTAD DE CIENCIAS

ESCUELA DE QUÍMICA

BUCARAMANGA

2015

Enantioselective and Chemoselective Acylation of (*R*,*S*)-Propranolol Catalyzed by *Candida antarctica* Lipase B: A Theoretical and Experimental Approach

Doctoral dissertation

Presented by:

Andrés Mauricio Escorcia Cabrera

Advisors:

Dr. Markus Hans Oliver Doerr

Universidad Industrial de Santander

Dr. Martha Cecilia Daza Espinosa

Universidad Industrial de Santander

UNIVERSIDAD INDUSTRIAL DE SANTANDER

FACULTAD DE CIENCIAS

ESCUELA DE QUÍMICA

BUCARAMANGA

2015

To the Lord Jesus Christ, who has taught me that: “No discipline seems pleasant at the time, but painful. Later on, however, it produces a harvest of righteousness and peace for those who have been trained by it (Hebrews 12:11)”.

To Ruthber and Marina, my parents, for all their support…

To Sharon, my wife, for her love and sweetness…

To Samuel, my son, my inspiration…

ACKNOWLEDGEMENTS

I want to thank the many people without whose help, support and friendship this thesis would not had been possible. I especially thank to my supervisors Prof. Dr. Martha Cecilia Daza and Prof. Dr. Markus Doerr for giving me the opportunity to pursue doctoral studies in their group as well as for their support and encouragement. Thanks for all you commitment during this long process. I also thank to all the colleagues at the "Grupo de Bioquímica Teórica" for the friendly atmosphere and many interesting scientific discussions as Angela Rodriguez, Jorge Quintero, Daniel Barrera and Pedro Acosta.

A great thanks to Dr. Daniel Molina from the "Laboratorio de Resonancia Magnética Nuclear" at "Universidad Industrial de Santander" for the valuable contributions to the analysis of the experiments by NMR. Also I thank to Dr. Rodrigo Torres from the "Grupo de Investigación en Bioquímica y Microbiología" for allowing me to use materials and equipments of his laboratory. Many thank to Dr. Jesús Olivero Verbel and Carlos Ortega Zuñiga from the "Universidad de Cartagena" for teaching me how to do Molecular Docking.

My gratitude goes also to Prof. Dr. Walter Thiel for his very kind hospitality, guidance and support at the Max-Planck-Institüt für Kohlenforschung in Germany. Many thanks to Dr. Kakali Sen for all the patience on teaching me how to do QM/MM calculations as well as for her scientific advice and ongoing support. Also I thank to all the friends in Germany for helping to feel at home as Daniel Escudero, Juan Manuel Ramirez, Mahendra Patil, Bora Karasulu, Rachel Crespo and Esra Bozkurt.

I express my deep gratitude to my wife and my parents for their constant support and encouragement. To my brother and sister (pechy and yuya) and all my friends for being there taking part of the process.

The financial support from COLCIENCIAS through the Fellowship of the PhD Program 2009 is gratefully recognized. I also acknowledge the financial support from COLCIENCIAS (project 8110256933409) and VIE-UIS (project 5702) given during my doctoral studies.

Finally I thank the referees: Dr. Cristian Blanco, Dr. Albeiro Restrepo, Dr. Constanza Cárdenas, Dr. Luis Javier López and Dr. Andres Illanes for dedicating time on revising my dissertation and for their kind suggestions.

Table of contents

List of Figures

List of tables

List of abbreviations

CalB	*Candida antarctica* lipase B
O-BP	*O*-butyryl-propranolol
N-AP	*N*-acetyl-propranolol
O-AP	*O*-acetyl-propranolol
N,O-AP	*N,O*-acetyl-propranolol
p-NPB	p-nitrophenylbutyrate
ee	enantiomeric excess
E	enantiomeric ratio or enantioselectivity
K_M	Michaelis-Mentent constant
k_{cat}	Turnover number
AcCalB	Acetylated CalB
SEA	Acylated catalytic serine
MCC	Michaelis complex
TI	Tetrahedral intermediate
TS	Transition state
PDC	Product complex
NAC	Near attack conformer
$\Delta_{R \text{ or } S}G^{\ddagger}$	Gibbs free energy of activation for each enantiomer
$\Delta_{R\text{-}S}\Delta G^{\ddagger}$	Difference in Gibbs free energy of activation for the enantiomers
$\Delta_{R\text{-}S}\Delta H^{\ddagger}$	Difference in activation enthalpy for the enantiomers
$\Delta_{R\text{-}S}\Delta S^{\ddagger}$	Difference in activation entropy for the enantiomers
MD	Molecular dynamics
QM/MM	Quantum Mechanics/Molecular Mechanics
DFT	Density functional theory
PES	Potential energy surface
TZVP	Triple-ζ basis set for valence electrons with (d,p) polarization functions
SCC-DFTB	Self-consistent charge-density functional tight binding
RS	Reactant state

List of papers

This thesis has contributed to the following publications:

1) A. M. Escorcia, D. Molina, M. C. Daza, M. Doerr. "Acetylation of (*R*,*S*)-propranolol catalyzed by *Candida antarctica* lipase B: An experimental and computational study" *J. Mol. Catal. B: Enzym.* 98 (2013) 21-29.

2) A. M. Escorcia, M. C. Daza, M. Doerr. "Computational study of the enantioselectivity of the *O*-acetylation of (*R*,*S*)-propranolol catalyzed by *Candida antarctica* lipase B" *J. Mol. Catal. B: Enzym.* 108 (2014) 21-31.

Manuscript drafts:

1) A. M. Escorcia, K. Sen, M. C. Daza, M. Doerr, W. Thiel. "QM/MM insights into enantioselectivity of the *O*-acetylation of (*R*,*S*)-propranolol catalyzed by *Candida antarctica* lipase B" *In preparation for submitting to JACS.*

Participation in conferences

1) A. M. Escorcia, R. Torres, M. C. Daza, M. Doerr. "Computational study of the *O*-acylation of (*R,S*)-propranolol catalyzed by *Candida antarctica* lipase B" Ninth Triennial Congress of the World Association of Theoretical and Computational Chemists (WATOC), July 17th - 22nd, Santiago de Compostela, España, 2011.

2) A. M. Escorcia, R. Torres, M. C. Daza, M. Doerr. "Modeling structure and flexibility of acylated *Candida antarctica* lipase B in an organic solvent" 43rd IUPAC World Chemistry Congress, July 30th to August 7th, San Juan, Puerto Rico, 2011.

3) A. M. Escorcia, R. Torres, M. C. Daza, M. Doerr. "Computational study of Michaelis conformers in the *O*-acylation of (*R,S*)-propranolol catalyzed by *Candida antarctica* lipase B" 43rd IUPAC World Chemistry Congress, July 30th to August 7th, San Juan, Puerto Rico, 2011.

4) A. M. Escorcia, R. Torres, M. C. Daza, M. Doerr. "Molecular modeling of enantioselectivity of *Candida antarctica* lipase B catalyzing *O*-acylation of (*R,S*)-propranolol" 43rd IUPAC World Chemistry Congress, July 30th to August 7th, San Juan, Puerto Rico, 2011.

5) A. M. Escorcia, K. Sen, M. C. Daza, M. Doerr, W. Thiel. "A QM/MM study of the enantioselectivity of the *Candida antarctica* lipase B (CalB) catalyzed *O*-acetylation of (*R,S*)-propranolol". 14th International Congress of Quantum Chemistry, June 25th-30th, Boulder, United States of America, 2012.

6) A. M. Escorcia, K. Sen, M. C. Daza, M. Doerr, W. Thiel. "Estudio QM/MM de la enantioselectividad de la acetilación de (*R,S*)-propranolol catalizada por lipasa B de *Candida antarctica*" I Congreso Latinoamericano de Estudiantes de Química Pura y Aplicada. XIV Encuentro Nacional de Estudiantes de Química UIS, November 6th - 9th, Bucaramanga, Colombia, 2012.

7) A. M. Escorcia. "Combined docking and molecular dynamics simulations" Seminario Internacional en Ciencias Aplicadas - Una mirada hacia la innovación y el desarrollo sostenible, May 9th - 10th, Bucaramanga, Colombia, 2013.

8) A. M. Escorcia, M. C. Daza, M. Doerr. "Computational study of the chemo- and enantioselectivity of the acetylation of (*R,S*)-propranolol catalyzed by *Candida antarctica* lipase B" V Encuentro Nacional de Químicos Teóricos y Computacionales - II Escuela de Teoría y Computación en las Ciencias Moleculares, April 27th - 30th, Guatapé, Colombia, 2014.

9) D. Barrera, A. M. Escorcia, M. C. Daza, M. Doerr. "Efecto de las mutaciones I189S y T138S sobre la enantioselectividad de la lipasa B de *Candida antarctica* en la acetilación de (*R,S*)-propranolol" V Encuentro Nacional de Químicos Teóricos y Computacionales - II Escuela de Teoría y Computación en las Ciencias Moleculares, April 27th - 30th, Guatapé, Colombia, 2014.

10) J. Avila, M. C. Daza, M. Doerr, A. M. Escorcia. "Complejos enzima-sustrato en la reacción de acilación de (*R/S*)-atenolol catalizada por lipasa B de *Candida antarctica*" V Encuentro Nacional de Químicos Teóricos y Computacionales - II Escuela de Teoría y Computación en las Ciencias Moleculares, April 27th - 30th, Guatapé, Colombia, 2014.

11) A. M. Escorcia, K. Sen, M. C. Daza, M. Doerr, W. Thiel. "Insights into the enantioselectivity of the *Candida antarctica* lipase B catalyzed *O*-acetylation of (*R,S*)-propranolol - a QM/MM study" 10th Congress of the World Association of Theoretical and Computational Chemists (WATOC), October 5th – 10th, Santiago, Chile, 2014.

12) A. M. Escorcia, M. C. Daza, M. Doerr. "Chemo- and enantioselectivity of *Candida antarctica* lipase B catalyzing acetylation of (*R,S*)-propranolol - a combined docking and molecular dynamics investigation" 10th Congress of the World Association of Theoretical and Computational Chemists (WATOC), October 5th – 10th, Santiago, Chile, 2014.

13) J. Avila, A. M. Escorcia, M. C. Daza, M. Doerr. "Molecular modeling of the Michaelis complexes in the acetylation of (*R,S*)-atenolol catalyzed by *Candida antarctica* lipase B" 10th Congress of the World Association of Theoretical and Computational Chemists (WATOC), October 5th – 10th, Santiago, Chile, 2014.

14) D. Barrera, A. M. Escorcia, M. C. Daza, M. Doerr. "Effect of mutations I189S and T138S on the population of near attack conformations during the *O*-acetylation of (*R*,*S*)-propranolol catalyzed by *Candida antarctica* lipase B" 10^{th} Congress of the World Association of Theoretical and Computational Chemists (WATOC), October 5^{th} – 10^{th}, Santiago, Chile, 2014.

RESUMEN

TÍTULO: ACILACIÓN ENANTIOSELECTIVA Y QUIMIOSELECTIVA DE (*R,S*)-PROPRANOLOL CATALIZADA POR LIPASA B DE *Candida antarctica*: UN ENFOQUE TEÓRICO Y EXPERIMENTAL*

AUTOR: ANDRÉS MAURICIO ESCORCIA CABRERA**

PALABRAS CLAVES: LIPASA B DE *Candida antarctica*, ACILACIÓN, ENANTIOSELECTIVIDAD, QUIMIOSELECTIVIDAD, DINÁMICA MOLECULAR, MECÁNICA CUÁNTICA/MECÁNICA MOLECULAR

DESCRIPCIÓN:

En esta tesis se realizó un estudio experimental y computacional de la acetilación de (*R,S*)-propranolol catalizada por lipasa B de *Candida antarctica* (CalB) en tolueno. Experimentalmente se encontró que CalB exhibe una enantioselectividad moderada (*E* = 61-63) y una quimioselectividad exclusiva que favorece la formación más rápida del *R-O*-acetil-propranolol, el cual se obtuvo con una pureza enantiomérica del 95-96 % a un grado de conversión del 21-33 %. Esta reacción involucra dos pasos. El primero (acilación) conduce a la formación de una acil-enzima reactiva. La quimio- y enantioselectividad se origina en el segundo (desacilación), cuando la acil-enzima transfiere el grupo acilo al propranolol. Ambos pasos ocurren vía la formación de un complejo enzima-sustrato no covalente inicial (complejo de Michaelis; CMC) y un intermediario tetraédrico (IT). La parte computacional de esta tesis se enfocó en la reacción de desacilación. Se modelaron los CMCs e ITs utilizando simulaciones combinadas de acoplamiento y dinámica molecular (DM). Adicionalmente, se calcularon los perfiles de reacción para la transformación de *R*- y *S*-propranolol utilizando un enfoque de mecánica cuántica/mecánica molecular (MC/MM). Únicamente se identificaron CMCs reactivos en los que el grupo hidroxilo del *R*- y *S*-propranolol se encuentra disponible para ser acilado por CalB. Se encontró además que la barrera de energía para la transformación de *R*-propranolol es 4.5 kcal/mol más baja que la del *S*-propranolol. También se identificaron las interacciones enzima-sustrato que son responsables de la enantioselectividad. Por otro lado, en contraste con lo que se sugiere comúnmente para las reacciones catalizadas por lipasas, se encontró que el IT no es una buena representación de los estados de transición. En general, los resultados computacionales proveen una explicación para la quimio- y enantioselectividad, así como elementos guía para mejorar la síntesis enantioselectiva del propranolol mediante un rediseño racional de CalB o de las condiciones de reacción.

---

*Tesis doctoral.

**Facultad de Ciencias, Escuela de Química, Director: Dr. Markus Hans Oliver Doerr, Directora: Martha Cecilia Daza Espinosa.

ABSTRACT

TITTLE: ENANTIOSELECTIVE AND CHEMOSELECTIVE ACYLATION OF (*R*,*S*)-PROPRANOLOL CATALYZED BY *Candida antarctica* LIPASE B: A THEORETICAL AND EXPERIMENTAL APPROACH*

AUTHOR: ANDRÉS MAURICIO ESCORCIA CABRERA**

KEYWORDS: *Candida antarctica* LIPASE B, ACYLATION, ENANTIOSELECTIVITY, CHEMOSELECTIVITY, MOLECULAR DYNAMICS, QUANTUM MECHANICS/MOLECULAR MECHANICS

DESCRIPTION:

In this thesis the kinetic resolution of (*R*,*S*)-propranolol via acetylation reaction catalyzed by *Candida antarctica lipase B* (CalB) in toluene was studied through an experimental and computational approach. It was experimentally found that CalB displays moderate enantioselectivity (*E* = 61-63) and exclusive chemoselectivity favoring the faster formation of *R*-*O*-acetyl-propranolol, which was obtained with an enantiomeric purity of 95-96 % at a conversion degree of 21-33 %. This reaction involves two steps. The first step leads to the formation of a reactive acyl-enzyme (acylation). The chemo- and enantioselectivity originates from the second step (deacylation), when the acyl-enzyme transfers the acyl group to the racemic substrate. Both steps proceed via an initial noncovalent enzyme substrate complex (Michaelis complex; MCC) and a tetrahedral intermediate (TI). The computational part of this thesis was focused on the deacylation reaction. A combined docking and molecular dynamics (MD) protocol was used to model the MCCs and TIs. In addition, the reaction profiles for the transformation of *R*- and *S*-propranolol were computed by using a Quantum Mechanics/Molecular Mechanics (QM/MM) approach. Only reactive MCCs were identified for *R*- and *S*-propranolol, in which their hydroxyl group is available to be acetylated by CalB. Moreover, the energy barrier for the transformation of *R*-propranolol into *O*-acetyl-propranolol was estimated to be 4.5 kcal/mol lower than that of *S*-propranolol. In addition, enzyme-substrate interactions responsible for the enantioselectivity of the reaction were identified. On the other hand, in contrast to what is commonly suggested for lipase-catalyzed reactions, the TI was not found to be a good representation of the transition states. Generally speaking, the computational results obtained here provide an explanation for the chemo- and enantioselectivity of the reaction, as well as guide elements for improving the enantioselective synthesis of *S*-propranolol through a rational redesign of CalB or the reaction conditions.

---

*Doctoral dissertation.

**Facultad de Ciencias, Escuela de Química, Director: Dr. Markus Hans Oliver Doerr, Directora: Martha Cecilia Daza Espinosa.

Introduction

Propranolol (1-iso-propylamino-3-(1-naphthoxy)-2-propanol), a beta-adrenergic blocking agent used for treatment of arterial hypertension and other cardiovascular disorders [1–3], is commercially available as a racemic mixture. However, the desired therapeutic effect is associated with the *S*-enantiomer, and administration of the racemic propranolol mixture causes serious side effects such as bronchoconstriction or diabetes [4–6]. Thus the design of strategies for obtaining the *S*-propranolol with high enantiomeric purity is of great importance. In this context, several chemoenzymatic or chemical synthesis routes for obtaining *R*- and *S*-propranolol in enantiomerically pure form have been proposed [7–12]. Several authors have also reported the biocatalytic resolution of (*R,S*)-propranolol through lipase catalyzed transesterification and hydrolysis reactions [13–16].

Lipase catalyzed reactions offer an environmentally friendly way for the synthesis of enantiomerically pure chiral drugs in comparison with conventional chemical methods. Many of these reactions are highly selective and can be performed under very mild reaction conditions [17]. Moreover, lipases are well established catalysts in organic synthesis nowadays, because they are highly stable and active in organic solvents [18–20], and they can catalyze a number of biotransformations which involve carboxylic-groups, such as esterification, transesterification and aminolysis [19,21–26].

Attempts to increase the rate and the enantioselectivity of lipase-catalyzed reactions are focused on the modulation of the catalytic properties of the enzyme using protein engineering (e.g. directed mutation and immobilization of the enzyme), different organic solvents and acyl donors, and by controlling the water activity [19,24–27]. Complementary to the experiments, computational modeling has become a useful tool to improve the understanding of lipase-catalyzed reactions, giving insight into these reactions at a level of detail which is experimentally not accessible. This often helps to improve the rate and enantioselectivity of these reactions through a more rational design of the reaction conditions [28–31]. The methodologies applied in the computational studies range from studies on small model systems over quantum mechanical/molecular mechanical (QM/MM) studies and docking studies to molecular dynamics (MD) studies [32–39].

Recently, immobilized *Candida antarctica* lipase B (CalB) has been used to carry out the acetylation of (*R,S*)-propranolol with vinyl acetate in toluene. The enantioselectivity was moderate (maximum *E* value of 57; *R*-selective), but higher than or comparable to the enantioselectivity observed in the kinetic

resolution of propranolol either via esterification or hydrolysis reactions using other lipases such as *Pseudomonas cepacia*, *Rhizopus niveus* and *Pseudomonas fluorescens* [13]. Using immobilized CalB allows to reuse the biocatalyst and to simplify its separation from the reaction products. Moreover, the stereopreference of CalB toward *R*-propranolol is advantageous since it allows the direct production of *S*-propranolol as unreacted substrate of the enzymatic acylation. All of this makes the reaction attractive for industrial application, but the enantioselectivity has to be improved for this purpose.

The aim of the present study was to gain insights into the origin of the enantioselectivity of the CalB catalyzed acetylation of (*R*,*S*)-propranolol in toluene, which may help to improve the enantioselective synthesis of this drug. In the first place a detailed analysis of all reactions which may occur in this system was carried out. Propranolol has two reactive centers (-NH and –OH) available to be acylated (**Fig. 1**) [40], thus one or two acylation reactions (*O*- and *N*-acylation) could be responsible for the enantioselectivity. In other words, the acetylation of propranolol catalyzed by CalB is expected to be chemo- and enantioselective (**Fig. 2**). Nevertheless, the chemoselectivity of CalB catalyzing this reaction was not known until the development of this thesis [41]. In this work, the acetylation reaction of propranolol catalyzed by CalB was carried out using the free enzyme, vinyl acetate as acyl donor, and a mixture of toluene/methanol as reaction medium. Methanol was added in small quantities as cosolvent for increasing the solubility of propranolol in toluene. ^{1}H- and ^{13}C-NMR spectroscopy was used for determining the chemoselectivity of the reaction. In addition, the enantioselectivity of the reaction was determined.

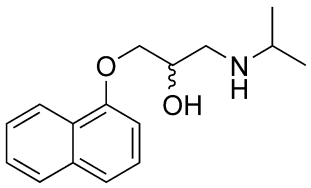

Fig. 1 (*R*,*S*)-propranolol.

Once a complete picture of the selectivity (chemo- and enantioselectivity) of the reaction was obtained through experiments, computational modeling was used to figure out what is the molecular basis of this selectivity. The generally accepted mechanism of lipase-catalyzed reactions was taken into account [19,42]. This involves two steps. The first step is the acylation of the enzyme by the acyl donor in the reaction medium –vinyl acetate in this study- (acylation step). In the second step, the acylated enzyme (acylenzyme) can transfer the acyl group to several nucleophiles, such as amines, alcohols or peroxides

–propranolol in this study- (deacylation step) (**Fig. 3**). Acylation as well as deacylation proceed via an initial noncovalent enzyme-substrate complex (Michaelis complex; MCC) and a tetrahedral intermediate (TI). The computational study of the CalB catalyzed acetylation of (*R*,*S*)-propranolol was focused on the deacylation step, since the chemo- and enantioselectivity of this reaction is originated when the racemic propranolol reacts with the previously generated acetylated enzyme (namely, AcCalB). AcCalB as well as the MCCs and TIs of the deacylation step were studied using combined docking and MD simulations. In addition, the energy profiles of the deacylation step for the transformation of *R*- and *S*-propranolol were computed by QM/MM calculations.

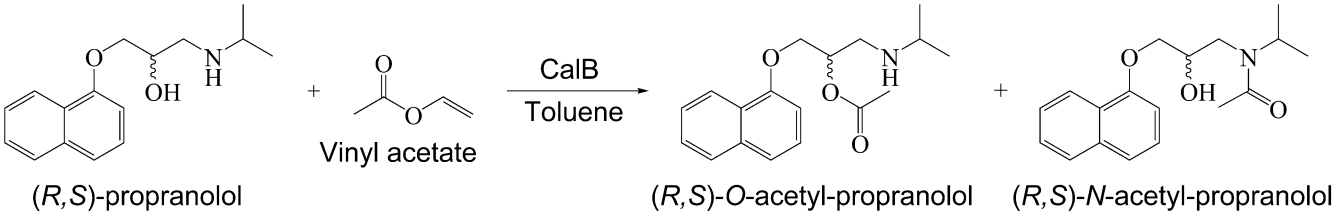

Fig. 2 General visualization of the CalB-catalyzed acetylation of (*R*,*S*)-propranolol.

Initially molecular modeling of AcCalB was carried out in order to generate target structures for the non-covalent docking of *R*- and *S*-propranolol (i.e. for building the MCCs). Then the MCCs between AcCalB and *R*- or *S*-propranolol were modeled by using a docking protocol similar to the implemented in other studies of lipase-catalyzed reactions. This allowed testing the accessibility of the nucleophilic groups of propranolol in the CalB-catalyzed acetylation reaction. The chemoselectivity of the reaction was explained from the results obtained up to this point of the research [41]. Thereafter MD simulations of the MCCs of *R*- and *S*-propranolol were performed for rationalisation of the enantioselectivity [43]. MD simulations were also carried out for molecular modeling of the corresponding TIs. The analysis of the MD simulations of the MCCs and TIs was focused on the dynamic behaviour of propranolol, essential hydrogen bond interactions for the catalytic process, and hydrophobic interactions between CalB and propranolol which were identified to be important for the stabilization of the respective transition states (TSs). Thereby, based on the analysis of the MD trajectories, key factors for the enantioselectivity of the reaction were identified. Finally, representative snapshots of the TIs were selected from the MD simulations to be used in subsequent QM/MM calculations. These structures were subjected to QM/MM geometry optimization at the B3LYP(TZVP)/CHARMM level and then used as starting points to compute the reaction energy profiles for the transformation of *R*- and *S*-propranolol at the same level of theory. In addition, other

DFT levels were evaluated in single-point calculations. QM/MM calculations were also carried out using semiempirical methods and the self-consistent charge-density functional tight binding (SCC-DFTB) method. The accuracy of these methods for describing the thermochemistry and kinetic of the reaction was analyzed. From the QM/MM calculations the energy barriers for the transformation of *R*- and *S*-propranolol via different TIs were obtained and thus more quantitative information about the origin of the enantioselectivity.

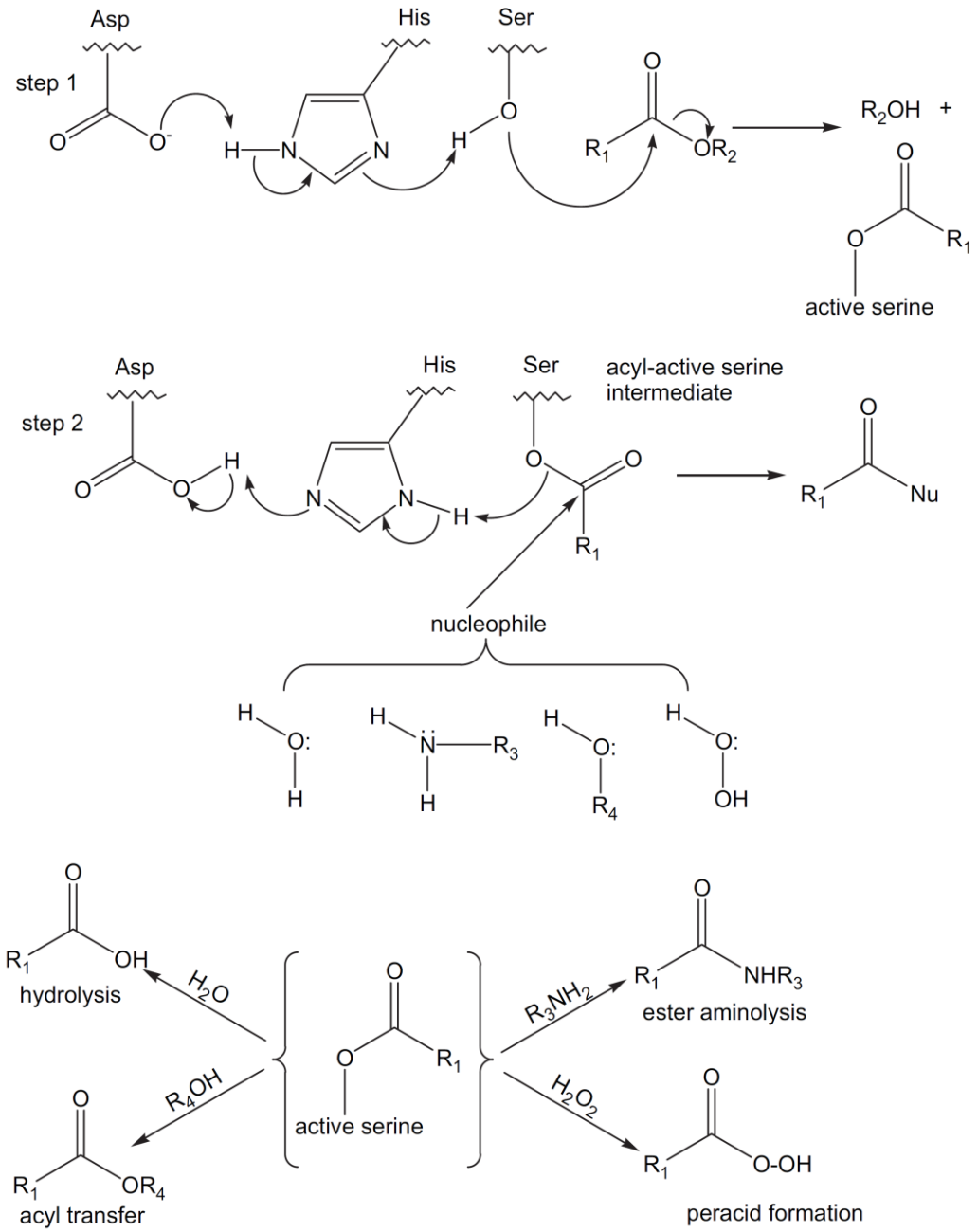

Fig. 3 Lipase catalyzed reactions. Enzymatic mechanism of lipases involves a catalytic triad consisting of Serine, Histidine and either Aspartate or Glutamate. Taken from Ghanem et al. [19].

In the computational work key residues for the enantioselectivity of the reaction were identified, which constitute the first guiding elements for the development of a new biocatalyst able to catalyze the acylation of propranolol with an elevated chemo- and enantioselectivity, by a rational redesign of CalB.

This doctoral dissertation consists of eight chapters plus appendices and is organized as follows. **Chapter 1** contains a theoretical background of lipase-catalyzed reactions and its application to the resolution of racemic compounds. This includes an analysis of the problem of enantioselectivity in the light of, but not exclusively, a computational approach. The following five chapters address the results of this investigation with the respective procedures used and should be read in succession. **Chapter 2** contains the experimental results of the chemo- and enantioselectivity of the CalB-catalyzed acetylation of (*R,S*)-propranolol. **Chapter 3** focuses on the rationalisation of the chemoselectivity of the reaction by molecular modeling of the MCCs using a docking protocol. **Chapter 4** is about the rationalisation of the enantioselectivity from MD simulations of the MCCs. In addition, a QM approach based on small model systems of the MCCs identified from the MD simulations is presented. **Chapter 5** corresponds to the rationalisation of the enantioselectivity by molecular modeling of the TIs. **Chapter 6** focuses on the analysis of the reaction energy profiles computed by QM/MM calculations. **Chapter 7** contains general conclusions of the research. On the other hand, appendices contain supplementary information for the **Chapter 2** to the **Chapter 6**, which has been separated from the main text in order to enhance readability. Appendices are referred to in the appropriated places and may be required for a full comprehension of the results obtained in this work.

Chapter 1. Theoretical background

1.1. Chirality

An object is said to be chiral if its mirror image cannot be brought to coincide with itself. The pair of non-superimposable entities are termed enantiomers. This definition applies to macroscopic objects (e.g. our left and right hands) but also exists on the molecular level. Molecules which are enantiomers have identical sum formulas and bonding patterns, but they differ in the arrangement of the constituent groups in space (i.e. present a different configuration) [44]. The stereoconfiguration of enantiomers is usually indicated by *R* and *S* according to the nomenclature of Cahn, Ingold and Prelog [45]. This spatial arrangement discriminating the enantiomers must be stable under predefined conditions, otherwise interconversion of one enantiomer into the other one occurs and a racemic mixture (racemate) is formed as a 1:1 mixture of the enantiomers. In other words, enantiomers are required to be minima on the Born-Oppenheimer surface separated by a sufficiently high barrier to suppress interconversion [46].

Enantiomers have identical physicochemical properties and show the same behaviour in a symmetric (i.e. achiral) environment, but may display very different behaviour in a chiral one. Thus enantiomers cannot be distinguished from each other unless an asymmetric probing (either chemical or physical) is applied. The physical method of choice for discrimination of enantiomers is the rotation of plane-polarized light. The magnitude of the rotation is the same for both enantiomers but in opposite direction (indicated by +/-). Hence chiral molecules and enantiomers are also referred to as optically active molecules and optical isomers, respectively [44]. An example of a chiral or optically active molecule is the lactic acid (**Fig. 4**).

Many examples where enantiomers function very differently when they are exposed to a chiral entity may be found, since chirality is a widespread phenomenon in nature. Particularly, the effects of chiral drugs on the body of the human being (in which a chiral receptor is usually the drug target) are a topic of great importance nowadays. Generally, only one enantiomer of a chiral drug presents optimal therapeutic action, while the other one can be less active, inactive or even responsible for adverse side

effects (**Fig. 5**) [47]. An example of the latter was the birth of a number of children with developmental malformations in the late 1950s after pregnant mothers had been prescribed thalidomide (as a racemic mixture) for the treatment of morning sickness. *R*-thalidomide was the therapeutic agent while *S*-thalidomide was responsible for the malformations [48,49]. Consequently, legislation now requires pharmacological effects of both enantiomers of a racemate drug to be studied [50]. Thus pharmaceutical industry is highly demanding for both new medicaments containing only enantiomers with desirable biological activities, and methods for obtaining enantiomerically pure chiral compounds [51–53].

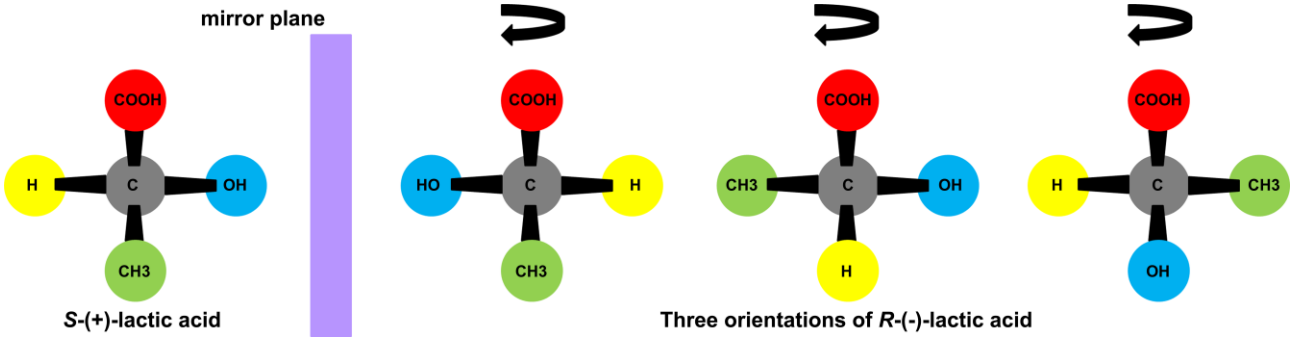

Fig. 4 Enantiomers of the lactic acid. *R*- and *S*-lactic acid are non-identical mirror images of each other. *R*-lactic acid cannot be rotated to be superimposable on *S*-lactic acid. The stereocenter responsible for the asymmetry of the molecule consists of a carbon atom (gray) with four different substituents.

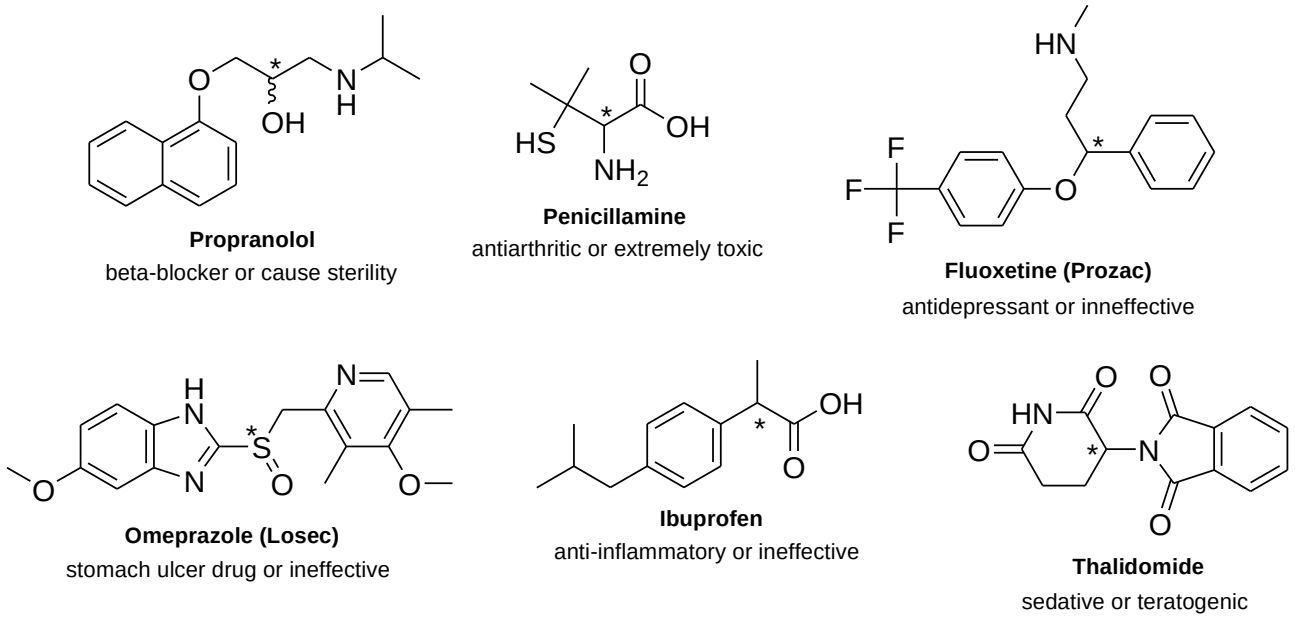

Fig. 5 Examples of chiral molecules with distinctly different biological functions of the enantiomers. The position of the stereocenter is indicated by *. This figure has been adapted from Ottosson [54].

1.2. Preparation of enantiomerically pure compounds

Different methods exist which may be used to access enantiomerically pure compounds. These methods can be classified into three groups depending on the type of starting material used (**Fig. 6**) [55]. The first approach is simply to use a chiral pool present in nature, as many natural products are enantiomerically pure and can be isolated at low cost. The second one is the resolution of racemic mixtures. Resolution is the separation of the enantiomers from the racemate with the recovery of at least one of the enantiomers. The third method is referred to as asymmetric synthesis. In the latter a chiral center is created in a non-chiral molecule (namely, prochiral substrate) by induction from a second source of chirality (i.e. a non-chiral molecule is converted into a non-racemic chiral compound) [56,57].

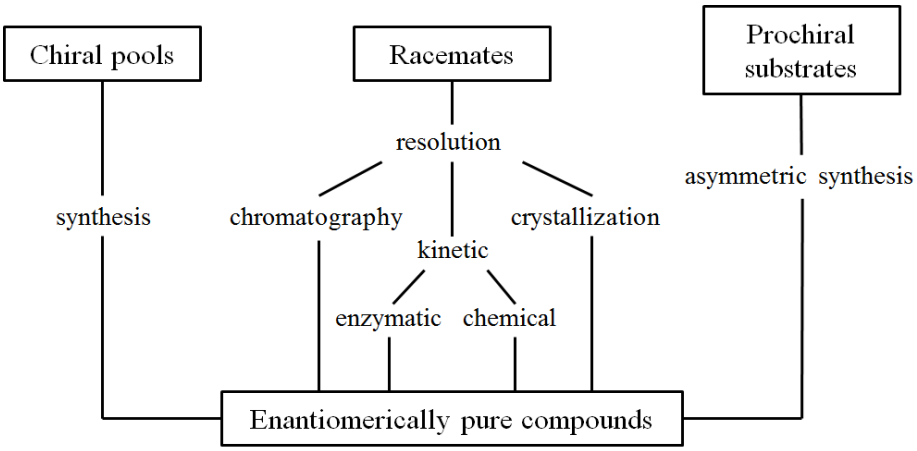

Fig. 6 Methods to obtain enantiomerically pure compounds. This figure has been adapted from Ghanem and Aboul-Enein [18].

The main method for obtaining enantiomerically pure compounds on an industrial scale is the resolution of racemic mixtures [18,58–60]. Approaches for resolution of racemic mixtures can be divided into four categories: i) direct preferential crystallization, ii) diastereomeric salt crystallization, iii) chiral chromatography, and iv) kinetic resolution. The success of the kinetic resolution approach depends on the fact that two enantiomers may react with different rates with a chiral entity. The chiral entity may be a biocatalyst (enzyme or microorganism) or a chemocatalyst (chiral acid or base or even a chiral metal complex), and should be present in catalytic amounts. Particularly, enzymatic kinetic resolution is considered as a versatile method for obtaining enantiomerically pure compounds. Reactions catalyzed by enzymes may be highly selective and offers an interesting alternative from an

economical and ecological point of view compared to classical chemical synthesis. The most used enzymes for carrying out the kinetic resolution of racemates are lipases [61–68]. The latter are the focus of the next sections.

1.3. Lipases

Lipases (triacyl glycerol hydrolases, EC 3.1.1.3) are established as the most versatile biocatalysts in organic synthesis nowadays, because the majority of lipases accept a wide range of non-natural substrates and show in many cases excellent selectivity [20,68,69]. These enzymes can catalyze hydrolysis reactions (in aqueous medium) as well as acylation reactions (in organic medium; e.g. esterification) from acyl donors and nucleophile compounds (e.g. alcohols, amines or peroxides). Kinetic resolution is the most common lipase-catalyzed chemical transformation, because the enzyme can discriminate between two enantiomers in a racemic mixture, transforming one enantiomer faster than the other one. This approach has been widely used for kinetic resolution of racemic mixtures of carboxylic acids, alcohols, esters and amines, among others compounds [70–76]. Several racemic drugs, precursors or intermediates have been resolved via hydrolysis, esterification or transesterification reactions catalyzed by lipases [16,77–79]. More applications of lipases in organic synthesis have been discussed in several reviews [17–19,80–82].

The success of the application of lipases in the kinetic resolution of racemates depends on the enantioselectivity (ability of the enzyme to discriminate between the enantiomers of a racemic mixture –see below-). The enantioselectivity of a lipase catalyzed reaction can be affected by changing the enzyme (either by screening for novel catalysts or by protein engineering of an existing catalyst) or the reaction conditions (e.g. temperature and solvent) and by modification of the substrates. An interesting overview of means to control the enantioselectivity of lipases has been reported by Berglund [80].

Different lipases have been used in different biotransformations, ranging from natural forms obtained with different organisms to bio-engineered forms. Due to their versatility and promising features, research on lipase catalyzed reactions is still a very active field. These reactions had been subject of a number of both computational and experimental studies. The general aim of the computational studies is to improve the understanding of the experimentally observed results (e.g. selectivities, effects of mutations, etc.), in order to improve reaction conditions and lipases as biocatalysts. Details about computational modeling of lipase-catalyzed reactions are given below in section **1.7**.

1.3.1. Enantioselectivity of lipases

There are two important concepts which are necessary to understand in lipase catalyzed kinetic resolution: the enantiomeric excess (ee) and the enantiomeric ratio *E*. The enantiomeric purity of any compound is expressed in terms of its ee value (**Equation 1**). For a racemic compound the ee value is zero while for an enantiomerically pure compound the ee value is 1 (or 100 % of ee). Moreover, as mentioned above, the ability of an enzyme to discriminate between the enantiomers of a racemic mixture is referred to as enantioselectivity or stereoselectivity. The parameter for describing the latter is called the enantiomeric ratio *E*, which is defined as the ratio of the specificity constant (k_{cat} / K_M) for the two enantiomers (**Equation 2**) [18].

Equation 1

$$\%\,\text{ee} = \frac{\text{concentration of major enantiomer - concentration of minor enantiomer}}{\text{concentration of major enantiomer + concentration of minor enantiomer}} \times 100$$

Equation 2

$$E = \frac{\left(k_{cat} / K_M\right)_{faster\ reactant\ enantiomer}}{\left(k_{cat} / K_M\right)_{slow\ reactant\ enantiomer}} \quad ; \quad \begin{array}{l} k_{cat}\ \textit{is the rate or turnover constant} \\ K_M\ \textit{is the Michaelis-Menten constant} \end{array}$$

Chen et al. [83] have developed **Equation 2** in terms of the enantiomeric excess of the product (ee_p), the unreacted substrate or slow reactant enantiomer (ee_s), and the conversion (*c*). Thus the *E* value for a given reaction can be expressed by **Equation 3**. *E* can also be expressed in terms of only the ee_s and ee_p by another equation presented by Rakels et al. (**Equation 4**). Thereby, to calculate the *E* value two of the three variables ee_s, ee_p and *c* can be measured. An *E* value of 1 corresponds to a non-enantioselective reaction, while an *E* value above 20 is the minimum for an acceptable resolution [68]. **Equation 3** and **Equation 4** apply to irreversible reactions. For reversible reactions the equilibrium constant (*K*) is incorporated to the equations [83].

Equation 3

$$E = \frac{\text{Ln}\left[1 - c\left(1 + \text{ee}_p\right)\right]}{\text{Ln}\left[1 - c\left(1 - \text{ee}_p\right)\right]} = \frac{\text{Ln}\left[\left(1 - c\right)\left(1 - \text{ee}_s\right)\right]}{\text{Ln}\left[\left(1 - c\right)\left(1 + \text{ee}_s\right)\right]} \quad ; \quad c = \frac{\text{ee}_s}{\text{ee}_s + \text{ee}_p}$$

Equation 4

$$E = \frac{\mathrm{Ln}\left[\frac{1\text{-}ee_s}{1+\left(ee_s/ee_p\right)}\right]}{\mathrm{Ln}\left[\frac{1+ee_s}{1+\left(ee_s/ee_p\right)}\right]}$$

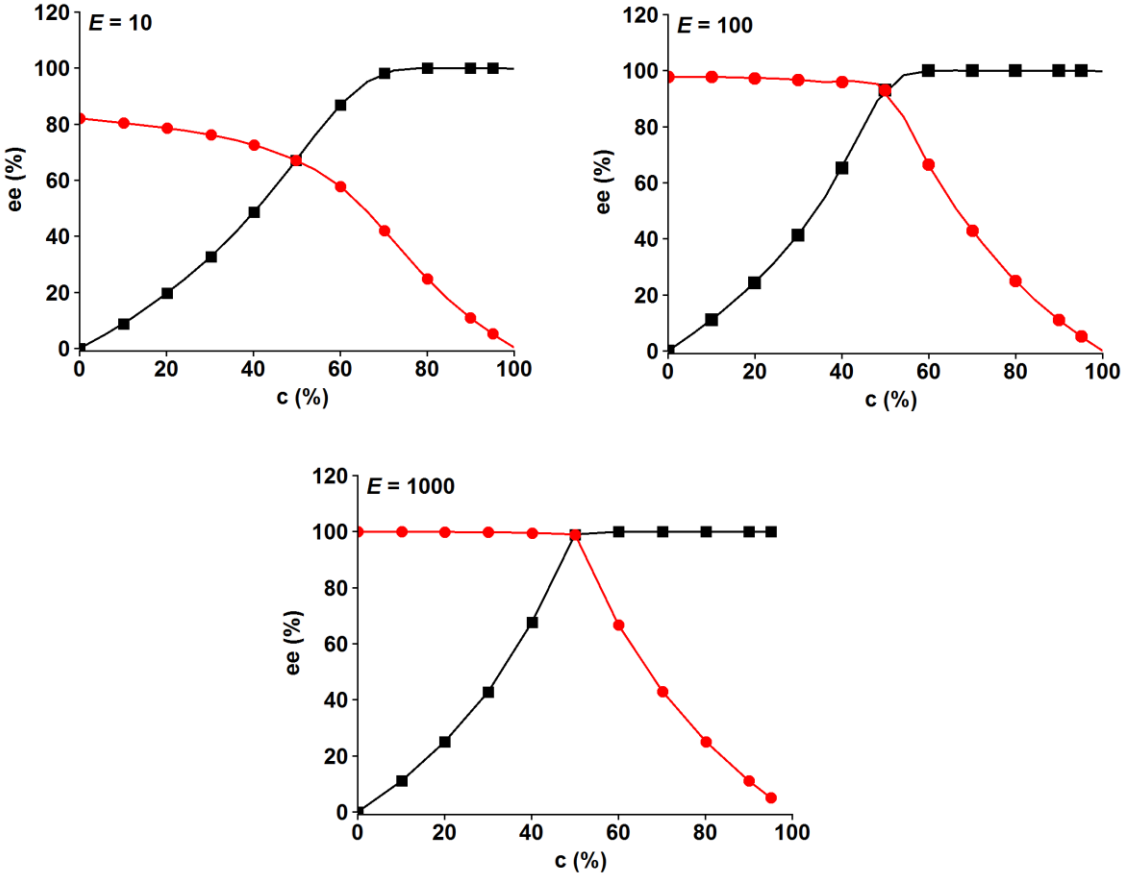

Fig. 7 Progression of the ee_s (black) and ee_p (red) at different *E* values for a lipase catalyzed irreversible kinetic resolution. Graphs have been built by using data obtained with the program *Selectivity* developed by the group of professor Faber at the University of Gratz (http://borgc185.kfunigraz.ac.at/).

The progress of the ee_s and ee_p versus the degree of conversion at different *E* values for a lipase catalyzed kinetic resolution is shown in **Fig. 7**. Generally speaking, at low conversion the enzyme is exposed to a nearly racemic concentration of the substrate and the faster reacting enantiomer is transformed yielding a high ee_p. As the reaction proceeds the concentration of the faster reacting enantiomer decreases and the enzyme is now exposed to a relatively higher concentration of the slow reacting enantiomer, raising its probability to be transformed, ee_s increases and ee_p decreases. The

progression of the ee_s and ee_p as the reaction proceeds depends on the *E* value (**Fig. 7**). Enzymes displaying high *E* values allow obtaining higher ee_s and ee_p values at a high conversion degree, which lead to obtain better yields of the enantiomerically pure materials.

1.4. Reaction mechanism of lipase-catalyzed reactions

All lipases are characterized by a catalytic triad consisting of Serine, Histidine and either Glutamate or Aspartate (Ser105, His224 and Asp187 in *Candida antarctica* lipase B –CalB-; the enzyme studied in this thesis). The generally accepted mechanism for reactions catalyzed by lipases involves two steps (**Fig. 8**). The first step (namely, acylation) is the addition of an acyl-group to the catalytic serine of the enzyme, yielding the acyl-enzyme. In the second step (namely, deacylation), the acyl-group can react with several nucleophiles, such as water, alcohols, amines or peroxides [19]. Acylation as well as deacylation proceed via a tetrahedral intermediate (TI), which is stabilized by the so-called oxyanion hole of the enzyme (constituted by the residues Thr40 and Gln106 in CalB).

All aminoacids of the catalytic triad play an important role for the reaction. Histidine exerts a general acid/base catalysis during the reaction which mediates in the acylation and subsequent deacylation of the serine. The deprotonated histidine acts as a base and enhances the nucleophilicity of the serine and the nucleophile in the reaction medium during the acylation and deacylation steps, respectively. In the doubly protonated form histidine acts as an acid donating the excess proton to the TIs. This ability of histidine to act both as an acid and a base is attributed to a pK value near neutrality in the enzyme [84,85]. On the other hand, the main role of the aspartate is to increase the basicity of the histidine, such that proton abstraction either from the serine (in the acylation step) or the nucleophile in the reaction medium (in the deacylation step) become probable.

The oxyanion hole is a very important structural feature of lipases as its function is the stabilization of the negative charge developing on the carbonyl oxygen coming from the acyl donor in the TIs. It is composed of NH functions in the backbone of aminoacids or hydrogen bond donating side chains (e.g. the OH side chain of Thr40 in CalB; **Fig. 8**) and is located in the vicinity of the catalytic serine. It was discovered in enzyme crystals that had an inhibitor attached to the active site serine [86,87]. Moreover, vibrational spectroscopy studies carried out by Carey and Tonge [88] showed that interactions between the carbonyl oxygen of the acylenzyme and the oxyanion hole exist. In fact, they

found a correlation between the C=O bond length of the acylenzyme and its deacylation rate. Acylenzymes with longer C=O bond lengths were more reactive than those with short ones.

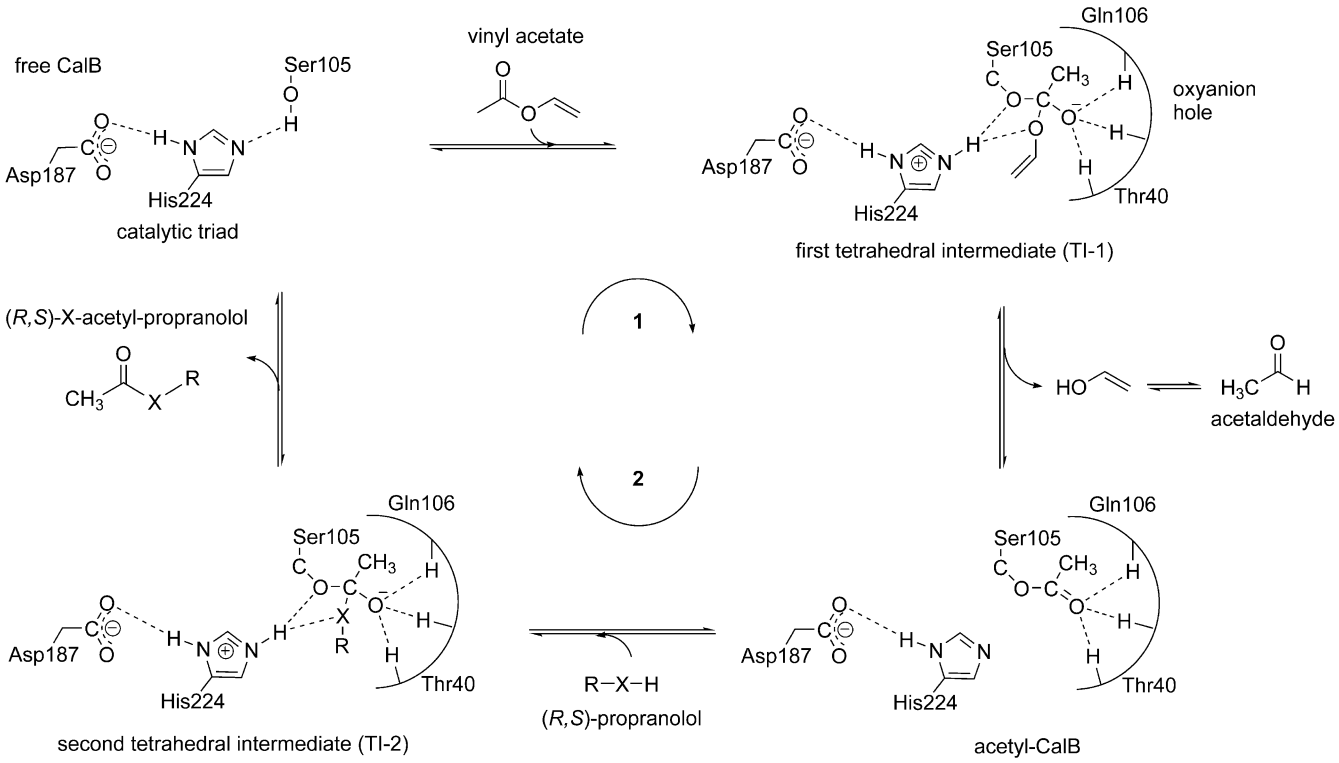

Fig. 8 Generally accepted reaction mechanism for lipase catalyzed reactions. The case of the CalB-catalyzed acetylation of (*R,S*)-propranolol is shown as example. The reaction is a two-step process: acylation (**1**) followed by deacylation (**2**) of CalB. X = N or O, according to the nucleophile groups of propranolol (**Fig. 1**).

The evidence supporting the reaction mechanism shown in **Fig. 8** has been reviewed extensively [89–91]. It is strongly recommended to revise the review of Hedstrom [42] to get a brief (but not incomplete) description about these evidences. On the other hand, it is important to note that this reaction mechanism has been subject of several computational studies [30,92–94], in which the TIs have been found to be energetically and structurally close to the transition states (TSs) of the reaction. Thus the TIs are usually regarded as transition state analogues [28,31,36,95].

1.4.1. Mechanism for the chemoselective acylation of amino alcohols catalyzed by lipases

Among the most frequently studied lipase catalyzed reactions is the enantioselective acylation of racemic amines and secondary alcohols in organic solvents [81,96–101]. In contrast, the lipase-catalyzed acylation of amino alcohols (compounds which contain at the same time an amino and an alcohol group available to be acylated; e.g. propranolol or ethanolamine) has been less studied and has

recently gained attention [102–108]. Particularly, the chemoselectivity of these reactions is still not completely understood. It has been suggested that the lipase-catalyzed chemoselective *N*-acylation of short chain amino-alcohols such as ethanolamine, serine and 3-amino-1-propanol proceeds through initial *O*-acylation (catalyzed by the enzyme according to the reaction mechanism shown in **Fig. 8**) followed by spontaneous *O*- to *N*-acyl migration [109,110]. However, recently Le Joubioux et al. [103] have reported experimental results on the lipase-catalyzed acylation of amino-alcohols and related compounds which are not in accordance with the hypothesis of acyl migration as an explanation of the observed chemoselectivity and rate enhancement for *N*-acylation. Therefore, a new reaction mechanism has been proposed [103,111]. This mechanism suggests an *N*-acylation reaction catalyzed by the enzyme and involves a proton shuttling in the transition state mediated by the nucleophilic groups present in the amino-alcohols linked together through an intramolecular hydrogen bond and by the availability of a suitable base (histidine) to act as a proton acceptor in the active site of the enzyme. This proton shuttle is concomitant with a nucleophilic attack of the nitrogen atom of the amino group at the acyl enzyme (see **Fig. 9**). This new mechanism explains the observed chemoselectivity in case of amino-alcohols exhibiting a variable carbon chain length between the amino and alcohol groups, such as alaninol, isopropranolamine, 4-amino-1-pentanol and 6-amino-1-hexanol [103]. It also explains the *N*-acylation observed in case of bifunctional compounds which are structurally related to alaninol but exhibit no alcohol group in their structure (1-methoxy-2-propylamine and 1,2-diaminopropane) and thus cannot possibly be *O*-acylated, ruling out the hypothesis of an *O*- to *N*-acyl migration.

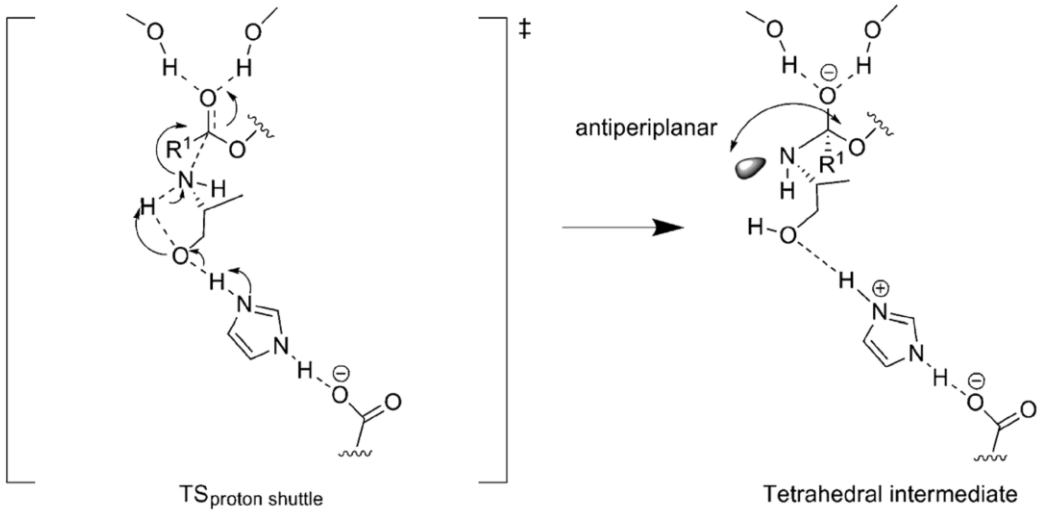

Fig. 9 TS (left) and TI (right) to be formed in the proposed proton shuttle reaction mechanism for the lipase catalyzed *N*-acylation of amino alcohols. The case of *R*-alaninol is shown as example. This proton shuttle mechanism works also for diamines. This figure has been taken from Syrén et al. [112].

Generally speaking, lipases catalyze *N*- or *O*- acylation of amino-alcohols with a chemoselectivity which depends on the amino-alcohol structure, the solvent, the acyl donor and the type of lipase used as biocatalyst [40,103,107,109,113,114]. In this thesis the chemoselectivity of the CalB-catalyzed acetylation of propranolol has been subject of an experimental and computational study, contributing to shed more light about the origin of the chemoselectivity of lipase-catalyzed acylation of amino alcohols.

1.5. Microscopic basis for the enantioselectivity of lipases

Different scenarios exist which may lead to an enantioselective lipase catalyzed reaction. These scenarios are described below for the acylation of racemic nucleophile compounds, which is the case of the system studied in this thesis. Similar scenarios occur when lipases catalyze the hydrolysis of racemic esters [115]. In the acylation of racemic nucleophile compounds catalyzed by lipases the acylation step is not enantiodiscriminative and identical acylenzymes are formed in the reaction. Enantioselectivity originates from the deacylation step when the racemic compound reacts with the acylenzyme molecules. This step requires that the substrate initially bind non-covalently to the acylenzyme (AcE), forming an acylenzyme substrate Michaelis complex (MCC). Then the MCC undergoes acyl cleavage to give the corresponding acylated product complex (PDC). This comprises two steps: forming of the second tetrahedral intermediate (TI-2) via a first transition state (TS1) and subsequent releasing of the acylated product via a second transition state (TS2) (**Fig. 8**). Enantioselection may occur at the binding and/or reaction steps and the enantioselectivity will be therefore determined by the free energy differences of both steps. Three types of scenarios are identified which lead to an enantioselective acylation reaction catalyzed by lipase: i) different activation energies for acyl transfer and identical binding free energies ii) identical activation energies for acyl transfer and different binding free energies iii) both the activation energies for acyl transfer and binding free energies are different. See **Fig. 10**.

Considering the overall reaction of enantiomers (enzyme + substrate $\longrightarrow$ $[TS]^{\ddagger}$ $\longrightarrow$ enzyme+product), the relation between the enantiomeric ratio *E* and the difference in activation free energy between the enantiomers ($\Delta_R G^{\ddagger}$ - $\Delta_S G^{\ddagger}$; $\Delta_{R\text{-}S}\Delta G^{\ddagger}$) that may be separated into an enthalpy and an entropic term, can be shown with transition state theory to be $\Delta_{R\text{-}S}\Delta G^{\ddagger} = \Delta_{R\text{-}S}\Delta H^{\ddagger} - T\Delta_{R\text{-}S}\Delta S^{\ddagger} = -RT \ln E$. Originally the contribution of entropy to the enantioselectivity was considered negligible as both enantiomers are significantly restricted in the small volume of the enzyme active site [116–118]. However it was

pointed out later that $\Delta_{R\text{-}S}\Delta S^{\ddagger}$ in fact can contribute significantly to enantioselectivity [119]. At the molecular level several events related to free energy components have been identified to be responsible for the enantioselectivity in lipase catalyzed reactions. Some of these events are briefly revised in the following.

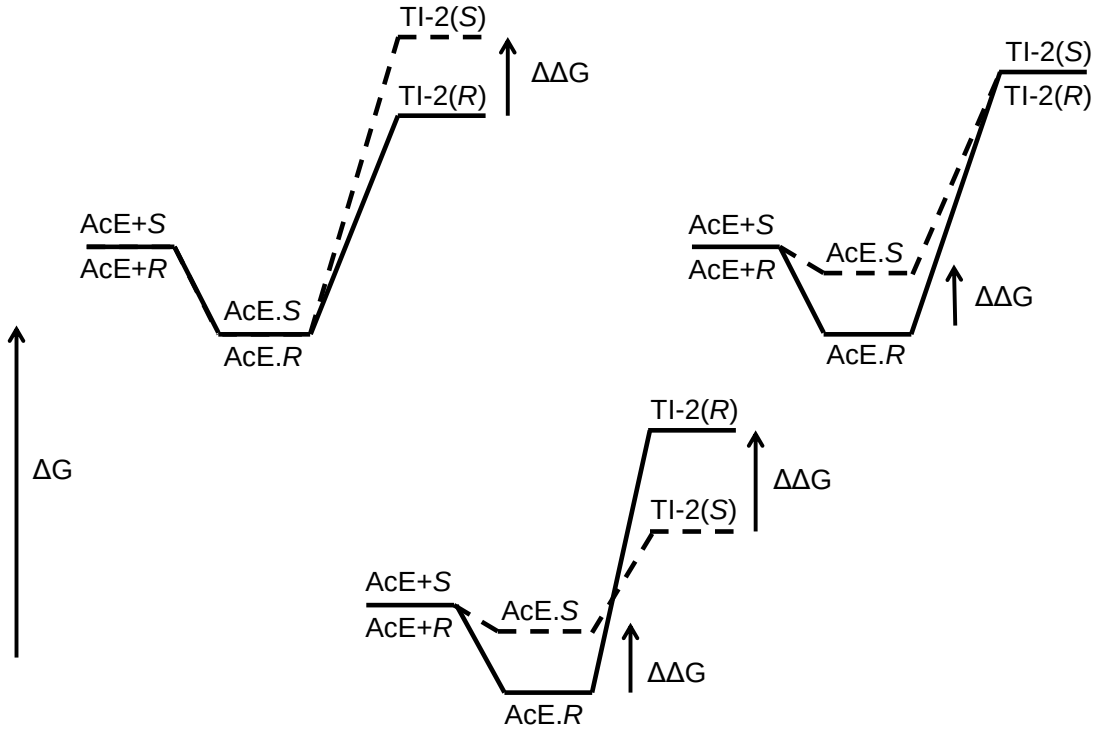

Fig. 10 Possible scenarios for an enantioselective lipase catalyzed acylation of racemic nucleophile compounds. Only the deacylation reaction, which is the enantioselective step, is shown. Initially the nucleophile compound (*R* or *S*) and the acylenzyme (AcE) are well separated providing a reference. Formation of the Michaelis complex (AcE.*R* or AcE.*S*) and subsequent reaction take place on the asymmetric surface of the acylenzyme and give rise to enantioselectivity. Here the TI-2 is treated as transition state (as is often done for the TIs [28,31,36,39,95,120]) for simplicity of the schemes. This graph has been adapted from that presented by Otte for the case of an enantioselective ester hydrolysis [115].

Enthalphic contributions to the enantioselectivity ($\Delta_{R\text{-}S}\Delta H^{\ddagger}$) arise from charge-charge or general multipole-multipole interactions, which may preferentially occur for only one enantiomer upon binding in the MCC or the TS (or the TI as an approximation) [28,31,36,120–123]. Thus, for example, Bocola et al. [31] attributed the enantioselective ester hydrolysis by a lipase in favor of the *S* enantiomer to the electrostatic stabilization of its TI-1 by an additional hydrogen bond in the oxyanion hole, which was sterically hindered for the *R* enantiomer. Similarly, Nyhlén et al. [28] attributed the enantioselectivity

in favor of the *R* enantiomer displayed by a mutant lipase catalyzing acylation of a keto alcohol to the ability of this enantiomer to form an additional hydrogen bond with a residue of the enzyme active site in the TI-2. In some studies, the probability of formation of an important hydrogen bond interaction for stabilization of the TIs (evaluated from MD simulations) has been related to reactivity (higher probability implying higher reactivity) [124–126]. In addition to polar interactions, attractive Van der Waals (VdW) interactions with the enzyme leading to better stabilization of the TI-(1 or 2; depending on the enantioselective step of the reaction) of the preferred enantiomer may also contribute to enantioselectivity [36,43].

On the other hand, though in terms of enthalpy any binding event (of either nonpolar or polar origin) may favorably contribute to the enantioselectivity of the reaction, it has an unfavorable contribution in terms of entropy. The latter is due to loss in translational and rotational motion, which decreases the entropy (i.e. $\Delta_{R\text{-}S}\Delta S^{\ddagger}$ becomes more negative) and leads the $T\Delta_{R\text{-}S}\Delta S^{\ddagger}$ term to make the process less spontaneous. However, $\Delta_{R\text{-}S}\Delta H^{\ddagger}$ is often observed to be negative and to outweigh the $T\Delta_{R\text{-}S}\Delta S^{\ddagger}$ [54,124,127,128]. Cases have also been reported in which the differential activation entropy is positive and increases the *E* value or even $T\Delta_{R\text{-}S}\Delta S^{\ddagger}$ is the dominant contribution [128,129].

Several studies treating on the molecular events which contribute to the enantioselectivity of lipase catalyzed reactions in terms of enthalpy or entropy may be found in the literature. The reader is encouraged to revise the review article of the enantioselectivity of lipases provided by Ema [130], which includes both a variety of experimental and theoretical examples.

1.6. *Candida antarctica* lipase B (CalB)

Most biotransformations carried out with lipase use commercial preparations and *Candida antarctica* lipase B (CalB) is often the most enantioselective lipase toward racemic amines and secondary alcohols [54,81,131,132]. Therefore CalB seems to be the ideal enzyme for the acylation of amino alcohols. Immobilized CalB has been recently used for carrying out the acylation of several amino alcohols using myristic acid as an acyl donor and different organic solvents and an ionic liquid as reaction medium [103,107]. Immobilized CalB has also been used as catalyst for the acetylation of racemic propranolol using vinyl acetate as acyl donor and toluene as reaction medium. The enantioselectivity of CalB catalyzing this reaction was moderate (*E*=57), but higher compared to other lipases used for the kinetic resolution of propranolol via hydrolysis and esterification reactions in previous studies [13]. In this

thesis valuable information is provided about the origin of the enantioselectivity of CalB catalyzing acetylation of propranolol, which may help to improve the resolution of propranolol via this reaction by a rational redesign of CalB or the reaction conditions.

1.6.1. Structure and origin of CalB

CalB is a globular protein with an α/β hydrolase fold [133]. It is composed of 317 amino acid residues and has a molecular weight of 33 kDa, which makes it fairly small protein compared to other lipases. The lipase was isolated from the yeast *Candida antarctica*. The latter also produces another lipase which is called CalA and is different from CalB [134,135]. The three dimensional structures of CalB and CalB complexes have been determined by X-ray crystallography (Protein Data Bank codes: 1LBS, 1LBT, 1TCA, 1TCB and 1TCC) [136,137]. The active site of the enzyme is buried in the core of its structure and the binding pocket has a funnel-like shape (**Fig. 11a**). As mentioned in section **1.4** the characteristic catalytic triad of lipases consist of the aminoacids Asp187, Ser105, and His224 in CalB. On the other hand, the oxyanion hole, which is responsible for the stabilization of the transition state, consist of the aminoacids Gln106 and Thr140. Viewed with the catalytic triad Asp-His-Ser oriented from left to right, the binding pocket of CalB is constituted by a large hydrophobic pocket above the catalytic triad and a medium size pocket below it. The large pocket is lined by Ile189 and Val190 on the left, Val154 on the far right, as well as Leu140 and Leu144 at the top. Deep in this pocket, Asp134 is on the left and Gln157 on the right. The medium pocket is below the catalytic Ser105 and is crowded by Trp104 below it and the Leu278–Ala287 helix (helix α10) to the right (**Fig. 11b**).

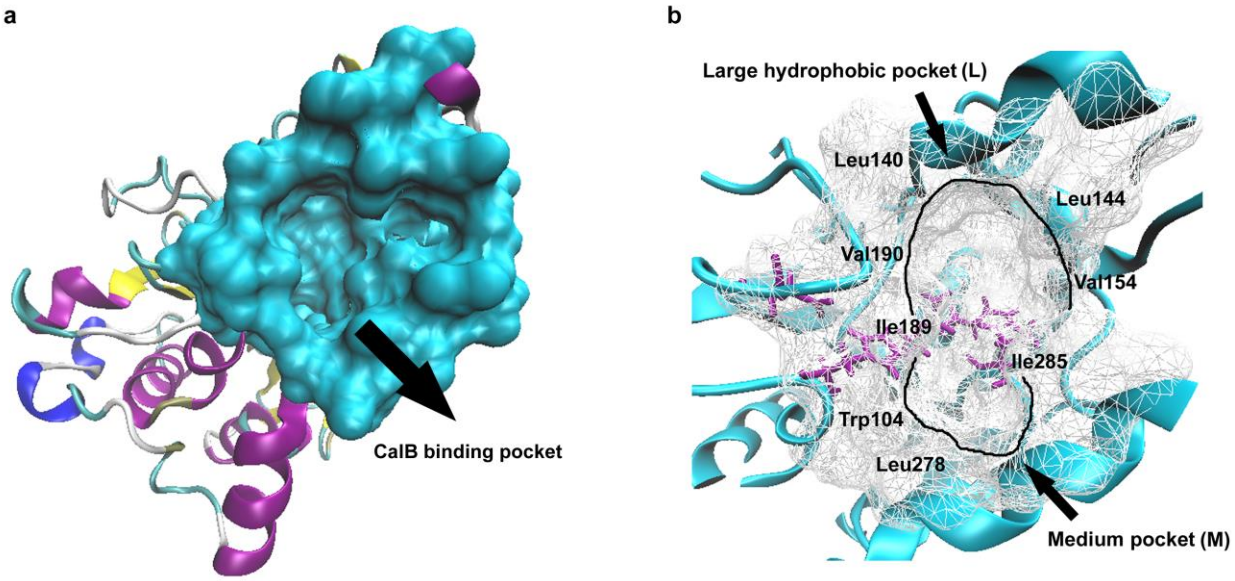

Fig. 11 Structure of CalB (a) with a zoom of its binding pocket (b). See the text for details.

1.7. Molecular modeling of lipase catalyzed reactions

As it was already mentioned above the aim of the computational modeling of lipase catalyzed reactions is to get information at atomistic level about the catalytic events which leads to the selectivity of these reactions [30,31,37,138]. Models aimed at reproducing such complex systems (enzyme-substrate-solvent) at the molecular level need to fulfill essentially three criteria: i) reproduction of intramolecular forces (e.g. bonding) ii) proper description of bond breaking and forming iii) inclusion of environmental effects (e.g. solvent effects or interactions with macromolecules) [115,139,140]. Quantum mechanical (QM) methods are in principle capable to satisfy all needs, but the high computational costs of these methods limit their usability to very small systems. Consequently QM methods are used with small models systems of the enzyme active site and the substrate [32,141]. In contrast, Molecular Mechanics (MM), which is an empirical force-field method, may be used for treating large systems such as enzymes [142]. However, chemical reactions in which bonds are formed and broken cannot be studied, as electrons are not treated explicitly with MM. Here, mixed quantum mechanical/molecular mechanical (QM/MM) approaches have become methods more suited for analysis of chemical reactions [143–146]. In these methods a subset of the system is identified which is deemed important in the reaction and is treated by QM. The rest of the system, which is considered to be less involved in the reaction under study, is treated with MM. QM method in a QM/MM approach can range from very fast (but often less accurate) semi-empirical methods to ab-initio (density functional theory, or even higher level methods like Møller Plesset perturbation theory or the coupled cluster method).

Interestingly, QM and QM/MM studies on the enantioselectivity in serine hydrolases (including lipases) have shown the TIs to be geometrically and energetically closely related to the corresponding transition states (TSs) [30,92–94]. Thus it is commonly accepted to consider the TIs as analogues of the TSs, and it is then suggested that the relative stability ($\Delta_{R\text{-}S}\Delta G$) of the TIs is a key factor in determining the enantioselectivity of lipase-catalyzed reactions. Thereby the most used computational approach to get insights at molecular level into the enantioselectivity of lipase catalyzed reactions is the molecular dynamics simulation (MD) of the tetrahedral intermediates (TIs) [28,31,36,39,95,120].

Chapter 2. Experimental study of the chemo- and enantioselectivity of the acetylation of (*R,S*)-propranolol catalyzed by CalB

2.1. Overview

The chemo- and enantioselectivity of the acetylation reaction of (*R,S*)-propranolol catalyzed by CalB (the free enzyme) using vinyl acetate as acyl donor and toluene as organic solvent was studied. Because of the poor solubility of propranolol in toluene small quantities of methanol were added as cosolvent. The effects of the propranolol/vinyl acetate ratio, the enzyme purification procedure and the methanol concentration on the reaction were investigated. Though using methanol in the reaction medium increased the solubility of propranolol, at the same time it increased the complexity of the reaction system, due to competing reaction of methanol in addition to hydrolysis of vinyl acetate (**Fig. 12**). ^{1}H- and ^{13}C-NMR spectroscopy was used for monitoring all reactions occurring in the system and for determining the chemoselectivity of the acetylation of propranolol. For a full assignment of the chemical shifts corresponding to each chemical compound in the reaction mixture, DEPT135° as well as HMBC and HSQC heteronuclear correlation techniques were used. The major reactions were the hydrolysis and alcoholysis of vinyl acetate. Furthermore, the NMR analysis confirmed that *O*-acetyl-propranolol was formed exclusively. The reaction was also found to be enantioselective favoring the faster transformation of the *R*-propranolol. *E* values similar to the observed with the immobilized enzyme were obtained.

2.2. Methodology

2.2.1. Materials

Candida antarctica lipase B (CalB) was obtained from Novozymes (Parana, Brazil). Racemic mixtures and pure enantiomers of (*R,S*)-propranolol-HCl, p-Nitrophenylbutyrate (pNPB), Triton X-100 and other reagents were purchased from Sigma–Aldrich (St. Louis, USA). All reagents and solvents used were of analytical or high-performance liquid chromatography grade.

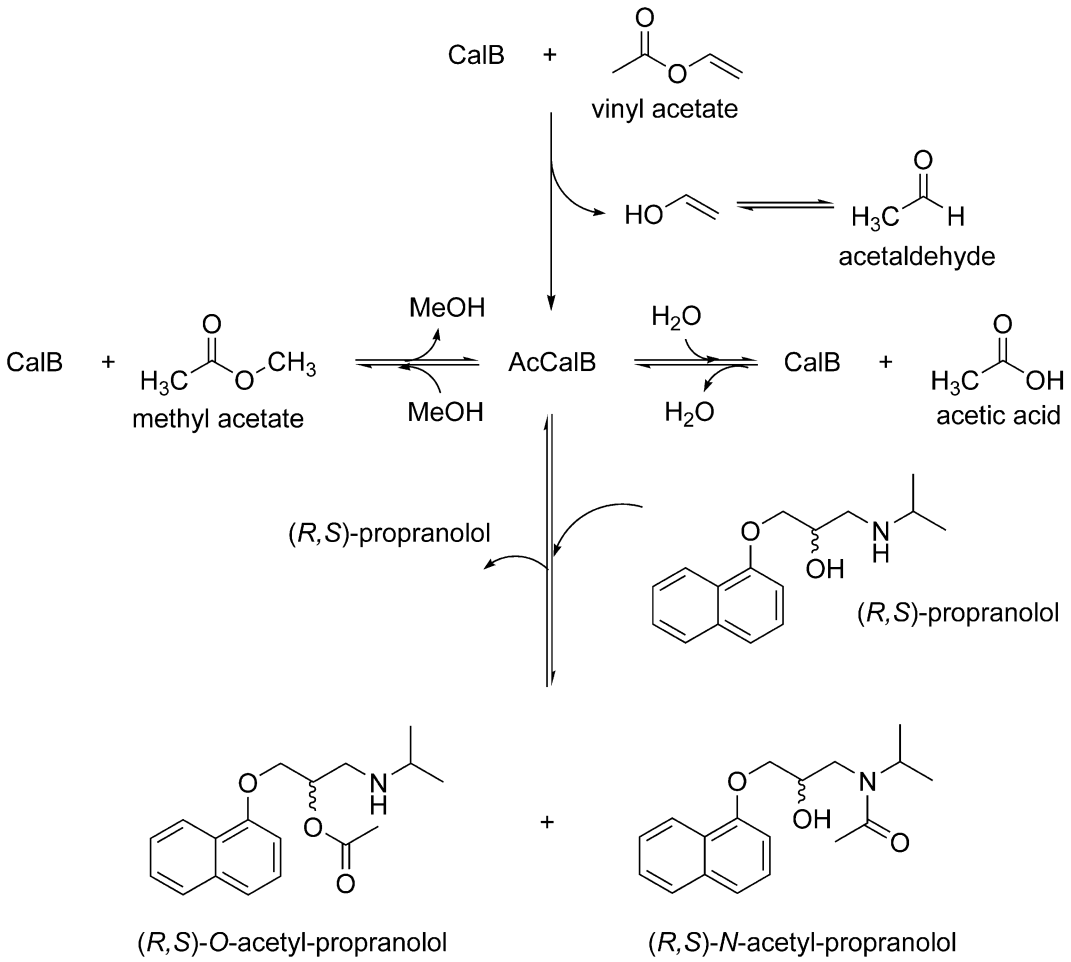

Fig. 12 Scheme of the reactions occurring in the CalB-catalyzed acetylation of propranolol using vinyl acetate as acyl donor and a solution of toluene/methanol as solvent. AcCalB denotes acetylated CalB or the acetyl-enzyme complex, an acyl-active intermediate in the reaction which can react with any of the nucleophiles participating of the reaction (methanol, water or propranolol). The competing reactions are the alcoholysis and hydrolysis of vinyl acetate, and the acetylation of propranolol.

2.2.2. Lipase purification

CalB was purified for being used in the acetylation of (*R*,*S*)-propranolol. The purification was done by chromatography based on the adsorption of the lipase on octyl agarose beads at low ionic strength [147]. A solution of CalB (20 mL, 0.7 mg/mL) in sodium phosphate buffer (5 mM, pH 7) having an activity of 167 U/mg in pNPB assay (see below) was incubated with octyl agarose beads (4 g) during 2h. Periodically, the activity of suspensions and supernatants was assayed using the p-nitrophenylbutyrate (p-NPB) assay as described below. The protein concentration in the supernatants was also determined, using Bradford´s method [148]. After immobilization, the adsorbed lipase was

filtered and washed with distilled water. Then the enzyme was desorbed using sodium phosphate buffer (20 mL, 5 mM, pH 7) containing Triton X-100 (1% v/v) [27,147]. This enzyme solution was diluted 5 fold in sodium phosphate buffer (5 mM, pH 7) to dilute the detergent. A fraction (50 mL) of this diluted enzyme solution was dialyzed to remove the detergent. The rest was kept as it was. Finally, both enzyme fractions were lyophilized and used for the acetylation of propranolol. These enzyme preparations are referred here as CalB-I and CalB-II respectively. As Triton X-100 has been shown to promote an increase of the activity of CalB [27], these two enzyme preparations were obtained to evaluate the effect of this detergent on the activity, the chemo- and the enantioselectivity of CalB.

2.2.3. Hydrolysis of p-NPB

This assay was performed by measuring the increase in absorbance at 348 nm produced by the released p-nitrophenol in the hydrolysis of p-NPB (0.4 mM) in sodium phosphate buffer (25 mM, pH 7.0) at 25 °C. To start the reaction, the lipase solution or suspension (0.02 mL) was added to the substrate solution (2.5 mL). One international unit of activity (U) was defined as the amount of enzyme that hydrolyzes 1 µmol of p-NPB per minute under the conditions described previously.

2.2.4. Chemical acetylation of (*R,S*)-propranolol

This reaction was carried out using an analogous procedure to the classical methodology of Gatterman [149] for the synthesis of (*R,S*)-*O*-butyryl propranolol (*RS*-*O*-BP): (*R,S*)-propranolol-HCl (0.2 g; 0.76 mmol) was refluxed with dichloromethane (20 mL) and acetyl chloride (0.08 mL; 0.76 mmol) was very slowly added. After two hours, the reaction mixture was washed successively with equal volumes of saturated aqueous sodium bicarbonate and brine. The organic layer was dried over anhydrous sodium sulfate and evaporated to dryness under reduced pressure to afford *N*-acetyl propranolol (*N*-AP) and *O*-acetyl propranolol (*O*-AP).

2.2.5. Lipase-catalyzed acetylation of (*R,S*)-propranolol

Different experiments were carried out in order to study the effect of the reaction conditions on the velocity, the chemo- and the enantioselectivity of the reaction. As propranolol is poorly soluble in toluene (<0.5 mg/mL), methanol was added as a cosolvent according to the amount of propranolol to be solvated: (a) (*R,S*)-propranolol (39 mM) was dissolved in a solution of toluene/methanol (20 mL, 93/7 v/v) containing vinyl acetate (117 mM). (b) (*R,S*)-propranolol (8 mM - 28 mM) was dissolved in a solution of toluene/methanol (5mL, 96/4 v/v) containing vinyl acetate (54 mM). To start these reactions

the purified enzyme was added (3 mg). The reaction mixtures were continuously shaken at 200 rpm and 25 °C.

Methanol was chosen as cosolvent based on the solubility of propranolol in this solvent (200 mg/mL). THF, hexane and ethanol were also tested, but the solubility of propranolol in these solvents is 9 mg/mL, 3 mg/mL and 10 mg/mL, respectively.

Blank experiments were carried out in addition, using the same reaction conditions but without addition of the enzyme. No acetylated product of propranolol was detected under these conditions.

2.2.6. HPLC analysis

The conversion of the enzyme reaction was determined by HPLC (Agilent 1100) using a Silica gel C-18 column (Zorbax C-18, Agilent Technologies). The mobile phase was composed of acetonitrile and phosphate buffer pH 6 (70:30) and the samples were eluted at 1.0 mL/min. A UV detector (at a wavelength of 289 nm) was used for quantification. The enantiomeric excess of the substrate (ee_s) and the product (ee_p) was determined using a chiral column (25cm, ES-OVM, Agilent-Technologies, USA) with methanol/phosphate buffer pH 6 (30:70) at 1.0 mL/min as mobile phase [13]. The enantioselectivity (*E*) was calculated using the equation reported by Chen et al. [83] (**Equation 3**).

2.2.7. NMR analysis

^{1}H-, ^{13}C-, DEPT135°, HMBC and HSQC-NMR spectra were recorded on a Bruker Avance III, 400 MHz spectrometer, using $CDCl_3$ as the solvent and tetramethylsilane (TMS) as internal reference. The experimental conditions were: for ^{1}H, spectral width (SW) = 4400 Hz (-0.5 to 10.5 ppm), Bruker pulse program zg30 and number of scans = 16; the quantitative ^{13}C-NMR spectra were obtained in the inverse gated mode for fully decoupled spectra with no Nuclear Overhauser Effect (NOE) with spectral width (SW) = 24038 Hz (-20 to 219 ppm), Bruker pulse program zgig30 and number of scans = 4096; the two-dimensional phase-sensitive gradient selected edited heteronuclear single quantum coherence -HSQC- spectra were obtained with the Bruker pulse program hsqcedetgp; for the two-dimensional heteronuclear multiple bond correlation –HMBC- spectra the Bruker pulse program hmbcgplpndqf was used; for distortionless enhancement by polarization transfer –DEPT135°- spectra the Bruker pulse program dept135 and 2048 scans were used. The products were identified by performing a full assignment of ^{1}H and ^{13}C chemical shifts using DEPT135° as well as ^{1}H-^{13}C HMBC and HSQC heteronuclear correlation techniques (see **Appendix A** for details).

2.3. Results and discussion

2.3.1. Chemical acetylation of (*R,S*)-propranolol

The chemical acetylation of (*R,S*)-propranolol was carried out as a first attempt to identify the possible acetylated products of propranolol directly from a mixture of these compounds using NMR spectroscopy. This was done in order to explore the feasibility of quantifying the chemoselectivity of any kind of acetylation reaction of propranolol, chemical or enzymatic, without any previous purification or separation of the reaction mixture. The NMR analysis of the reaction mixture revealed that a mixture of the mono-acetylated compounds *O*-AP and *N*-AP was formed. The di-acetylated product (*N,O*-AP: *N,O*-acetyl-propranolol) was not detected under the experimental conditions used here. The ^{13}C-NMR data of propranolol and its acetylated products are shown in **Table 1**. The ^{13}C- and ^{1}H-NMR signals corresponding to the carbon and hydrogen atoms of the acetate group (-**C**O**C**H_3 in **Table 1**) were chosen to determine the chemoselectivity of the reaction. It was found by integration of any of these peaks that the chemical acetylation of (*R,S*)-propranolol with acetyl chloride leads to the formation of both *N*-AP and *O*-AP, with a ratio of 3:1 in favor of *N*-AP (**Table 2**). This is consistent with the higher nucleophilicity of the amino compared to the hydroxyl group. A similar reactivity of the amino group has been observed in the chemical acetylation of other amino-alcohols [150,151].

2.3.2. CalB-catalyzed acetylation of (*R,S*)-propranolol

A first experiment was performed using 39 mM (*R,S*)-propranolol and 117 mM vinyl acetate in 20 mL of toluene/methanol (93:7 v/v). The reaction was very slow and was stopped after 18 days when the conversion rates reached 22% and 25% for CalB-I and CalB-II respectively. The higher conversion obtained with CalB-II may be attributed to hyperactivation of the enzyme due to the presence of Triton X-100 during its lyophilization. When CalB is exposed to Triton X-100, the formation of bimolecular lipase aggregates is avoided and the active site of the enzyme is expected to be more exposed to the reaction medium and the substrate, which results in a faster transformation of the substrate [27].

From the NMR analysis of the reaction mixtures the following reaction products were identified: acetaldehyde (aldehyde proton resonance at 9.38 ppm), acetic acid (carboxylic proton resonance at 9.98 ppm), methyl acetate (acetyl protons resonance at 2.04 ppm) and *O*-AP (acetyl protons resonance at 2.18 ppm). The amount of acetaldehyde, acetic acid and methyl acetate increased faster than the amount of *O*-AP. This indicates that the main reactions were the alcoholysis and hydrolysis of vinyl acetate and not the desired acetylation of (*R,S*)-propranolol. ^{13}C- or ^{1}H-NMR chemical shifts for *N*-AP

and *N,O*-AP were not observed. The absence of *N*-AP and *N,O*-AP may be due to the inaccessibility of the amino group of propranolol for the acyl transfer by the AcCalB complex or its unavailability for an intramolecular *O*- to *N*-acyl transfer in the structure of *O*-AP as a consequence of the preferred conformation of propranolol in the active site of CalB (see section **3.3.2.1** to section **3.3.2.2**).

Table 1 ^{13}C-NMR chemical shifts (in ppm) of propranolol and its acetylated products in the reaction mixture of the chemical acetylation reaction.

Carbon[a]	Propranolol	Acetyl propranolol	
		O-AP[b]	*N*-AP[c]
Ar-**C**	154.33 134.49 127.50 126.46 125.89 125.53 121.87 121.57 120.62 104.88	154.26 134.47 127.56 126.42 125.87 125.38 121.85 121.57 120.66 104.81	154.06 134.51 127.68 126.42 125.98 125.28 121.85 121.57 120.66 104.81
Ar-O**C**H_2-	70.65	68.20	69.78
Ar-OCH_2**C**H-	68.40	71.63	72.41
-CH**C**H_2N-	49.46	45.40	46.15
-**C**H$(CH_3)_2$	49.03	49.56	50.29
-CH(**C**$H_3)_2$	23.04 22.92	22.21 21.78	21.38 21.23
C=O[d]		171.38	173.92
-CO**C**H_3[d]		21.02	20.64

[a] Chemical shifts correspond to the underlined carbon atoms in bold.
[b] *O*-acetyl-propranolol.
[c] *N*-acetyl-propranolol.
[d] Chemical shifts used for quantification of the chemoselectivity of the reaction. The ^{1}H-NMR chemical shift of the methyl of the acetate group (-COC**H$_3$**), with value of 2.16 and 2.22 ppm for *O*-AP and *N*-AP respectively was used in addition.

In order to verify the chemoselectivity of CalB in favor of *O*-AP at higher conversions, the effect of the propranolol concentration on the synthesis of acetyl propranolol was evaluated with the aim of decreasing the reaction time. Using CalB-II as biocatalyst, the reaction was carried out with 8 mM-28 mM of (*R,S*)-propranolol and 54 mM vinyl acetate in 5 mL of toluene/methanol (96:4 v/v).

Table 2 Chemo- and Enantioselectivity of the chemical and enzymatic acetylation of propranolol.

Enzyme preparation	Solvent	c[a] (%)	t (h)	Ratio[b] *N*-AP/*O*-AP	ee_s (%)	ee_p (%)	*E*	Sp[c]
Chemical acetylation[d]	Dichloromethane	85	2	75/25	nd[g]	nd[g]	nd[g]	nd[g]
CalB-I[e]	toluene/methanol (93:7)	22	432	<3/>97	nd[g]	nd[g]	nd[g]	nd[g]
CalB-II[e]	toluene/methanol (93:7)	25	432	<3/>97	nd[g]	nd[g]	nd[g]	nd[g]
CalB-I[f]	toluene/methanol (96:4)	21	12	<3/>97	26	96	63	*R*
CalB-I[f]	toluene/methanol (96:4)	62	99.7	<3/>97	>99	61	63	*R*
CalB-I[f]	toluene/methanol (96:4)	70	140	<3/>97	>99	42	63	*R*
CalB-II[f]	toluene/methanol (96:4)	33	12	<3/>97	46	95	61	*R*
CalB-II[f]	toluene/methanol (96:4)	73	99.7	<3/>97	>99	37	61	*R*
CalB-II[f]	toluene/methanol (96:4)	82	140	<3/>97	>99	22	61	*R*

[a] Conversion.
[b] Determined by NMR spectroscopy. Assuming an error of 3 %.
[c] Stereochemical preference.
[d] Reaction conditions: propranolol (38 mM), acetyl chloride (38 mM) and 20 mL of solvent.
[e] Reaction conditions: propranolol (39 mM), vinyl acetate (117 mM), CalB (3 mg) and 20 mL of solvent.
[f] Reaction conditions: propranolol (28 mM), vinyl acetate (54 mM), CalB (3 mg) and 5 mL of solvent. The enantioselectivity of CalB-I and CalB-II was determined at a conversion of 21 % and 33 %, respectively.
[g] Not determined.

Under these reaction conditions the alcoholysis of vinyl acetate is notably decreased and the transformation of propranolol occurs faster.

As shown in **Fig. 13**, the reaction rate increases as the concentration of propranolol increases. The conversion rate of the substrate increased from 38% to 82% after 140 h by increasing the concentration of the substrate from 8 mM to 28 mM. The almost linear dependence of the reaction rate on the propranolol concentration suggests that CalB has not a very high affinity for this substrate. The same behavior has previously been observed in the acetylation of propranolol and atenolol (a similar compound) catalyzed by immobilized derivatives of CalB [13,24]. It is also observed that the competitive effect of both the hydrolysis and alcoholysis of vinyl acetate decreases as the concentration of propranolol is increased. The hydrolysis and alcoholysis of vinyl acetate are 2.6 and 4.4 times faster than the acetylation reaction, respectively, when 8mM of propranolol is used. With 28 mM of propranolol the alcoholysis of vinyl acetate is 1.2 times faster than the propranolol acetylation and the hydrolysis of vinyl acetate is not detected.

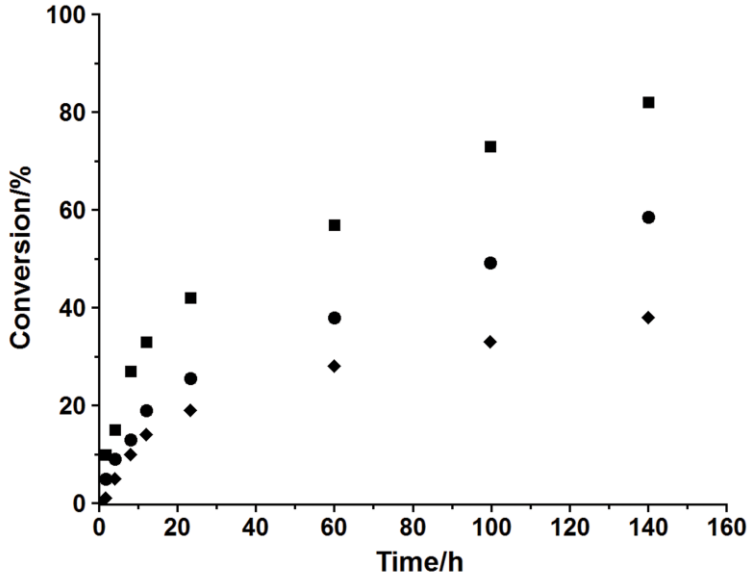

Fig. 13 Effect of the propranolol concentration on the rate of the CalB-catalyzed acetylation of (*R*,*S*)-propranolol. The biocatalyst was CalB-II. Experiments were performed as described in the section **2.2.5**. (*R*,*S*)-propranolol: (♦) 8 mM (●) 18 mM (■) 28 mM.

Because a reasonable conversion rate was obtained using 28 mM propranolol, the reaction was carried out under the same reaction conditions with the enzyme preparation CalB-I as biocatalyst. As it was

found previously, the reaction occurred faster with CalB-II (**Fig. 14**). The chemoselectivity of the reaction was then determined in the conversion range 21-82 %. Interestingly, as shown in **Table 2**, with all enzyme preparations of CalB the *O*-acetylated product is formed exclusively, even at high conversion of the substrate. This suggests the same acylation mechanism for both propranolol enantiomers.

The chemoselectivity of the CalB-catalyzed acetylation of propranolol mainly depends on the ability of the nucleophilic groups of propranolol to be transformed to the corresponding product in the active site of CalB. This suggests that the structure of the substrate is a determining factor for the chemoselectivity of CalB and not only the nucleophilicity of the hydroxyl and amino groups of propranolol. This conclusion is in agreement with the experimental results of this study and with recent results of Le Joubioux et al., who found that the chemoselectivity of the CalB catalyzed acylation of amino-alcohols depends on the structure of the substrate [103].

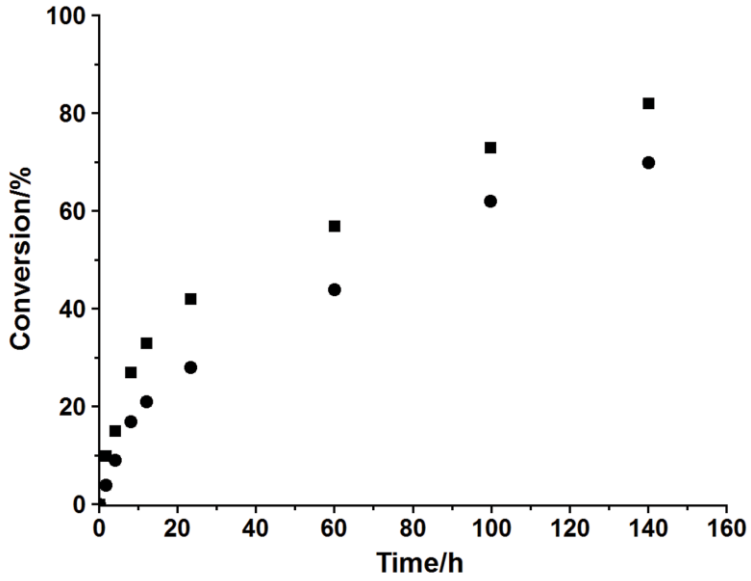

Fig. 14 Effect of the enzyme purification procedure on the rate of the CalB-catalyzed acetylation of (*R*,*S*)-propranolol. Experiments were performed as described in the section **2.2.5** using 28 mM of (*R*,*S*)-propranolol. Biocatalyst: (■) CalB-II (●) CalB-I.

The enantioselectivities of CalB-I and CalB-II were also investigated. The *E* values are 63 and 61, respectively, and the same enantiopreference in favor of the transformation of the *R*-propranolol (**Table 2**). The *E* values obtained for CalB-I and CalB-II are quite similar, which means that the presence of

Triton X-100 during the purification procedure did not affect significantly the enantioselectivity of CalB. These *E* values are also similar (although slightly higher) to those obtained with immobilized CalB on Eupergit C (*E*=57) [13].

Thus the reaction conditions affect mainly the reaction rate of the acetylation of propranolol and of the competing alcoholysis and hydrolysis of vinyl acetate, and not the chemo- and enantioselectivity of the reaction.

2.4. Conclusions

The chemo- and enantioselectivity of the *Candida antarctica* lipase B (CalB)-catalyzed acetylation of (*R,S*)-propranolol using vinyl acetate as acyl donor and a mixture of toluene/methanol as solvent were studied. A competing hydrolysis and alcoholysis of vinyl acetate occurred in addition to the acetylation of propranolol. However, these reactions could be controlled by increasing the propranolol concentration, allowing suppress completely the hydrolysis and the alcoholysis of vinyl acetate to the extent that it was only 1.2 times faster than the acetylation of propranolol. The reaction conditions affected mainly the acetylation reaction rate but not the chemo- and enantioselectivity. Exclusive formation of the *O*-acetyl-propranolol was observed under all reaction conditions. CalB was also found to be enantioselective (*E* = 61-63) favoring the transformation of *R*-propranolol.

Chapter 3. Computational insights into the chemoselectivity of the CalB-catalyzed acetylation of (*R,S*)-propranolol

3.1. Overview

The chemoselectivity of the acetylation of (*R,S*)-propranolol catalyzed by CalB originates from the deacylation step of the reaction. In the latter the acetylated CalB (AcCalB) reacts with the propranolol forming a non-covalent AcCalB-propranolol complex (Michaelis complex; MCC) which undergoes acyl cleavage to give the acetylated product complex (PDC) via the second tetrahedral intermediate (TI-2) **(Fig. 15).** To gain a deeper understanding of the experimentally observed chemoselectivity (section **2.3.2**), molecular modeling was used to study the formation of productive Michaelis complexes between AcCalB and propranolol, using a combined molecular docking and molecular dynamics procedure. This allowed testing the accessibility of the nucleophilic groups of propranolol in the CalB-catalyzed acetylation reaction. Only for the *O*-acetylation binding modes of the substrate leading to the formation of the product were found, which explains the exclusive chemoselectivity of CalB in favor of the formation of *O*-AP observed in experiments.

This study involved the following stages: preparation of the starting structures corresponding to the protein and the substrate (*R* or *S*-propranolol), modeling of the acetylated CalB (the docking target), docking of both enantiomers of propranolol, optimization and structural analysis of the poses with highest interaction free energy from the docking procedure, and finally 100 ps of molecular dynamics simulations to check the reliability of the final models.

3.2. Methodology

3.2.1. Preparation of the acetylated CalB (AcCalB) structure

The initial coordinates of CalB were taken from the crystal structure with entry number 1TCA in the Protein Data Bank [136]. This structure contains two units of *N*-acetyl-glucosamine (NAG) which are

far from the active site and are not expected to have any influence on the selectivity. Therefore these NAGs were removed. The PDB2PQR software package was used to add the missing hydrogen atoms, check the CalB structure together with its crystal waters by PROPKA in order to generate proposals for protonation states of amino acid side chains, and to correct flipped side chains of asparagine, histidine or glutamine residues [152–156]. All proposed protonation states and the side chains of asparagine, histidine or glutamine residues were rechecked for plausibility. Based on this procedure no flips of any residue were applied and all the polar and potentially charged amino acids were used in their ionized form, except Asp-134 which was protonated.

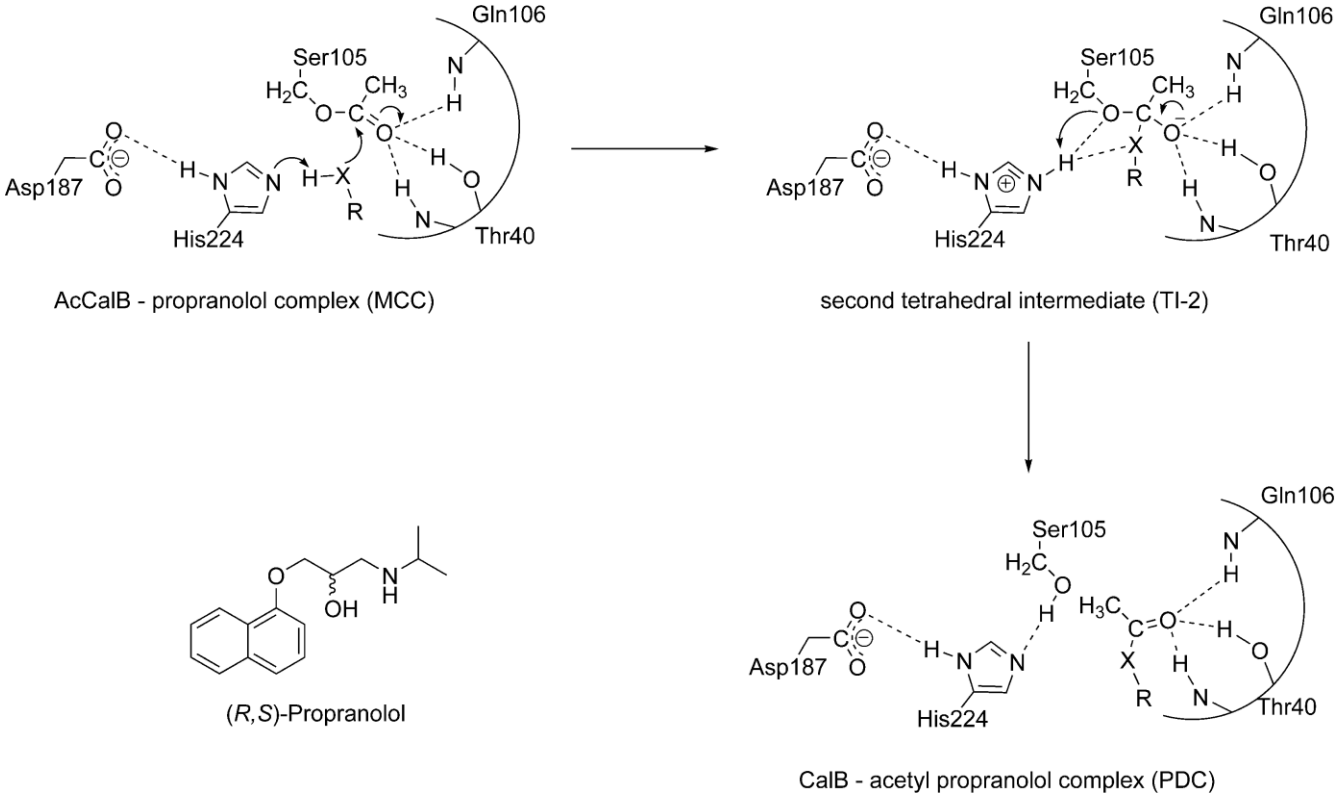

Fig. 15 Deacylation step in the CalB-catalyzed acetylation of (*R*,*S*)-propranolol (X = N or O, according to the nucleophile groups of propranolol –down to the left-). This reaction step occurs sequentially via an initial noncovalent acetyl-CalB (AcCalB) substrate complex (Michaelis complex; MCC) and the second tetrahedral intermediate (TI-2), to give a noncovalent CalB-product complex (PDC).

Once the structure of CalB was protonated, the hydroxyl group of the Ser105 side chain was replaced by acetate in order to mimic the acylenzyme complex, and the new residue corresponding to the acetylated catalytic serine was labeled SEA. The acetate oxygen was placed in three different conformations in the oxyanion hole, ensuring that it can form hydrogen bonds with the residues of the

oxyanion hole, and mimicking the oxyanion orientation in the second tetrahedral intermediate. The structures obtained for the acylenzyme were named ACE01, ACE02 and ACE03 according to the order in which they were created. Each of the three structures was then saved and transferred to the CHARMM program [157] (version 35b5) to be used as initial structures for a first series of MD simulations in explicit toluene molecules. The CHARMM22 force field was used [158,159]. CHARMM force field parameters for the acetylated serine (SEA) were adopted from serine and methyl acetate.

3.2.1.1. MD setup

First, the positions of all hydrogen atoms in the acylenzyme were optimized performing 500 steps of a steepest descent (SD) energy minimization, keeping all other atom coordinates fixed. In this and all subsequent steps all distances involving hydrogen atoms were constrained by SHAKE [160]. On the other hand, the nonbonded interactions were treated using group-based extended electrostatics [161]. In this approach, the electrostatic interactions between particles closer than a cutoff distance (14 Å in this study) are treated by the conventional pairwise additive scheme, while the interactions at larger distance are approximated by a computationally cheaper multipole approach. Then a sphere of 40 Å radius containing 4454 toluene molecules cut out from an equilibrated simulation of toluene under periodic boundary conditions was superimposed on the enzymatic system, centered at the alpha carbon of the acetylated serine (SEA:CA). All added toluene molecules whose non-hydrogen atoms were within 2.8 Å of any existing non-hydrogen atom were deleted. This solvent sphere covered the entire enzyme (**Fig. 16**). An active region including all residues within 30 Å of the SEA:CA atom was defined. All atoms of protein residues outside this active region were kept fixed during the MD simulations. Furthermore, to keep the shape of the solvent spherical and to prevent evaporation of solvent molecules in the MD simulations, toluene molecules and crystal waters were restrained by a quartic spherical boundary potential which is zero until 38.5 Å, has a shallow minimum of -0.25 kcal/mol at 39.5 Å and increases at larger distances. This was done by using the parameters FORCE = 0.2, P1 = 2.25, and DROFF = 38.5. Thereafter the toluene molecules within the sphere and the crystal waters were geometry-optimized, performing first 250 steps of steepest descent (SD) followed by 250 steps of adapted-basis Newton–Raphson minimization (ABNR), keeping all other atoms fixed. Two more minimizations of 250 steps each (SD and ABNR) were performed, optimizing the active region with the water and toluene molecules, adding a restraint of k = 30 mol/Å^2 on the active region. Then a heating molecular dynamics simulation (15000 steps) was performed starting at 50 K and ending at 300 K, raising the temperature in steps of 10 K every 100 MD steps. The Verlet

algorithm was used with a time step of 1 fs. This solvation procedure was repeated 12 times, and in the last two cycles the number of steps used in the dynamics was increased to 30000. Resolvation is necessary since volume contraction of the solvent results from the enhanced interaction and relaxation of toluene on the enzyme surface. During the solvation procedure, harmonic positional restraints were applied to the protein atoms in the active region, which were successively lowered in each of the iterations. Finally, all the constraints were removed and a production molecular dynamics simulation of 2 ns was run to complete the preparation of the acylenzyme. Again, the temperature was raised from 50 K to 300 K in steps of 10 K every 100 MD steps. The system was equilibrated after 10 ps, so the remaining 1990 ps were used for analyses. Information about the different solvation cycles is given in **Appendix B**.

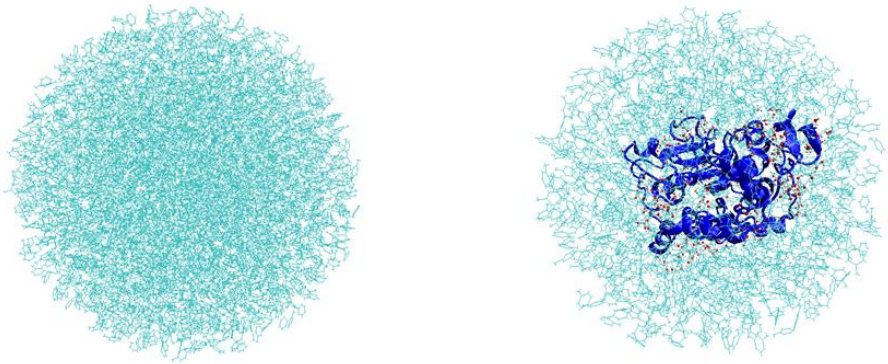

Fig. 16 Sphere of equilibrated toluene molecules (left) and a representative snapshot of the solvated system taken from the MD simulations (right).

3.2.2. Molecular modeling of the Michaelis complexes of acetyl-CalB propranolol

To build the Michaelis complexes (MCCs), *R* and *S*-propranolol were non-covalently docked against each acetyl-CalB structure using the Autodock Vina software [162,163]. The protein was treated as a rigid receptor and seven water molecules (HOH130, HOH136, HOH149, HOH219, HOH238, HOH265, HOH285) were removed from the binding pocket to accommodate the substrate, following similar studies on lipase-catalyzed reactions [39,126]. Different searches using cubic grid boxes of different size (20 Å, 30 Å and 40 Å) centered at SEA:CA were done with each enantiomer, and the exhaustiveness parameter of the search was set to 20. This approach allowed exploring different orientations of these substrates within the binding pocket of CalB. The best complexes were chosen on the basis of the binding affinity as well as on the basis of geometrical criteria, namely the distance of the amine and hydroxyl groups of propranolol from the acetylated serine. These complexes were optimized and further analyzed (see below).

As the applied docking procedure treats the protein as a rigid body, the acetyl enzyme–substrate complexes selected were submitted to a careful post-docking optimization, in order to take into account a potential induced fit effect (little displacements in the protein structure due to the presence of the ligand) [164]. Because there are no CHARMM force field parameters for propranolol, a QM/MM approach was used. The QM region corresponding to *R* or *S*-propranolol was treated by the self-consistent charge-density functional tight binding (SCC-DFTB) method [165] and the MM region (acetylated CalB and crystal waters) by CHARMM. Three consecutive energy minimizations were performed using a similar procedure as De Oliveira et al. [166] but with some modifications, by using the steepest descent (SD) and adapted-basis Newton–Raphson (ABNR) algorithms: (1) a fixed constraint was applied to the protein backbone and all remaining parts of the systems were tethered with a harmonic restraint ($k = 30$ mol/Å^2) in 100 steps of a steepest-decent minimization; (2) the protein backbone was kept fixed, the side chains and crystal waters were kept tethered and the docked ligand was free to move in 800 steps of a steepest decent minimization followed by 550 steps of an ABNR minimization; (3) only the backbone was kept fixed, with the rest of the system free to move in two minimizations of 2500 steps each (SD and ABNR).

From the post-docking QM/MM optimization procedure possible productive binding modes (binding modes of the substrate which lead to formation of the product) for *R* and *S*-propranolol were identified. These complexes were then submitted to 100 ps of QM(SCC-DFTB)/MM MD simulation in explicit toluene in order to evaluate their dynamic behaviour. The QM region corresponded to *R* or *S*-propranolol and the MM region to acetylated CalB, crystal waters and toluene. The same MD procedure as for acetyl-CalB was used, treating the substrate as part of the active region.

The results of all MD simulations were analyzed using the program VMD [167].

3.3. Results and discussion

3.3.1. The acetyl-CalB (AcCalB) complex

MD simulations of the AcCalB complex were performed in presence of explicit toluene molecules. Three possible orientations of the acetyl group were tested, which were named as ACE01, ACE02 and ACE03. The most predominant orientation of the acetyl group in each MD simulation is shown in **Fig. 17**. It was found that the acetyl-CalB structure is well conserved after the MD simulations. The root

mean square deviation (RMSD) to the initial structure by superimposition of all the heavy atoms of the protein backbone increased gradually during the first 10 ps in each simulation due to the increasing temperature. After this equilibration phase the RMSD was in the range from 0.24 Å to 0.29 Å and each AcCalB complex was in equilibrium without any significant conformational change (**Fig. 18**). The size of the RMSD value shows that CalB has a reduced flexibility in toluene and conserves its structure close to the crystal structure (**Fig. 19**). As a measure of the flexibility of CalB the root mean square fluctuation (RMSF) averaged over all the residues and the total B-factor (sum of B-factors per residue) were also calculated over the last nanosecond of the MD simulation. The RMSF average value was 0.21, 0.19 and 0.18 Å for ACE01, ACE02 and ACE03, respectively, which is in agreement with a low flexibility of CalB. The total B-factor was 2534, 2555 and 2548 $Å^2$ for ACE01, ACE02 and ACE03, respectively, which also indicated a reduced flexibility of the protein as the total B-factor for CalB in water is 5267 $Å^2$ [168].

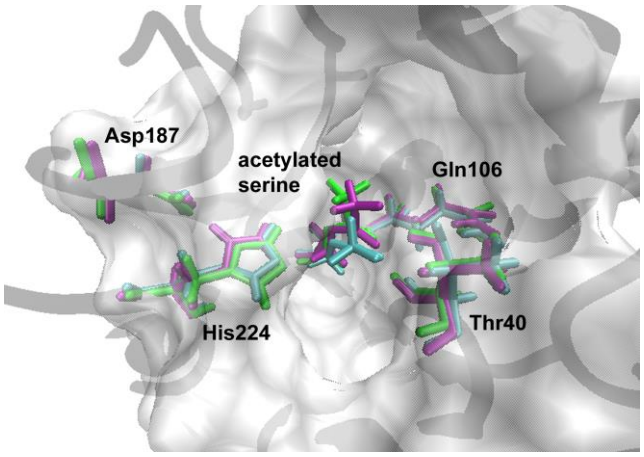

Fig. 17 Predominant orientation of the acetyl group of the acetylated catalytic serine into the binding pocket of CalB in each MD simulation: ACE01 (violet), ACE02 (cyan), ACE03 (green). The catalytic triad and the oxyanion hole are shown in licorice representation. The entrance to the binding pocket of CalB is represented as grey surface.

Essential hydrogen bonds in the AcCalB complex which are important for the catalytic activity were also studied. As shown in **Table 3**, the hydrogen bonds between the side chains of the residues Asp187 and His224 have an average distance of 1.91 Å, 1.90 Å and 1.96 Å, for ACE01, ACE02 and ACE03, respectively. This interaction increases the basicity of the catalytic histidine in the acetyl-enzyme complex, such that proton abstraction from a nucleophile becomes likely, facilitating the nucleophilic attack on the carbonyl group of the acetylated serine. On the other hand, the hydrogen bonds between the carbonyl oxygen atom of the acetylated serine (SEA:O) and the residues of the oxyanion hole

(Thr40 and Gln106) are also important, as they are responsible for the stabilization of the anion intermediate to be formed once the nucleophilic attack occurs. Furthermore, these hydrogen bonds enhance the partial positive charge of the carbonyl carbon atom (SEA:C) enabling the nucleophilic attack. The average distances for these hydrogen bonds are also given in **Table 3**. In case of the configuration ACE02 only two of the three possible hydrogen bonds with the residues of the oxyanion hole were present; the average distance between the SEA:O atom and the side chain of Thr40 (-OH) was 3.25 Å for this configuration. Both hydrogen bonds between the Asp187 and His224 residues, and between the SEA:O atom and the residues of the oxyanion hole were stable throughout the MD simulations (**Fig. 20**).

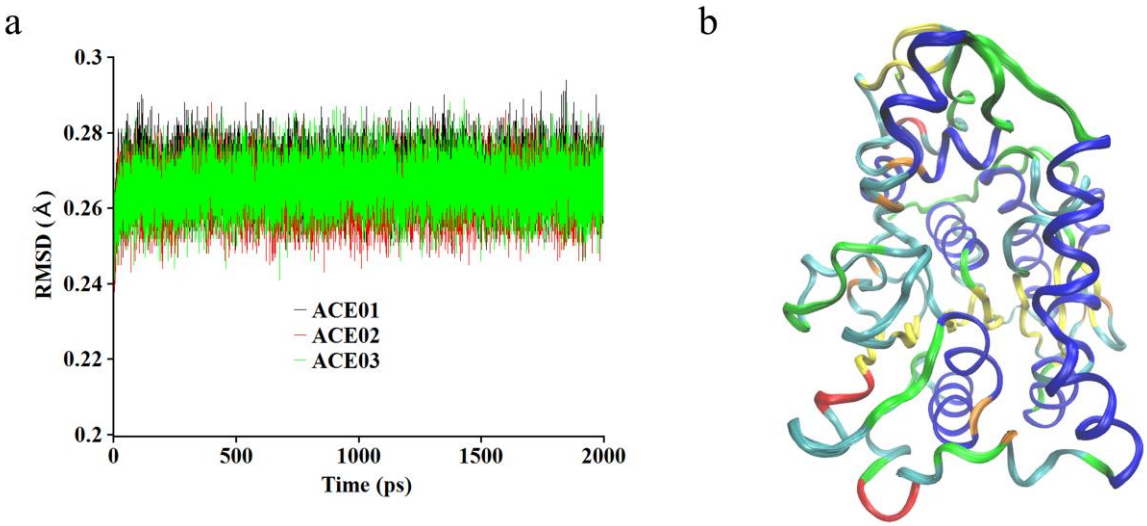

Fig. 18 (a) Root mean square deviation (RMSD) of all heavy atoms of the AcCalB backbone from the X-ray structure during the 2 ns MD simulation. **(b)** Superimposed AcCalB structures at intervals of 0.1 ns over the last 1 ns of the MD simulation.

Table 3 Essential hydrogen bond distances (in Å) for the catalytic activity of the AcCalB complex averaged over the last nanosecond of the MD simulations[a].

	AcCalB complex		
	ACE01	ACE02	ACE03
Asp187:O_D-His224:H_{ND}	1.91	1.90	1.96
SEA:O-Gln106:NH	2.12	1.91	2.13
SEA:O-Thr40:NH	1.93	1.74	2.09
SEA:O-Thr40:OH	1.98	3.25	1.80

[a] SEA is the acetylated serine of CalB.

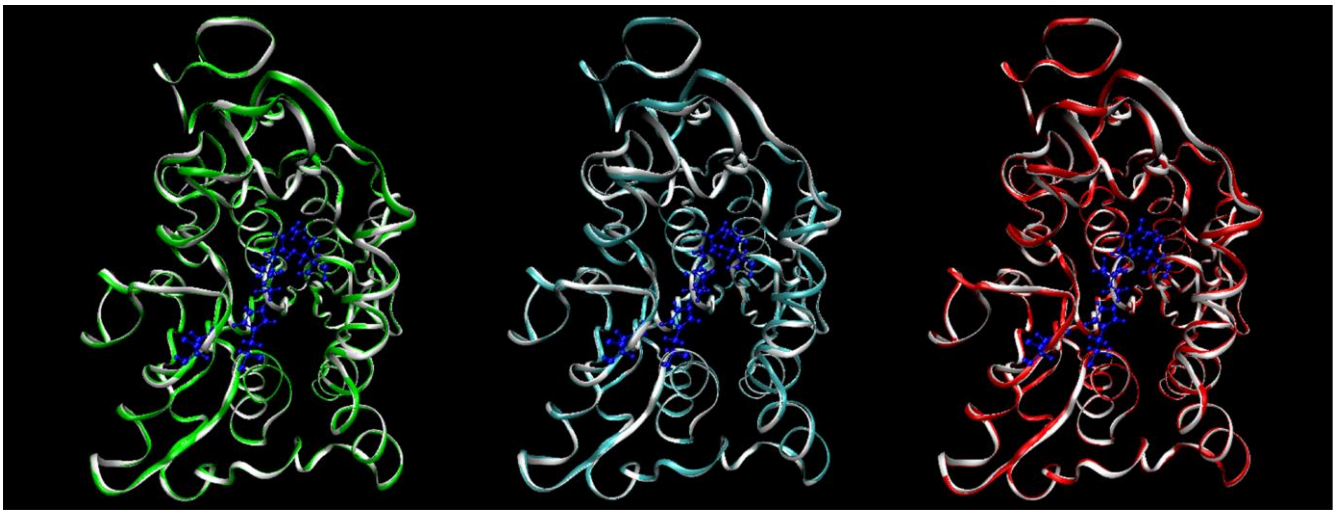

Fig. 19 Crystal structure of CalB (ribbon representation) superimposed with the most predominant acetyl-CalB structures during the MD simulations: ACE01 (green), ACE02 (cyan) and ACE03 (red). The catalytic triad is shown in blue. Only in some loops minimal distortions were found after the MD simulations.

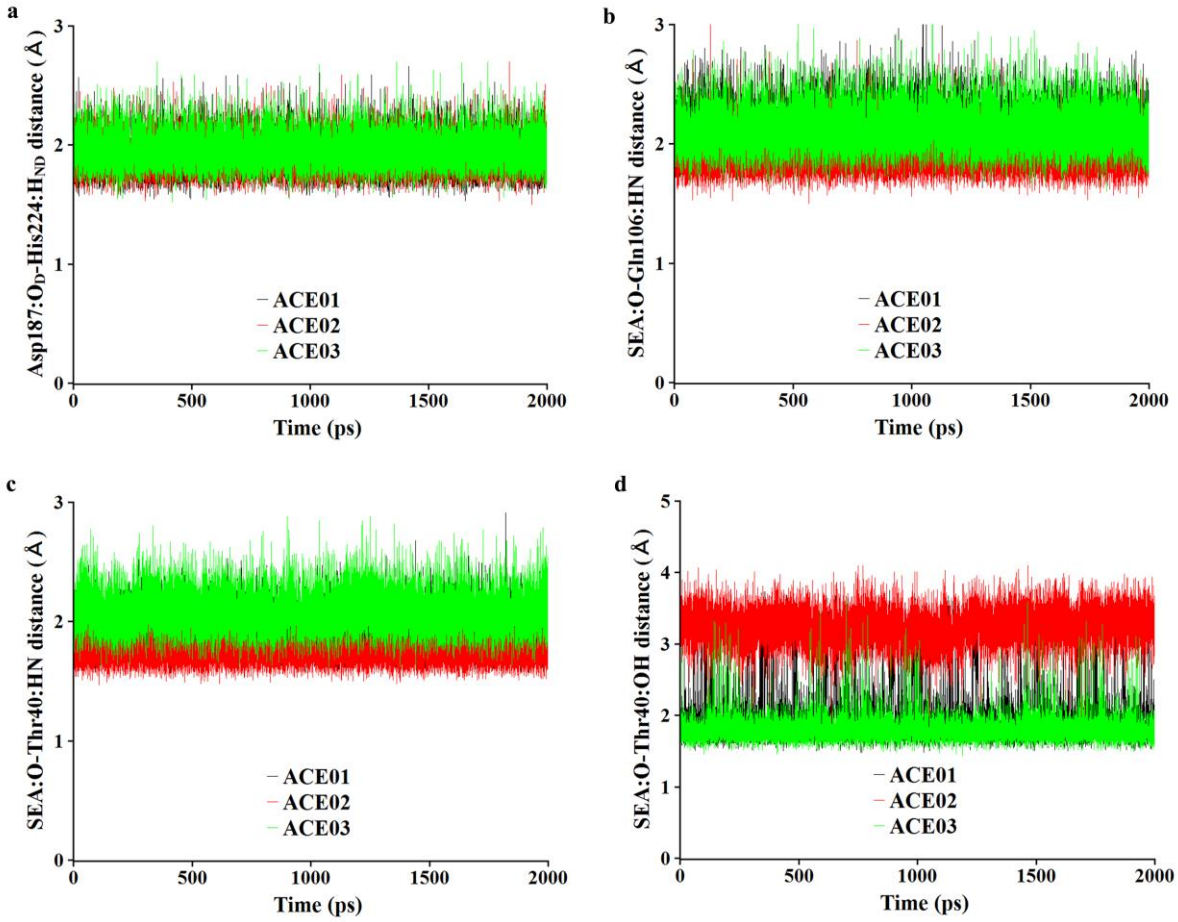

Fig. 20 Time evolution of the essential hydrogen bonds for the catalytic activity of the AcCalB complexes in the MD simulations: **(a)** Hydrogen bond between the catalytic aspartate and histidine residues **(b-d)** Hydrogen bonds between the acetate oxygen of the acetylated serine and the residues of the oxyanion hole.

According to the information given above, in the three structures obtained for the AcCalB complex the catalytic triad is stable and well conserved after the MD simulations. Therefore these structures are reactive. Thus it was decided to use all of them as targets for the docking of *R*- and *S*-propranolol.

3.3.2. AcCalB-propranolol complexes

A total number of 163 (*R*-propranolol) and 149 (*S*-propranolol) complexes met the conditions described for the docking procedure (section **3.2.2**). These complexes could be grouped according to two binding modes, which are referred here as binding modes I and II. In binding mode I the naphthoxy side chain of propranolol is located in the large hydrophobic pocket of CalB. The isopropylamine side chain is in the medium pocket and part of it may extend toward the entrance of the pocket (i.e. toward the solvent). In binding mode II the orientation of propranolol is reversed (**Fig. 21**). The binding free energies of both enantiomers are similar and in the range from -4.7 to -7.1 kcal/mol. In case of *R*-propranolol the complexes present a binding free energy between -4.9 and -7.0 kcal/mol, and those of *S*-propranolol between -4.7 to -7.1 kcal/mol. These values are in good agreement with the expected low affinity of CalB for propranolol according to the reaction rates observed in the experiments (section **2.3.2**).

According to the general mechanism of lipase catalyzed acylations, for *N*- or *O*-acetylation of propranolol, the amino or hydroxyl group of propranolol has to be positioned simultaneously close to the His224: Nε and SEA:C atoms of AcCalB, respectively. Only complexes satisfying this criterion for the hydroxyl group were found, which gives an explanation for the exclusive formation of *O*-acetyl-propranolol observed in the experiments. This can be understood taking into account that a proper position of the amino group in order to be acetylated by any of the AcCalB complexes requires that a large side chain with a naphthyl group is positioned in the binding pocket of CalB without unfavorable steric contacts. In contrast to this, in case of the acetylation of the hydroxyl group, two side chains of medium size have to be positioned in the binding pocket, resulting in more favorable structures. This also explains why complexes in which the amino group of propranolol is able to be acetylated by AcCalB via the mechanism proposed by Le Joubioux et al. [111] (see section **1.4.1**) were not found.

In the next step only complexes with a binding affinity stronger than -5.5 kcal/mol were considered and those in which the reaction could take place easily according to the proximity of the atoms involved in the reaction were selected for optimization. A total number of 12 and 7 complexes were selected for the

R- and *S*-enantiomer, respectively. These complexes are representative for the two binding modes found for *R*- and *S*-propranolol. The reader is referred to **Appendix B** for details about these complexes. Once the complexes were optimized, they were analyzed to determine if they correspond to productive binding modes according to three criteria used in previous studies dealing with molecular modeling of lipase-catalyzed reactions: (a) protein distortion (b) conservation of the hydrogen bond interactions between the acetate oxygen of SEA and the residues of the oxyanion hole (c) a short distance of the nucleophile groups of propranolol to the His224:Nε and SEA:C atoms [166,169,170].

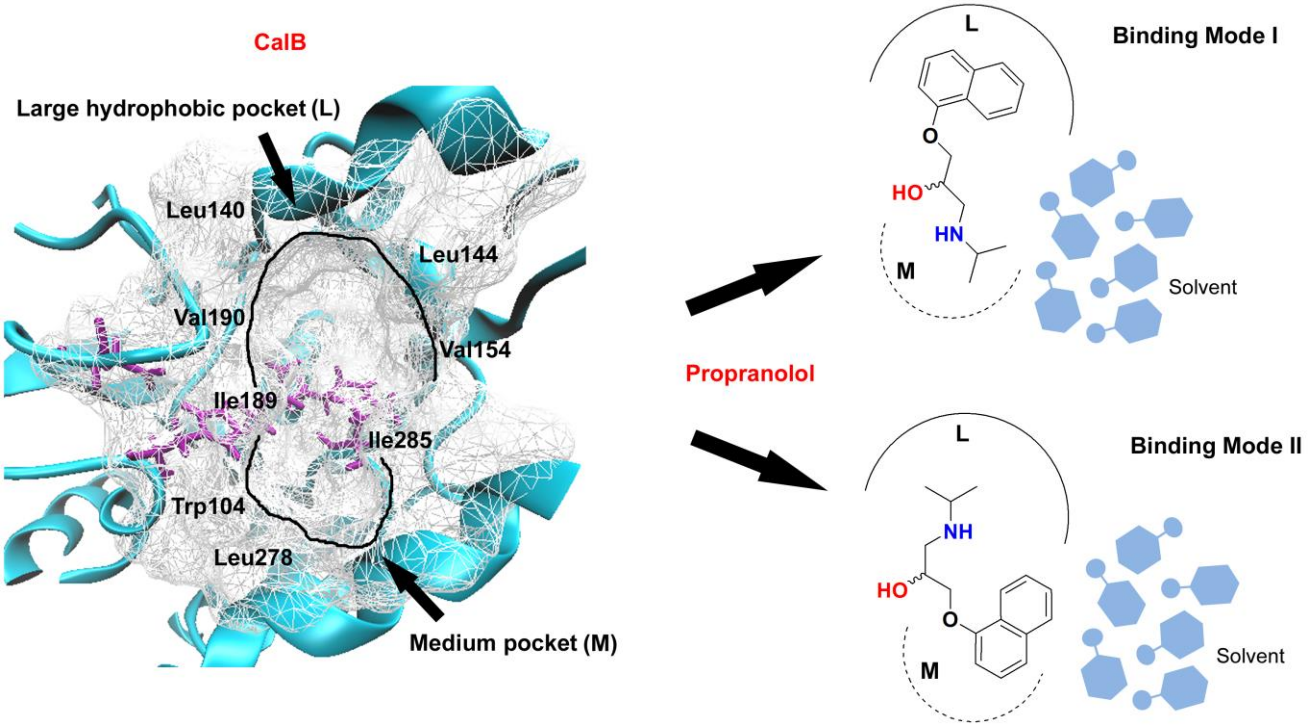

Fig. 21 Schematic view of the binding modes of propranolol in the CalB binding pocket. The structure of acetyl-CalB (AcCalB) is shown on the left with the catalytic triad Asp-His-Ser oriented from left to right. In binding mode I (up to the right) the naphthoxy side chain of propranolol lies in the large hydrophobic pocket of CalB while its isopropylamine side chain in the medium pocket and may extends to toward the entrance of the binding pocket. Conversely, in binding mode II (down to the right) the former lies in the medium pocket and the latter in the large pocket.

Although some conformational rearrangements of the protein could improve the binding affinity, a high distortion of the CalB structure would result in a loss of activity if some essential residues for the catalytic activity such as the residues of the oxyanion hole are disturbed. Therefore the RMSD value between the initial CalB crystal structure and the final optimized complex must be small. Vallikivi et al. [170] found that in case of complexes between AcCalB and prostaglandins, RMSD

values higher than 3.0 Å were experimentally well correlated with non-productive complexes. Therefore this RMSD value was chosen as a limit. This RMSD value has also been successfully used as a limit in other studies on lipase-catalyzed reactions [166,169]. In this work, the superimposition of all heavy atoms of the protein in the optimized AcCalB-propranolol complexes to the CalB crystal structure resulted in RMSD values of only about 0.55 Å, even though the side chains were finally free to move.

To facilitate the acetylation reaction it is necessary that the AcCalB-propranolol complexes form hydrogen bonds with amino acids of the oxyanion hole, namely with the backbone (–NH) of the residues Thr40 and Gln106 and the side chain (–OH) of Thr40. A complex was considered as productive if at least two of these three hydrogen bonds are conserved after the post-docking optimization. Hydrogen bond distances and angles involving the substrate in the optimized complexes are given in **Appendix B** (**Table 27**).

Finally, the third condition for considering a complex as productive is the proximity of the hydroxyl or amino group of propranolol to the catalytic residues. As mentioned above, any of these groups has to be positioned simultaneously close to the His224:Nε and SEA:C atoms. The proton transfer to the catalytic histidine enhances the nucleophilicity of the amino or hydroxyl group attacking the SEA:C atom. It was decided to use a maximal value of 4 Å for these distances, following other authors studying lipase-catalyzed acetylation reactions [166,169,171]. The distances involved in the nucleophilic attack corresponding to each complex after optimization are given in **Appendix B** (**Table 28**).

All complexes selected from the docking procedure satisfy the first two criteria after optimization. However, not all of them satisfy the third criterion. The best complexes obtained for *R*- and *S*-propranolol after the post-docking optimization (according to whether the nucleophile groups of propranolol have distances and angles suitable for the nucleophilic attack) are shown in **Fig. 22**. All of these complexes correspond to possible productive complexes for the *O*-acetylation of propranolol.

3.3.2.1. Productive complexes between R-propranolol and AcCalB

Three complexes were retained for *R*-propranolol after optimization, namely ORI, ORIV and ORIX (**Fig. 22**). In ORI and ORIX the substrate is oriented in binding mode I. In these complexes the naphthyl group of propranolol is positioned in the same plane, but pointing toward the exterior of the

binding pocket in ORI and toward the interior of it in ORIX. The isopropylamine group is oriented toward the exterior of the binding pocket in both ORI and ORIX. In the complex ORIV the substrate is positioned in binding mode II, with the naphthyl group pointing to the exterior of the binding pocket and the isopropylamine group toward the interior of it.

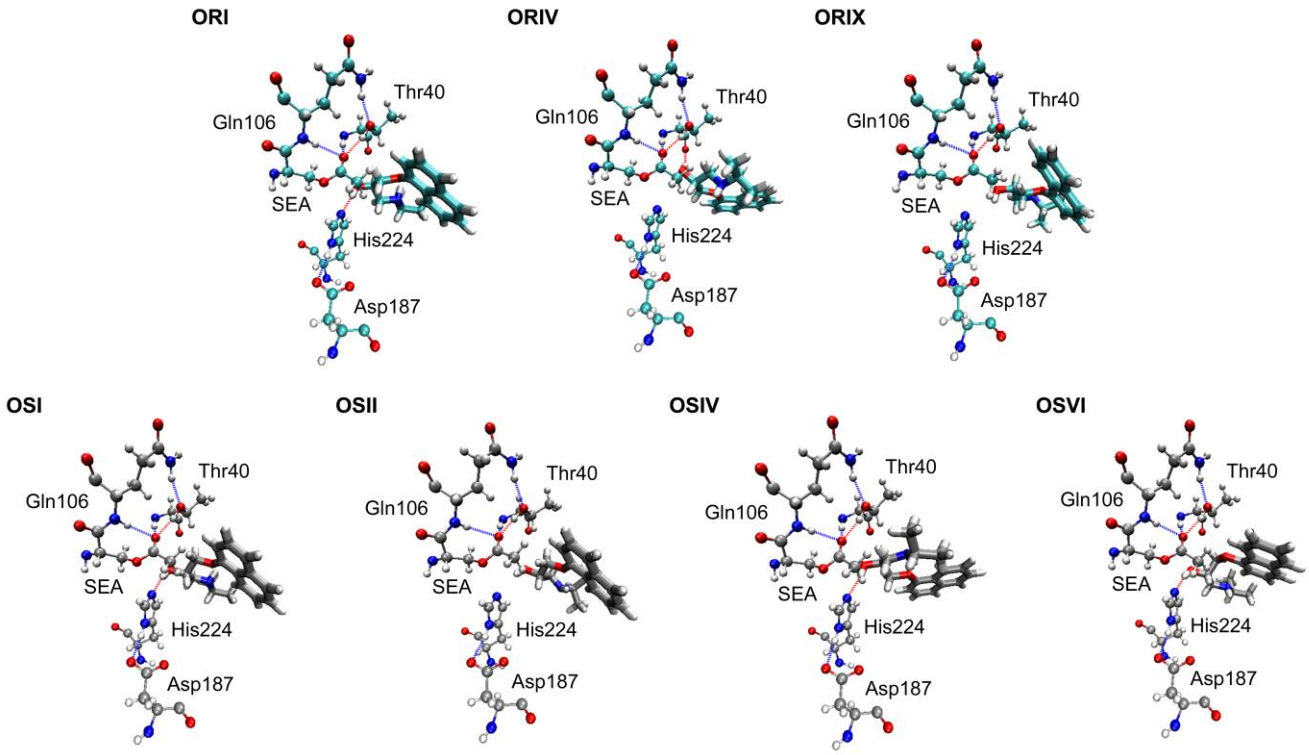

Fig. 22 Top view of the best complexes obtained for *R*-propranolol (ORI, ORIV and ORIX) and *S*-propranolol (OSI, OSII, OSIV and OSVI) after optimization. The catalytic triad and the oxyanion hole are shown in CPK representation. The substrate is shown in licorice representation. Hydrogen bonds are shown as blue and red dashed lines, indicating whether the proton donor is a nitrogen or oxygen atom, respectively.

The relevant interatomic distances corresponding to these complexes, including those used as criteria to consider a complex as productive, are given in **Table 4**. ORI is the only complex which satisfies the distance criteria to react, as the hydroxyl group of propranolol is positioned simultaneously at 3.99 Å from SEA:C and 1.98 Å from His224:Nε. Furthermore, the angle for the nucleophilic attack is 98°, which is just slightly smaller than the ideal angle (107°) for a nucleophilic addition to a carbonyl group as described by Burgi et al. [172]. Thus, ORI may be considered as a productive complex leading to formation of the *O*-acetylated product. In contrast, the *N*-acetylation of propranolol cannot occur via ORI as the amino group of propranolol is positioned at a distance larger than 4 Å from the catalytic residues.

Table 4 Relevant interatomic distances, bond lengths and angles corresponding to the best AcCalB-propranolol complexes after optimization[a].

Distance (Å)	*R*-propranolol			*S*-propranolol			
	ORI	ORIV	ORIX	OSI	OSII	OSIV	OSVI
His224:Nε-Sub:**H**	1.98 (173)	4.78	3.18 (135)	1.96 (169)	2.78 (162)	2.09 (167)	1.92 (170)
SEA:C-Sub:**O**	3.99 (98)	3.50 (120)	4.65 (108)	3.90 (101)	4.67 (102)	3.68 (105)	4.03 (99)
His224:Nε-Sub:*H*	5.89	4.71	7.85	6.20	5.83	5.66	5.14
SEA:C-Sub:*N*	6.59	4.88	7.90	6.73	7.33	4.87	6.73
Asp187:O_D-His224:H_{ND}	1.87 (168)	1.78 (171)	1.88 (165)	1.85 (168)	1.93 (164)	1.89 (168)	1.83 (166)
SEA:O-Gln106:NH	2.09 (149)	2.03 (151)	2.31 (138)	2.11 (152)	2.29 (137)	2.08 (147)	2.15 (152)
SEA:O-Thr40:NH	2.05 (161)	1.97 (160)	1.86 (165)	1.96 (162)	1.90 (164)	2.12 (160)	1.96 (163)
SEA:O-Thr40:OH	1.86 (169)	1.83 (167)	1.66 (172)	1.85 (169)	1.65 (173)	1.89 (166)	1.87 (166)
Gln106:H2N-Thr40:Oγ	1.98 (165)	1.99 (165)	2.04 (159)	1.98 (165)	2.06 (158)	1.99 (164)	1.98 (165)
Sub:*H*-Sub:O	2.45 (95)	3.10	3.86	2.28 (99)	2.28 (123)	2.01 (133)	3.77
Sub:**H**-Thr40:O	4.44	1.86 (154)	4.52	4.49	4.18	4.33	4.67

[a] The atoms corresponding to the hydroxyl and amino group of the substrate (Sub) are marked in bold and italic respectively. The Oxygen of the naphthoxy group of propranolol is indicated as Sub:O. Angles in degrees for both the corresponding hydrogen bonds and the nucleophilic attack (Sub:**O**···SEA:C=O) are given in brackets. SEA is the acetylated serine of CalB.

In ORIV and ORIX the amino group of propranolol is also positioned far from the catalytic residues, while its hydroxyl group is well positioned. However, these complexes do not satisfy completely the distance criteria to react. In ORIV the oxygen atom of the hydroxyl group of propranolol is positioned to a distance of 3.50 Å from SEA:C, but the hydrogen atom of the hydroxyl group is forming a hydrogen bond with the backbone of Thr40 (with a distance of 1.86 Å), such that the interaction with the His224:Nε atom is quite weak (4.78. Å). In contrast, in ORIX the hydrogen atom of the hydroxyl group is positioned at a distance of 3.18 Å from the His224:Nε atom, but the distance for the nucleophilic attack is 0.65 Å larger than required, although the angle of attack is 108°, which is very close to the ideal angle.

In all complexes for *R*-propranolol, the naphthyl and isopropylamine side chains of propranolol are stabilized in their positions in the binding pocket by the respective non-polar residues surrounding: Leu140, Ala141, Leu144, Val154, Ile189, Ile285, Ala281, Ala282, Leu278 and Trp104 (**Fig. 23**). Additionally, in ORI and ORIV there is an intramolecular hydrogen bond between the amino group and the oxygen atom of the naphthoxy group of *R*-propranolol, which also contributes to stabilize these complexes. This hydrogen bond is stronger in case of ORI with a distance of 2.45 Å.

Considering the feasibility of a spontaneous *O*- to *N*-acyl migration, this hydrogen bond as well as the orientation of the amino group of propranolol would be responsible for the chemoselectivity observed in the reaction. In all complexes obtained for *R*-propranolol it is clearly observed that the nitrogen atom of the substrate is not well positioned for a nucleophilic attack at the *O*-acyl group. In addition, in the complexes where the proton of the amino group of propranolol is forming an intramolecular hydrogen bond with the naphthoxy oxygen, such *O*- to *N*-acyl migration is more difficult, as this interaction would avoid the proton transfer from the amino group of propranolol to the carbonyl oxygen.

3.3.2.2. Productive complexes between S-propranolol and AcCalB

Four complexes were retained for *S*-propranolol after optimization, namely OSI, OSII, OSIV and OSVI (**Fig. 22**). The substrate is positioned in binding mode I in OSI, OSII and OSVI. In these complexes the isopropylamine side chain of the substrate is oriented toward the exterior of the binding pocket, while its naphthyl group is oriented pointing toward the exterior of the pocket in OSI and OSII, and toward the pocket in OSVI, but in the same plane. OSI and OSII are very similar; the main difference is the orientation of the isopropylamine group of propranolol in the binding pocket. In the complex OSIV, the

substrate is oriented in binding mode II, with the naphthyl group positioned toward the exterior of the binding pocket and the isopropylamine group toward the interior.

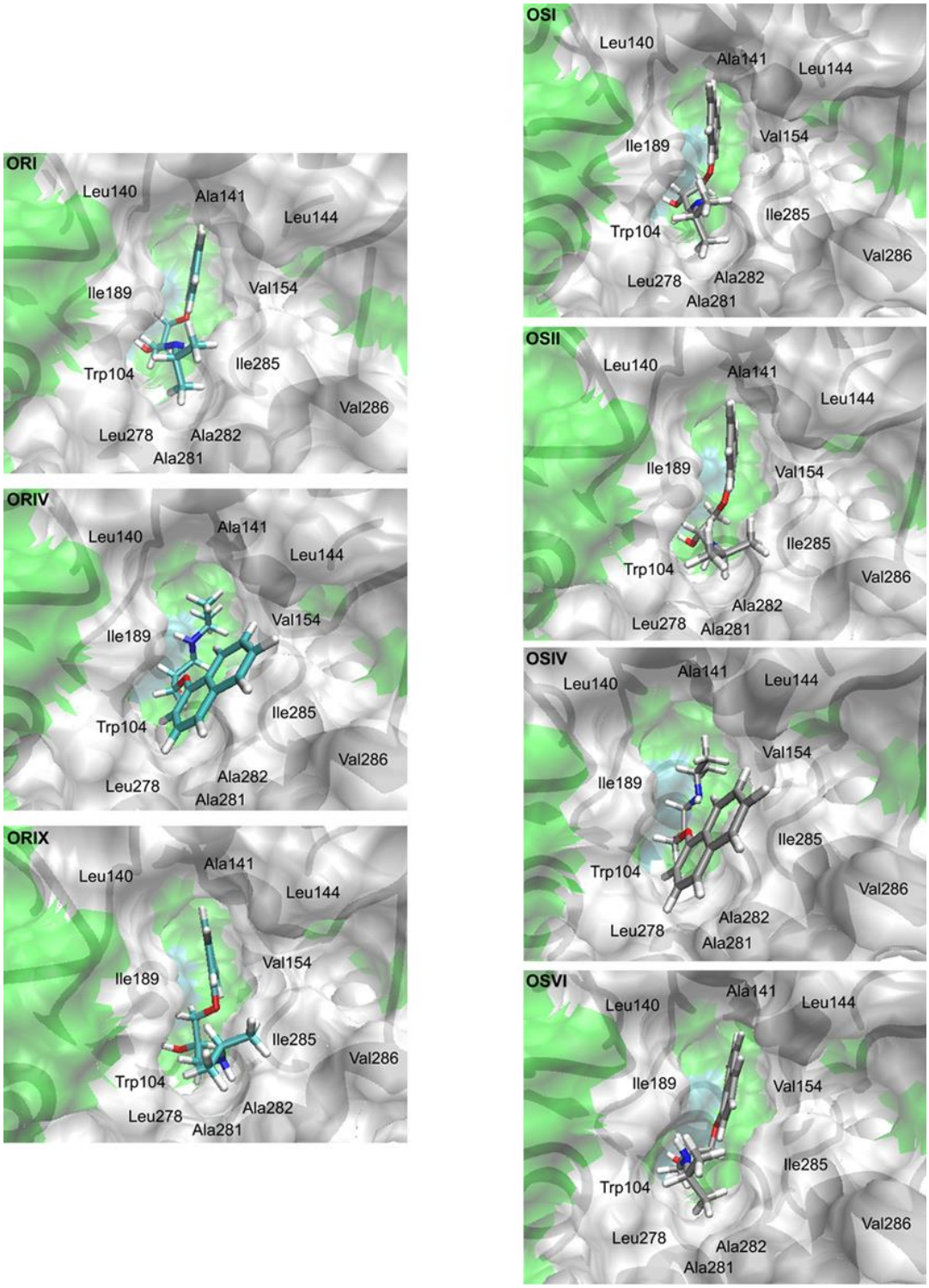

Fig. 23 Surface representation of the CalB binding pocket showing the non-polar residues stabilizing the substrate in the productive complexes of *R*- and *S*-propranolol. Hydrophobic regions of the enzyme pocket are shown in white and polar ones in green. The acetylated serine is shown in cyan.

The relevant interatomic distances involving the *S*-propranolol complexes are also given in **Table 4**. Similar to the *R*-propranolol complexes, the hydroxyl group of propranolol is positioned close to the catalytic residues while its amino group is far from these residues. OSI and OSIV fulfill the distance criteria to react. The hydroxyl group of *S*-propranolol is positioned toward the SEA:C and His224:Nε atoms with distances of less than 4 Å in these complexes. Furthermore the angle of attack is 101° and 105° respectively, which is close to the Burgi angle. Therefore these complexes may be considered as productive complexes for *S*-propranolol.

OSVI and OSII do not fulfill the distance criteria strictly. The hydrogen atom of the hydroxyl group of *S*-propranolol is positioned at a distance less than 4 Å from the His224:Nε atom, but the distance for the nucleophilic attack is 4.03 Å and 4.67 Å for OSVI and OSII, respectively. It can be noted that in case of OSVI this distance is only slightly larger than the threshold. In case of OSII this distance is larger but the angle of attack is 102°, which is close to the ideal angle.

As in the case of *R*-propranolol, in the *S*-propranolol complexes, the naphthyl and isopropylamine groups of propranolol are also stabilized by interactions with non-polar residues of the binding pocket surrounding (**Fig. 23**). Furthermore, the intramolecular hydrogen bond between the amino and naphthoxy groups is also observed in the complexes OSI, OSII and OSIV, and is stronger than in the *R*-propranolol complexes. This hydrogen bond has a distance of 2.28 Å in OSI and OSII, and 2.01 Å in OSIV. Thus, the *S*-propranolol complexes exhibit a similar behavior as the *R*-propranolol complexes. Because *S*-propranolol is the slowly reacting enantiomer, this intramolecular hydrogen bond and the orientation of the amino group of propranolol explains why no *N*-acetylated product resulting from a possible *O*- to *N*-acyl migration was found even at high conversion of the substrate. This corroborates the previous suggestion given in section **2.3.2** that the acylation mechanism is the same for both propranolol enantiomers.

3.3.2.3. MD simulations of the complexes

In order to complement this computational study, 100 ps of molecular dynamics simulations were carried out on the complexes retained after optimization. Essentially the stability of both the hydrogen bond interactions and the position of the hydroxyl group and the dynamic behaviour of the docked substrates were revised. The results showed that the protein did not undergo significant conformational changes; the maximal RMSD values considering all the heavy atoms of the protein backbone were about 1.0-1.2 Å. The visual analysis of trajectories showed that the hydrogen bonds between the

carbonyl oxygen (SEA:O) and the residues of the oxyanion hole (Thr40 and Gln106) were stable during the MD simulations. The stability of the position of the hydroxyl group was evaluated by monitoring the acetylation distances (SEA:C-Sub:O) along the trajectories. The minimal and maximal values for the distance between the hydroxyl oxygen atom of propranolol and the carbonyl carbon of SEA are given in **Table 5**. All complexes were able to form productive complexes during the MD simulation except ORIX. In particular, in the MD simulation of ORIV it was observed that the hydrogen atom of the hydroxyl group of propranolol flips to form a hydrogen bond with the His224:Nε atom without affecting the distance for the nucleophilic attack, leading therefore to a productive complex. A different temporal stability was observed for each complex as revealed by the value of the maximal fluctuation in the acetylation distance. ORI, ORIV, OSIV and OSVI were the most stable complexes. ORIV and OSVI presented the lower maximal fluctuation of this distance, with a value of 3.7 Å and 1.6 Å, respectively. The amino group of propranolol was never found at a distance less than 4 Å from SEA in the MD simulations, which reinforces the previous conclusion about the chemoselectivity of the reaction.

Table 5 Minimal and maximal values of the interatomic distance between the propranolol hydroxyl oxygen and the carbonyl carbon of SEA[a] in the MD simulations of the productive complexes found after the post-docking optimization.

SEA:C-Sub:O Distance (Å)[a]	*R*-propranolol			*S*-propranolol			
	ORI	ORIV	ORIX	OSI	OSII	OSIV	OSVI
Minimum	3.1	2.9	4.2	2.9	3.4	3.3	2.8
Maximum	6.8	7.2	13.5	9.5	6.4	6.5	4.4

[a] SEA is the acetylated serine of CalB.

3.4. Conclusions

Molecular modeling of the Michaelis complexes between propranolol and acetylated CalB (AcCalB) was carried out. Only productive AcCalB-propranolol complexes leading to the formation of *R*- or *S*-*O*-acetyl-propranolol were identified, which is consistent with the experimental results. In these productive complexes, both propranolol enantiomers fit into the CalB binding pocket in two binding modes, with the naphthyl or amino group positioned either at the large or the medium pocket of CalB. Two events were identified as responsible for the observed chemoselectivity of CalB in favor of the

formation of *O*-AP. In the first place the direct acylation of the amino group of *R*- or *S*-propranolol by CalB is not possible, as a proper position of this group for executing the nucleophilic attack at the acetylated catalytic serine involves unfavorable steric contacts with the residues of the binding pocket. Secondly, in the identified productive conformations of *R*- and *S*-propranolol the amino group is not well positioned for a spontaneous *O*- to *N*-acyl migration. In some cases the latter is further avoided by the formation of an intramolecular hydrogen bond between the amino group and the naphthoxy oxygen of propranolol.

Chapter 4. Understanding the enantioselectivity since the first stages of the deacylation reaction: from the MCC to formation of the TI-2

4.1. Overview

In **Chapter 3** molecular modeling of the Michaelis complexes of the deacylation step of the CalB-catalyzed acetylation of propranolol by using a docking protocol was presented. Only AcCalB-propranolol Michaelis complexes leading to the formation of *O*-acetyl-propranolol were identified, which explained the chemoselectivity of the reaction. In these complexes both propranolol enantiomers fit into the CalB binding pocket in two binding modes, with the naphthyl group positioned either at the large or medium pocket of CalB (binding mode I and II, respectively). To check the reliability of the complexes identified by docking, they were subjected to short (100 ps) MD simulations in explicit toluene. Interestingly, a different temporal stability was observed for each complex (see section **3.3.2.3**), which is expected to play an important role for the enantioselectivity of the reaction [112]. With the aim to gain a deeper understanding of the molecular basis for the observed enantioselectivity in favor of the faster formation of *R*-*O*-acetyl-propranolol (section **2.3.2**), a more extensive sampling of the AcCalB-propranolol MCCs was performed. Starting from the optimized MCCs obtained in the previous study by docking (**Fig. 23**), multiple 1.5 ns MD simulations were carried out using different initial velocity distributions in order to improve the sampling of the conformational space [173–175]. The results obtained from these MD simulations are discussed in this chapter.

The analysis of the MD trajectories was focused on the interatomic distances important for the catalytic process (**Fig. 24**), the enzyme-substrate-solvent interactions involved in the binding modes of the substrate, the temporal stability (lifetime) of the productive complexes, and the ability of the propranolol enantiomers to form near attack conformations (NACs). NACs are conformers in which the atoms involved in the bond formation are at van der Waals distance and the angle of approach is ±15º of the angle of the bond formed in the transition state (TS). NACs are turnstiles through which the reactants must pass in order to reach the TS. A higher population of the NACs indicates a lower free energy change required to reach the NACs, thus the population of NACs is indicative of the reaction

rate [38,138,176,177]. Thereby, based on the analysis of the MD trajectories, the reactivities of several conformations of both *R*- and *S*-propranolol were estimated and the enzyme-substrate interactions which are essential for the enantioselectivity were identified.

In addition, quantum chemical (QM) calculations were carried out on small models of the enzyme-substrate complexes in order to assess the reactivity of both enantiomers and to get a first estimation of the energy barriers involved in their transformations.

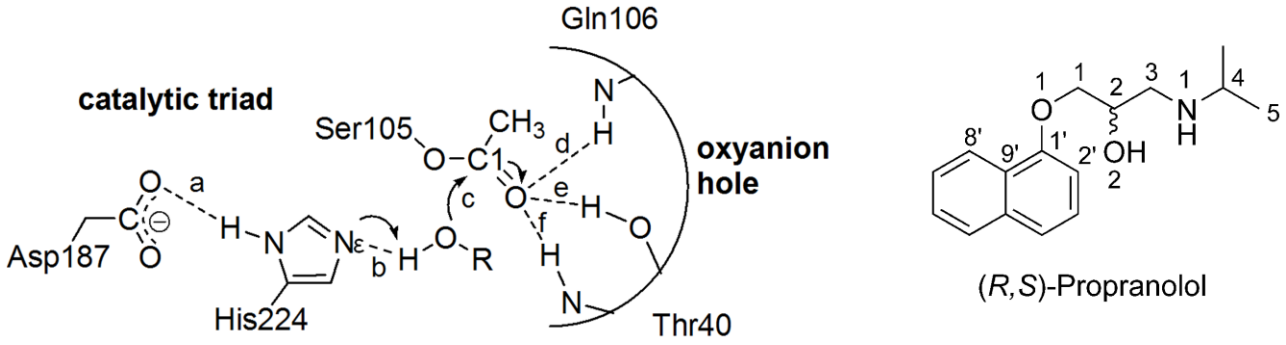

Fig. 24 Michaelis complexes (MCCs) between AcCalB and propranolol in the *O*-acetylation of propranolol catalyzed by CalB. **a-f** are the most important interatomic distances for the catalytic process. The acylated catalytic serine is referred to as SEA. The structure of propranolol with the atom numbering used in this chapter is shown at the right.

4.2. Methodology

4.2.1. MD simulations

In the computational study described in **Chapter 3** three and four possible productive complexes for *R*- and *S*-propranolol were identified, respectively (**Fig. 23)**. For *R*-propranolol, two complexes in binding mode I and one complex in binding mode II were found. These complexes are referred to as R1-R3 in this chapter, respectively. For *S*-propranolol three complexes in binding mode I and one complex in binding mode II were identified. These complexes are referred to as S1-S4 in this chapter, respectively. These optimized complexes were used as starting structures for 1.5 ns MD simulations in explicit toluene. For each complex three MD simulations with different initial velocity distributions were performed, corresponding to values of the random seed parameter iseed of 314159, 835 and 234. The MD simulations carried out using the iseed values 835 and 234 are indicated by * and ** respectively.

The same procedure described in **Chapter 3** (section **3.2.2**) for 100 ps of MD simulation of the MCCs was used.

In these MD simulations the temporal stability of the AcCalB-propranolol complexes and their ability to lead to the formation of the second tetrahedral intermediate (TI-2) and then to acetyl-propranolol were checked (**Fig. 15**). As a measure of the structural stability of the protein, the root mean square deviations (RMSD) with respect to the initial structure were calculated by superimposing all backbone heavy atoms of the protein. As it was done for the analysis of the optimized MCCs in **Chapter 3** (section **3.3.2**), the MD trajectories were analyzed based on four criteria which have been successfully used in previous studies of lipase-catalyzed reactions for characterizing productive binding modes. These criteria are: (a) protein distortion, (b) hydrogen bond interactions between the acetate oxygen of the acetylated catalytic serine (SEA:O) and the residues of the oxyanion hole (distances **d-f** in **Fig. 24**), (c) the distance of the hydroxyl group of propranolol to the His224:Nε and SEA:C1 (carboxylic carbon of the acetylated catalytic serine) atoms (distances **b** and **c** in **Fig. 24**), (d) steric clashes with the enzyme **[37,120,166,169,170]**. Binding modes were considered as productive if all catalytically essential hydrogen bonds were maintained, the substrate avoided steric clashes with the enzyme, and its hydroxyl group was simultaneously positioned close to the catalytic residues His224 and SEA. The results of all MD simulations were analyzed using the program VMD **[167]**.

4.2.2. QM calculations

Quantum chemical calculations based on small model systems of the productive complexes identified for both propranolol enantiomers during the MD simulations were carried out. The aim was to determine whether a bond is formed between the alcohol oxygen of propranolol and the carbonyl carbon atom of the acetate group of the acetylated serine when the alcohol hydrogen is manually bonded to the His224:Nε atom, leading to the formation of the second tetrahedral intermediate (TI-2). These calculations were run with the GAUSSIAN 09 program ***[178]***. A similar procedure to that described by De Oliveira et al. for analysing the reactivity of CalB-flavonoids complexes and to understand the selectivity of CalB catalysing the acetylation reaction of these substrates was used [32]. The QM models of the AcCalB-propranolol complexes were constituted by the substrate (*R*- or *S*-propranolol), the side chain carboxylate of Asp187, the imidazole ring of His224, the backbone –NH of Gln106, and the backbone and side chains of the residues SEA (acetylated serine) and Thr40. The remaining free valences in these systems were filled with methyl groups ($-CH_3$). Thus the resulting

systems included a total of 107 atoms. These systems were used as input structures of the reactants for the QM optimizations.

Geometry optimizations were performed using the self-consistent charge-density functional tight binding (SCC-DFTB) method ***[165]***, in order to execute the QM calculations at a reasonable computational cost for the size of the system. SCC-DFTB often yields good results (geometries and energetics) and performs well for biological systems ***[179,180]***. The spatial coordinates of all heavy atoms constituting the protein backbone and the carbon atoms of the added methyl group were fixed, in order to conserve the spatial disposition of the protein residues and substrates in the complexes. A total charge of -1 was assigned to the system, due to the deprotonated Asp187 carboxylate.

Thereafter, from the optimized reactant structures starting geometries for optimization of the TI-2s were constructed as follows: the hydroxyl group of propranolol was deprotonated, the His224:Nε atom was protonated and the SEA:C atom was assigned as sp^3. After these modifications, the systems were again optimized, using the same procedure as for the reactant structures optimizations.

Considering that the tetrahedral intermediates are commonly accepted as analogues of the transition states in the lipase catalyzed reactions (see section **1.4**) [28,36], the energy barriers for the transformation of the propranolol enantiomers were calculated as the difference between the energies of the corresponding optimized reactants and TI-2s.

4.3. Results and discussion

4.3.1. MD simulations of the AcCalB-propranolol complexes

4.3.1.1. Protein distortion

1.5 ns MD simulations of the AcCalB-propranolol complexes were carried out. The RMSD value for all heavy atoms of the protein backbone with respect to the initial structure increased gradually during heating and equilibration time for the first 10 ps. After this phase a plateau with a RMSD value of about 1 Å is reached in all simulations (see **Fig. 62** in **Appendix C**). The largest movements are observed in several surface loops (residues 250-267, 215-222, 1-12, 22-26, 67-75 and 170-178), a β-sheet constituting the C-terminal (residues 310-317), two short α-helix (α2:residues 44-49 and α5: residues

139-150), a long α-helix (α10: residues 267-289) and several residues constituting the binding pocket of CalB (residues 104, 154, 189, 190 and those making part of the α10 and α5 helix) (**Fig. 25**). This is in agreement with the results reported by other authors about the flexibility of CalB in organic solvents (e.g. chloroform, methanol and cyclohexane) and water [168,181,182]. In these studies it has also been reported that the regions with higher flexibility in CalB are the same in water and organic solvents and that only the degree of flexibility depends on the solvent [168]. On the other hand, the average RMSD values with respect to the crystal structure of the protein are about 0.90 Å and 1.22 Å (see **Table 29** in **Appendix C**), which shows that the CalB structure is well conserved during the MD simulations. In particular the hydrogen bond interaction between Asp187 and His224 is maintained (see the next section) and the average distance between the SEA:Oγ and His224:Nε atoms is about 3.21-3.36 Å (see **Table 30** in **Appendix C**), indicating that the disposition of the catalytic triad is stable during the simulations.

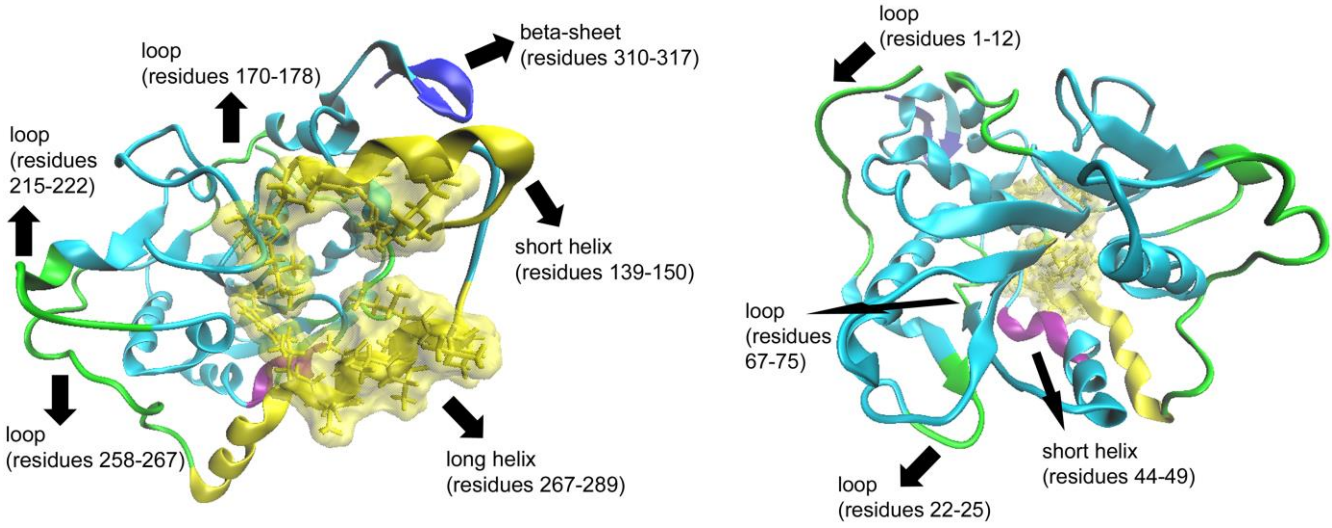

Fig. 25 Regions of CalB which exhibit more flexibility (or movements) during the MD simulations. These regions are colored in green (loop), blue (β-sheet) and yellow/purple (α-helix with residues being part of the CalB binding pocket/any other α-helix). A view from the front (left) and the back (right) with respect to the CalB binding pocket are shown. The regions with more flexibility involve several residues of the protein surface as well as residues constituting the medium and large pocket of CalB. The latter are shown in surface representation (yellow).

As found by Vallikivi et al. [170] for acetylation of prostaglandins, and as has successfully been used by other researches working with lipase catalyzed reactions [166,169], a RMSD value of < 3 Å between the protein structures during the MD simulations and the CalB crystal structure was chosen as

the limit to consider a complex to be in a productive binding mode. Because this criterion is satisfied in all simulations, all complexes formed during the MD simulations which satisfy the other three criteria mentioned above (section **4.2.1**) may be considered productive complexes. Therefore, subsequent analysis of the MD simulations was focused on those criteria.

4.3.1.2. Hydrogen bonds between the catalytic residues

The MD trajectories of the AcCalB-propranolol complexes were first analyzed with respect to the orientation of the acetylated serine (SEA) in the oxyanion hole, in order to check if this residue preserves a catalytic configuration. The average distances **d-f** (**Fig. 24**) for each complex in the MD simulations are given in **Appendix C** (**Table 31**). In all MD simulations the acetylated serine shows a similar behaviour. The carbonyl oxygen (SEA:O) of the acetate points towards the oxyanion hole during the whole simulation. A strong hydrogen bond is formed between the SEA:O atom and the side chain –OH of the residue Thr40 (distance **e** in **Fig. 24**) with an average distance between 1.78 and 1.83 Å. The hydrogen bonds between the SEA:O atom and the -NH functions of the residues Gln106 and Thr40 (distances **d** and **f** in **Fig. 24**) have average distances of 2.12-2.26 Å and 2.02-2.44 Å respectively. In general, the hydrogen bonds with the oxyanion hole are stable throughout the MD simulations of all complexes. There are only short periods (less than 2 % of the total simulation time in most of the MD simulations) in which mainly the SEA:O-Thr40:NH hydrogen bond (distance **f** in **Fig. 24**) is disrupted due to the conformational changes of the substrate during the MD simulations. Thus at least two of the hydrogen bonds with the oxyanion hole are formed throughout the MD trajectory. See **Fig. 63** to **Fig. 68** in **Appendix C**.

The hydrogen bond between the catalytic residues Asp187 and His224 (distance **a** in **Fig. 24**) has an average distance between 1.90 and 2.06 Å and is stable throughout the MD simulations of all complexes (See **Table 31** and **Fig. 63** to **Fig. 68** in **Appendix C**). This hydrogen bond is also important for the catalytic process as this interaction increases the basicity of the catalytic histidine, such that proton abstraction from the hydroxyl group of propranolol becomes likely, facilitating the nucleophilic attack on the carbonyl group of the acetylated serine (SEA).

The stability of these hydrogen bonds throughout all the simulations suggests that neither the orientation of the acetyl group toward the oxyanion hole nor the catalytic role of the residue Asp187 are determining factors for the formation of productive complexes between AcCalB and *R*- or *S*-propranolol and thus for the enantioselectivity of the reaction. Instead the enantioselectivity of the

reaction mainly depends on the ability of the propranolol enantiomers to adopt conformations inside the binding pocket of CalB which are suitable for a reaction and on the difference of the reactivities of these conformations.

4.3.1.3. The nucleophilic attack

As explained in section **4.2.1**, for considering a complex as productive the hydroxyl group of propranolol has to be positioned simultaneously close to the His224:Nε and SEA:C1 atoms and steric contacts with the protein must not be observed. It was decided to use a maximal value of 4 Å for the distances **b** and **c** (see **Fig. 24**), following other authors studying lipase-catalyzed acetylation reactions **[37,166,169]**. Several conformers satisfying these distance criteria were identified for *R*- and *S*-propranolol, which exhibit H-H contact distances with the protein which are longer than 2.6 Å (i.e. no steric clashes are observed). Thus several reactive conformers were identified for both *R*- and *S*-propranolol. The reactivities of these conformers are analysed below in terms of the distances **b** and **c**, the enzyme-substrate interactions, the temporal stability and the formation of NACs.

4.3.1.3.1. AcCalB-propranolol complexes in binding mode I

In most of the MD simulations of the AcCalB-propranolol complexes in binding mode I propranolol is stabilized with its hydroxyl group close to the catalytic residues only during some time of the MD trajectories (see details below). Then the substrate undergoes conformational changes leading to non-productive complexes or movement of propranolol from the binding pocket to the solvent. The stabilization of propranolol close to the catalytic residues is mediated mainly by CH-π interactions established between its naphthyl group and the aliphatic side chains of the residues at the large pocket of CalB (Ile189, Ala141, Leu144, Val154 and Thr138) (**Fig. 26** and **Fig. 28**). On the other hand, the destabilization of the complexes is mainly due to hydrophobic interactions established between the isopropyl side chain of propranolol and the solvent (toluene) during the simulations, which leads to the loss of the hydrophobic interactions between the isopropyl side chain of propranolol and the side chains of the residues at the medium pocket (Leu278, Ala281, Ala282, Ile285). Because the binding pocket of CalB is accessible to the solvent and in binding mode I the isopropyl side chain of propranolol may extends toward the entrance of the binding pocket, propranolol interacts continuously with toluene, leading to the loss of the CH-π interactions between the naphthyl group of propranolol and the residues at the large pocket. Thereby, as described in the following sections, it is found that the better exposition of the isopropyl group of propranolol toward the entrance of the binding pocket the shorter the

temporal stability of propranolol close to the catalytic residues (thus of the productive complexes) in binding mode I.

(a) R-propranolol complexes in binding mode I

The MD simulations of the *R*-propranolol complexes in binding mode I were carried out using two initial structures corresponding to the complexes R1 and R2 (ORI and ORIX in **Fig. 23**). In these structures the naphthyl group of propranolol is positioned in the same plane, but pointing toward the exterior of the binding pocket of CalB in R1 and toward the interior of the binding pocket in R2. Propranolol is near to the catalytic residues (SEA and His224) for a longer time in the simulations of R1 (more than 200 ps) than in the simulations of R2 (less than 5 ps). This is attributed to the better ability of the solvent to interact with the isopropyl group of propranolol in the system R2, as this isopropyl group is more exposed toward the exterior of the binding pocket in this system (see **Appendix C** for details). The predominant conformations of *R*-propranolol in the MD simulations of these complexes are shown in **Fig. 26**. The observed interaction between propranolol and the solvent in R2 does not permit the formation of productive complexes and only for R1 productive complexes are found (**R1a** and **R1b**). **R1a** is characterized by the formation of an intramolecular hydrogen bond between the amino and ether groups of propranolol (N1-H⋯O1). The average distance of this hydrogen bond is 2.43 ± 0.06 Å **(Fig. 27**). **R1b** is similar to **R1a**, but in this conformer the N1-H⋯O1 intramolecular hydrogen bond is not formed due to the orientation of the isopropylamine side chain. Propranolol is switching between **R1a** and **R1b** while it is close to the catalytic residues, by rotation of the C2-C3-N1-C4 dihedral angle (**Fig. 27**).

The average distances **b** and **c** for **R1a** and **R1b** are given in **Table 6**. It can be seen that the distance **c** is similar for both conformers, while the distance **b** is remarkably shorter for **R1a** compared to **R1b**. This shows that **R1a** is more accessible to be acylated by the enzyme, as a stronger hydrogen bond interaction with His224 (distance **b**) increases the nucleophilicity of the alcohol oxygen. Visual inspection shows that this behaviour is strongly related to the folding of the propranolol structure due to the formation of the N1-H⋯O1 intramolecular hydrogen bond.

The average distances corresponding to the CH-π interactions stabilizing the reactive conformers of *R*-propranolol in binding mode I are shown in **Table 7**. Because of their linearity the CH-π interactions between the naphthyl group of propranolol and the side chains of the residues Ile189, Val154 and

Leu144 are expected to be stronger [183]. The side chains of these residues are pointing toward the center of the naphthyl rings, especially the side chain of Ile189. Thus Ile189 is expected to have a large contribution to the stabilization of the TS involved in the transformation of the *R*-propranolol in binding mode I (see the next section).

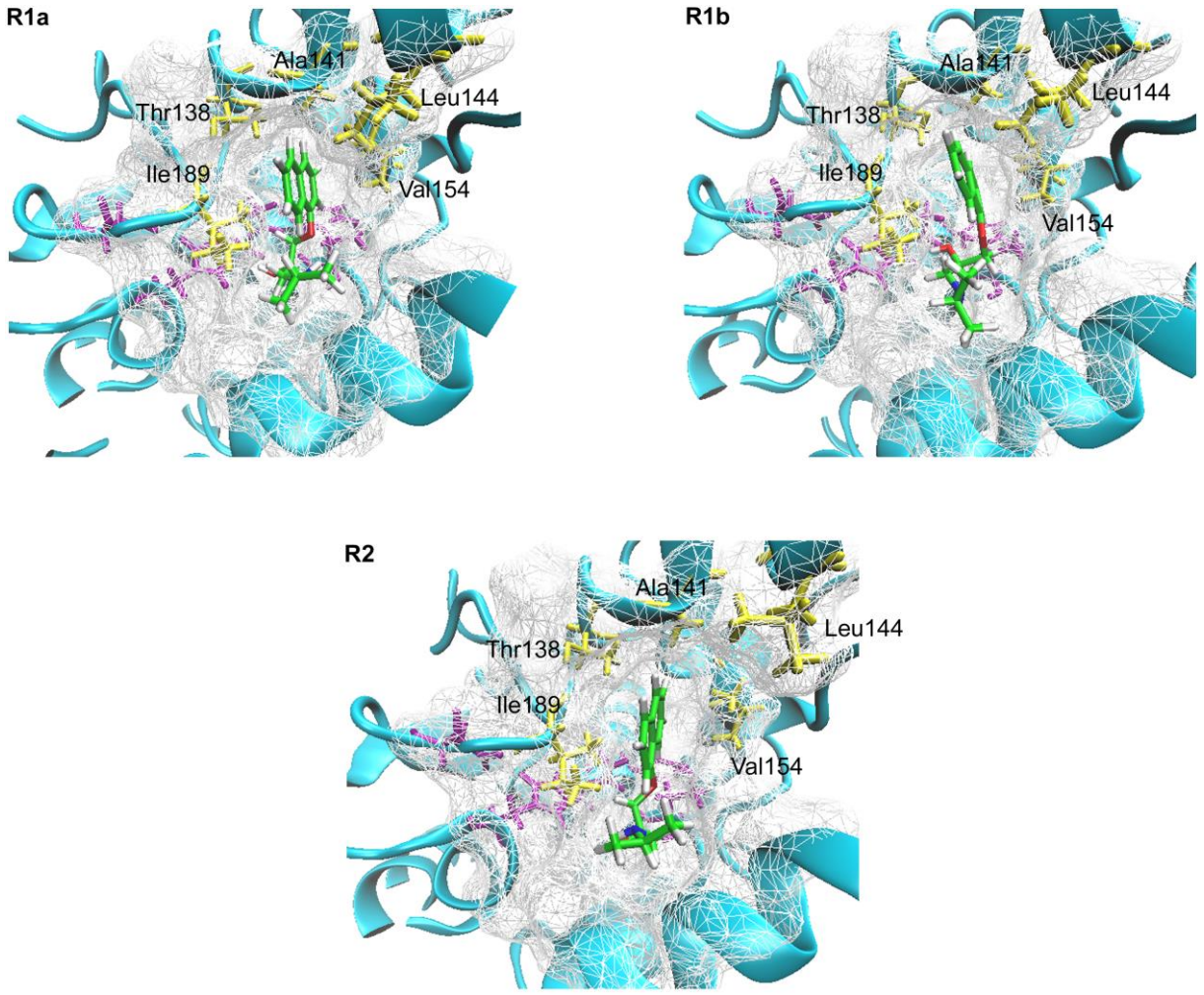

Fig. 26 Predominant conformations of *R*-propranolol in the MD simulations of the Michaelis complexes between AcCalB and *R*-propranolol in binding mode I. R1a and R1b correspond to the major reactive conformers of *R*-propranolol observed in the MD simulations of the complex R1. The catalytic triad (Asp187, His224 and acetylated Ser105) and the oxyanion hole (Thr40 and Gln106) are shown in purple. The residues constituting the binding pocket of CalB are shown in wireframe representation (gray). The most important residues contributing to the stabilization of propranolol by CH-π interactions are shown in yellow.

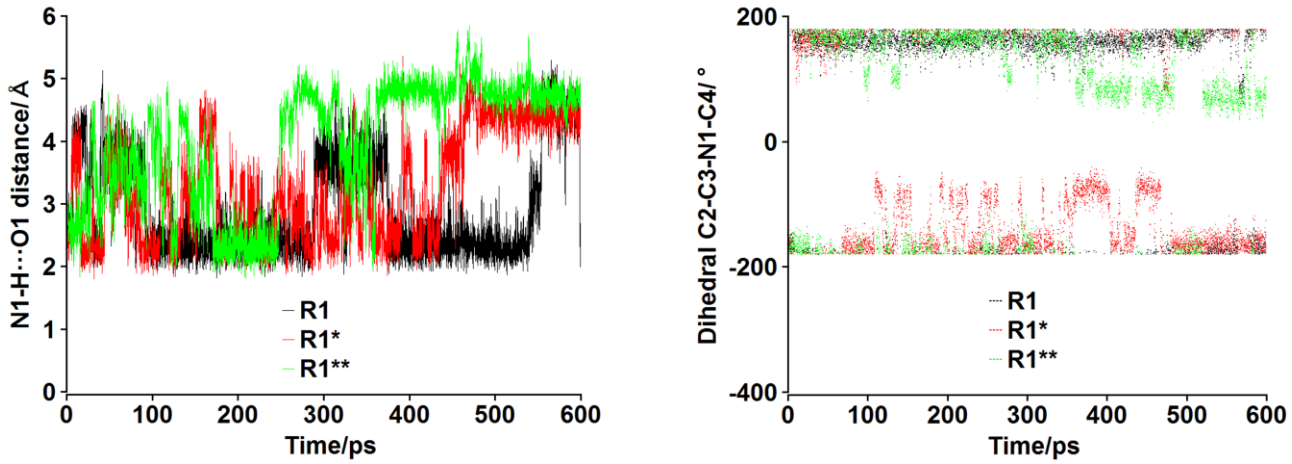

Fig. 27 Time evolution of the N1-H···O1 intramolecular hydrogen bond and the C2-C3-N1-C4 dihedral angle of propranolol in the MD simulations of the complex R1. Only the first 600 ps of the simulations are shown. Simulations with different initial velocities are indicated by *.

(b) S-propranolol complexes in binding mode I

The MD simulations of the *S*-propranolol complexes in binding mode I were carried out using three initial structures corresponding to the complexes S1, S2 and S3 (OSI, OSII and OSVI in **Fig. 23**). In S1 and S2 the naphthyl group of propranolol is oriented pointing toward the exterior of the binding pocket while in S3 it is oriented pointing toward the interior of the binding pocket. In general, propranolol is located near to the catalytic residues for a longer period of time in the simulations of S3 (more than 1300 ps) than in simulations of S2 and S1 (less than 600 ps). This behaviour observed for *S*-propranolol in binding mode I differs from that of *R*-propranolol, which is stabilized close to the catalytic residues for a longer time in the system in which its naphthyl group is oriented pointing toward the exterior of the binding pocket (R1). This is explained by a better exposition of the isopropyl group of propranolol toward the exterior of the binding pocket (facilitating the interaction with the solvent) in systems S1 and S2 than in S3. This contrasts with what is observed in R1 and R2, respectively. Details are given in **Appendix C**.

The predominant conformations of *S*-propranolol in the MD simulations of these complexes are shown in **Fig. 28**. In all MD simulations propranolol is able to form productive complexes. As in the case of *R*-propranolol, when the naphthyl group of *S*-propranolol is oriented pointing toward the exterior of the binding pocket (complexes S1 and S2), propranolol switches between two reactive conformations during the MD simulations. These conformations are generated by rotation of the same C2-C3-N1-C4

Table 6 Average distances[a] (in Å) between the hydroxyl group of propranolol and the carbonyl carbon of the acetylated serine and the Nε atom of the catalytic histidine in the MD simulations[b] of the Michaelis complexes between AcCalB and *R*- or *S*-propranolol in binding mode I.

Complex	Distance					
	b	c	b*	c*	b**	c**
R1a	2.31 (0.30)	3.77 (0.17)	2.26 (0.38)	3.67 (0.21)	2.25 (0.31)	3.71 (0.17)
R1b	2.86 (0.40)	3.60 (0.21)	3.06 (0.45)	3.70 (0.12)	2.70 (0.47)	3.61 (0.21)
S12a[c]	2.47 (0.42)	3.61 (0.22)	2.31 (0.48)	3.60 (0.23)	2.22 (0.37)	3.49 (0.26)
S12b[c]	2.38 (0.29)	3.71 (0.24)	2.28 (0.44)	3.51 (0.29)	2.27 (0.38)	3.49 (0.24)
S3a	2.15 (0.31)	3.28 (0.21)	2.19 (0.30)	3.63 (0.24)	2.29 (0.35)	3.42 (0.23)
S3b	2.18 (0.35)	3.25 (0.20)	2.18 (0.28)	3.28 (0.23)	2.20 (0.31)	3.37 (0.22)

[a] Distances b and c correspond to those shown in **Fig. 24**. Only periods during which the distances b and c were simultaneously less than 4 Å were taken into account. Numbers in brackets correspond to standard deviations from average values.
[b] MD simulations with different initial velocity distribution are indicated by *.
[c] Averages have been performed over the MD simulations of S1 and S2.

Table 7 Average distances[a] (in Å) of the interactions between the carbon atoms[b] of the naphthyl rings of propranolol and the residues of the binding pocket of the surrounding protein, in the MD simulations of the Michaelis complexes between AcCalB and *R*- or *S*-propranolol in binding mode I.

Non polar interactions	Complex					
	R1a	R1b	S12a	S12b	S3a	S3b
Val154 Cγ2···C2'	4.27 (0.08)	4.20 (0.06)	4.26 (0.14)	4.32 (0.25)		
Val154 Cγ2···C7'					4.22 (0.03)	4.22 (0.05)
Val154 Cγ1···C3'	4.10 (0.07)	4.08 (0.04)	3.90 (0.03)	4.00 (0.11)		
Val154 Cγ1···C4'	4.24 (0.33)	4.21 (0.38)	3.78 (0.04)	3.71 (0.05)		
Val154 Cγ1···C10'	4.37 (0.12)	4.33 (0.08)	4.38 (0.04)	4.27 (0.10)	4.54 (0.16)	4.64 (0.01)
Val154 Cγ1···C5'					3.97 (0.07)	4.02 (0.02)
Val154 Cγ1···C6'					3.68 (0.03)	3.70 (0.04)
Leu144 Cδ1···C5'	4.18 (0.16)	4.15 (0.11)	4.00 (0.10)	4.14 (0.16)		
Leu144 Cδ1···C6'	3.88 (0.09)	3.85 (0.06)	3.96 (0.22)	4.00 (0.22)		
Ala141 Cβ···C5'	3.99 (0.06)	3.99 (0.06)	4.14 (0.17)	4.22 (0.06)	4.21 (0.17)	4.35 (0.13)
Thr138 Cγ2···C4'	4.05 (0.08)	3.99 (0.03)	3.93 (0.21)	3.98 (0.23)		
Thr138 Cγ2···C6'					3.82 (0.11)	3.87 (0.06)
Ile189 Cγ2···C10'	3.92 (0.07)	3.88 (0.06)	4.09 (0.06)	4.10 (0.11)	3.96 (0.00)	3.97 (0.03)
Ile189 Cγ2···C9'	3.76 (0.05)	3.74 (0.05)	3.66 (0.04)	3.66 (0.09)	3.79 (0.05)	3.73 (0.01)

[a] Averages have been performed over the three MD simulations with different seed velocities. Numbers in brackets correspond to standard deviations from average values.
[b] Labels for the carbon atoms of propranolol are given in **Fig. 24**.

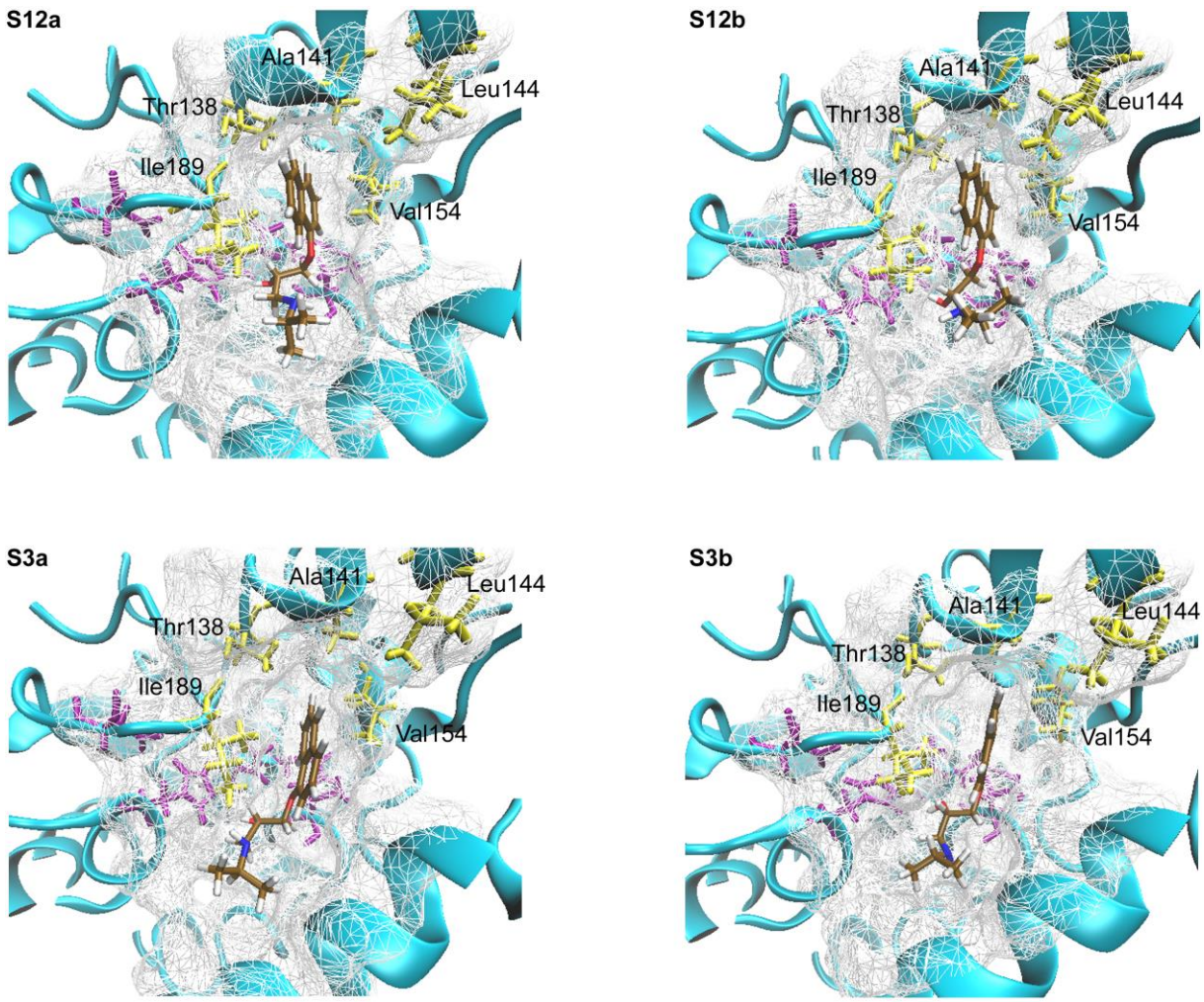

Fig. 28 Predominant reactive conformations of *S*-propranolol in the MD simulations of the Michaelis complexes between AcCalB and *S*-propranolol in binding mode I. The catalytic triad (Asp187, His224 and acetylated Ser105) and the oxyanion hole (Thr40 and Gln106) are shown in purple. The residues constituting the binding pocket of CalB are shown in wireframe representation (gray). The most important residues contributing to the stabilization of propranolol by CH-π interactions are shown in yellow.

dihedral angle, and differ by a N1-H···O1 intramolecular hydrogen bond. As this behaviour is observed in the MD simulations of S1 and S2, it is referred to these two conformations as **S12a** and **S12b**, **S12a** being the conformation in which the N1-H···O1 hydrogen bond is present. The average distance of this hydrogen bond is 2.46 ± 0.09 Å, which is close to the value obtained for **R1a**. A similar behaviour is observed in the simulations of S3, where two major reactive conformers of propranolol are observed (**S3a** and **S3b**) differing in the C2-C3-N1-C4 dihedral angle, but without formation of a N1-H···O1 intramolecular hydrogen bond. This hydrogen bond cannot be formed because the oxygen atom O1 is

positioned far from the amino group (N1-H) when the naphthyl group of propranolol is oriented pointing toward the interior of the binding pocket.

The average distances **b** and **c** for the productive complexes of *S*-propranolol in binding mode I are also shown in **Table 6**. These complexes present a different dynamic behaviour compared to the *R*-propranolol complexes. Productive complexes of *S*-propranolol in which the naphthyl group is oriented pointing toward the exterior of the binding pocket (**S12a** and **S12b**) present a similar ability to be transformed by the enzyme, as in these complexes the hydroxyl group of propranolol is simultaneously positioned near to His224 and SEA at similar distances. Furthermore, the *S*-enantiomer is also able to form productive complexes when its naphthyl group is oriented pointing toward the interior of the binding pocket, which is not the case for *R*-propranolol, due to the destabilization of the corresponding complex (R2) by the solvent (see the previous section).

The hydroxyl group of propranolol is closer to the catalytic residues in the *S*-propranolol complexes than in the *R*-propranolol complexes, especially in comparison to the **R1b** complex. This means that in binding mode I *S*-propranolol fits into the CalB binding pocket in conformations in which its hydroxyl group is in a better position to be acetylated by CalB than the *R*-propranolol. This suggests a faster transformation of the *S*-propranolol over *R*-propranolol. However, analysis of the CH-π interactions contributing to the stabilization of the reactive *S*-propranolol conformers shows that these conformers are more weakly stabilized by this type of interaction (according to the average distances and standard deviations, and to the linearity of the interactions) in comparison to the reactive *R*-propranolol conformers (**Table 7**). This suggests a better stabilization of the TS involved in the transformation of the *R*-enantiomer, which would enhance the reactivity of this enantiomer. Particularly it should be noted that **S3a** and **S3b** loose the interaction with Leu144 (**Fig. 28**). Furthermore, as is reflected in the average distances and standard deviations, **R1a** and **R1b** are more strongly stabilized by the residues Leu144, Ala141, Thr138 and Ile189 in comparison to **S12a** and **S12b.** For example, the average distances between the atom Cγ2 of Ile189 and the atoms C10' and C9' of propranolol are 3.92 ± 0.07 Å and 3.76 ± 0.05 Å in case of **R1a**, while in case of **S12a** (specular binding mode of **R1a**) are 4.09 ± 0.06 Å and 3.66 ± 0.04 Å, respectively. The average distance between the atom Cβ of Ala141 and the atom C5' of propranolol is 3.99 ± 0.06 Å in case of **R1a**, while in case of **S12a** it is 4.14 ± 0.17 Å. Finally, the average distance between the atom Cδ1 of Leu144 and the atom C6' of propranolol, which is 3.88 ± 0.09 Å for **R1a** and 3.96 ± 0.22 Å for **S12a**.

Several studies have been reported showing experimental and theoretical evidence of a major stabilization of the transition state involved in the transformation of the faster enantiomer by hydrophobic interactions. One example is the resolution of methyl (±)-3-hydroxypentanoate catalyzed by *Candida antarctica* lipase B using ammonia and benzyl amine as nucleophiles. Molecular dynamics simulations carried out over the second tetrahedral intermediate revealed that the higher number of contacts involving non-polar atoms of both the acyl chain (substrate) and some of the residues of the CalB binding pocket (including Ile189) are responsible for the higher enantioselectivity observed in the aminolysis reaction [36]. Another good example showing specifically the contribution of the CH-π interactions to the enantioselectivity is the improvement of the catalytic activity and enantioselectivity of *Burkholderia cepacia* toward secondary alcohols through the I287F/I290A double mutation. Substrate mapping analysis strongly suggested that Phe287 contributes to enhancement the reactivity of the *R*-enantiomer by a CH-π interaction with the substrate, of which the estimated energy was -0.4 kcal/mol [184]. The CH-π interactions have also shown to be responsible for the enantioselectivity observed in other reactions such as the transfer hydrogenation of aromatic carbonyl compounds catalyzed by chiral n^6-Arene-Ruthenium (II) complexes [185].

4.3.1.3.2. AcCalB-propranolol complexes in binding mode II

In contrast to binding mode I, in the MD simulations of the AcCalB-propranolol complexes in binding mode II the substrate never leaves the binding pocket. This is because in this binding mode the solvent interacts mainly with the naphthyl group of propranolol, which is strongly stabilized by CH-π interactions with the residues at the medium pocket of CalB (Ile285, Val286, Ala282 and Leu278, see **Fig. 29** and **Fig. 30**). As the strength of a CH-interaction depends on its linearity [183], the temporal stabilization of propranolol (in binding mode II) with its hydroxyl group close to the catalytic residues depends on the orientation of its naphthyl group in the medium pocket. Generally speaking, the better the stabilization of the naphthyl rings by the residues of the surrounding protein and the less exposed they are to the solvent, the longer the temporal stability of propranolol close to the catalytic residues (thus of the productive complexes) in binding mode II (see **Appendix C**).

(a) R-propranolol complexes in binding mode II

In the MD simulations of R3 a total of six productive complexes of *R*-propranolol are found (**R3a-R3f** in **Fig. 29**). Interestingly, not all complexes are observed in all MD simulations, except **R3a** and **R3b**.

R3c and **R3d** occur in two of the three MD simulations while **R3e** and **R3f** only in one MD simulation. These results show the versatility of using multiple MD simulations with different initial velocity distributions for sampling the conformational space in this type of systems. See **Appendix C**.

Similar to the simulations of the complexes in binding mode I, a rotation of the C2-C3-N1-C14 dihedral angle of propranolol is observed, resulting in a temporal formation of the N1-H···O1 intramolecular hydrogen bond. **R3a**, **R3c** and **R3e** are characterized by the formation of this hydrogen bond, with an average distance of 2.60 ± 0.21 Å, 2.41 ± 0.07 Å and 2.47 ± 0.24 Å, respectively. The main difference between these complexes is the orientation of the naphthyl group of propranolol in the medium pocket of CalB. **R3c** is generated from **R3a** by the simultaneous rotation of the O1-C1-C2-C3 and C1'-O1-C1-C2 dihedral angles, from 44 ± 6° to 57 ± 1° and from 139 ± 0.3° to 102 ± 0.9°, respectively. These rotations move the naphthyl group of propranolol from a plane almost perpendicular to the Leu278-Ala287 helix (helix α10) in **R3a** to an orientation parallel to this helix in **R3c**. In turn **R3e** is generated from **R3c** by the simultaneous rotations of the same dihedral angles, from 57 ± 1° to 79 ± 9° and from 102 ± 0.9° to 69 ± 11°, respectively. These rotations move the naphthyl group of propranolol toward the interior of the medium pocket. **R3b**, **R3d** and **R3f** are structural analogues of **R3a**, **R3c** and **R3e**, respectively. They only differ in the orientation of the amino group of propranolol, which does not favour the formation of the N1-H···O1 hydrogen bond in **R3b**, **R3d** and **R3f**.

The average distances **b** and **c** for the productive complexes of *R*-propranolol in binding mode II are given in **Table 8**. In the complexes **R3a-R3d** the hydroxyl group of propranolol is simultaneously positioned closer to the catalytic residues when the N1-H···O1 intramolecular hydrogen bond is formed. While in **R3e** and **R3f** the hydroxyl group is positioned at a similar distance, suggesting that these complexes have the same ability to be acetylated by CalB. In general, the distances **b** and **c** in **R3e** and **R3f** are shorter than the ones observed in **R3a-R3d**. Furthermore, even though **R3e** and **R3f** are only found in one of the MD simulations, they are temporally more stable than the other *R*-propranolol conformers (more than 500 ps; see **Table 10** and **Appendix C**). This is attributed to the higher number of protein residues contributing to the stabilization of these conformers through CH-π interactions as well as to a reduced exposition of the naphthyl group of propranolol to the solvent. In **R3a-R3d** propranolol is mainly stabilized through CH-π interactions between their naphthyl rings and the residues Ile285, Ala282, Leu278 and Val286, while in **R3e** and **R3f** it is also stabilized by the residues Ile189 and Glu188 as shown in **Fig. 29** (see also **Table 9**). The larger number of CH-π

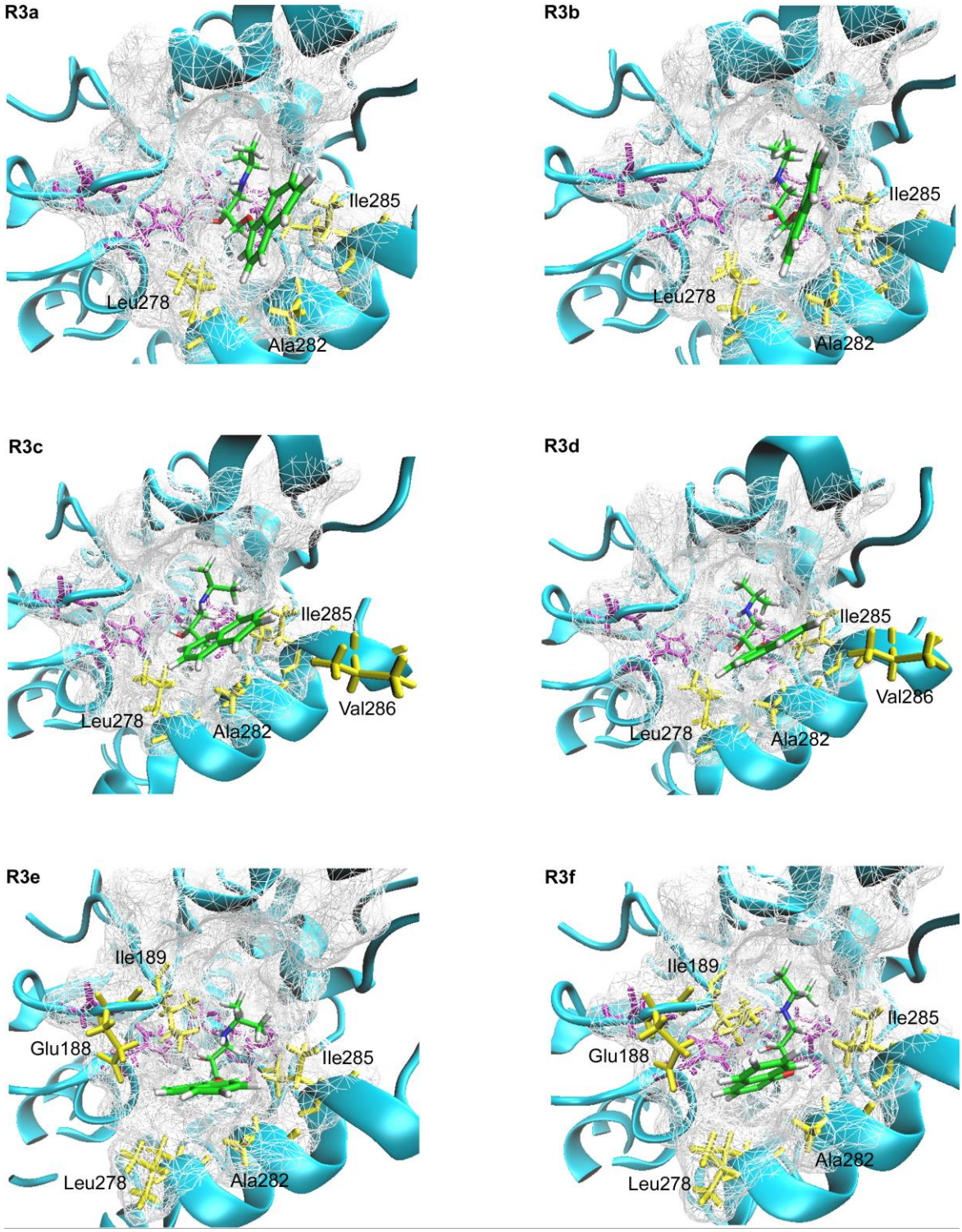

Fig. 29 Predominant reactive conformations of *R*-propranolol in the MD simulations of the Michaelis complexes between AcCalB and *R*-propranolol in binding mode II. The catalytic triad (Asp187, His224 and acetylated Ser105) and the oxyanion hole (Thr40 and Gln106) are shown in purple. The residues constituting the binding pocket of CalB are shown in wireframe representation (gray). The most important residues contributing to the stabilization of propranolol by CH-π interactions are shown in yellow.

interactions contributing to the stabilization of these conformers may also play an important role in stabilizing the corresponding transition states. Thus these results suggest that the acetylation of **R3e** and **R3f** by CalB is favored compared to the other *R*-propranolol conformers.

(b) S-propranolol complexes in binding mode II

In the MD simulations of S4 two productive complexes of *S*-propranolol could be identified (**S4a** and **S4b** in **Fig. 30**). **S4a** and **S4b** are specular binding modes of **R3c** and **R3d**, respectively. They are also stabilized in the binding pocket of CalB by the residues Ile285, Ala282, Leu278 and Val286 by CH-π interactions. **S4a** and **S4b** differ in the orientation of their amino group, which forms an N1-H···O1 hydrogen bond only in **S4a**. This hydrogen bond is stronger than in the other reactive conformers of *R*- and *S*-propranolol, with an average distance of 2.29 ± 0.03 Å.

The average distances **b** and **c** of the **S4a** and **S4b** complexes are shorter than in the **R3a-R3d** complexes (**Table 8**). According to this, the transformation of **S4a** and **S4b** is favoured over **R3a-R3d**. In contrast, in terms of these distances, **R3e** and **R3f** display a similar ability to **S4a** and **S4b** to be acetylated by CalB. However, as observed in the complexes in binding mode I, the reactive conformers of *R*-propranolol are more strongly stabilized (by CH-π interactions with the surrounding protein residues) than the reactive conformers of *S*-propranolol in binding mode II (**Table 9**). For example, it can be seen in **Fig. 29** and **Fig. 30** that **R3e** and **R3f** are stabilized by a larger number of CH-π interactions than **S4a** and **S4b**. This suggests that these interactions are also responsible for a better stabilization of the transition states involved in the transformation of the *R*-propranolol complexes in binding mode II, leading to a faster transformation of this enantiomer, which would explain the experimentally observed enantioselectivity.

It is important to note that from the MD simulations of the Michaelis complexes between AcCalB and propranolol is not possible to quantitatively estimate the contribution of the hydrophobic interactions between the substrate and CalB to the stabilization of the corresponding transition states, and therefore to the enantioselectivity. However, at least a qualitative idea is obtained, which may help to improve the enantioselective synthesis of propranolol through a rational redesign of CalB. The actual contribution of these interactions to the stabilization of the TS can be estimated from hybrid quantum chemical/molecular mechanical (QM/MM) calculations [186]. The latter are the focus of **Chapter 6**.

Table 8 Average distances[a] (in Å) between the hydroxyl group of propranolol and the carbonyl carbon of the acetylated serine and the Nε atom of the catalytic histidine in the MD simulations[b] of the Michaelis complexes between AcCalB and *R*- or *S*-propranolol in binding mode II.

Complex	Distance					
	b	c	b*	c*	b**	c**
R3a	2.87 (0.33)	3.55 (0.21)	2.82 (0.69)	3.63 (0.27)	2.69 (0.56)	3.69 (0.21)
R3b	2.81 (0.41)	3.61 (0.19)	3.11 (0.52)	3.74 (0.21)	3.08 (0.56)	3.65 (0.21)
R3c			2.74 (0.51)	3.70 (0.18)	2.34 (0.46)	3.60 (0.24)
R3d			3.11 (0.57)	3.76 (0.19)	2.99 (0.54)	3.76 (0.21)
R3e					2.20 (0.36)	3.43 (0.24)
R3f					2.39 (0.40)	3.15 (0.21)
S4a	2.18 (0.34)	3.28 (0.21)	2.18 (0.28)	3.62 (0.23)	2.28 (0.35)	3.41 (0.23)
S4b	2.14 (0.31)	3.24 (0.20)	2.18 (0.29)	3.45 (0.30)	2.23 (0.32)	3.39 (0.22)

[a] Distances b and c correspond to those shown in the **Fig. 24**. Only periods during which the distances b and c were simultaneously less than 4 Å were taken into account. Numbers in brackets correspond to standard deviations from average values.
[b] MD simulations with different initial velocity distribution are indicated by *.

Table 9 Average distances[a] (in Å) of the interactions between the carbon atoms[b] of the naphthyl rings of propranolol and the residues of the binding pocket of the surrounding protein in the MD simulations of the Michaelis complexes between AcCalB and *R*- or *S*-propranolol in binding mode II.

Non polar interactions	Complex							
	R3a	R3b	R3c	R3d	R3e	R3f	S4a	S4b
Ile285 Cγ2···C8’	4.24 (0.55)	4.21 (0.38)	3.97 (0.01)	3.87 (0.13)			3.98 (0.20)	4.16 (0.13)
Ile285 Cγ2···C7’	4.36 (0.51)	4.37 (0.37)	4.04 (0.01)	4.07 (0.18)			4.21 (0.13)	4.25 (0.17)
Ala282 Cβ···C3’	3.59 (0.07)	3.69 (0.15)	4.19 (0.25)	4.13 (0.15)			4.05 (0.03)	4.03 (0.12)
Ala282 Cβ···C4’	3.95 (0.19)	4.02 (0.23)	4.05 (0.28)	3.99 (0.10)			4.31 (0.11)	4.13 (0.01)
Ala282 Cβ···C8’					3.66 (0.27)	3.68 (0.29)		
Ala282 Cβ···C7'					3.77 (0.31)	3.75 (0.31)		
Val286 Cγ2···C7’			4.78 (0.71)	4.41 (0.57)			4.48 (0.27)	4.33 (0.01)
Val286 Cγ2···C6’			4.75 (0.71)	4.55 (0.45)			4.44 (0.34)	4.30 (0.02)
Leu278 Cδ2···C2’	4.02 (0.18)	4.10 (0.06)	4.00 (0.16)	3.95 (0.07)			4.19 (0.26)	4.10 (0.01)
Leu278 Cδ2···C3’	4.15 (0.10)	4.07 (0.07)	3.90 (0.00)	3.91 (0.07)			4.45 (0.29)	4.37 (0.01)
Leu278 Cβ···C3’					3.75 (0.31)	3.82 (0.27)		
Leu278 Cβ···C4’					3.84 (0.36)	3.86 (0.36)		
Leu278 Cβ···C10’					4.41 (0.46)	4.44 (0.50)		
Leu278 Cγ···C4’					4.54 (0.28)	4.05 (0.31)		
Leu278 Cδ1···C4’					4.19 (0.44)	3.58 (0.45)		
Ile189 Cδ···C10’					3.84 (0.26)	4.19 (0.29)		
Ile189 Cδ···C9’					3.86 (0.24)	4.12 (0.30)		
Glu188 Cγ···C4’					4.36 (0.36)	4.54 (0.35)		

[a] Averages have been computed over the three MD simulations with different seed velocities. Numbers in brackets correspond to standard deviations from average values. [b] Labels for the carbon atoms of propranolol are given in **Fig. 24**.

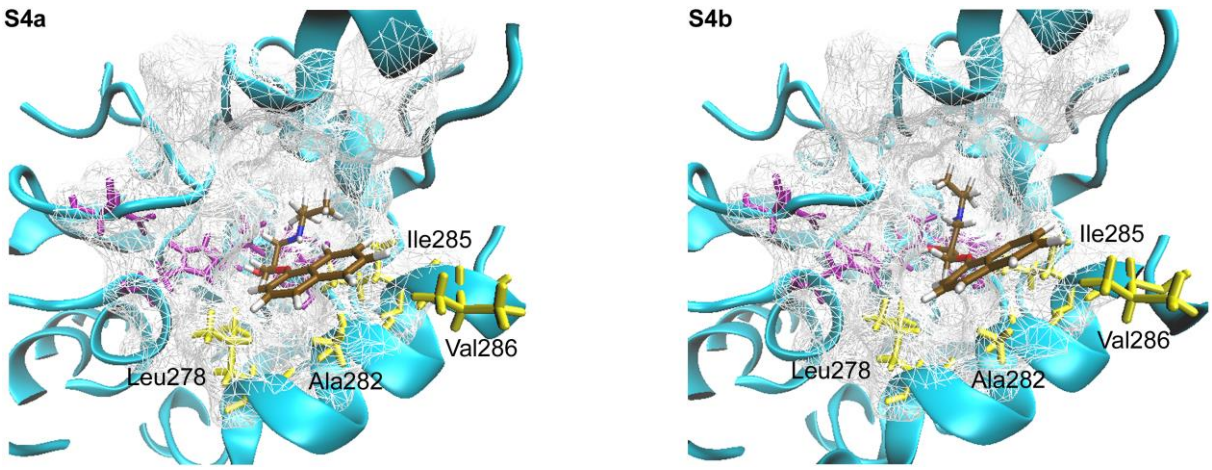

Fig. 30 Predominant reactive conformations of *S*-propranolol in the MD simulations of the Michaelis complexes between AcCalB and *S*-propranolol in binding mode II. The catalytic triad (Asp187, His224 and acetylated Ser105) and the oxyanion hole (Thr40 and Gln106) are shown in purple. The residues constituting the binding pocket of CalB are shown in wireframe representation (gray). The most important residues contributing to the stabilization of propranolol by CH-π interactions are shown in yellow.

4.3.1.4. Formation of near attack conformers (NACs)

Finally the ability of the reactive conformers of propranolol to form near attack conformers (NACs) was analyzed. Because the reactants must pass through the NACs in order to reach the TS, the population of NACs is an indicative of the reaction rate [176]. NACs for the AcCalB-propranolol complexes were defined as those in which the distances **b** and **c** are simultaneously ≤ 2.7 Å and ≤ 3.2 Å, respectively. The fraction of the lifetime of each reactive conformer of propranolol in which NACs are formed during the MD simulations was analyzed. All reactive conformers are able to form NACs and thus will reach the TS. The percentage of NACs of the two propranolol enantiomers is similar in all MD simulations with different initial velocity distributions. Therefore only the results of the analysis of the MD simulations with the third initial velocity distribution (iseed 234) are shown in **Table 10**. In this simulation all reactive propranolol conformers are present. It can be seen that in binding mode I the reactive conformers of *S*-propranolol occur more frequently and have a better ability to form NACs than the reactive conformers of *R*-propranolol. The lifetime of the reactive conformers of *R*-propranolol is < 120 ps and the percentage of NACs is < 2 %, while for the reactive conformers of *S*-propranolol the lifetime is > 300 ps and the percentage NACs is > 4 %. In contrast, in binding mode II, the percentage of NACs in the productive complexes of *S*-propranolol is higher than in the **R3a-R3d** complexes but lower than in the **R3e** and **R3f** complexes. This is explained by the strong binding of propranolol to the active site of CalB in the **R3e** and **R3f** complexes (see **Appendix C**). The percentage

of NACs in these complexes is higher than in the other complexes. This means that this stage of the reaction is kinetically favored for *R*-propranolol, which is in agreement with the experimental results. The moderate enantioselectivity of CalB may be partly attributed to the high percentage of NACs formation observed for the *S*-propranolol. See **Table 32** to **Table 33** in **Appendix C** for details on the other simulations.

Table 10 Lifetime and percentage of NACs[a] of each reactive conformer of *R*- and *S*-propranolol in the MD simulations of the AcCalB-propranolol complexes carried out with the third initial velocity distribution.

Binding Mode I			Binding Mode II		
Conformer	Lifetime** (ps)	NACs** (%)	Conformer	Lifetime** (ps)	NACs** (%)
R1a	116.7	0.09	R3a	9.5	1.05
R1b	118.4	1.18	R3b	24.5	0.41
S12a[b]	372.5	4.00	R3c	38.7	0.78
S12b[b]	715.8	13.90	R3d	214.4	0.05
S3a	1024.9	13.01	R3e	520.6	26.89
S3b	465.1	21.29	R3f	679.4	36.74
			S4a	577.4	1.52
			S4b	912.6	1.89

[a] The percentage of NACs formation is given related to the lifetime of each reactive conformer.
[b] Averages have been calculated over the MD simulations of S1 and S2 (see section **5.3.1.3.1(b)**).

4.3.2. QM calculations

The implemented QM methodology allowed identifying the TI-2 structure for most of the productive complexes of *R*- and *S*-propranolol (see **Table 11**). The key geometrical parameters in the optimized reactant states (RS) and TI-2s as well as the corresponding atomic charges of the involved atoms (calculated by the Mülliken population analysis approach [187,188]) are reported in **Appendix C** (**Table 34** to **Table 37**). Most of the observed geometrical changes and the variations of the atomic charges as the reaction proceeds are different for each reactive conformer of propranolol. The first observed geometrical change is the decrease of the distance between the His224:Nε atom and the alcohol hydrogen of propranolol (His224:Nε-Sub:**H**), from 1.85-1.90 Å to 1.04-1.06 Å. This change occurs simultaneously with the increase in the O-H distance of the alcohol group of propranolol (Sub:**O**-Sub:**H**), from 1.00 Å to 1.73-2.17 Å. This is further accompanied by a decrease in the charge of

the His224:Nε atom about 10 folds (from -0.4 to -0.04, approximately). Together, these changes indicate that the proton transfer from the alcohol group of propranolol to His224 actually results in the formation of a NH bond, with a bond length about 1.06 Å. Another noticeable change is that the distance between the alcohol oxygen of propranolol and the carbonyl carbon of the acetate group of the acetylated serine (SEA:C-Sub:**O**) decreases until 1.56-1.76 Å, which is compatible with formation of an ester bond between propranolol and the acetylated serine. Simultaneously, the SEA:Oγ atom becomes more negative (atomic charge variation from -0.3 to -0.5 in all complexes, approximately) and the distance of the SEA:C-SEA:Oγ bond increases (from 1.37-1.38 Å to 1.50-1.54 Å), suggesting a weakening of this bond in the formed intermediate. A slight increase in the distance between the carbonyl oxygen and the carbonyl carbon of the acetate group of SEA (SEA:C-SEA:O) as well as in the negative charge of the SEA:O atom are also observed. In addition, the three hydrogen bonds with the oxyanion hole remain stable, but depending on the reactive conformer they become stronger or weaker in the TI-2.

All these findings corroborated that the TI-2 is actually expected to be formed when propranolol docks in the AcCalB complex with its hydroxyl group positioned to a distance less than 4 Å from the catalytic residues His224 and SEA. In case of the propranolol conformers for which it was not possible to get the TI-2 structure by the QM methodology used here, it not necessarily means that they are not able to reach the TS as they are able to form NACs (section **4.3.1.4**). This may be a consequence of some protein residues important for the catalytic process missing in the QM model, for example, some residues of the CalB binding pocket which participate in stabilizing propranolol in a particular reactive conformation. One of the reasons why the TI-2 was not found for some of the reactant QM systems is that the substrate drastically changes its conformation during the optimization.

On the other hand, a proton transfer from His224 to Asp187 is observed during optimization of the TI-2, such that the His224:N_D proton is covalently bound to Asp187 and forming a hydrogen bond with the deprotonated His224:N_D atom in the optimized TI-2s (**Fig. 31**). This suggests that the reaction follows a double proton transfer mechanism. However, in QM/MM calculations which were carried out for this system, the His224:N_D proton is observed to stay coordinated to this atom as the reaction proceeds (**Chapter 6**). Thus the proton transfer from His224 to Asp187 is attributed to the QM model used, as in this model Asp187 is naked respect to its environment in the protein, in which conversely is forming hydrogen bonds with the backbone (-NH) of nearby residues (namely, Ile189 and Val190). These interactions would be responsible for avoiding a possible proton transfer from His224 to Asp187

by increasing the associated energy barrier to this process. Similar results have been reported in the computational study of the lipase-catalyzed hydrolysis of 1-(2-naphthyl)-ethyl-acetate by using a QM gas-phase model and QM/MM calculations at a high level of theory (BLYP) [115], and have been attributed to the same event (missing residues in the QM model which participate in hydrogen bonds with the catalytic Asp in the protein environment). In this study the energy barrier associated to this proton transfer is calculated to be more than 4 kcal/mol higher in presence of the residues participating in hydrogen bond interactions with the catalytic Asp compared to a "naked" Asp. This indicates that the QM model used here is somewhat artificial. However, it was useful to get a first impression of the factors which may affect the enantioselectivity of the reaction such as the changes in the hydrogen bond patterns with the oxyanion hole as the reaction proceeds (see below).

Another important aspect which has to be noted about the QM calculations is that the optimized reactant states resulted to be basically a NAC. The hydrogen bond between the alcohol hydrogen and the His224:Nε atom has a distance less than 2.00 Å in all optimized reactants, and the distance between the alcohol oxygen and the carbonyl carbon of the acetate is less than 3.2 Å in most of them (see **Table 34** and **Table 36** in **Appendix C**). Thus the QM calculations provide information about the formation of the TI-2 from the respective NAC. The discussion given in the next sections is focused on this step of the reaction.

4.3.2.1. Transformation of R- and S-propranolol in binding mode I

According to the calculated energy barriers (**Table 11**), in binding mode I the transformation of *R*-propranolol is kinetically favoured over the *S*-propranolol. The observed difference between the energy barriers for the transformation of the *R*- and *S*-propranolol conformers in binding mode I may be easily understood by analysing the hydrogen bonds with the oxyanion hole and the position of the hydroxyl group of propranolol to execute the nucleophilic attack. It can be seen in **Table 36** (**Appendix C**) that in case of the **S12b** system, which presents the lower energy barrier of the *S*-propranolol conformers in binding mode I, the hydrogen bonds with the oxyanion hole in both the RS and the TI-2 are stronger than in the other *S*-propranolol systems in binding mode I. Furthermore, the variations in these hydrogen bonds as the reaction proceeds contribute to a major stabilization of the TI-2 formed in the **S12b** system. One of the hydrogen bonds with the oxyanion hole (SEA:O-Thr40:NH) become weaker in the TI-2 of **S12b** and **S3b**, but the variation is smaller for **S12b** (0.19 Å) than for **S3b** (0.47 Å). With similar variations in both of these systems the other two hydrogen bonds become stronger. In case of **S3a** the SEA:O-Thr40:NH hydrogen bond does not suffer a significant

change while the other two hydrogen bonds become slightly stronger; the SEA:O-Thr40:OH distance change from 1.86 Å to 1.71 Å and the SEA:O-Gln106:NH distance is the same, but the angle of the latter become more planar. In the TI-2 of **S12b** an intramolecular hydrogen bond is also formed between the amino and naphthoxy groups of propranolol (with a distance of 2.67 Å), which may also contribute to a major stabilization of the TI-2 of this conformer. On the other hand, in case of the RS of the **R1a** system (see **Table 34** in **Appendix C**) the interaction with the oxyanion hole is slightly weaker than that observed in the RS of **S12b**. However, all the hydrogen bonds with the oxyanion hole in the **R1a** system become stronger as the reaction proceeds, to the point that the interaction with the oxyanion hole in the TI-2 of this conformer is stronger than in the TI-2 of **S12b**. In addition, in the RS of **R1a** propranolol is forming an intramolecular hydrogen bond (with a distance of 2.10 Å), which remains in the corresponding TI-2 (with a distance of 2.36 Å). The TI-2 of **R1a** is further stabilized by a hydrogen bond formed between its amino group and the carbonyl oxygen of Thr40 (with a distance of 2.09 Å). Furthermore, the SEA:C atom in the RS of **R1a** is slightly more electrophilic (with an atomic charge of +0.684; **Table 35** in **Appendix C**) than in the RS of **S12b** (with an atomic charge of +0.667; **Table 37** in **Appendix C**), and the hydroxyl group of propranolol is closer to this atom in the RS of **R1a** than in the RS of **S12b**. All of this makes easier the transformation of **R1a** respect to the other propranolol conformers in binding mode I, which explain the obtained lower energy barrier for this conformer. The optimized reactant state and TI-2 for this conformer are shown in **Fig. 31**.

Table 11 Energy barriers for the transformation of the AcCalB-propranolol complexes into the corresponding second tetrahedral intermediates estimated by quantum chemical calculations using small model systems[a].

Binding Mode I		Binding Mode II	
Complex	ΔE^b (kcal/mol)	Complex	ΔE^b (kcal/mol)
R1a	-6.0	R3a	-[c]
R1b	-[c]	R3b	11.2
S12a	-[c]	R3c	-[c]
S12b	0.1	R3d	9.8
S3a	3.8	R3e	4.5
S3b	8.1	R3f	7.5
		S4a	9.1
		S4b	-4.8

[a] The small model systems were only constituted by the substrate, the catalytic triad and the oxyanion hole, according to the procedure described in the section **4.2.2**. [b] ΔE corresponds to the energy barrier. It was obtained by calculating the difference between the energies of the optimized reactant systems and the corresponding optimized tetrahedral intermediates. [c] No second tetrahedral intermediate could be localized.

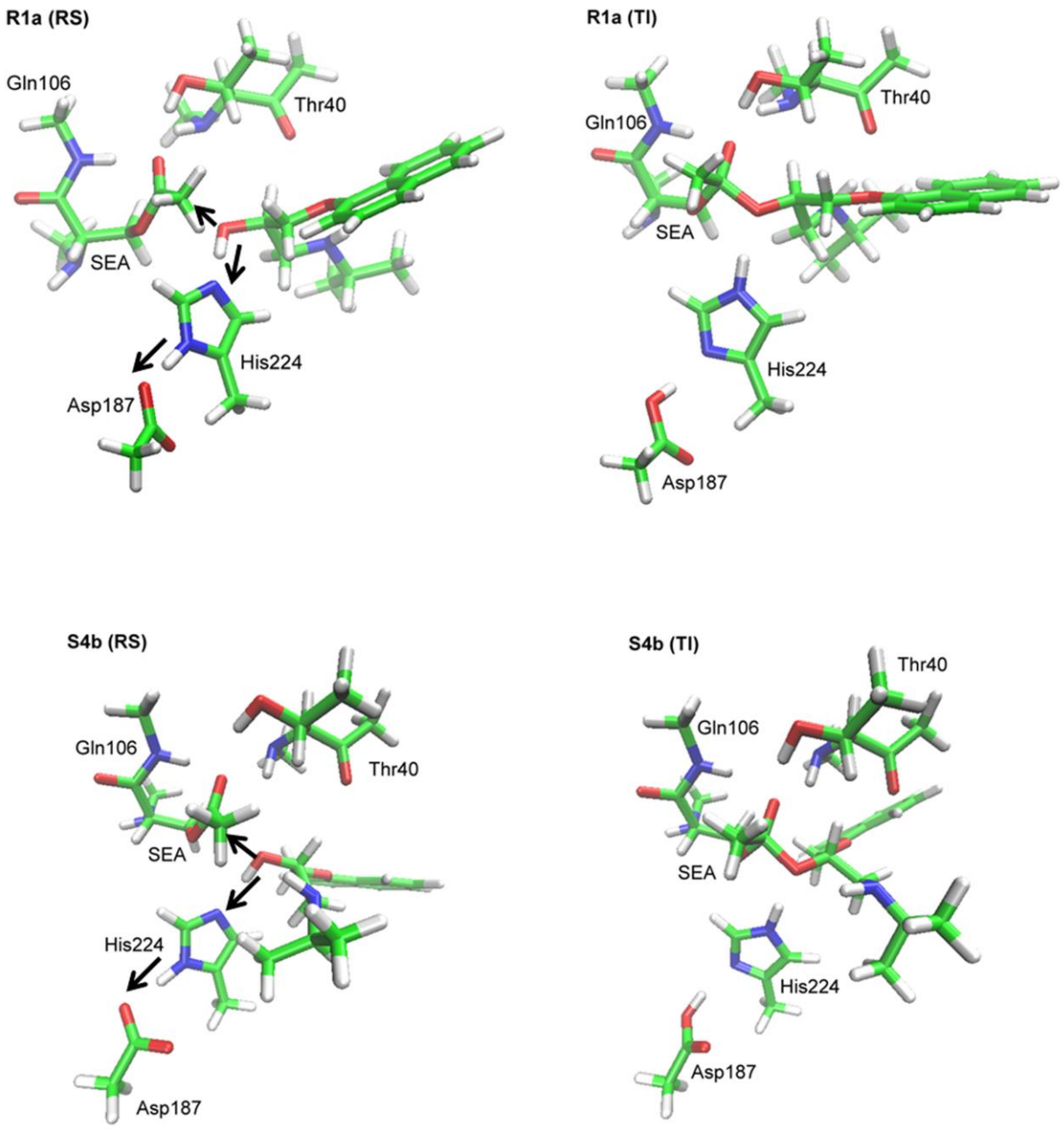

Fig. 31 Optimized reactant state (RS) and the corresponding second tetrahedral intermediate (TI) for the conformer of *R*- and *S*-propranolol with the lower energy barrier.

4.3.2.2. Transformation of R- and S-propranolol in binding mode II

In contrast to the binding mode I, in binding mode II the transformation of *S*-propranolol is favoured over the *R*-propranolol, being the conformer **S4b** that with the lower energy barrier (see **Table 11** and **Fig. 31**). A similar analysis to the given above for the propranolol conformers in binding mode I may be done for the conformers in binding mode II. Thus, the higher energy barrier obtained for **S4a** respect to **S4b** is mainly attributed to the distance of the hydroxyl group of propranolol to execute the

nucleophilic attack, which is 3.52 and 2.55 Å in the RS of **S4a** and **S4b**, respectively (**Table 36** in **Appendix C**). The higher energy barrier obtained for **R3b** respect to the rest of *R*-propranolol conformers in binding mode II is also attributed to the position of the hydroxyl group for the nucleophilic attack (**Table 34** in **Appendix C**). The distance and angle for the nucleophilic attack in the RS of **R3b** are 3.68 Å and 99°, respectively. This distance is larger than the observed in the RS of **R3e** (2.52 Å) and **R3f** (2.73 Å), and is quite similar to that in the RS of **R3d** (3.69 Å). On the other hand, the angle for the nucleophilic attack is similar to that in the RS of **Re** (97°) and **R3f** (94°), and is quite smaller than the angle in the RS of **R3d (**105°). The ideal angle for a nucleophilic attack to a carbonyl carbon is 107° [172]. Others key parameters for the catalytic process which contribute to the observed energy barrier values are: the electrophilicity of the SEA:C atom in the RS, the nucleophilicity of the hydroxyl group of propranolol (this depends on the strength of the His224:Nε-Sub:**H** hydrogen bond, which in turn depends on the Asp187:O_D-His224:H_{ND} hydrogen bond that can increase the basicity of the His224:Nε atom), and the interaction with the oxyanion hole in the RS and the corresponding TI-2.

4.3.2.3. Understanding the enantioselectivity of CalB from the QM calculations

The QM model of the AcCalB-propranolol complexes used was very useful to estimate the reactivity of the different propranolol conformers available to be acetylated by CalB. In general the model gives good results, as they explain the enantioselectivity of the reaction. The energy barriers obtained for the conformers **R3a** (-6.0 kcal/mol) and **S4b** (-4.8 kcal/mol) show that effectively the transformation of *R*-propranolol is favored over the *S*-propranolol. However, it is important to note that this QM model omits many factors that may play an important role for the stabilization or destabilization of the system as the reaction proceeds, such as the interaction of the protein and the substrate with the solvent and the interaction of the substrate with the residues of the protein surrounding. Thus, this QM model offers only a small picture about the origin of the enantioselectivity in the CalB catalyzed acetylation of propranolol. A more precise estimation of the energy barriers involved in this reaction is given in **Chapter 6** by QM/MM calculations.

4.4. Conclusions

The dynamic behaviour of the Michaelis complexes of the deacylation reaction of the *O*-acetylation of propranolol catalyzed by CalB has been studied by multiple molecular dynamics simulations in explicit toluene. The analysis of the MD trajectories shows that different reactive conformations of *R*- and

S-propranolol exist, which may be transformed to the corresponding second tetrahedral intermediate (TI-2). These reactive conformations differ in their temporal stability and ability to reach the corresponding transition states. In Binding mode I, the reactive conformers of *S*-propranolol are temporally more stable and have a better ability to form NACs than those of *R*-propranolol. On the other hand, in binding mode II, reactive conformers of *R*-propranolol are identified, which have a better ability to form NACs than all reactive *S*-propranolol conformers (either in binding mode I or II). This provides an explanation for the preference of CalB to transform *R*-propranolol. The moderate enantioselectivity of CalB may be explained by the frequency of NACs observed for several reactive *S*-propranolol conformers, which is just slightly lower than the frequency of NACs for the *R*-propranolol conformers.

The CH-π interactions established between the naphthyl group of propranolol and the surrounding protein residues are the major source of the stabilization of propranolol with its hydroxyl group near to the catalytic residues. These interactions are in general stronger in the productive complexes of *R*-propranolol than in those of *S*-propranolol. Thus these interactions are expected to play an important role in stabilizing the corresponding transition states involved in the transformation of the *R*-propranolol, enhancing the reactivity of this enantiomer. Based on the strength of their interactions with the naphthyl group of *R*-propranolol, Ile189, Ala282 and Leu278 have been identified as key residues for the enantioselectivity of CalB. Ile189 is particularly important as this residue is involved in CH-π interactions with *R*-propranolol in both binding mode I and II. These results suggest key residues for improving the enantioselective acylation of propranolol catalyzed by CalB, through the rational redesign of CalB.

On the other hand, it has been explored the viability of using a simple gas-phase QM model for computing the energy barriers involved in the transformation of the productive MCCs identified from the MD simulations into the corresponding TI-2. The QM model used resulted to be somewhat artificial. However, it provided valuable information about some factors which may play an important role for the enantioselectivity of the reaction. According to the calculated QM energy barriers, in binding mode I a NAC of *R*-propranolol exists whose transformation into the TI-2 is kinetically favoured over the rest of NACs of *R*- and *S*-propranolol (either in binding mode I or II), which is in agreement with faster transformation of *R*-propranolol observed in experiments. Three factors are identified to be responsible for the lower energy barrier observed for the transformation of *R*-propranolol: a higher electrophilicity of the carbonyl carbon of the acetate group of the acetylated

serine (SEA:C) in the reactant state (RS), a strengthening of the hydrogen bond interactions with the residues of the oxyanion hole as the reaction proceeds to the formation of the TI-2, and the formation of a hydrogen bond interaction between the amino group of propranolol and the –NH function of Thr40 in the TI-2.

Chapter 5. Molecular modeling of the second tetrahedral intermediate (TI-2)

5.1. Overview

Parallel to the MD simulations of the MCCs of the deacylation reaction presented in **Chapter 4** molecular modeling of the second tetrahedral intermediate (TI-2) was carried out in order to get more insights into the enantioselectivity of the reaction in favor of the formation of *R*-*O*-acetyl-propranolol (section **2.3.2**). This is the most used computational approach for rationalisation of the enantioselectivity of lipase catalyzed-reactions, as the tetrahedral intermediates are commonly accepted as transition state (TS) analogues in these reactions (see section **1.4**). As it was done for molecular modeling of the MCCs (**Chapter 3** and **Chapter 4**) a combined docking and MD simulations protocol was used to model the TI-2. The analysis of the simulations was focused on aspects like the protein distortion, the hydrogen bonding patterns which are essential for the catalytic process (**Fig. 32**), and the interactions between the side chains of propranolol and the surrounding protein residues. Based on this analysis the enantioselectivity of the reaction was rationalised and key residues for it were identified. As another result several models of the TI-2 were selected to be used as starting structures for computing the reaction profiles of the deacylation step for the conversion of *R*- and *S*-propranolol into *O*-acetyl-propranolol, which is described in the next chapter.

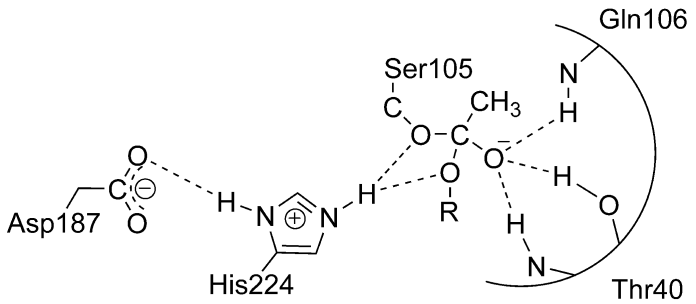

Fig. 32 Schematic view of the second tetrahedral intermediate (TI-2) for the *O*-acetylation of (*R*,*S*)-propranolol catalyzed by CalB. The essential hydrogen bond interactions for the catalytic process are shown in dashed lines. The acylated catalytic serine is referred in the text to as SEA.

5.2. Methodology

Generally speaking, molecular modeling of the TI-2 involved the following stages: covalent docking of *R*- and *S*-propranolol against acetylated CalB (AcCalB), optimization and structural analysis, and finally MD simulations in explicit toluene using different initial velocity distributions for improving the sampling of the conformational space and checking the reliability of the final models.

5.2.1. Docking target (AcCalB)

Molecular modeling of AcCalB was presented in **Chapter 3.** As described in this chapter three AcCalB structures (corresponding to three different orientations of the acyl group into the CalB binding pocket) were tested for modeling of the MCCs. One of these structures (namely, ACE03; **Fig. 17**) was involved in most of the productive MCCs identified for *R*- and *S*-propranolol. Therefore ACE03 was used for the covalent docking of *R*- and *S*-propranolol.

5.2.2. Building the TI-2: covalent docking of *R*- and *S*-propranolol against AcCalB

The TI-2 was built by manual docking and taking into account the torsion angles observed for *R*- and *S*-propranolol in the respective Michaelis complexes (**Chapter 3**). Thereby, conformationally distinct structures were created by varying the dihedral angles shown in **Fig. 33**. During the docking procedure the protein was treated as a rigid body and five water molecules (HOH130, HOH149, HOH238, HOH265 and HOH285) were removed from the binding pocket of CalB to accommodate the substrate. It was ensured that steric contacts with the residues of the binding pocket were avoided and all essential hydrogen bond interactions for the catalytic process were formed (**Fig. 32**).

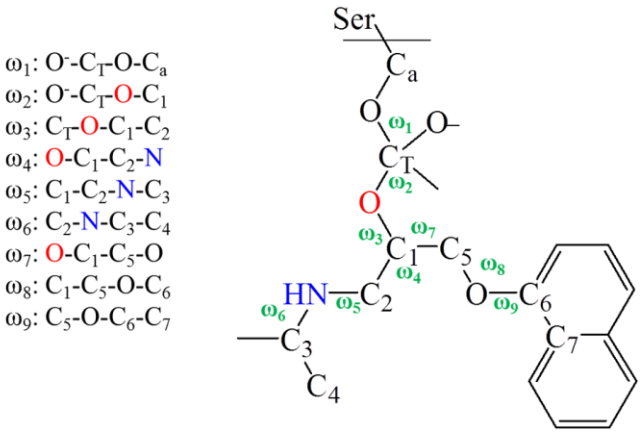

Fig. 33 Torsion angles (ω_1-ω_9) considered for building the TI-2.

5.2.3. Post-docking optimization

The TI-2 structures obtained from the docking procedure were submitted to a careful post-docking optimization, in order to take into account a potential induced fit effect (little displacements in the protein structure due to the presence of the ligand) [164]. Because there are no CHARMM force field parameters for propranolol, a QM/MM approach was used. The QM region corresponded to the Cα atom of the residue Ser105 bound to *R*- or *S*-propranolol, such that Ser105 was truncated at its Cα-Cβ atoms (sp3-hybridized carbon atoms). The QM region was treated by the SCC-DFTB method [165] and the MM region (residual enzyme and crystal waters) by CHARMM force fields. The QM/MM boundary atoms were treated by the Generalized Hybrid Orbital Method (GHO) [189]. Three consecutive energy minimizations were performed by using the same procedure as for the molecular modeling of the MCCs (see section **3.2.2**).

5.2.4. MD simulations of the TI-2

To complement the molecular modeling of the TI-2, the optimized structures were submitted to 1.5 ns of QM(SCC-DFTB)/MM MD simulation in explicit toluene. The QM region corresponded to the Cα atom of the residue Ser105 bound to *R*- or *S*-propranolol and the MM region to the residual enzyme, crystal waters and toluene. For each TI-2 structure two MD simulations with different initial velocity distributions were performed, corresponding to values of the random seed parameter iseed of 314159 and 835. The MD simulations carried out using the iseed value 835 are indicated by *. The same MD setup as for the MD simulations of AcCalB (section **3.2.1.1**) was used, treating the QM region as part of the active region.

5.3. Results and discussion

5.3.1. Docking results

From the docking procedure described in section **5.2.2** six TI-2 structures were identified for both *R*- and *S*-propranolol. These structures were named as TI-R or TI-S to emphasize whether it is the *R* or *S* enantiomer, followed by 1, 2, 3, … according to the order they were created. In four of these structures propranolol is oriented in binding mode I (namely, TI-R1(S1) – TI-R4(S4)) while in the other two it is oriented in binding mode II (namely, TI-R5(S5) – TI-R6(S6)) (**Fig. 34** to **Fig. 35**). The lower number of structures obtained in binding mode II is due to the bulky size of the naphthyl group of propranolol, which is difficult to fit at the medium pocket of CalB avoiding steric contacts with the protein residues.

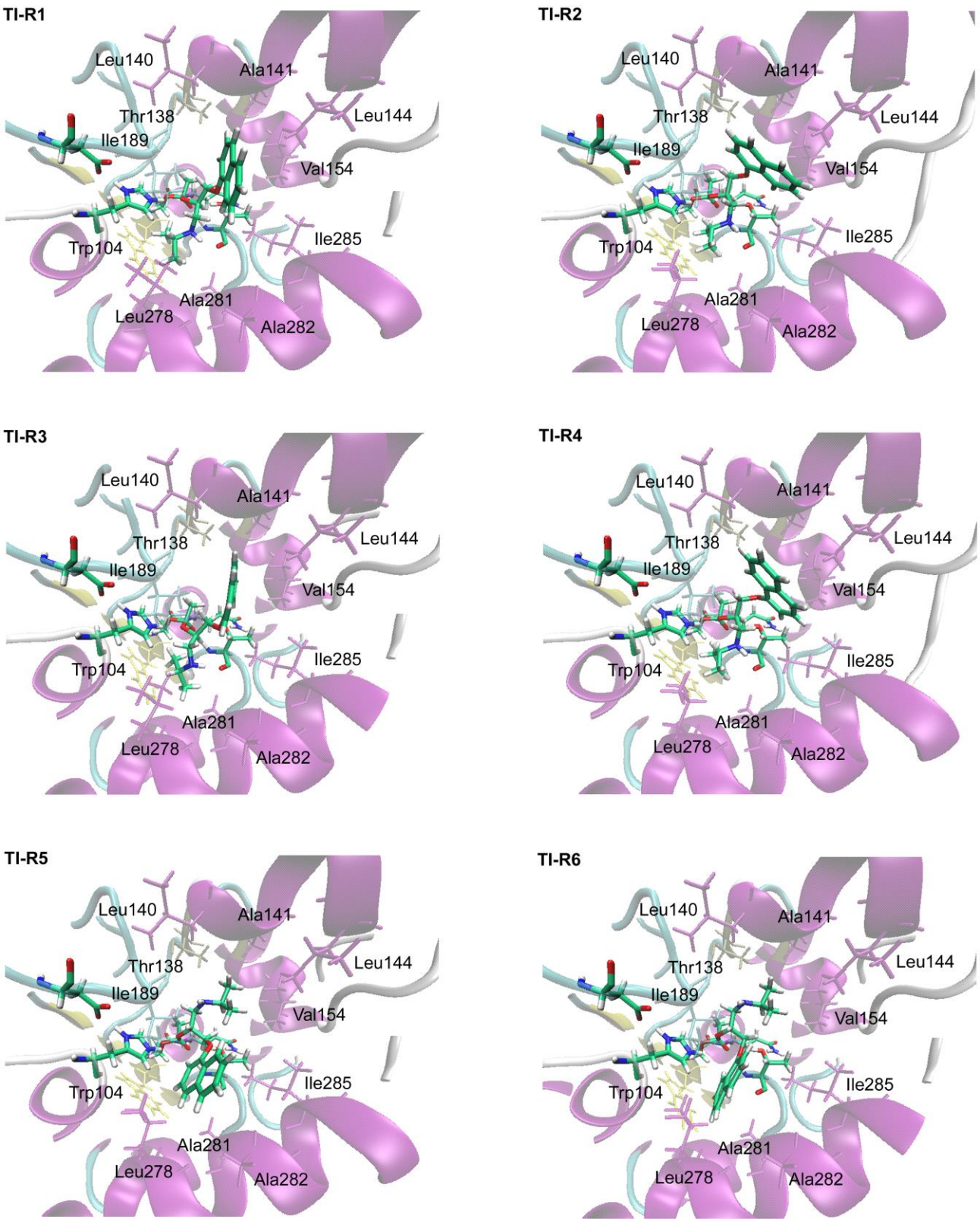

Fig. 34 TI-2 structures of *R*-propranolol after post-docking optimization. The TI-2 and the catalytic triad are shown in licorice with the carbon atoms in green. The residues stabilizing the side chains of propranolol into the binding pocket are also shown in licorice, and with a unique color indicating the secondary structure to which they belong: α-helix (purple), β-conformation (yellow) and loops (cyan).

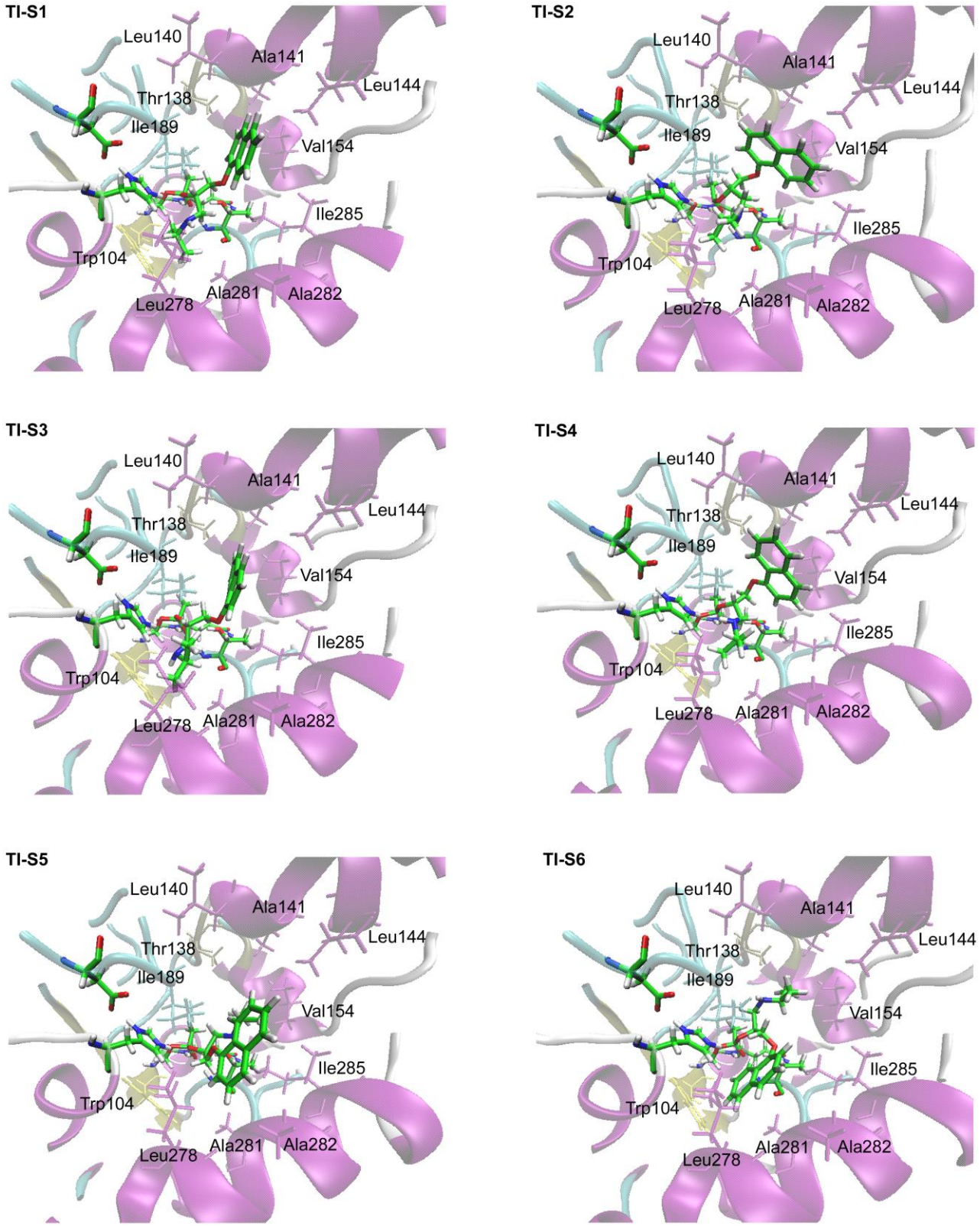

Fig. 35 TI-2 structures of *S*-propranolol after post-docking optimization. The TI-2 and the catalytic triad are shown in licorice with the carbon atoms in green. The residues stabilizing the side chains of propranolol into the binding pocket are also shown in licorice, and with a unique color indicating the secondary structure to which they belong: α-helix (purple), β-conformation (yellow) and loops (cyan).

Post-docking optimization was the first opportunity to judge whether the proposed structures were stable. After optimization these structures were analyzed to determine if they correspond to possible productive binding modes (binding modes of the substrate leading to formation of the product). The analysis was focused on the protein distortion and the essential hydrogen bond interactions for the catalytic process. The latter are the hydrogen bond interactions with the oxyanion hole, the hydrogen bonds between the protonated His224 and the reactive oxygen atoms (the SEA:Oγ atom and the alcohol oxygen of propranolol -Sub:**O**-), and the hydrogen bond between the residues Asp187 and His224 (see **Fig. 32**) [42,126]. As it was done for analysis of the MCCs (following other studies of lipase-catalyzed reactions), a RMSD value less than 3 Å between the initial CalB crystal structure and the final optimized TI-2 was chosen as a limit for considering a TI-2 as productive [170]. As shown in **Appendix D** (**Table 38**) this criterion is satisfied in all TI-2s, as the superimposition of all heavy atoms of the protein in the optimized TI-2s to the CalB crystal structure resulted in RMSD values of only about 0.55 Å, even though the side chains were finally free to move during the optimization. On the other hand, in all optimized TI-2s of *R*- and *S*-propranolol all hydrogen bonds important for the catalytic process are formed (**Table 12**). Thus all of them may be considered as possible productive binding modes.

Interestingly, in all TI-2 structures of *R*-propranolol in binding mode I a hydrogen bond interaction between its amino group and the carbonyl oxygen of Thr40 (Sub:*H*-Thr40:O) is observed, with a distance between 1.85 Å and 2.39 Å. In contrast, this hydrogen bond is only formed in one of the TI-2 structures of *S*-propranolol (in binding mode I), with a distance of 2.52 Å (**Table 12**). This interaction may be partly responsible for the selective acetylation of *R*-propranolol, as it may contribute significantly to the stabilization of the respective TSs (those connecting the MCC with TI-2 and the latter with the PDC). This is similar to the observed for the acetylation of hexane-2,5-diol (a δ-functionalized secondary alcohol) catalyzed by CalB [28].

On the other hand, in the TI-2 structures the naphthoxy and isopropylamine side chains of *R*- and *S*-propranolol are stabilized in their positions in the binding pocket by the respective non-polar residues surrounding them: Trp104, Thr138, Leu140, Ala141, Leu144, Val154, Ile189, Leu278, Ala281, Ala282 and Ile285. It is especially observed that the naphthyl rings of propranolol form CH-π interactions with these residues. Because the strength of a CH-π interaction depends on its distance and directionality (the stronger the interaction, the stronger the trend for the linearity) [183], the contribution of these interactions to the stabilization of the TI-2s vary from one structure to another, due to the

Table 12 Hydrogen bond distances[a] and angles[b] involving the TI-2s of *R*- and *S*-propranolol[c] after post-docking optimization.

TI-2	SEA:O[d]-Gln106:NH	SEA:O[d]-Thr40:NH	SEA:O[d]-Thr40:OH	His224:**H**-SEA:O_γ[e]	His224:**H**-Sub:**O**	Asp187:O_D-His224:H_{ND}	Sub:*H*-Thr40:O
TI-R1	1.81 (164)	1.70 (165)	2.01 (174)	2.19 (125)	1.74 (159)	1.60 (177)	1.85 (149)
TI-R2	1.78 (161)	1.81 (164)	2.11 (174)	2.06 (124)	1.88 (150)	1.64 (174)	2.39 (106)
TI-R3	1.84 (166)	1.64 (165)	2.01 (172)	2.03 (135)	1.84 (143)	1.62 (166)	1.92 (170)
TI-R4	1.81 (162)	1.77 (165)	2.09 (173)	2.12 (124)	1.87 (150)	1.63 (173)	2.02 (128)
TI-R5	1.92 (155)	1.96 (168)	2.07 (174)	2.02 (124)	1.95 (134)	1.67 (171)	7.70
TI-R6	1.89 (150)	2.18 (169)	2.36 (171)	2.17 (116)	2.09 (123)	1.71 (169)	7.76
TI-S1	1.89 (164)	1.66 (166)	1.95 (173)	2.09 (135)	1.80 (144)	1.60 (168)	3.94
TI-S2	1.72 (160)	1.74 (158)	1.89 (175)	1.83 (139)	2.22 (139)	1.65 (171)	2.52 (113)
TI-S3	2.02 (162)	1.76 (173)	2.12 (170)	2.14 (133)	1.98 (128)	1.64 (164)	4.00
TI-S4	1.93 (158)	1.80 (165)	1.91 (175)	1.92 (132)	1.96 (137)	1.65 (171)	4.72
TI-S5	1.80 (166)	1.67 (164)	2.02 (171)	2.03 (129)	1.79 (149)	1.63 (172)	3.98
TI-S6	1.83 (156)	1.90 (164)	1.99 (172)	2.13 (120)	1.97 (144)	1.67 (173)	7.78

[a] Distances are given in Å. A maximum distance of 3 Å was chosen as a limit to be considered a hydrogen bond.
[b] Angles are in degrees (º) and given in brackets.
[c] The atoms corresponding to the amino and hydroxyl group of propranolol (Sub) are shown in italic and bold respectively.
[d] Oxyanion.
[e] Reactive oxygen of the acylated catalytic serine (SEA).

conformational diversity of the TI-2s identified. Thereby these interactions are expected to have an important influence on the stabilization of the corresponding TSs and thus on the enantioselectivity of the reaction. As it was already mentioned in section **5.3.1.3.1(b)** several studies on enantioselective reactions have been reported showing experimental and theoretical evidence of a major stabilization of the TS involved in the transformation of the faster reactant enantiomer by CH-π interactions [184,185].

In the subsequent sections, a detailed analysis of the enzyme-substrate interactions occurring in the optimized TI-2s of *R*- and *S*-propranolol is presented. According to this analysis the TSs involved in the transformation of *R*-propranolol are expected to be better stabilized than those for *S*-propranolol, which is in agreement with faster formation of *R*-*O*-acetyl-propranolol as observed in experiments.

5.3.1.1. Enzyme-substrate interactions in the TI-2s of R- and S-propranolol in binding mode I

In the TI-2 structures of both *R*- and *S*-propranolol in binding mode I, the naphthyl group of propranolol is positioned at the large pocket of CalB in four different orientations, where it is stabilized by the residues Thr138, Leu140, Ala141, Leu144, Ile189 and Ile285, through CH-π interactions. This type of interaction is also formed between the isopropylamine side chain of propranolol and the residue Trp104 at the medium pocket of CalB, most specifically with the six-member ring of this residue, which is in agreement with its energetic preference to form CH-π interactions over the five-member ring [190]. The isopropylamine side chain is also stabilized through hydrophobic interactions by the surrounding aliphatic residues of the medium pocket (namely, Leu278 and Ala281). However, these interactions are similar in all TI-2s in binding mode I and are not expected to have a major influence on the relative stabilization of the TI-2s (i.e. the stabilization of a TI-2 configuration respect to another one) in comparison to the CH-π interactions.

The distances of the CH-π interactions established between the side chains of propranolol and the surrounding non-polar residues, in the TI-2s in binding mode I, are shown in **Fig. 36**. Comparison of the CH-π interactions presented in the TI-2s of *R*-propranolol with those in the corresponding analogues TI-2s of *S*-propranolol (according to the orientation of the naphthyl group) shows that the major differences related to these interactions are observed for TI-R1 and TI-S1 respect to TI-R2 and TI-S2, respectively. In TI-R1 and TI-S1 the naphthyl group of propranolol is oriented pointing toward the entrance of the binding pocket, where it is strongly stabilized through CH-π interactions by the residues Ile189 and Val154; the side chains of these residues (mainly that of Ile189) are partly directed to the center of the naphthyl rings, favoring the formation of CH-π interactions more lineal in

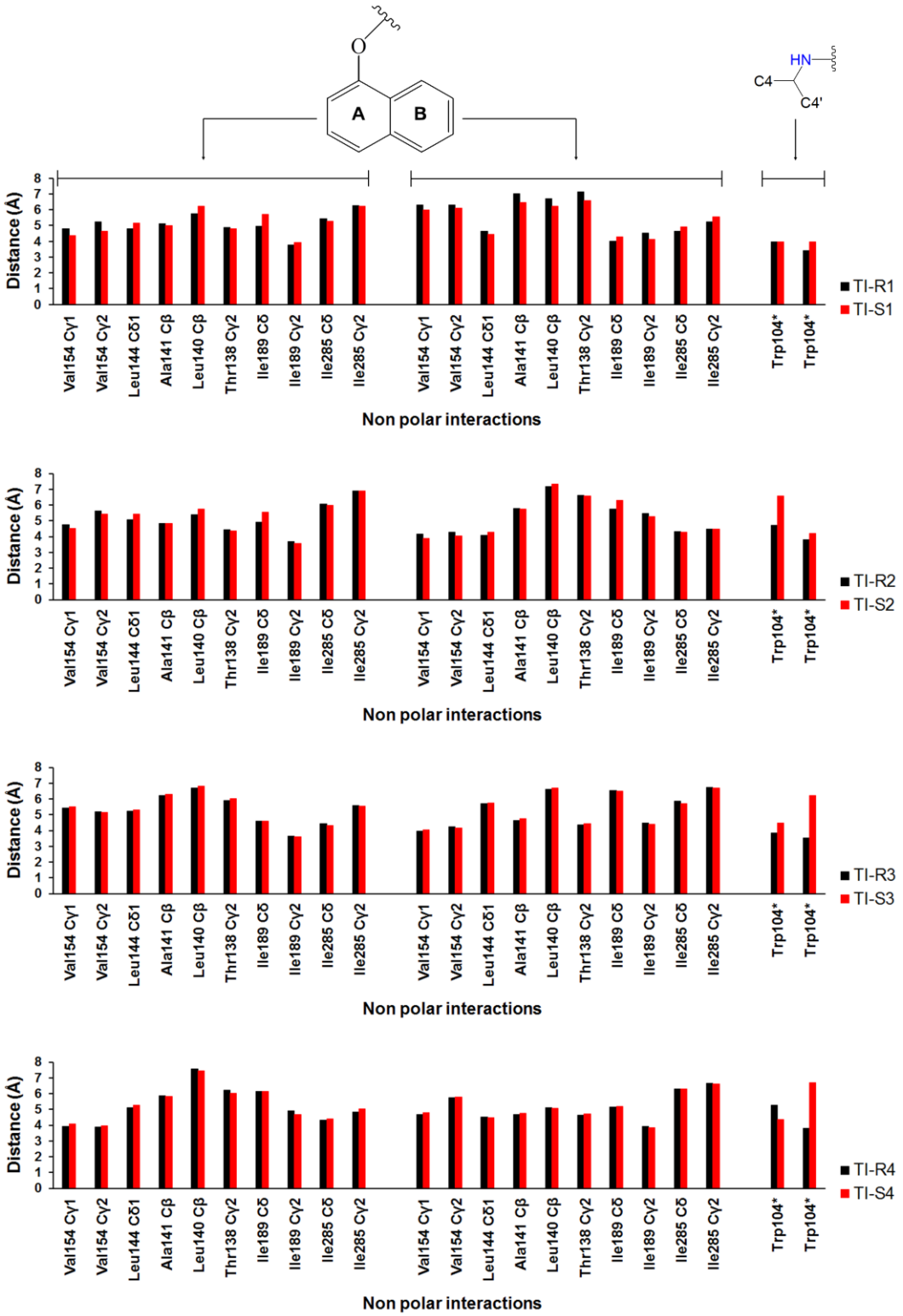

Fig. 36 Distances between the side chains (center of mass of naphthyl rings and the carbon atoms of the isopropyl methyl groups) of *R*- and *S*-propranolol and the surrounding residues of the binding pocket, in the TI-2s in binding mode I after post-docking optimization. Every set of analogues structures (related to the orientation of the naphthyl group) is shown separately. * Center of mass of the six-member ring.

comparison to the other residues at the large pocket. Ile189 stabilizes both naphthyl rings while Val154 interacts mainly with the naphthyl ring A (that which is forming the ether bond in the propranolol molecule). Furthermore, the CH-π interactions with Ile189 are in general stronger in TI-R1 than in TI-S1, while the CH-π interactions with Val154 are stronger in TI-S1. The strongest CH-π interaction with Ile189 in TI-R1 is between the Cγ2 atom of this residue and the center of mass of the naphthyl ring A, with a distance of 3.77 Å. While in TI-S1 the strongest CH-π interaction with Val154 has a distance of 4.35 Å. On the other hand, the CH-π interactions between the isopropyl group of propranolol and Trp104 are slightly stronger in TI-R1. All this plus the additional Sub:*H*-Thr40:O hydrogen bond formed in TI-R1 (**Table 12**) suggest a better stabilization of the corresponding TSs involved in the transformation of TI-R1 respect to those of TI-S1. This would favor in turn the faster transformation of TI-R1 respect to TI-S1.

In TI-R2 and TI-S2, the naphthyl group of propranolol is oriented pointing toward the residues Ile285, Val154 and Leu144. The position of the naphthyl rings in these TI-2s favors the formation of strong CH-π interactions (trend to the linearity) between them and the residues Ala141, Leu144 and Val154. The CH-π interactions between the naphthyl rings and Val154 (through its Cγ1 and Cγ2 atoms) are stronger in TI-S2 than in TI-R2, while the CH-π interactions with Leu144 (through its Cδ1 atom) are stronger in the latter. In contrast, the CH-π interactions with Ala141 are similar in both structures. On the other hand, the CH- π interactions between the isopropyl group of propranolol and Trp104 are quite stronger in TI-R2 than in TI-S2. All this suggests a better stabilization of the TSs involved in the transformation of TI-R2 respect to those of TI-S2, which would lead in turn to a faster transformation of TI-R2 over TI-S2. The Sub:*H*-Thr40:O hydrogen bond is formed in both TI-R2 and TI-S2, therefore it is not considered to have a major effect on the transformation of TI-R2 relative to TI-S2.

In the rest of TI-2s in binding mode I the CH-π interactions between the naphthyl group of propranolol and the surrounding protein residues are similar for both enantiomers. However, the formation of the Sub:*H*-Thr40:O hydrogen bond in TI-R3 and TI-R4 may contribute to a better stabilization of the corresponding TSs involved in the transformation of these TI-2s, favoring their transformations over TI-S3 and TI-S4, in which such hydrogen bond is not formed.

5.3.1.2. Enzyme-substrate interactions in the TI-2s of R- and S-propranolol in binding mode II

In the TI-2s of both propranolol enantiomers in binding mode II, the naphthyl group of propranolol is positioned at the medium pocket of CalB in two distinct orientations (pointing outward or inward the

binding pocket), where it is also stabilized through CH-π interactions, by the nonpolar residues Trp104, Ile189, Leu278, Ala281, Ala282 and Ile285. In contrast to binding mode I, in binding mode II the isopropylamine side chain of propranolol is not forming CH-π interactions and is only stabilized through hydrophobic interactions by the surrounding aliphatic residues of the large pocket. These interactions are similar in all TI-2s in binding mode II. Thus, as in binding mode I, the relative stabilization of the TI-2s in binding mode II is expected to depend mainly on the CH-π interactions established between propranolol and the surrounding protein residues. The distances for these CH-π interactions are shown in **Fig. 37**.

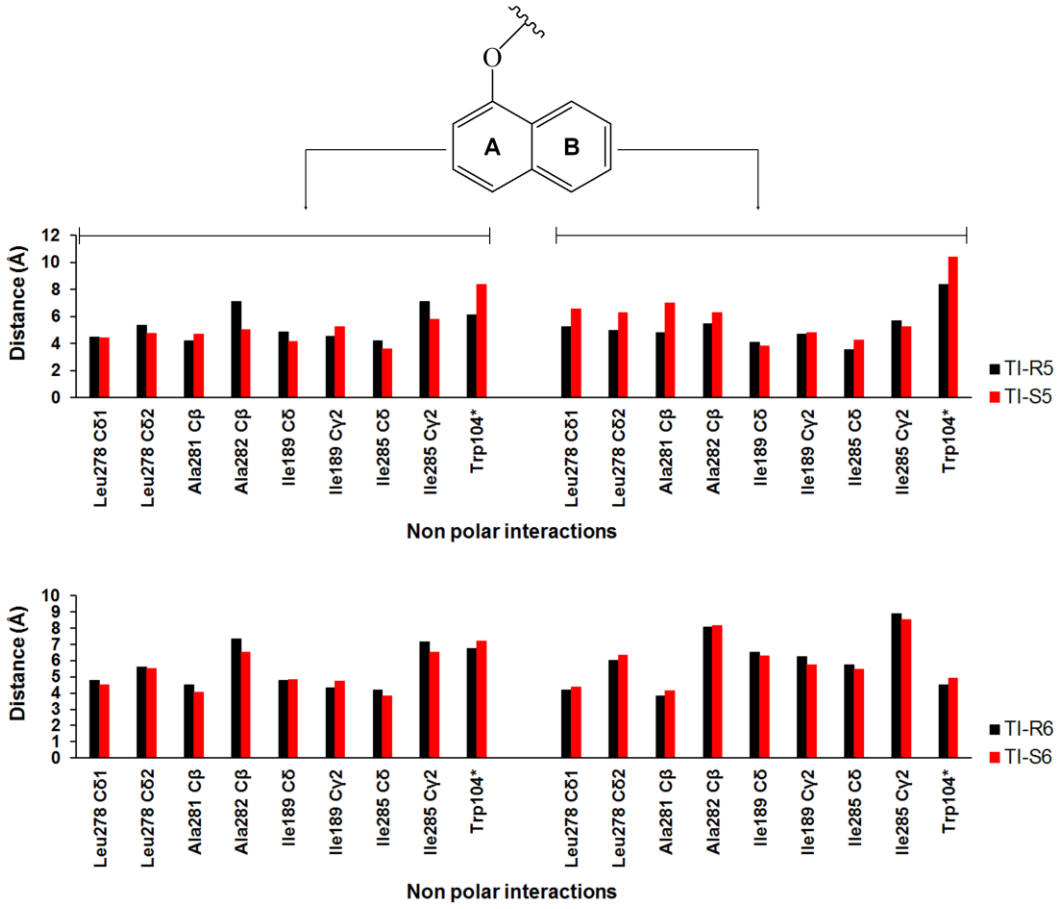

Fig. 37 Distances between the centers of mass of naphthyl rings of *R*- and *S*-propranolol and the surrounding residues of the binding pocket, in the TI-2s in binding mode II after post-docking optimization. Every set of analogues structures (related to the orientation of the naphthyl group) is shown separately. * Center of mass of the six-member ring.

Following the same scheme of analysis used for the TI-2s in binding mode I, the transformation of TI-R5 is expected to be favored over TI-S5. In these TI-2s the naphthyl group of propranolol is

pointing toward the entrance of the binding pocket, but is more exposed toward the entrance of the pocket in TI-S5 than in TI-R5. This affects the strength of the CH-π interactions established with the residues Leu278, Ala281, Ile189 and Trp104. The CH-π interaction between naphthyl ring A and Trp104 is stronger in TI-R5 than in TI-S5. Furthermore, in TI-R5 both naphthyl rings of propranolol are strongly stabilized by Leu278 and Ala281, while in TI-S5 the CH-π interactions between these residues and the naphthyl ring B are partly lost. In addition, considering the orientation of the naphthyl rings in these TI-2s, the CH-π interactions with Ala281 and Ile189 (through its Cγ2 atom) are stronger (more lineal) in TI-R5 than in TI-S5 (see **Fig. 34** to **Fig. 35**). All this suggest a better stabilization of the TSs involved in the transformation of TI-R5 respect to those of TI-S5, which would favor in turn a faster transformation of TI-R5.

In TI-R6 and TI-S6 the naphthyl group of propranolol is oriented toward the interior of the binding pocket. This leads to the formation of CH-π interactions between the naphthyl ring B and the residues Ala281 and Leu278 stronger compared to the naphthyl ring A (based on the linearity of the interactions). In addition, the residue Trp104 forms a CH-π interaction with this ring. In contrast, the residue Ile189 is interacting mainly with the naphthyl ring A. The observed distances for these interactions show TI-R6 to be better stabilized than TI-S6, suggesting a better stabilization of the TSs involved in the transformation of the former.

5.3.2. MD simulations of the TI-2s

To complete the molecular modeling of TI-2, all optimized TI-2s were submitted to 1.5 ns MD simulations in explicit toluene, using different initial velocity distributions. Essentially, the stability of the hydrogen bond interactions relevant for the catalytic process and the dynamic behaviour of the docked substrates were revised. The MD results show that the protein does not undergoes significant conformational changes, as given by the average RMSD values (respect to the CalB crystal structure) considering all heavy atoms of the protein backbone (see **Table 39** in **Appendix D**) The maximal average RMSD values observed for the TI-2s of *R*- and *S*-propranolol are 1.08 ± 0.17 Å and 1.14 ± 0.22 Å, respectively. Related to the stability of the essential hydrogen bond interactions for the catalytic process, some differences are observed for *R*- and *S*-propranolol depending on the binding mode. Furthermore, not all TI-2s are stable throughout the MD simulations. A complete description of the dynamic behaviour of the TI-2s of both propranolol enantiomers is given in the next sections.

5.3.2.1. MD simulations of the TI-2s of R-propranolol

5.3.2.1.1. Stability of the essential hydrogen bonds for the catalytic process in the MD simulations of the TI-2s of R-propranolol

The time evolution of the essential hydrogen bonds for the catalytic process in the MD simulations of the TI-2s of *R*-propranolol is given in **Appendix D** (**Fig. 77** to **Fig. 82**). It can be seen that the hydrogen bond between Asp187 and His224 is stable throughout the MD simulations. Furthermore, the average distance of this hydrogen bond is similar for all TI-2s (1.71-1.75 Å; **Table 13**). The hydrogen bond interactions between the oxyanion and the residues of the oxyanion hole are also stable throughout the MD simulations. However, the average distance of the hydrogen bond with Gln106 (SEA:O-Gln106:NH) is particularly different depending on the binding mode of *R*-propranolol. As shown in **Table 13**, this hydrogen bond is shorter in the TI-2s of *R*-propranolol in binding mode II (1.70-1.71 Å) than in binding mode I (1.98-2.01 Å). This is strongly related to the dynamic behaviour of the hydrogen bonds between the protonated His224 and the reactive oxygen atoms. The alcohol oxygen of propranolol (Sub:**O**) is displaced toward the oxyanion hole in the MD simulations of the TI-2s of *R*-propranolol in binding mode II, leading to that the hydrogen bond between the oxyanion and Gln106 becomes stronger, in order to keep the stabilization of the oxyanion. In turn, the hydrogen bond between the protonated His224 and the Sub:**O** atom (His224:**H**-Sub:**O**) is disrupted in these TI-2s; this interaction has an average distance of 2.09-2.30 Å in the TI-2s in binding mode I and 3.21-3.49 Å in the TI-2s in binding mode II. Meanwhile, the hydrogen bond between the protonated His224 and the SEA:Oγ atom becomes stronger; this hydrogen bond has an average distance of 2.01-2.14 Å in the TI-2s in binding mode I and 1.79-1.81 Å in the TI-2s in binding mode II (see **Fig. 77** to **Fig. 82** in **Appendix D** and **Table 13**).

The disruption of the His224:**H**-Sub:**O** hydrogen bond and the displacement of the Sub:**O** atom toward the oxyanion hole in the TI-2s in binding mode II, show that in this binding mode *R*-propranolol undergoes difficulties for reaching an orientation which allows the reaction to proceed (i.e. to reach the TS leading to formation of the TI-2 from the respective MCC) [28].

5.3.2.1.2. Dynamic behaviour of R-propranolol throughout the MD simulations of their TI-2s

In the MD simulations of the TI-2s of *R*-propranolol in binding mode I two major configurations are identified (TI-R[number]**a** and TI-R[number]**b**), which differ in the orientation of the isopropylamine side chain of propranolol in the medium pocket. Configuration **a** is characterized by the formation of

Table 13 Hydrogen bond distances[a] involving the TI-2s of *R*-propranolol[b] averaged throughout the 1.5 ns MD simulations[c]

TI-2	SEA:O[d]-Gln106:NH	SEA:O[d]-Thr40:NH	SEA:O[d]-Thr40:OH	His224:**H**-SEA:O_γ[e]	His224:**H**-Sub:**O**[f]	Asp187:O_D-His224:H_{ND}	Sub:*H*-Thr40:O
TI-R1	1.99 (0.15)	1.81 (0.14)	1.70 (0.14)	2.14 (0.25)	2.10 (0.31)	1.72 (0.11)	2.69 (0.64)
TI-R1*	1.98 (0.15)	1.82 (0.12)	1.71 (0.12)	2.13 (0.25)	2.14 (0.28)	1.73 (0.11)	2.69 (0.78)
TI-R2	1.99 (0.15)	1.83 (0.15)	1.70 (0.12)	2.05 (0.23)	2.15 (0.28)	1.73 (0.13)	3.30 (1.05)
TI-R2*	1.99 (0.15)	1.81 (0.14)	1.72 (0.13)	2.12 (0.25)	2.09 (0.26)	1.72 (0.11)	3.12 (1.01)
TI-R3	2.01 (0.15)	1.75 (0.11)	1.72 (0.13)	2.03 (0.24)	2.14 (0.33)	1.71 (0.11)	2.81 (0.64)
TI-R3*	1.99 (0.15)	1.75 (0.11)	1.73 (0.13)	2.09 (0.25)	2.09 (0.31)	1.72 (0.11)	5.08 (0.78)
TI-R4	1.99 (0.15)	1.79 (0.15)	1.72 (0.13)	2.04 (0.24)	2.18 (0.37)	1.72 (0.11)	2.73 (0.70)
TI-R4*	1.98 (0.15)	1.81 (0.17)	1.71 (0.13)	2.01 (0.25)	2.30 (0.41)	1.72 (0.11)	3.01 (0.60)
TI-R5	1.70 (0.09)	1.76 (0.12)	1.65 (0.10)	1.80 (0.11)	3.24 (0.31)	1.72 (0.12)	⋯
TI-R5*	1.70 (0.09)	1.78 (0.13)	1.65 (0.10)	1.79 (0.11)	3.23 (0.32)	1.72 (0.12)	⋯
TI-R6	1.71 (0.09)	1.73 (0.10)	1.66 (0.10)	1.79 (0.10)	3.49 (0.22)	1.75 (0.14)	⋯
TI-R6*	1.70 (0.10)	1.79 (0.13)	1.65 (0.10)	1.81 (0.13)	3.21 (0.37)	1.74 (0.13)	⋯

[a] Distances are given in Å. Numbers in brackets correspond to standard deviations from average values. A maximum distance of 3 Å was chosen as a limit to be considered a hydrogen bond.
[b] The atoms corresponding to the amino and hydroxyl group of propranolol (Sub) are shown in italic and bold respectively.
[c] Two MD simulations of each TI-2 were carried out using a different initial velocity distribution as indicated by *.
[d] Oxyanion.
[e] Reactive oxygen of the acylated catalytic serine (SEA).
[f] This hydrogen bond is disrupted when the Sub:**O** atom moves toward the oxyanion hole.

the hydrogen bond between the amino group of *R*-propranolol and Thr40 (Sub:*H*-Thr40:O), while in the configuration **b** this hydrogen bond is missing. Propranolol is switching between these two configurations throughout the MD simulations of these TI-2s, by rotation of the ω_5 dihedral angle of TI-2 (see **Fig. 33**). The Sub:*H*-Thr40:O hydrogen bond is present more than 50 % of the simulation

time in almost all MD simulations of these TI-2s, except in the MD simulation of TI-R3 with the second initial velocity distribution, in which is only present during 96 ps (see **Fig. 83** in **Appendix D**). Particularly, this hydrogen bond is quite stable in the MD simulations of TI-R1, in which is present about 80 % of the simulation time and has an average distance of 2.69 Å (**Table 13**). Thus, the configuration **a** of TI-R1 is temporally more stable than the configuration **a** of the other TI-2s in binding mode I (**Table 14**). Considering only the orientation of the naphthoxy group of propranolol in the large pocket, TI-R1 and TI-R3 are temporally more stable than TI-R2 and TI-R4. This naphthoxy group preserves its initial orientation throughout the MD simulations of TI-R1 and TI-R3, while in the MD simulations of TI-R2 and TI-R4 adopts the orientation observed in TI-R1 (after less than 80 ps) and TI-R3 (after less than 570 ps), respectively (**Table 14**). Interestingly, in the MD simulations of TI-R1 or when it is formed in the MD simulations of TI-R2, the residue Leu140 is reoriented establishing a stronger CH-π interaction with the naphthyl group of propranolol (**Fig. 38**), which remains stable throughout the MD simulations and is therefore not dependent on the observed change on the orientation of the isopropylamine side chain of propranolol during the simulations. This reorientation of Leu140 is expected to contribute to a better stabilization of TI-R1.

The rotation of the ω_5 dihedral angle is also observed in the MD simulations of the TI-2s of *R*-propranolol in binding mode II. This results in the temporal formation of an intramolecular hydrogen bond between the amino and naphthoxy groups of propranolol (Sub:*H*-Sub:O) in the MD simulations of TI-R5 (see **Fig. 84** in **Appendix D**). Thus two configurations are observed, one in which this hydrogen bond is formed (TI-R5a) and one in which is missing (TI-R5b). However, as shown in **Table 14**, TI-R5a is temporally more stable (more than 990 ps) than TI-R5b (less than 500 ps). In contrast, in the MD simulations of TI-R6, distinct configurations (significantly) are not identified. Considering only the orientation of the naphthoxy group of propranolol in the medium pocket, the TI-2s identified in the MD simulations of TI-R5 and TI-R6 are stable throughout the MD trajectories. However, it is important to note that they are different from the starting structures (**Fig. 38**); during heating and equilibration time an structural rearrangement is presented in response to the movement of the Sub:**O** atom toward the oxyanion hole and the interaction of the naphthyl group with the solvent.

Based on the stability of the essential hydrogen bond interactions for the catalytic process observed in the MD simulations of the TI-2s of *R*-propranolol in binding mode I, as well as on the ability of *R*-propranolol to form the Sub:*H*-Thr40:O hydrogen bond in these TI-2s, the transformation of *R*-propranolol is expected to be favored in binding mode I respect to the binding mode II. Particularly,

its transformation is expected to be faster when its naphthyl group is pointing toward the exterior of the binding pocket and its isopropylamine side chain is oriented such that the Sub:*H*-Thr40:O hydrogen bond is formed (TI-R1a). This conclusion is based on the observed temporal stability for TI-R1a in the MD simulations of TI-R1 (about 1200 ps), which is longer in comparison to the observed for the other *R*-propranolol configurations in which the Sub:*H*-Thr40:O hydrogen bond is also formed (**Table 14**) [112].

Table 14 Lifetime[a] (in ps) of the TI-2s of *R*-propranolol identified during the MD simulations[b]

TI-2[c]	Lifetime	Lifetime*
TI-R1a	1175.5	1204.5
TI-R1b	314.5	285.5
TI-R2a[d]	71.4	68.3
TI-R2b[d]	7.6	9.7
TI-R3a	925.6	96
TI-R3b	564.4	1394
TI-R4a[e]	147.7	227.5
TI-R4b[e]	170.3	333.5
TI-R5a[f]	1215.5	995.2
TI-R5b[f]	274.5	494.8
TI-R6[f]	1490	1490

[a] Lifetime corresponds to the simulation time during which each TI-2 is present.
[b] Two MD simulations with different initial velocity distribution were carried out as indicated by *.
[c] In all MD simulations of the TI-2s (except TI-R6) two distinct configurations (a and b) are observed. Configuration a is characterized either by the formation of the Sub:*H*-Thr40:O hydrogen bond (in the TI-2s in binding mode I) or the Sub:*H*-Sub:O hydrogen bond (in TI-R5; binding mode II). The total lifetime of the TI-2s considering only the orientation of the naphthoxy group in the binding pocket is the sum of the lifetimes of the corresponding configurations.
[d] The naphthoxy group is oriented as in TI-R1 after the first 79 ps and 78 ps of the MD simulations with the first and second seed velocity (*), respectively.
[e] The naphthoxy group is oriented as in TI-R3 after the first 318 ps and 561 ps of the MD simulations with the first and second seed velocity (*), respectively.
[f] These TI-2s are different from the corresponding starting structures (see section **5.3.2.1.2** and **Fig. 38**).

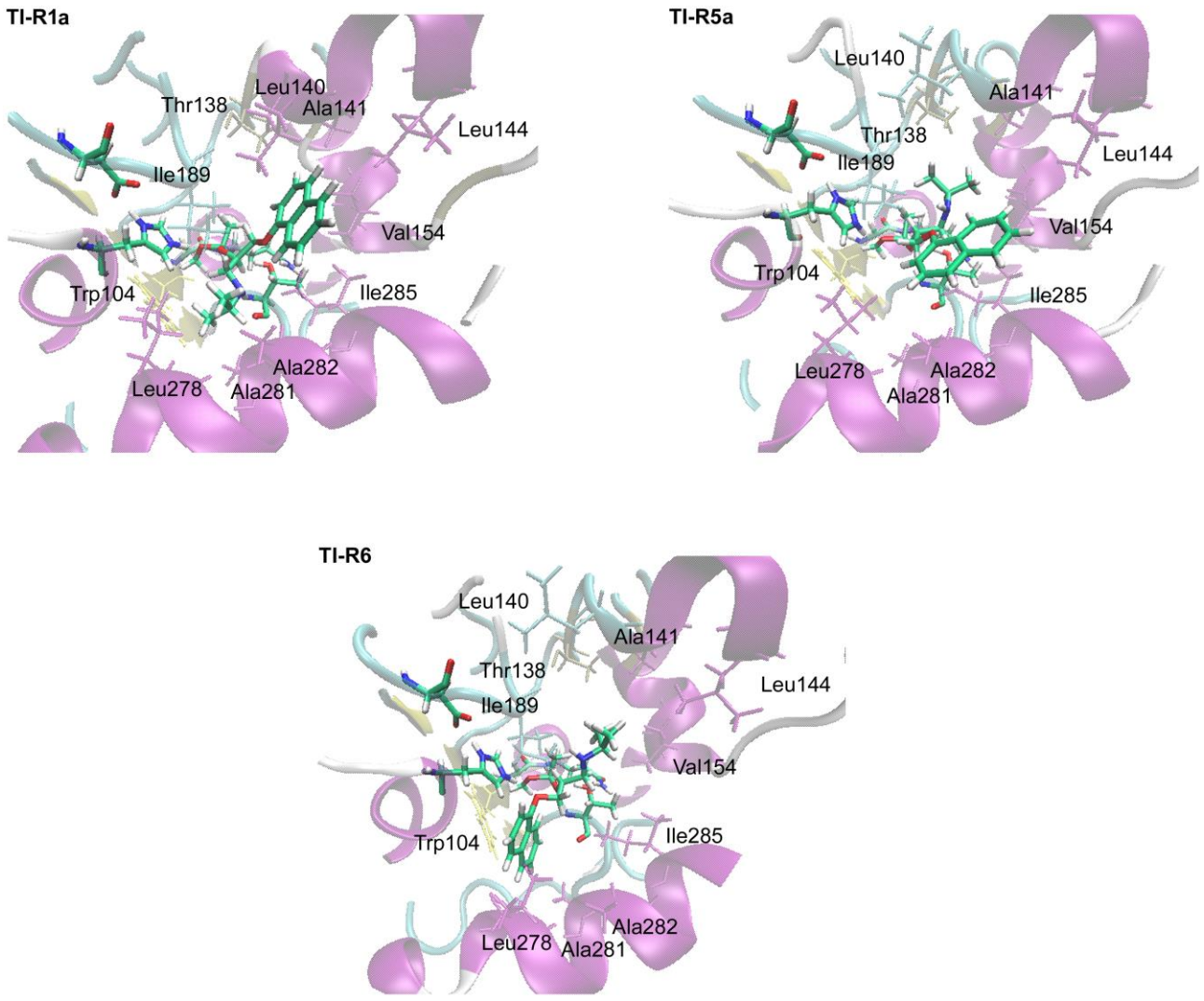

Fig. 38 Most predominant structures of the TI-2s in the MD simulations of TI-R1, TI-R5 and TI-R6. These structures are shown because they are significantly different from the starting structures. In the MD simulations of TI-R1 the residue Leu140 is reoriented establishing a stronger CH-π interaction with the naphthyl rings of propranolol. In the MD simulations of TI-R5 the naphthoxy group of propranolol is moved toward the entrance of the binding pocket. Finally, in the MD simulations of TI-R6 this group is moved toward the interior of the binding pocket. Furthermore, the Sub:**O** atom is displaced toward the oxyanion hole in the MD simulations of TI-R5 and TI-R6.

5.3.2.2. MD simulations of the TI-2s of S-propranolol

5.3.2.2.1. Stability of the essential hydrogen bonds for the catalytic process in the MD simulations of the TI-2s of S-propranolol

The time evolution of the essential hydrogen bonds for the catalytic process in the MD simulations of the TI-2s of *S*-propranolol is shown in **Appendix D** (**Fig. 85** to **Fig. 90**). As found for the TI-2s of

R-propranolol, the hydrogen bond between Asp187 and His224 is stable throughout the MD simulations of the TI-2s of *S*-propranolol and presents a similar average distance in all TI-2s (1.71-1.73 Å; **Table 15**). The hydrogen bond interactions between the oxyanion and the residues of the oxyanion hole are also stable throughout the MD simulations. Furthermore, the average distance of the SEA:O-Gln106:NH hydrogen bond as well as those of the hydrogen bonds between the protonated His224 and the Sub:**O** and SEA:Oγ atoms are observed to be dependent on the movement of the Sub:**O** atom toward the oxyanion hole. However, in contrast with the TI-2s of *R*-propranolol, the Sub:**O** atom is not observed to be displaced toward the oxyanion hole in the MD simulations of the TI-2s of *S*-propranolol in binding mode II but in binding mode I (see **Fig. 85** to **Fig. 90** in **Appendix D** and **Table 15**). This shows that in binding mode I the *S*-propranolol undergoes difficulties for reaching an orientation which allows the reaction to proceed [28], and not in binding mode II as observed for the *R*-propranolol. In addition, in the MD simulations of some TI-2s in binding mode I (TI-S1 and TI-S3) this displacement of the Sub:**O** atom is observed only after more than 45 ps, and not from the beginning of the production phase (after 10 ps) as observed in the MD simulations of the TI-2s of *R*-propranolol in binding mode II. Thus in the MD simulations of TI-S1 and TI-S3 two major configurations are clearly visible, one in which the His224:**H**-Sub:**O** hydrogen bond is formed (configuration i: TI-S[1 or 3]i) and one in which is disrupted due to the displacement of the Sub:**O** atom toward the oxyanion hole (configuration ii: TI-S [1 or 3]ii). In the MD simulations of TI-S3 and that of TI-S1 with the second seed velocity, the configuration i (TI-S3i and TI-S1i, respectively) is stable during less than 190 ps and then the configuration ii (TI-S3ii and TI-S1ii, respectively) is formed. In contrast, in the MD simulation of TI-S1 with the first seed velocity, TI-S1i is stable during 1360 ps and then TI-S1ii is formed (see **Fig. 85** and **Fig. 87** in **Appendix D** and **Table 16**). Since in the MD simulations of TI-S2 and TI-S4 the configuration ii predominates throughout the trajectories (see **Fig. 86** and **Fig. 88** in **Appendix D**), it is expected that among all TI-2s of *S*-propranolol in binding mode I the transformation of TI-S1 will be favored.

5.3.2.2.2. Dynamic behaviour of S-propranolol throughout the MD simulations of their TI-2s

Similar to the observed in the MD simulations of the TI-2s of *R*-propranolol, the orientation of the isopropylamine side chain of *S*-propranolol is observed to be continuously changing throughout the MD simulations of the TI-2s by rotation of the ω_5 dihedral angle. This leads to the temporal formation of the Sub:*H*-Thr40:O hydrogen bond in the MD simulations of the TI-2s of *S*-propranolol in binding mode I (see **Fig. 91** in **Appendix D**), resulting in two major configurations: configuration **a** (TI-S[number]a) -this hydrogen bond is formed- and the configuration **b** (TI-S[number]b) –it is not formed.

Table 15 Hydrogen bond distances[a] involving the TI-2s of *S*-propranolol[b] averaged throughout the 1.5 ns MD simulations[c]

TI-2	SEA:O[d]-Gln106:NH	SEA:O[d]-Thr40:NH	SEA:O[d]-Thr40:OH	His224:**H**-SEA:O_γ[e]	His224:**H**-Sub:**O**[f]	Asp187:O_D-His224:H_{ND}	Sub:*H*-Thr40:O
TI-S1	2.18 (0.26)	1.94 (0.20)	1.68 (0.11)	1.88 (0.18)	2.48 (0.39)	1.72 (0.12)	2.37 (0.47)
TI-S1*	1.71 (0.14)	1.74 (0.12)	1.66 (0.10)	1.81 (0.14)	3.27 (0.36)	1.72 (0.12)	4.10 (1.47)
TI-S2	1.68 (0.09)	1.72 (0.10)	1.67 (0.10)	1.81 (0.12)	3.27 (0.29)	1.73 (0.12)	2.70 (0.66)
TI-S2*	1.67 (0.08)	1.74 (0.11)	1.66 (0.10)	1.78 (0.10)	3.40 (0.21)	1.71 (0.11)	5.49 (0.42)
TI-S3	1.67 (0.12)	1.71 (0.10)	1.68 (0.10)	1.77 (0.10)	3.51 (0.30)	1.73 (0.13)	5.61 (0.47)
TI-S3*	1.72 (0.20)	1.73 (0.12)	1.68 (0.11)	1.80 (0.17)	3.32 (0.54)	1.72 (0.12)	5.49 (0.82)
TI-S4	1.69 (0.09)	1.74 (0.11)	1.66 (0.10)	1.80 (0.11)	3.50 (0.24)	1.72 (0.11)	3.76 (0.98)
TI-S4*	1.68 (0.08)	1.72 (0.10)	1.66 (0.10)	1.81 (0.11)	3.39 (0.28)	1.71 (0.11)	2.87 (0.77)
TI-S5	2.01 (0.16)	1.86 (0.15)	1.71 (0.13)	1.92 (0.19)	2.08 (0.22)	1.72 (0.12)	⋯
TI-S5*	2.01 (0.15)	1.89 (0.15)	1.72 (0.13)	1.92 (0.19)	1.92 (0.20)	1.72 (0.11)	⋯
TI-S6	2.01 (0.15)	1.77 (0.12)	1.72 (0.13)	2.35 (0.31)	2.06 (0.26)	1.71 (0.11)	⋯
TI-S6*	2.03 (0.17)	1.88 (0.17)	1.70 (0.12)	2.39 (0.32)	2.47 (0.37)	1.73 (0.12)	⋯

[a] Distances are given in Å. Numbers in brackets correspond to standard deviations from average values. A maximum distance of 3 Å was chosen as a limit to be considered a hydrogen bond.
[b] The atoms corresponding to the amino and hydroxyl group of propranolol (Sub) are shown in italic and bold respectively.
[c] Two MD simulations of each TI-2 were carried out using a different initial velocity distribution as indicated by *.
[d] Oxyanion.
[e] Reactive oxygen of the acylated catalytic serine (SEA).
[f] This hydrogen bond is disrupted when the Sub:**O** atom moves toward the oxyanion hole.

As shown in **Table 16**, the configuration **b** is temporally more stable than the configuration **a** in almost all MD simulations of the TI-2s in binding mode I. There is only two particular cases in which it is not observed: (1) the MD simulation of TI-S1 with the first seed velocity, in which the configuration TI-S1ia (that in which the His224:**H**-Sub:**O** hydrogen bond interaction is formed –see the previous section-) is temporally more stable (1285.7 ps) than TI-S1ib (74.3 ps); (2) the MD simulation of TI-S4

with the second seed velocity, in which the configuration TI-S4iia is temporally more stable (332.6 ps) than TI-S4iib (257.4 ps). This suggests that *R*-propranolol has a major ability than the *S*-propranolol to form the Sub:*H*-Thr40:O hydrogen bond in the TI-2 (generally speaking). Considering only the orientation of the naphthoxy group of propranolol in the large pocket of CalB, TI-S1 and TI-S3 are temporally more stable than TI-S2. The naphthoxy group preserves its initial orientation throughout the MD simulations of TI-S1 and TI-S3, while in the MD simulations of TI-S2 adopts the orientation observed in TI-S1 after less than 90s. This group also preserves its initial orientation throughout the MD simulation of TI-S4 with the first seed velocity, but in the MD simulation with the second seed velocity adopts the orientation observed in TI-S1 after 590 ps (see **Table 16**). Interestingly, when TI-S1 is formed in the MD simulations of TI-S2 and TI-S4, the Sub:**O** atom remains displaced toward the oxyanion hole (configuration ii) throughout the MD simulations (more than 60 % of the simulation time; see **Fig. 86** and **Fig. 88** in **Appendix D**). This shows that in binding mode I the preferred configuration of the TI-2s of *S*-propranolol is in fact the configuration ii, even though in the MD simulation of TI-S1 with the first seed velocity the configuration i is found to be stable during 1360 ps, since finally after this time the configuration ii is formed (see previous section).

Related to the TI-2s of *S*-propranolol in binding mode II, the rotation of the ω_5 dihedral angle results in the temporal formation of an intramolecular hydrogen bond between the amino and naphthoxy groups of propranolol (Sub:*H*-Sub:O) in the MD simulations of TI-S5 (see **Fig. 92** in **Appendix D**), similar to the observed in the MD simulations of TI-R5 (analogue structure of TI-S5). Thus two configurations are observed, one in which this hydrogen bond is formed (TI-S5a) and one in which is missing (TI-S5b). However, as shown in **Table 16**, TI-S5b is temporally more stable (more than 870 ps) than TI-S5a (less than 620 ps). This shows that the *R*-propranolol has a major ability to form this hydrogen bond, as TI-R5a is stable by more than 900 ps (see **Table 14**). Meanwhile, in the MD simulations of TI-S6, distinct configurations (significantly) due to the rotation of the ω_5 dihedral angle are not identified. But, interestingly, in the MD simulation of TI-S6 with the second seed velocity two configurations are identified due to the rotation of the ω_9 dihedral angle of TI-2 (see **Fig. 33**) after 1293 ps (see **Table 16**). The most predominant structures in the MD simulations of TI-S5 and TI-S6 are shown in **Fig. 39**, as they are different from the starting structures respect to the orientation of the naphthoxy group in the medium pocket of CalB; similar to the observed for the *R*-propranolol in binding mode II, during heating and equilibration time a structural rearrangement is presented, which is mainly attributed to the presence of the solvent.

Table 16 Lifetime[a] (in ps) of the TI-2s of *S*-propranolol identified during the MD simulations[b]

TI-2[c]	Lifetime	Lifetime*
TI-S1ia	1285.7	1.4
TI-S1ib	74.3	68.6
TI-S1iia	61	582.8
TI-S1iib	69	837.2
TI-S2iia[d]	0.6	0.8
TI-S2iib[d]	76.4	42.2
TI-S3ia	3.4	21.4
TI-S3ib	31.6	161.6
TI-S3iib	1455	1307
TI-S4iia[e]	504.3	332.6
TI-S4iib[e]	985.7	257.4
TI-S5a[f]	616.3	491.5
TI-S5b[f]	873.7	998.5
TI-S6i[f]	1490	1283
TI-S6ii[f]	0	207

[a] Lifetime corresponds to the simulation time during which each TI-2 is present.
[b] Two MD simulations with different initial velocity distribution were carried out as indicated by *.
[c] Different configurations of the TI-2s are identified throughout the MD simulations. In the TI-2s in binding mode I the configuration i is characterized by the formation of the His224:**H**-Sub:**O** hydrogen bond, while in the configuration ii this hydrogen bond is disrupted as the Sub:**O** atom is displaced toward the oxyanion hole. In turn, the configuration a (ia or iia) is characterized by the formation of the Sub:*H*-Thr40:O hydrogen bond. By the other hand, TI-S5a is characterized by the formation of the Sub:*H*-Sub:O hydrogen bond. The total lifetime of the TI-2s TI-S1 to TI-S5 considering only the orientation of the naphthoxy group of propranolol in the binding pocket is the sum of the lifetimes of the corresponding configurations. Meanwhile, configurations i and ii of TI-S6 differ on the orientation of the naphthoxy group at the medium pocket.
[d] The naphthoxy group is oriented as in TI-S1 after the first 77 ps and 43 ps of the MD simulations with the first and second seed velocity (*), respectively.
[e] The naphthoxy group is oriented as in TI-S1 after the first 590 ps of the MD simulation with the second seed velocity (*).
[f] These TI-2s are different from the corresponding starting structures (see section **5.3.2.2.2** and **Fig. 39**).

Based on the stability of the essential hydrogen bond interactions for the catalytic process, the transformation of the *S*-propranolol is expected to be favored in binding mode II respect to the binding mode I. However, as it was mentioned in section **5.3.2.2.1** an important transformation of TI-S1 is also expected.

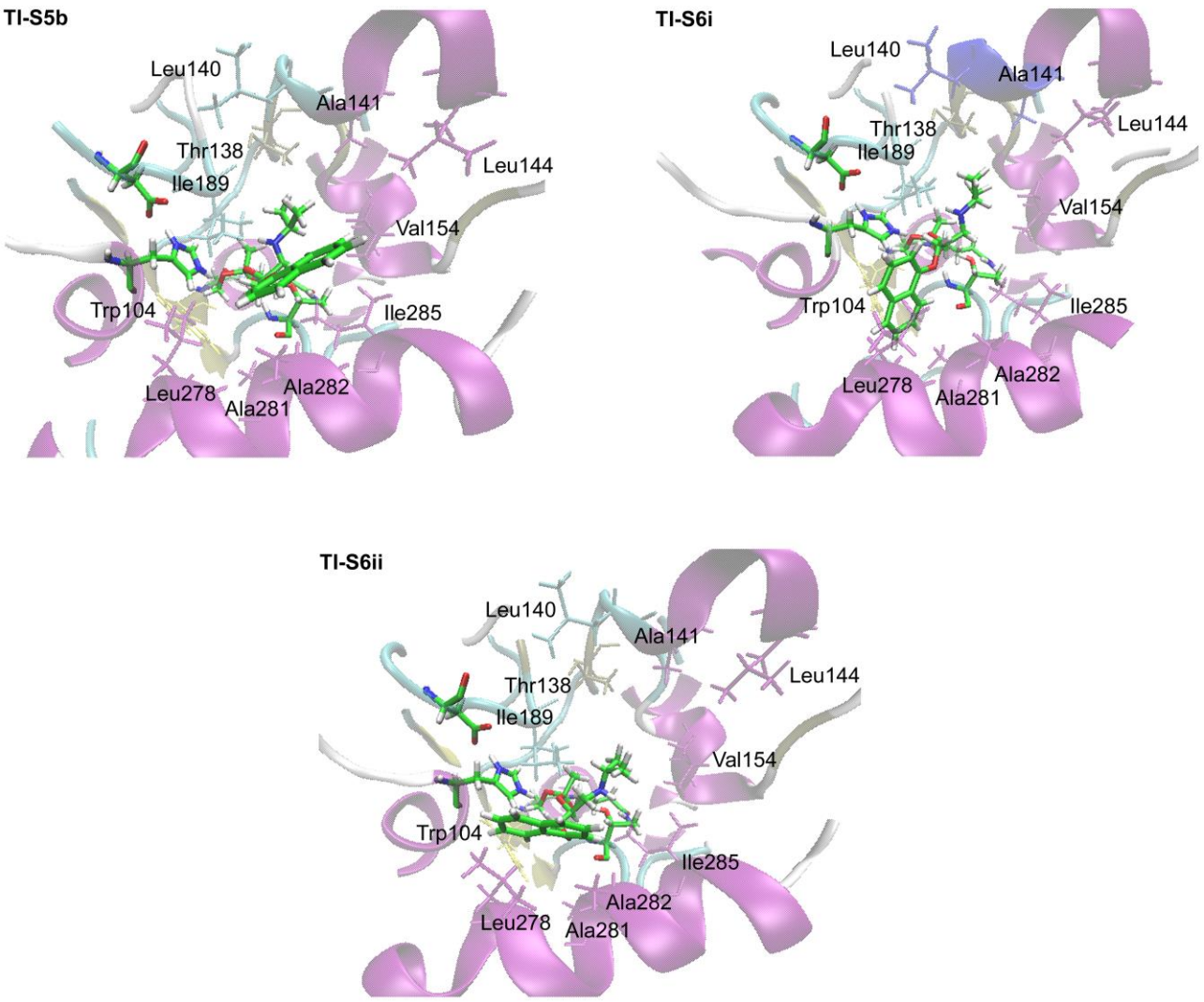

Fig. 39 Most predominant structures of the TI-2s in the MD simulations of TI-S5 and TI-S6. These structures are shown because they are significantly different from the starting structures. In the MD simulations of TI-S5 the naphthoxy group of propranolol is oriented parallel to the Leu278-Ala287 helix (helix α10). In the MD simulations of TI-S6 two configurations differing on the orientation of the naphthoxy group at the medium pocket of CalB are identified (TI-S6i and TI-S6 ii). In TI-S6i the naphthoxy group is oriented toward the interior of the pocket. TI-S6ii is generated from TI-S6i by rotation of the ω_9 dihedral.

5.3.2.3. Explaining the enantioselectivity from the MD simulations of the TI-2s

The MD simulations of the TI-2s show that in binding mode II *R*-propranolol undergoes difficulties to reach an orientation in which the reaction may proceed. The same is observed for the *S*-propranolol in binding mode I. Therefore, the competition between *R*- and *S*-propranolol to be transformed by CalB is expected to occur mainly via *R*-propranolol in binding mode I and *S*-propranolol in binding mode II. This explains (at least partly) the enantioselectivity of the reaction, as in binding mode I the amino

group of *R*-propranolol is able to forms a hydrogen bond with the carbonyl oxygen of Thr40 (Sub:*H*-Thr40:O), which may play an important role on stabilizing the TI-2s and the corresponding TSs. On the other hand, even though an important transformation of *S*-propranolol in binding mode I may occurs via TI-S1, its specular binding mode (TI-R1) is better stabilized by the surrounding protein residues through CH-π interactions, as shows the analysis of these interactions in the corresponding optimized TI-2s (see section **5.3.1.1**). Furthermore, in the MD simulations of TI-R1 the residue Leu140 is reoriented to form a stronger CH-π interaction with the naphthyl group of propranolol (**Fig. 38**), which is not observed in the MD simulations of TI-S1. Thus a faster transformation of TI-R1 respect to TI-S1 is expected. All this reinforces the previous conclusion about that these CH-π interactions may play an important role for the enantioselectivity of the reaction.

5.4. Conclusions

The TI-2 of the *O*-acetylation of (*R,S*)-propranolol catalyzed by CalB was studied by using a combined docking and MD simulations protocol. As it was found from molecular modeling of the MCCs, several conformers of *R*- and *S*-propranolol were identified which may be transformed by CalB to *O*-acetyl-propranolol. Interestingly, in the MD simulations of the TI-2s of *R*- and *S*-propranolol in binding mode II and I, respectively, a displacement of the alcohol oxygen of propranolol (Sub:**O**) toward the oxyanion hole is observed, which leads to the disruption of the hydrogen bond between the protonated His224 and the Sub:**O** atom (His224:**H**-Sub:**O**) in these TI-2s. This reveals that *R*- and *S*-propranolol undergo difficulties to reach the TS which leads to formation of the TI-2 when they are oriented in these binding modes. Thereby the enantioselectivity of the reaction is expected to be mainly originated from the competing transformation of *R*-propranolol in binding mode I and *S*-propranolol in binding mode II. The enantioselectivity of the reaction is thus attributed to the ability of the amino group of *R*-propranolol to form a hydrogen bond interaction with Thr40 in binding mode I, which may contribute significantly to the stabilization of the TSs. Moreover, the conformers of *R*-propranolol are found to be better stabilized than those of *S*-propranolol by the surrounding residues of the CalB binding pocket through CH-π interactions, which may enhance the reactivity of *R*-propranolol. Several residues are identified as key for the enantioselectivity, which constitute guide elements for improving the enantioselective synthesis of *S*-propranolol through a rational redesign of CalB. Particularly, the residue Ile189 is considered to be very important for the enantioselectivity, as the orientation of its side

chain facilitates the formation of CH-π interactions with the naphthyl rings of propranolol stronger in comparison to the other residues of the binding pocket.

Chapter 6. Reaction energy profiles: QM/MM calculations

6.1. Overview

In the precedent chapter the TI-2 of the *O*-acetylation of (*R*,*S*)-propranolol catalyzed by CalB was studied by combined docking and MD simulations. Valuable qualitative information about the origin of the enantioselectivity of CalB in favor of the formation of *R*-*O*-acetyl-propranolol was obtained from these simulations. To complete the computational study of this reaction the energy profile of the deacylation step was computed for several configurations of the TI-2 by using QM/MM calculations. This allowed calculating the reaction barriers for the conversion of *R*- and *S*-propranolol to *O*-acetyl-propranolol. In QM/MM geometry optimizations and reaction path calculations, it was essentially applied density functional theory (B3LYP/TZVP) to describe the QM region while the MM region is represented by CHARMM force fields. Semi-empirical methods (AM1, PM3, MNDO, OM2 and OM3) and the SCC-DFTB method were tested in addition. Moreover the electrostatic influence of individual aminoacids on the reaction profiles was calculated by a perturbation approach. The results of these calculations are analyzed in this chapter.

6.2. Methodology

Representative snapshots of TI-2 were taken from the MD simulations carried out in **Chapter 5** to be used as starting point for the QM/MM calculations (see **Fig. 40a**). The chosen QM/MM methodology is analogous to that used in other studies on enzymatic reactions [191,192]. The QM/MM calculations were performed with the ChemShell package [193]. QM/MM geometry optimizations were carried out with the hybrid delocalized internal coordinates optimizer (HDLCopt) [194]. The QM part of the system was treated at different levels of theory: (a) density functional theory -DFT- (BP86 [195–199], B3LYP [195–197,200], M06 [201], M06-2X [201] and wB97XD [202] functionals) with the TZVP [203] basis set, (b) semiempirical methods (AM1 [204], PM3 [205,206], MNDO [207], OM2 [208,209] and OM3 [179,210]) and (c) the SCC-DFTB [165] method. The BP86 and B3LYP functionals were applied using the TURBOMOLE 6.3 program [211], while in the case of the M06, M06-2X and

wB97XD functionals the Gaussian09 program [178] was used. The calculations with semiempirical methods and SCC-DFTB were done using MNDO2005 [212]. The energy and gradients of the MM part were computed by the DL_POLY code [213] applying the CHARMM22 force field. An electrostatic embedding scheme [214] was adopted incorporating the MM point charges into the one-electron Hamiltonian during the QM calculation. To treat the QM/MM boundary hydrogen link atoms with the charge shift model were employed [215,216]. No cutoffs were applied for the nonbonding MM and QM/MM interactions.

The QM region consisted of the catalytic residues Asp187, His224 and the Ser105 covalently bound to propranolol (**Fig. 40b**). The included residues were truncated at their Cα−Cβ bonds (sp3-hybridized carbon atoms). The total charge of the QM region was -1. During the QM/MM geometry optimizations, the active region to be optimized (**Fig. 40a**) included all QM atoms as well as all residues, crystal waters and toluene molecules of the MM region within 7 Å of the QM region. This radius was chosen such that all enzyme residues around the binding pocket and some toluene molecules surrounding the substrate were part of the active region.

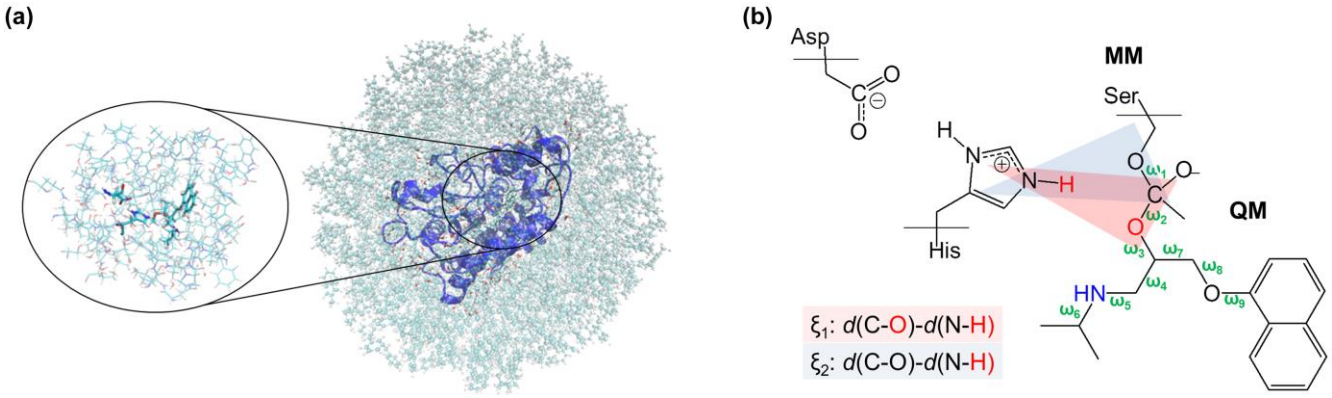

Fig. 40 (a) Representative snapshot of the TI-2 system. The active region in the QM/MM calculations is enlarged on the left with the QM region highlighted. (b) QM region and reaction coordinates (ξ_1 and ξ_2) used in the QM/MM calculations: ξ_1 and ξ_2 lead from TI-2 to the corresponding MCC and PDC, respectively. Torsion angles leading to distinct orientations of TI-2 into the CalB binding pocket are shown in green (ω_1-ω_9). Atoms coming from hydroxyl group of propranolol are marked in red.

Reaction paths were scanned by performing constrained optimizations along properly defined reaction coordinates (see **Fig. 40b**) in steps of 0.1-0.2 Å. This provided starting structures for subsequent full optimization of all relevant stationary points. In the case of minimizations the low-memory Broyden-Fletcher-Goldfarb-Shanno (L-BFGS) algorithm was employed [217,218]. While the microiterative

optimizer combining both the partitioned rational function optimizer [219,220] (P-RFO) and L-BFGS was used during the transition state search. All these algorithms are implemented in the HDLCopt module of ChemShell. Frequency calculations performed for the QM region confirmed that all optimized transition states are characterized by a single imaginary frequency and a suitable transition vector that corresponds to the investigated reaction. Subsequent intrinsic reaction coordinate (IRC) calculations and visual inspection ensured that the TS is indeed connected to the proper minima by a continuous pathway.

QM/MM geometry optimizations at the DFT level were essentially carried out using the B3LYP functional. The BP86 functional was only used for an initial optimization of the TI-2 structures selected from the MD trajectories, in combination with the resolution of the identity (RI) approximation [221,222]. The TI-2 structures were then reoptimized at the B3LYP level before using them in the subsequent B3LYP/CHARMM pathway explorations. To check the influence of dispersion the stationary points were subjected to single-point calculations at the B3LYP level applying empirical dispersion corrections for DFT [223] (DFT-D2 and D3). Single-point calculations were also carried out using the M06, M06-2X and wB97XD density functionals for further validation using modern functionals that performs particularly well for main-group thermochemistry and kinetics. Furthermore, the electrostatic contribution of different amino acids on the reaction barriers was estimated by deleting their MM partial charges in additional single-point calculations. Finally, for the purpose of comparison, single-point pure QM calculations were performed at the B3LYP/TZVP level in the gas phase for the QM region.

To complement the work, relaxed QM potential energy surface (PES) scans at the B3LYP/TZVP level along the dihedral angles of a propranolol model (*R*-1-methyl-3-(1-naphthoxy)-2-propanol) (**Fig. 41**) were carried out. This was done to identify the local minima for the dihedral angles of the naphthoxy side chain of propranolol, which allowed evaluating the influence of small variations of these dihedral angles as the reaction proceeds on the reaction profiles.

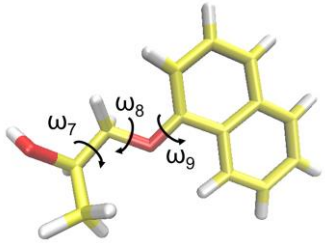

Fig. 41 *R*-1-methyl-3-(1-naphthoxy)-2-propanol. ω_7- ω_9 are the dihedrals of interest for the PES scans.

6.3. Results and discussion

6.3.1. QM/MM reaction paths for the transformation of *R*-propranolol

The QM/MM reaction profiles for the transformation of *R*-propranolol were computed for a total of four configurations of TI-2, two in binding mode I and two in binding mode II. These TI-2s are referred to as ORI-ORIV, respectively (see **Fig. 42**)**.** In the TI-2s in binding mode I (ORI and ORII) the naphthyl group of propranolol is forming CH-π interactions with the residues at the large pocket of CalB (Leu140, Ala141, Leu144, Val154 and Ile189). In these TI-2s this naphthyl group is practically positioned in the same plane, but pointing toward the entrance of the pocket in ORI and toward the interior of the pocket in ORII. Thus in ORI the naphthyl rings of propranolol are in a better position to form CH-π interactions with the surrounding protein residues. Meanwhile, the isopropylamine side chain of propranolol is oriented such that a hydrogen bond between the amino group of propranolol and the carboxyl oxygen of Thr40 (Sub:*H*-Thr40:O) is formed in both ORI and ORII. In addition, its isopropyl group is forming hydrophobic interactions with the residues at the medium pocket (Leu278, Ala281 and Ala282), and a CH-π interaction with Trp104. The latter is stronger in ORI.

In the TI-2s in binding mode II (ORIII and ORIV) the naphthyl group of propranolol is forming CH-π interactions with the residues at the medium pocket of CalB. However, this naphthyl group is exposed to the solvent in ORIII, while it is hindered in ORIV. Furthermore, it is observed to be in a more relaxed configuration and interacting through CH-π interactions with more protein residues in ORIII. Meanwhile, the isopropylamine side chain of propranolol is oriented toward the entrance of the binding pocket in ORV and toward the interior of the binding pocket in ORIII. In both TI-2s this side chain is stabilized by the nonpolar residues at the large pocket through hydrophobic interactions. Moreover, in ORIII it is oriented such that an intramolecular hydrogen bond between the amino and naphthoxy groups of propranolol (Sub:*H*-Sub:O) is formed. On the other hand, ORIV also significantly differs from ORIII about the hydrogen bond between the protonated His224 and the alcohol oxygen of propranolol (His224:**H**-Sub:**O**); this hydrogen bond is larger in ORIII (3.09 Å) than in ORIV (1.69 Å), as the Sub:**O** atom is slightly displaced toward the oxyanion hole in ORIII (its preferred orientation in the TI-2s of *R*-propranolol in binding mode II as observed in the MD simulations –see section **5.3.2.1.1**-). As delineated later this contributes to significant differences between the reaction profiles obtained for these TI-2s. It was also tried a configuration of ORIV in which the Sub:**O** atom was slightly displaced toward the oxyanion hole, but attempts to connect the MCC to the TI-2 starting from this configuration failed and were not followed further.

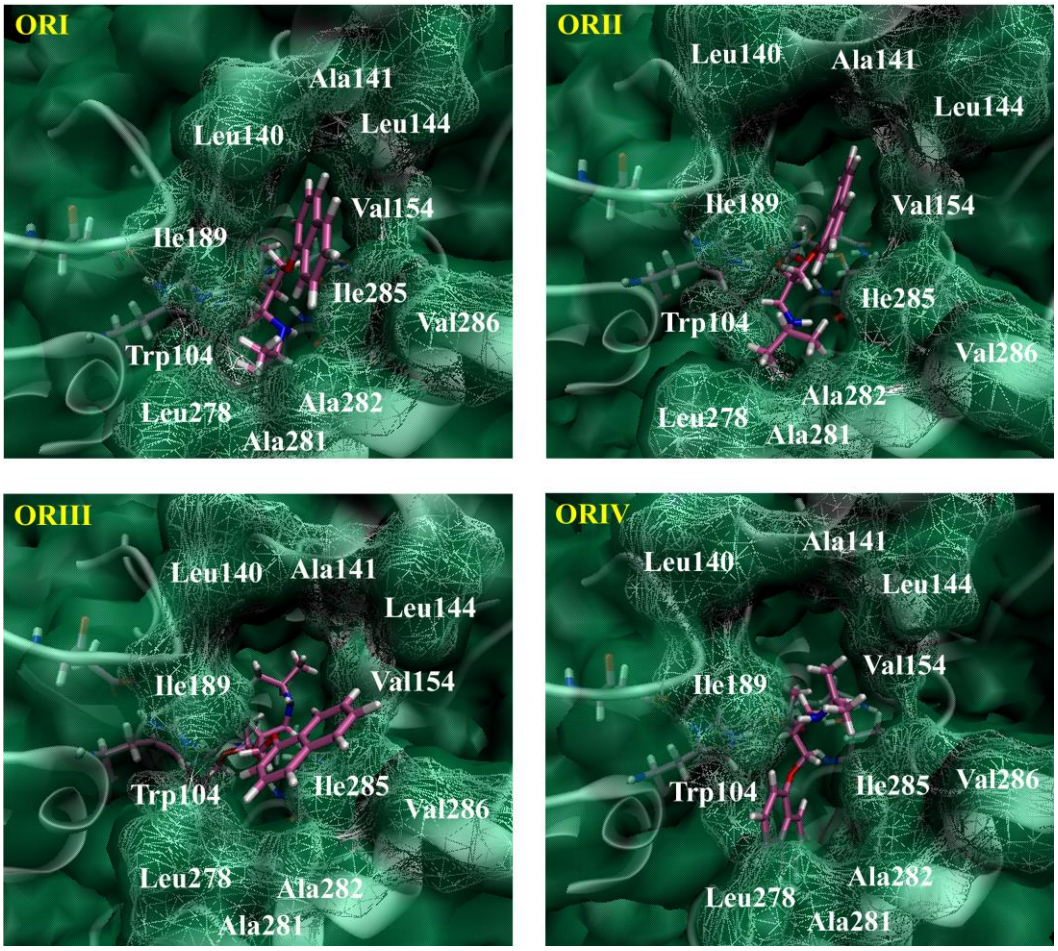

Fig. 42 Second tetrahedral intermediates for *R*-propranolol in binding mode I (ORI-ORII) and binding mode II (ORIII-ORIV), optimized at the QM(B3LYP/TZVP)/CHARMM level. Protein residues surrounding the substrate are shown in wireframe surface (white). The substrate, catalytic triad and oxyanion hole are in licorice.

6.3.1.1. Reaction profiles for the transformation of R-propranolol in binding mode I

The QM(B3LYP/TZVP)/CHARMM energy profiles for the transformation of *R*-propranolol via the TI-2s ORI and ORII are shown in **Fig. 43**. They are more or less similar. In both cases the initial phase of the deacylation reaction is the rate-limiting step, which is the formation of TI-2 from the MCC via a first TS (TS1). The energy barriers for the formation of the TI-2s ORI and ORII are similar (7.1 kcal/mol and 6.5 kcal/mol, respectively), thus the formation of ORII is kinetically favored over ORI just by 0.6 kcal/mol. However, a better stabilization of ORI respect to ORII is observed, as their energies (relative to their respective MCCs) are 0.5 kcal/mol and 3.2 kcal/mol, respectively. In the second step of the deacylation reaction (formation of the PDC from the TI-2 via a second transition state -TS2-), the energy barrier for the transformation of ORI to its respective PDC is 1.1 kcal/mol higher relative to ORII. This is due to the major stabilization of ORI respect to ORII, because the

relative energy of TS2 for ORI is lower (4.6 kcal/mol) than that of TS2 for ORII (6.2 kcal/mol). In other words, ORI acts as a thermodynamic sink and heightens the energy barrier to be overcome. Finally, the overall reaction (from the MCC to the PDC) is found to be exothermic via ORI (by -2.6 kcal/mol) while it is endothermic (or almost thermoneutral) via ORII (by 0.9 kcal/mol). This makes the transformation of *R*-propranolol via ORI energetically more favorable than via ORII.

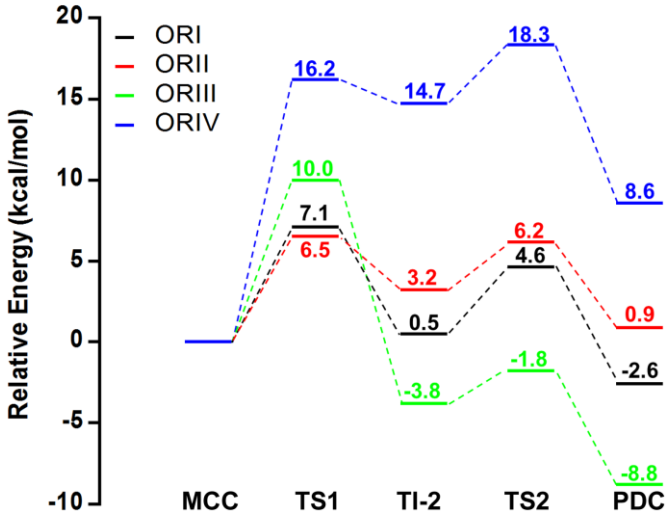

Fig. 43 QM(B3LYP/TZVP)/MM energy profiles for the conversion of *R*-propranolol to *R*-acetyl-propranolol, relative to the energy of the reactive complexes between AcCalB and *R*-propranolol (MCCs). ORI-ORIV correspond to different configurations of TI-2 in the CalB binding pocket.

The major stabilization observed for ORI respect to ORII may be understood from the decomposition of the QM/MM energy into the QM (including the electrostatic interactions with the MM point charges) and MM contributions along their reaction profiles (see **Table 40** in **Appendix E**). Relative to the MCC the MM energy of ORI is -3.1 kcal/mol, while that of ORII is 0.9 kcal/mol. Meanwhile, their relative QM energies are 3.6 kcal/mol and 2.3 kcal/mol, respectively. Thus a considerable decrease of the MM energy is responsible for the major stabilization of ORI. As these reactions proceed to the formation of the TI-2s ORI and ORII significant motions in the CalB binding pocket are not observed, except for the *R*-propranolol getting closer to the carbonylic carbon of the acetyl group (Ace:C) and undergoing slight rotations along its dihedral angles, which is accompanied by slight motions of the residues of the binding pocket (see **Fig. 93** to **Fig. 95** in **Appendix E** and **Table 17**). Therefore, considering that all atoms directly involved in the formation of TI-2 are part of the QM region, the decrease and rise of the MM energy in ORI and ORII are mainly attributed to the strengthening and weakening of the van der Waals interactions between propranolol and the

Table 17 Distribution of dihedral angles characterizing TI-2[a] at the stationary points along the reaction profiles obtained at the B3LYP(TZVP)/CHARMM level for the transformation of *R*-propranolol in binding mode I via the TI-2s ORI and ORII

Dihedral (°)	**ORI**					**ORII**				
	MCC	**TS1**	**TI-2**	**TS2**	**PDC**	**MCC**	**TS1**	**TI-2**	**TS2**	**PDC**
ω_1	2	10	15	-20	-26	11	22	32	-3	3
ω_2	30	34	38	6	10	17	24	28	-2	9
ω_3	-148	-150	-151	-122	-114	-117	-124	-128	-102	-110
ω_4	160	159	157	160	154	178	-179	-178	178	177
ω_5	-168	-170	-171	-176	178	94	94	94	95	94
ω_6	63	61	59	61	63	-138	-140	-140	-132	-130
ω_7	120	127	133	136	152	-65	-68	-71	-62	-63
ω_8	-170	-171	-173	-172	-177	172	174	177	168	166
ω_9	-168	-174	-176	-174	-179	-161	-164	-162	-151	-148

[a] ω_1-ω_3 are the dihedral angles directly involved in the formation of TI-2. ω_4-ω_9 are the dihedral angles involving the propranolol molecule. See **Fig. 40b**.

surrounding protein residues, respectively. This shows that the CH-π interactions between propranolol and the surrounding protein residues play an important role on the stabilization of ORI, as the total energy of this type of interaction has a great contribution of the dispersion energy [183], which is computed at the MM level as part of the van der Waals interactions. In this sense, these CH-π interactions are also observed to be very important for the stabilization of the TSs obtained for ORI, as the relative MM energies of TS1 and TS2 for ORI are -2.3 kcal/mol and -2.2 kcal/mol, respectively.

To check the influence of the MM region on the reaction profiles obtained for ORI and ORII in more detail, single-point QM(B3LYP/TZVP) calculations in the gas phase were performed for the QM region of all stationary points along these reaction profiles (**Fig. 44a**). In the gas phase the energy profiles of ORI and ORII resulted to be very similar up to the formation of TS2. This shows that up to this point the geometrical changes occurring in the QM regions of ORI and ORII are not directly responsible for the energetic differences observed between their respective QM/MM reaction profiles, but how they may affect the interactions between the QM and MM regions. Moreover, in the gas phase the relative energies of the TI-2s ORI and ORII (21.6 kcal/mol and 23 kcal/mol, respectively) and their corresponding TSs (about 13-16 kcal/mol) are higher compared to the B3LYP/CHARMM calculations. Thus these TI-2s are the highest point in their respective gas-phase energy profiles. This is expected since the residues of the oxyanion hole (which contribute to the stabilization of the oxyanion) make part of the MM region. In contrast, the relative energy of the PDC of ORI in the gas phase is the same observed in the B3LYP/CHARMM calculations (-2.6 kcal/mol), and that of the PDC of ORII is just slightly lower (0.4 kcal/mol). Thus the overall reaction is found to be exothermic via ORI and endothermic (or almost thermoneutral) via ORII even in the gas phase calculations. This reveals that a structural rearrangement in the QM regions of the PDCs of ORI and ORII respect to their MCCs exists, which is directly responsible for the thermodynamic nature of these reactions. Such structural rearrangement is identified to be related to the naphthoxy side chain of propranolol (see below).

From the energy values obtained in the gas phase, the contribution of the MM region to the electrostatic stabilization/destabilization of the QM system along the reaction profiles of ORI and ORII was calculated (**Fig. 44b**). In both cases the contribution of the MM region to the stabilization of TI-2 is the most prominent, with 18 kcal/mol and 20.7 kcal/mol for ORI and ORII, respectively (relative to their MCCs). Conversely, it abruptly decreases in the PDCs; the PDC of ORI is destabilized respect to its MCC by 0.8 kcal/mol, and the PDC of ORII is stabilized just by 0.3 kcal/mol. This is mainly attributed to the weakening of the hydrogen bonds between the acetate oxygen (Ace:O) and the residues of the

oxyanion hole in these PDCs: in the PDC of ORI the hydrogen bond interactions between the Ace:O atom and the –NH functions of Gln106 (Ace:O-Gln106:NH) and Thr40 (Ace:O-Thr40:NH) are diminished respect to its MCC, by 0.31 Å and 0.23 Å, respectively; the former is also diminished in the PDC of ORII by 0.59 Å (**Table 18**). This conclusion is based on the fact that the residues of the oxyanion hole are found to be the major source of the electrostatic stabilization/destabilization of the QM system along the reaction profiles of ORI and ORII. As shown in **Table 19**, the contribution of these residues to the stabilization of the TI-2s ORI and ORII represents about 94 % (16.9 kcal/mol) and 75 % (15.6 kcal/mol) of the total contribution of the MM region, respectively. These residues also contribute with more than 60 % of the electrostatic stabilization of the TSs of ORI and ORII. By the other hand, Thr40 is the major responsible for the destabilization of the PDC of ORI (with 2.7 kcal/mol). Meanwhile, Gln106 contributes to the destabilization of the PDC of ORII with 1.4 kcal/mol.

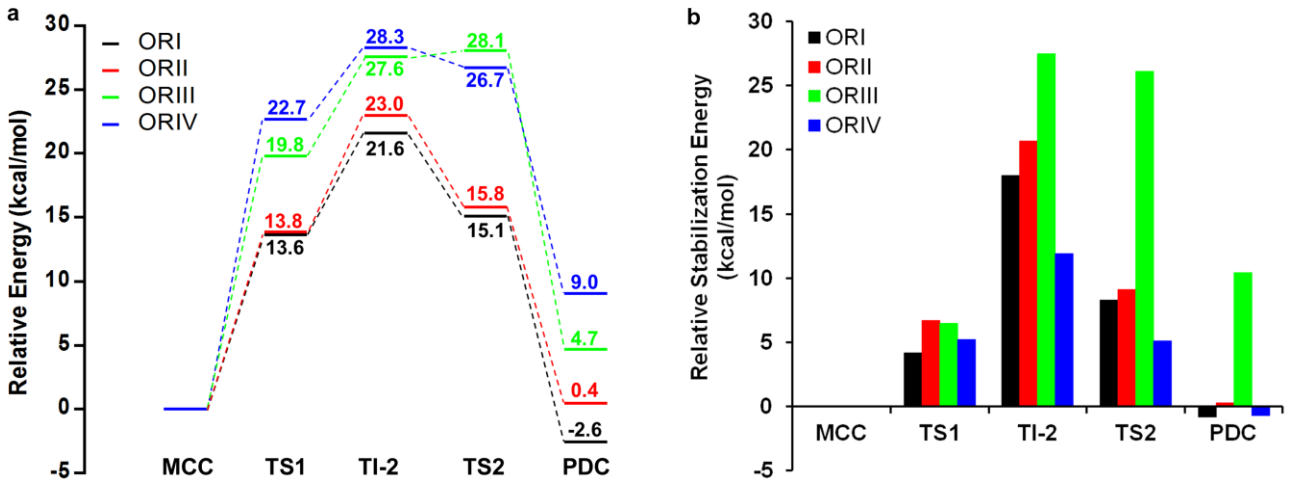

Fig. 44 (a) Gas-phase pure QM (B3LYP/TZVP) energy profiles for the conversion of *R*-propranolol to *R*-acetyl-propranolol, relative to the energy of the reactive complexes between AcCalB and *R*-propranolol (MCCs). Only the QM region is considered. (b) Electrostatic contribution of the MM region to the stabilization (positive values) or destabilization (negative values) of the QM region at the stationary points along the reaction profiles obtained for *R*-propranolol, relative to the MCCs.

PES scans (at the B3LYP/TZVP level) along the dihedral angles involving the naphthoxy side chain of propranolol (ω_7-ω_9) were also performed, by using *R*-1-methyl-3-(1-naphthoxy)-2-propanol as a model of the propranolol molecule (see **Fig. 96** in **Appendix E**). This allowed evaluating the contribution to the reaction energy profiles of ORI and ORII of small torsions that *R*-propranolol undergoes along such dihedral angles as these reactions proceed from the MCC to the formation of the PDC (**Table 17**).

Table 18 Relevant interatomic distances and bond lengths[a] corresponding to the stationary points along the reaction profiles obtained at the B3LYP(TZVP)/CHARMM level for the transformation of *R*-propranolol[b] in binding mode I via the TI-2s ORI and ORII[c]

Distance (Å)	ORI					ORII				
	MCC	**TS1**	**TI-2**	**TS2**	**PDC**	**MCC**	**TS1**	**TI-2**	**TS2**	**PDC**
Asp187:O_D-His224:H_{ND}	1.74 (169)	1.66 (169)	1.54 (170)	1.57 (174)	1.66 (173)	1.83 (169)	1.75 (168)	1.67 (168)	1.62 (174)	1.69 (175)
His224:H_{ND}-His224:N_D	1.05	1.06	1.09	1.07	1.05	1.04	1.05	1.06	1.06	1.04
His224:**H**-Ser105:Oγ	-	-	2.35(129)	1.37 (170)	1.01	-	-	2.40 (123)	1.36 (170)	1.02
Ace:C-Ser105:Oγ	1.34	1.37	1.47	2.01	2.54	1.33	1.37	1.46	1.96	2.43
His224:Nε-Sub:**H**	1.83 (164)	1.22 (172)	1.03	1.15 (170)	1.65 (173)	1.71 (168)	1.17 (174)	1.04	1.14 (170)	1.57 (175)
Sub:**H**-Sub:**O**	1.00	1.31	1.88 (162)	-	-	1.00	1.34	1.69 (166)	-	-
Ace:C-Sub:**O**	2.46 (100)	2.07 (105)	1.53 (114)	1.37 (122)	1.33 (124)	2.49 (98)	2.05 (106)	1.56 (114)	1.37 (122)	1.33 (124)
Ace:C-Ace:O	1.23	1.24	1.29	1.25	1.22	1.23	1.24	1.29	1.25	1.23
Ace:O-Gln106:NH	2.04 (145)	2.00 (154)	1.93 (165)	2.03 (153)	2.35 (141)	2.01 (149)	2.01 (157)	2.00 (166)	2.17 (158)	2.60 (149)
Ace:O-Thr40:NH	1.90 (167)	1.87 (169)	1.79 (170)	1.94 (165)	2.13 (158)	1.87 (172)	1.80 (174)	1.73 (175)	1.76 (171)	1.84 (164)
Ace:O-Thr40:OH	1.71 (173)	1.72 (172)	1.71 (175)	1.73 (174)	1.68 (176)	1.74 (170)	1.74 (170)	1.72 (171)	1.74 (170)	1.69 (169)
Sub:*H*-Thr40:O	1.93 (167)	1.90 (166)	1.87 (167)	1.89 (161)	1.96 (157)	1.93 (163)	1.85 (168)	1.83 (168)	1.90 (174)	1.94 (172)

[a] Distances and bond lengths are given in Å. Angles in degrees for both the corresponding hydrogen bonds and the nucleophilic attack (Sub:**O**⋯Ace:C=O) are given in brackets.
[b] The atoms corresponding to the hydroxyl and amino group of propranolol (Sub) are marked in bold and italic respectively.
[c] Ace is the acetyl group which is transferred from the acetylated catalytic serine (SEA) to the alcohol oxygen of propranolol.

When the transformation of *R*-propranolol occurs via ORI, ω_8 and ω_9 are shifted from -170° and -168° in the MCC to -177° and -179° in the PDC, respectively (closer to the global minimum which is 180°). Meanwhile, ω_7 is shifted from 120° to 152° (closer to a local minimum). In contrast, when the transformation of *R*-propranolol occurs via ORII, ω_8 and ω_9 are shifted from 172° and -161° in the MCC to 166° and -148° in the PDC, respectively. ω_7 is shifted only 2°. According to the PES scans results obtained for the propranolol model, such torsions that *R*-propranolol undergoes during its transformation via ORI are expected to stabilize the PDC (about 2.1 kcal/mol) respect to the MCC, while those via ORII are expected to destabilize the PDC (about 0.7 kcal/mol). Therefore such torsions are partly responsible for the exothermic formation of the PDC of ORI and the endothermic formation of the PDC of ORII.

Table 19 Electrostatic contribution (in kcal/mol) of the residues of the oxyanion hole to the stabilization or destabilization of the QM region at the stationary points along the B3LYP/CHARMM reaction profiles of *R*-propranolol[a]

Reaction profile	TS1		TI-2		TS2		PDC	
	Thr40	Gln106	Thr40	Gln106	Thr40	Gln106	Thr40	Gln106
ORI	3.0	2.4	9.6	7.3	2.0	3.9	-2.7	0.2
ORII	3.6	2.2	9.8	5.8	3.7	2.2	0.2	-1.4
ORIII	2.7	2.7	11.5	11.0	6.1	7.3	1.3	3.0
ORIV	5.0	2.2	8.7	3.8	0.8	-2.0	-1.2	-2.5

[a] The contribution of each residue was estimated by setting their point charges to zero in additional energy calculations (i.e. by electrostatic perturbation). Energy values are given relative to the MCC. Positive values mean stabilization, whereas negative values mean destabilization.

6.3.1.2. Reaction profiles for the transformation of R-propranolol in binding mode II

The QM(B3LYP/TZVP)/CHARMM energy profiles for the transformation of *R*-propranolol via ORIII and ORIV are also shown in **Fig. 43**. In contrast to the observed for ORI and ORII, these energy profiles are very different. The overall reaction is exothermic via ORIII by -8.8 kcal/mol, while it is endothermic via ORIV by 8.6 kcal/mol. The energy barriers for the formation of the TI-2s ORIII and ORIV from their respective MCCs are 10 kcal/mol and 16.2 kcal/mol, respectively. Furthermore, the formation of the former is exothermic by -3.8 kcal/mol, while the formation of the latter is endothermic by 14.7 kcal/mol. Finally, the energy barriers for the formation of the corresponding PDCs from these TI-2s are 2.0 kcal/mol and 3.6 kcal/mol, respectively. Thereby it is found that the transformation of *R*-propranolol is both kinetically and thermodynamically more favorable via ORIII than via ORIV. On

the other hand, as observed in binding mode I, the formation of the TI-2 is the rate-limiting step for the transformation of *R*-propranolol in binding mode II. Thus the conversion of *R*-propranolol is kinetically favored in binding mode I over the binding mode II, as the energy barrier for the formation of the TI-2 ORI is 2.9 kcal/mol lower relative to that for the TI-2 ORIII.

Valuable information about the origin of the significant differences observed for the reaction profiles of ORIII and ORIV is obtained from the decomposition of the QM/MM energy into the QM and MM contributions (see **Table 41** in **Appendix E**). In the reaction profile of ORIII the relative MM energies of TS1, TI-2, TS2 and PDC are -3.3, -3.9, -3.8 and -3.1 kcal/mol, while in the reaction profile of ORIV are -1.3, -1.7, -3.3 and -1.1 kcal/mol, respectively. This suggests a strengthening of the van der Waals interactions between propranolol and the surrounding protein residues in such stationary points respect to the MCC, which is more pronounced along the reaction profile of ORIII. Thus the CH-π interactions between the naphthyl rings of propranolol and the surrounding MM residues are found to be very important for the stabilization of these stationary points (see the case of the stabilization of the TI-2 ORI described in section **6.3.1.1**). Similar to the observed for the transformation of *R*-propranolol in binding mode I, as the reaction proceeds either via ORIII or ORIV, slight motions of the residues of the binding pocket are observed, as given by their RMSD values less than 1 Å (respect to the MCC) at the stationary points along such reaction profiles (see **Fig. 97** in **Appendix E**). Interestingly, the motions of the residues at the loop making part of the CalB binding pocket (Glu188, Ile189 and Val190) are more pronounced when the transformation of *R*-propranolol occurs via ORIII. Visual inspection shows that such motions are destined to make stronger the CH-π interaction between the naphthyl group of propranolol and the Ile189:Cδ atom as the reaction proceeds. Thus this may be partly responsible for the lower relative MM energies observed for the stationary points along the reaction profile of ORIII.

Though there is an important contribution of the MM energy, the fluctuations in the QM energy are the major source of the energetic differences between the reaction profiles of ORIII and ORIV (e.g. the relative QM energy of TI-2 ORIII is 0.1 kcal/mol while that of ORIV is 16.4 kcal/mol). Because the QM energy includes the electrostatic interactions between the QM and MM systems, gas-phase QM(B3LYP/TZVP) single-points calculations for the QM region of all stationary points along the reaction profiles of ORIII and ORIV were performed in order to better understand the origin of their energetic differences (**Fig. 44a**). This allowed calculating the electrostatic contribution of the MM region to the stabilization/destabilization of the QM system along these reaction profiles (see **Fig. 44b**). Interestingly, in the gas-phase calculations the formation of the PDCs of ORIII and ORIV resulted to

be endothermic by 4.7 kcal/mol and 9.0 kcal/mol, respectively. This shows that the MM region contributes significantly to the stabilization of the PDC of ORIII, as its formation is found to be quite exothermic in the QM/MM calculations (see above). In fact, it is found that the MM region contributes to the electrostatic stabilization of this PDC with 10.4 kcal/mol compared to the MCC. Conversely, it contributes to the electrostatic destabilization of the PDC of ORIV (with 0.7 kcal/mol), which explains the observed endothermic formation of this PDC in the QM/MM calculations.

Moreover, in the gas-phase the relative energy of the TS1 for ORIV is 2.9 kcal/mol higher than that of the TS1 for ORIII. Accordingly about 47 % of the energy difference observed for these TSs in the QM/MM reaction profiles (6.2 kcal/mol) is directly due to the distinct geometrical changes occurring in the respective QM systems as the reaction proceeds (see **Table 20** to **Table 21**). Interestingly, in the MCC and TS1 for ORIII the distance between the atoms involved in the formation of the ester bond (Ace:C-Sub:**O**) is 2.61 Å and 2.07 Å, while in these for ORIV is 2.73 Å and 1.87 Å, respectively. Meanwhile the key distance in the breaking alcohol bond (Sub:**H**-Sub:**O**) presents a similar pattern in both reaction systems, with 1.43 Å in the TS1 for ORIII and 1.47 Å in that for ORIV. This means that in the reaction system of ORIII the TS1 is reached earlier than in that of ORIV, which explains the lower relative energy obtained for the TS1 of ORIII even in the gas-phase. This is attributed to a shorter distance for the nucleophilic attack and a major nucleophilicity of the Sub:**O** atom in the MCC for ORIII respect to that for ORIV. The latter is due to a stronger hydrogen bond interaction between His224 and the hydroxyl group of propranolol (His224:Nε-Sub:**H**); this hydrogen bond has a distance (angle) of 1.81 Å (175°) in the MCC for ORIII, and 1.91 Å (168°) in that for ORIV. On the other hand, it is found that the TS1 for ORIII is electrostatically better stabilized by the MM region (with 6.5 kcal/mol) in comparison to the TS1 for ORIV (with 5.2 kcal/mol).

Finally, the relative energies of the TI-2s ORIII and ORIV as well as of their respective TS2s are found to be similar in the gas-phase; both of them differ by less than 1.5 kcal/mol. Thus the energetic difference observed for these stationary points in the QM/MM calculations comes mainly from the different contribution of the MM region to their stabilization. As shown in **Fig. 44b**, the contribution of the MM region to the electrostatic stabilization of such stationary points along the reaction profile of ORIII is notably higher (TI-2: 27.5 kcal/mol, TS2: 26.1 kcal/mol) than the observed for these along the reaction profile of ORIV (TI-2: 11.9 kcal/mol, TS2: 5.1 kcal/mol).

Table 20 Distribution of dihedral angles characterizing TI-2[a] at the stationary points along the reaction profiles obtained at the B3LYP(TZVP)/CHARMM level for the transformation of *R*-propranolol in binding mode II via the TI-2s ORIII and ORIV

Dihedral (°)	ORIII					ORIV				
	MCC	**TS1**	**TI-2**	**TS2**	**PDC**	**MCC**	**TS1**	**TI-2**	**TS2**	**PDC**
ω_1	-13	-13	-12	-8	-6	1	14	19	-8	-11
ω_2	105	89	122	137	159	63	52	52	30	22
ω_3	-46	-32	-69	-71	-79	45	58	59	74	80
ω_4	138	139	153	155	154	171	157	154	147	144
ω_5	-81	-83	-83	-84	-82	176	177	177	-175	-171
ω_6	-155	-155	-147	-151	-150	-178	-176	-176	-177	-175
ω_7	171	176	168	164	159	-47	-55	-55	-57	-57
ω_8	177	172	-179	-171	-168	-100	-100	-103	-118	-114
ω_9	163	167	158	155	153	-146	-134	-129	-101	-110

[a] ω_1-ω_3 are the dihedral angles directly involved in the formation of TI-2. ω_4-ω_9 are the dihedral angles involving the propranolol molecule. See **Fig. 40b**.

Table 21 Relevant interatomic distances and bond lengths[a] corresponding to the stationary points along the reaction profiles obtained at the B3LYP(TZVP)/CHARMM level for the transformation of *R*-propranolol[b] in binding mode II via the TI-2s ORIII and ORIV[c]

Distance (Å)	ORIII					ORIV				
	MCC	**TS1**	**TI-2**	**TS2**	**PDC**	**MCC**	**TS1**	**TI-2**	**TS2**	**PDC**
Asp187:O_D-His224:H_{ND}	1.94 (166)	1.82 (166)	1.65 (171)	1.69 (172)	1.76 (174)	1.88 (170)	1.69 (172)	1.63 (172)	1.60 (177)	1.70 (177)
His224:H_{ND}-His224:N_D	1.03	1.04	1.07	1.06	1.04	1.04	1.06	1.07	1.06	1.04
His224:**H**-Ser105:Oγ	-	-	1.64 (173)	1.40 (175)	1.02	-	-	2.37 (128)	1.38 (169)	1.01
Ace:C-Ser105:Oγ	1.34	1.38	1.58	1.97	2.49	1.33	1.40	1.48	1.93	2.66
His224:Nε-Sub:***H***	1.81 (175)	1.15 (176)	1.05	1.14 (175)	1.58 (176)	1.91 (168)	1.11 (169)	1.05	1.14 (169)	1.66 (171)
Sub:**H**-Sub:***O***	1.00	1.43	3.09 (138)	-	-	0.99	1.47	1.69 (161)	-	-
Ace:C-Sub:***O***	2.61 (96)	2.07 (106)	1.44 (112)	1.38 (114)	1.34 (117)	2.73 (103)	1.87 (112)	1.55 (116)	1.39 (122)	1.33 (124)
Ace:C-Ace:O	1.22	1.24	1.29	1.25	1.22	1.23	1.25	1.28	1.25	1.22
Ace:O-Gln106:NH	1.98 (146)	1.94 (154)	1.73 (166)	1.77 (160)	1.90 (156)	2.03 (152)	2.18 (163)	2.27 (168)	2.55 (161)	3.19 (152)
Ace:O-Thr40:NH	1.96 (168)	1.99 (168)	1.83 (168)	1.86 (167)	1.89 (165)	2.04 (161)	1.89 (167)	1.85 (168)	1.93 (163)	2.25 (151)
Ace:O-Thr40:OH	1.74 (172)	1.73 (172)	1.67 (176)	1.69 (179)	1.72 (174)	1.69 (178)	1.70 (176)	1.69 (175)	1.69 (170)	1.68 (162)
Sub:*H*-Sub:O	2.74 (112)	2.64 (113)	2.47 (118)	2.40 (118)	2.47 (116)	4.57	4.48	4.42	4.36	4.47
Sub:**O**-Thr40:NH	3.96 (131)	3.93 (144)	3.20 (139)	3.20 (139)	3.22 (137)	4.05	3.86	3.77	3.94	4.24
Sub:**O**-Thr40:OH	3.58 (137)	3.57 (140)	2.92 (131)	2.81 (128)	2.75 (122)	4.00	3.77	3.64	3.61	3.77

[a] Distances and bond lengths are given in Å. Angles in degrees for both the corresponding hydrogen bonds and the nucleophilic attack (Sub:**O**⋯Ace:C=O) are given in brackets.

[b] The atoms corresponding to the hydroxyl and amino group of propranolol (Sub) are marked in bold and italic respectively. The naphthoxy oxygen of propranolol is indicated as Sub:O.

[c] Ace is the acetyl group which is transferred from the acetylated catalytic serine (SEA) to the alcohol oxygen of propranolol.

The individual electrostatic contribution of the residues of the oxyanion hole to the stabilization of the QM system along the reaction profiles of ORIII and ORIV was also evaluated (**Table 19**). According to the energy values obtained such residues are identified to play an important role on the stabilization/destabilization of the QM system along these reaction profiles, similar to the observed for the transformation of *R*-propranolol in binding mode I (e.g. these residues (together) represent about 83 %, 82 %, 51 % and 41 % of the total electrostatic contribution of the MM region to the stabilization of the TS1, TI-2, TS2 and PDC involving the reaction system of ORIII, respectively). It is also observed a strong correlation between the total contribution of the MM region and that of the residues of the oxyanion hole to the stabilization of the reaction profiles of ORIII and ORIV after formation of the TI-2. For example, the contribution of the residues of the oxyanion hole to the stabilization of ORIII is 10 kcal/mol higher relative to ORIV. These residues are also observed to contribute to the stabilization of the PDC of ORIII (with 4.3 kcal/mol), while contribute to the destabilization of the PDC of ORIV (with 3.7 kcal/mol). Thereby the hydrogen-bond patterns with the oxyanion hole presented at the stationary points along these reaction profiles are found to contribute significantly to the energetic differences between them, and thus to the thermodynamic nature of such reactions. Interestingly, when the reaction proceeds via ORIV, the Ace:O-Gln106:NH hydrogen bond interaction decreases continuously; this hydrogen bond has a distance of 2.03 Å, 2.18 Å, 2.27 Å, 2.55 Å and 3.19 Å, in the MCC, TS1, TI-2, TS2 and PDC, respectively. In addition, the Ace:O-Thr40:NH hydrogen bond is diminished in the PDC compared to the MCC (by 0.21 Å). In contrast, these hydrogen bonds are preserved when the reaction proceeds via ORIII, and in fact they become shorter (about 0.1-0.3 Å respect to the MCC) in the TI-2 and TS2. Moreover, the Sub:**O** atom is found slightly displaced toward the oxyanion hole in the TI-2, such that it may forms a weak hydrogen bond interaction with the –OH function of Thr40 (2.92 Å), which is not present neither in the MCC nor in the TS1. This hydrogen bond becomes stronger as this reaction proceeds to the formation of the PDC. See **Fig. 98** to **Fig. 99** in **Appendix E** and **Table 21**.

6.3.2. QM/MM reaction paths for the transformation of *S*-propranolol

The B3LYP(TZVP)/CHARMM reaction profiles for the transformation of *S*-propranolol were computed for a total of four configurations of TI-2, one in binding mode I and three in binding mode II. These TI-2s are referred to as OSI-OSIV, respectively (**Fig. 45**). OSI is practically the specular binding mode of ORI. The most significant differences between them are related to the orientation of the residue Leu140 and the Sub:*H*-Thr40:O and His224:**H**-Sub:**O** hydrogen bonds. The latter are stronger in ORI (with a distance of 1.87 Å and 1.88 Å, respectively) than in OSI (with a distance of 2.53 Å and

3.16 Å, respectively). In turn, the orientation of Leu140 in ORI favors the formation of CH-π interactions between its side chain and the naphthyl group of propranolol stronger than those observed in OSI (see **Fig. 42** and **Fig. 45**). By the other hand, OSII and OSIII are more or less similar to ORIII and ORIV, respectively. The most relevant difference between such structures is about the orientation of the isopropylamine side chain of propranolol in the medium pocket of CalB. Its orientation in OSII does not favors the formation of the Sub:*H*-Sub:O intramolecular hydrogen bond as is the case in ORIII. Moreover, it is less exposed to the solvent in OSIII compared to ORIV. Finally, OSIV is characterized by a particular orientation of the naphthyl group of propranolol in the medium pocket, which favors the formation of strong CH-π interactions between this group and the residues of the Leu278-Ala287 helix (helix α10). It is also important to note that in OSII-OSIV the His224:**H**-Sub:**O** hydrogen bond is stronger than in OSI, with a distance about 2.3-2.6 Å. This is because in OSI the Sub:**O** atom is slightly displaced toward the oxyanion hole (its preferred orientation in the TI-2s of *S*-propranolol in binding mode I as observed in the MD simulations –see section **5.3.2.2.1**-).

The B3LYP/CHARMM reaction profiles obtained for the transformation of *S*-propranolol are shown in **Fig. 46**. As observed for the *R*-propranolol the formation of the TI-2 is the rate-limiting step for the transformation of *S*-propranolol either in binding mode I or II. Interestingly, the formations of OSI and OSII involve similar energy barriers (about 11 kcal/mol), which are lower than those observed for the formations of OSIII and OSIV (higher than 14 kcal/mol). However, the overall reaction via the TI-2 OSI is exothermic (by -2.8 kcal/mol), while the reactions occurring via the TI-2s OSII-OSIV are endothermic (by 9.9 kcal/mol, 1.8 kcal/mol and 6.9 kcal/mol, respectively). Accordingly the transformation of *S*-propranolol is found to be favored in binding mode I over the binding mode II, which is also the case of *R*-propranolol. The enantioselectivity of the reaction is thus explained by the difference between the energy barriers obtained for the formations of the TI-2s ORI and OSI. The energy barrier for the formation of ORI is 4.5 kcal/mol lower relative to that for OSI, which corroborates with faster formation of *R*-*O*-acetyl-propranolol as observed in experiments. It is also important to note that even the transformation of *R*-propranolol in binding mode II (via ORIII) is kinetically favored over that of *S*-propranolol via OSI (hence also over its transformation in binding mode II), as the energy barrier for the formation of ORIII is 1.6 kcal/mol lower relative to OSI. This is added to the fact that the formation of the PDC of ORIII is quite exothermic, which contrasts in turn with the observed endothermic formation of the PDCs of *S*-propranolol in binding mode II. Thereby CalB is observed to favor the transformation of *R*-propranolol over *S*-propranolol in both binding mode I and II (see **Fig. 43** and **Fig. 46**).

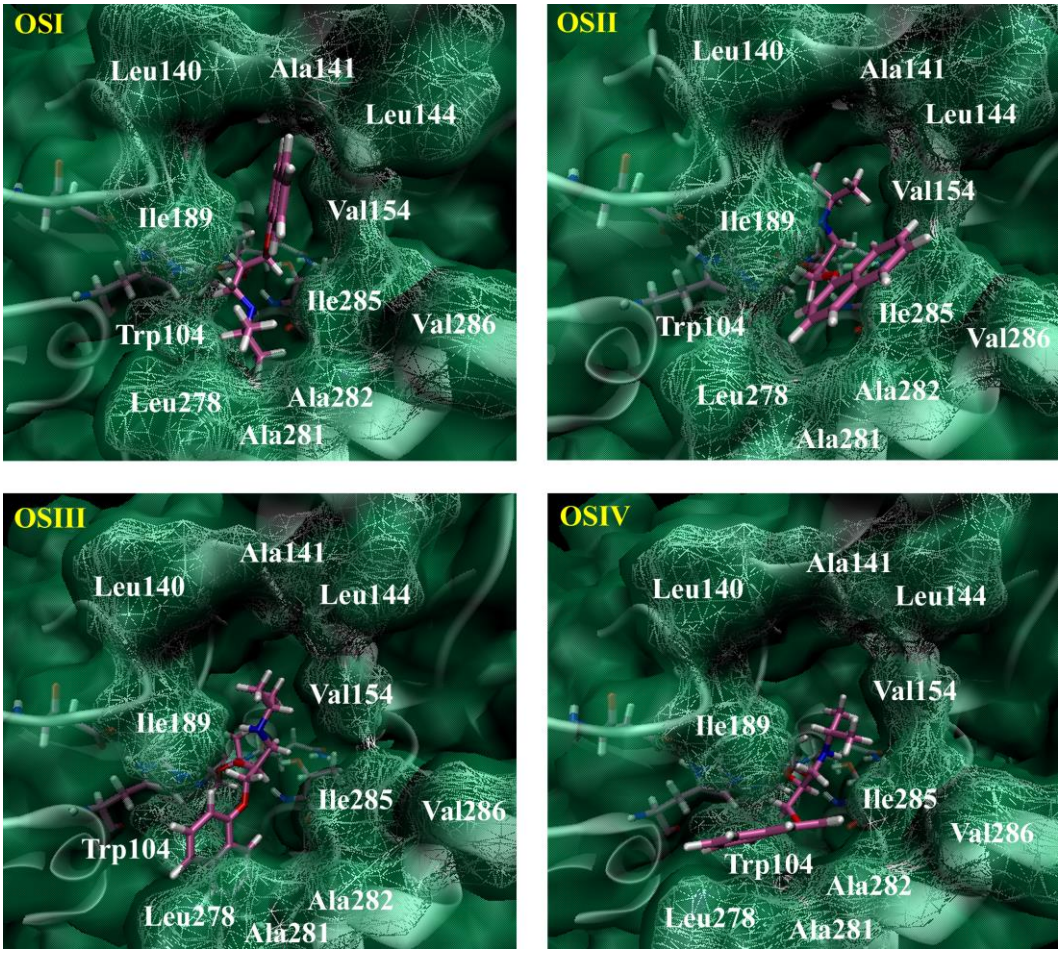

Fig. 45 Second tetrahedral intermediates for *S*-propranolol in binding mode I (OSI) and binding mode II (OSII-OSIV), optimized at the QM(B3LYP/TZVP)/CHARMM level. Protein residues surrounding the substrate are shown in wireframe surface (white). The substrate, catalytic triad and oxyanion hole are in licorice.

In order to get insights about the major factors contributing to the selectivity of CalB in favor of the conversion of *R*-propranolol over *S*-propranolol either in binding mode I or II, it was followed for the QM/MM reaction profiles of *S*-propranolol the same analysis scheme used for those of *R*-propranolol: (i) the decomposition of the QM/MM energy into the QM and MM contributions was analyzed (ii) gas-phase QM(B3LYP/TZVP) single-points calculations for the QM region of all stationary points were carried out (iii) the electrostatic contribution of all MM region as well as of the residues of the oxyanion hole to the stabilization/destabilization of the QM system was calculated. Based on this analysis a more detailed description about the transformation of *S*-propranolol is given in the next sections.

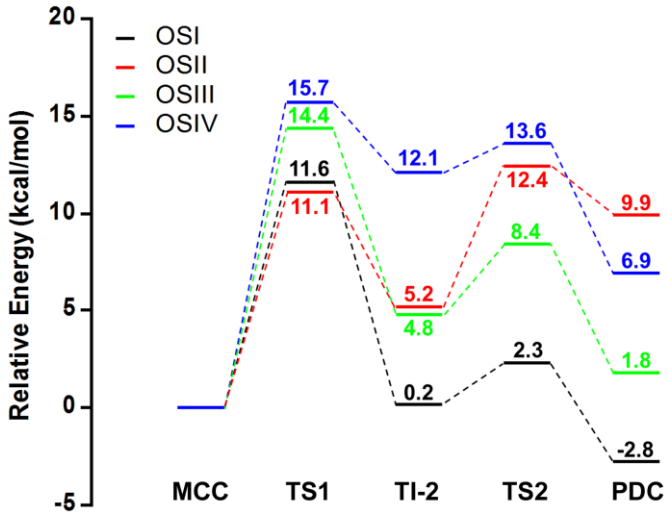

Fig. 46 QM(B3LYP/TZVP)/MM energy profiles for the conversion of *S*-propranolol to *S*-acetyl-propranolol, relative to the energy of the reactive complexes between AcCalB and *S*-propranolol (MCCs). OSI-OSIV correspond to different configurations of TI-2 in the CalB binding pocket.

6.3.2.1. Details about the transformation of S-propranolol in binding mode I

Generally speaking, the transformation of *S*-propranolol in binding mode I (via OSI) is a similar case to the transformation of *R*-propranolol in binding mode II via ORIII. As shown in **Fig. 47**, a remarkable electrostatic contribution of the MM region to the stabilization of the stationary points along the reaction profile of OSI is observed, particularly from the formation of the TI-2 (TS1: 9.7 kcal/mol, TI-2: 34.1 kcal/mol, TS2: 22.6 kcal/mol and PDC: 11.7 kcal/mol). Hence the noteworthy stabilization of the TI-2 and TS2 respect to TS1 as well as the exothermic formation of the PDC (see **Fig. 46**).

The residues of the oxyanion hole are responsible for much of the electrostatic stabilization energy provided by the MM region along the reaction profile of OSI. The contributions of these residues to the stabilization of the TS1, TI-2, TS2 and PDC in this reaction profile represent about 73 % (7.1 kcal/mol), 74 % (25.3 kcal/mol), 62 % (14 kcal/mol) and 46 % (5.4 kcal/mol) of the total electrostatic contribution of the MM region, respectively (**Table 22**). These stabilization energies provided by the residues of the oxyanion hole are attributed to the observed strengthening of the Ace:O-Gln106:NH, Ace:O-Thr40:NH and Sub:*H*-Thr40:O hydrogen bond interactions as this reaction proceeds from the MCC to the formation of the PDC, which is further accompanied by the establishment of hydrogen bond interactions between the Sub:**O** atom and the -OH and -NH functions of Thr40 once the TI-2 is formed (**Table 23**). The latter interactions are established due to the displacement of the Sub:**O** atom toward the oxyanion hole (see **Fig. 101** in **Appendix E**). In fact, the

Ace:O-Gln106:NH and Ace:O-Thr40:NH hydrogen bond interactions become noticeably stronger in the TI-2 and TS2, which explains the higher energetic contribution of the residues of the oxyanion hole to the stabilization of these stationary points. Thereby the hydrogen bond patterns with the oxyanion hole are found to contribute significantly to the observed high stabilization of the TI-2 and TS2 in the reaction profile of OSI as well as to the exothermic formation of the respective PDC, which is also the case in the reaction profile of ORIII. This result contrasts with the observed for the competing transformation of *R*-propranolol in binding mode I (via ORI), which is exothermic mainly due to the conformational changes that *R*-propranolol undergoes as the reaction proceeds and not to the hydrogen bond interactions with the oxyanion hole. Conversely, the latter contribute to the destabilization of the PDC of ORI respect to its respective MCC (section **6.3.1.1**).

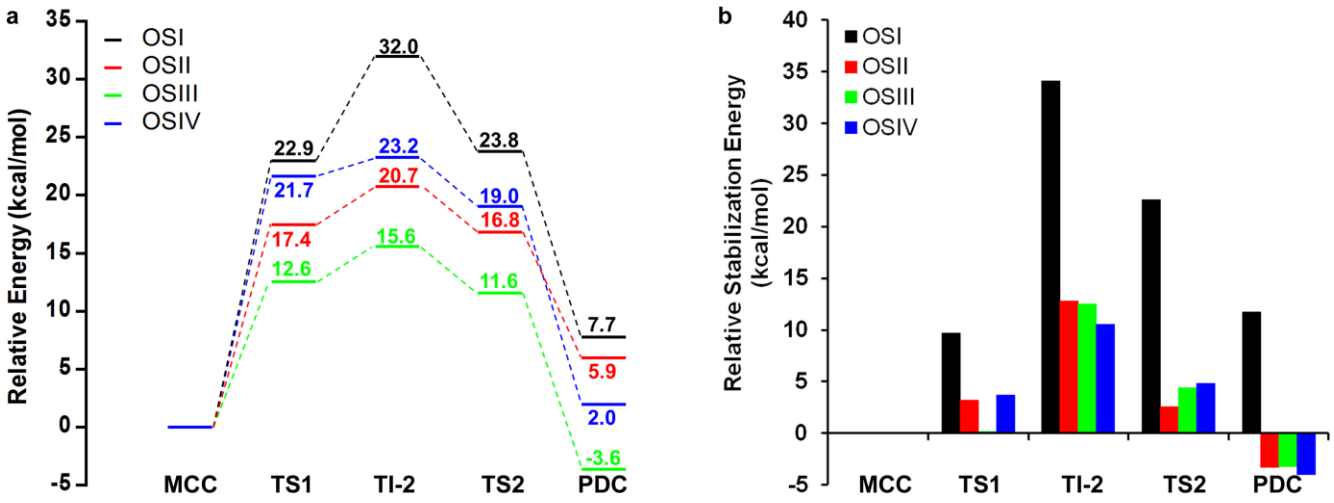

Fig. 47 (a) Gas-phase pure QM (B3LYP/TZVP) energy profiles for the conversion of *S*-propranolol to *S*-acetyl-propranolol, relative to the energy of the reactive complexes between AcCalB and *S*-propranolol (MCCs). Only the QM region is considered. (b) Electrostatic contribution of the MM region to the stabilization (positive values) or destabilization (negative values) of the QM region at the stationary points along the reaction profiles obtained for *S*-propranolol, relative to the MCCs.

Though there is certain similarity between the reaction profiles of OSI and ORIII about the electrostatic contribution of both the MM region and the residues of the oxyanion hole to the stabilization of the stationary points along them, from the formation of the TI-2 the relative energies of the stationary points along the reaction profile of ORIII are remarkably lower in comparison to those along the reaction profile of OSI (see **Fig. 43** and **Fig. 46**). This is mainly associated with the behaviour of the MM energy. In contrast to the overall decreasing of the MM energy observed along the reaction profile of ORIII, in the reaction profile of OSI an increasing of this energy is observed from the formation of

the TI-2 (see **Table 41** and **Table 42** in **Appendix E**). Thus, for example, the PDC of ORIII presents a QM energy of -5.7 kcal/mol and a MM energy of -3.1 kcal/mol (resulting in a QM/MM energy of -8.8 kcal/mol), while in the PDC of OSI these energies are -4.0 kcal/mol and 1.2 kcal/mol respectively (resulting in a QM/MM energy of -2.8 kcal/mol). Meanwhile the relative MM energy of the TS1 for ORIII is 1.7 kcal/mol lower (-3.3 kcal/mol) compared to that of the TS1 for OSI (-1.6 kcal/mol), which results in the lower QM/MM energy barrier observed for the formation of the TI-2 ORIII, since the QM energies of these TSs differ just by 0.1 kcal/mol. Considering that a major decreasing of the MM energy (-2.3 kcal/mol) also contributes to the stabilization of the TS1 for ORI (section **6.3.1.1**), these results show that the van der Waals interactions (hence the CH-π interactions) between propranolol and CalB play an important role for the favored transformation of *R*-propranolol over *S*-propranolol either in binding mode I or II.

Table 22 Electrostatic contribution (in kcal/mol) of the residues of the oxyanion hole to the stabilization or destabilization of the QM region at the stationary points along the B3LYP/CHARMM reaction profiles of *S*-propranolol[a]

Reaction profile	TS1		TI-2		TS2		PDC	
	Thr40	Gln106	Thr40	Gln106	Thr40	Gln106	Thr40	Gln106
OSI	4.1	3.0	14.2	11.1	7.7	6.3	3.1	2.3
OSII	3.0	1.6	6.8	4.8	0.2	0.7	-3.4	-1.4
OSIII	2.1	1.5	7.8	6.0	2.2	2.6	-2.2	-0.5
OSIV	2.5	1.9	5.9	3.5	1.4	0.9	-2.8	-2.9

[a] The contribution of each residue was estimated by setting their point charges to zero in additional energy calculations (i.e. by electrostatic perturbation). Energy values are given relative to the MCC. Positive values mean stabilization, whereas negative values mean destabilization.

On the other hand, it is important to note that the relative QM energy of the TS1 for OSI is 3.8 kcal/mol higher compared to the TS1 for ORI (see **Table 40** and **Table 42** in **Appendix E**). Thus the QM energy is the major source of the favored transformation of *R*-propranolol in binding mode I. Two events have been identified which may contribute to this QM energy difference between these TSs and thus to the enantioselectivity of the reaction. In the first place the internal energy of *S*-propranolol in the TS1 for OSI is expected to be higher in comparison to that of *R*-propranolol in the TS1 for ORI. This is based on the observed difficulty of the TI-2s of *S*-propranolol in binding mode I to keep the His224:**H**-Sub:**O** hydrogen bond interaction during the MD simulations (see section **5.3.2.2.1**) [28], which is necessarily formed in the TS1 (see **Fig. 101** in **Appendix E**). Secondly in the MCC of ORI the Sub:**O** atom is

better positioned for executing the nucleophilic attack on the acetate group, as judged by the respective distance and angle (see **Table 18** and **Table 23**) [172]. The energy contribution of these events is notable in the gas-phase QM calculations, in which the energy of the TS1 for OSI is 9.3 kcal/mol higher relative to the TS1 for ORI.

Table 23 Relevant interatomic distances and bond lengths[a] corresponding to the stationary points along the reaction profile obtained at the B3LYP(TZVP)/CHARMM level for the transformation of *S*-propranolol[b] in binding mode I via the TI-2 OSI[c]

Distance (Å)	**OSI**				
	MCC	**TS1**	**TI-2**	**TS2**	**PDC**
Asp187:O_D-His224:H_{ND}	1.88 (166)	1.76 (166)	1.61 (172)	1.65 (173)	1.72 (174)
His224:H_{ND}-His224:N_D	1.04	1.05	1.07	1.06	1.04
His224:**H**-Ser105:Oγ	-	-	1.71 (168)	1.39 (171)	1.02
Ace:C-Ser105:Oγ	1.33	1.38	1.59	2.03	2.44
His224:Nε-Sub:**H**	1.82 (173)	1.10 (169)	1.05	1.14 (171)	1.59 (172)
Sub:**H**-Sub:**O**	1.00	1.57	3.16 (140)	-	-
Ace:C-Sub:**O**	2.71 (95)	2.04 (106)	1.44 (109)	1.37 (114)	1.33 (116)
Ace:C-Ace:O	1.23	1.24	1.29	1.25	1.23
Ace:O-Gln106:NH	1.96 (151)	1.94 (160)	1.71 (170)	1.79 (166)	1.94 (161)
Ace:O-Thr40:NH	2.00 (168)	1.93 (168)	1.74 (171)	1.77 (169)	1.83 (167)
Ace:O-Thr40:OH	1.72 (171)	1.71 (171)	1.68 (174)	1.71 (174)	1.72 (171)
Sub:*H*-Thr40:O	3.27 (126)	3.31 (117)	2.53 (141)	2.52 (142)	2.53 (141)
Sub:**O**-Thr40:NH	3.91 (128)	3.76 (137)	2.92 (131)	2.93 (131)	2.97 (130)
Sub:**O**-Thr40:OH	3.76 (130)	3.61 (140)	2.88 (129)	2.90 (127)	2.95 (124)

[a] Distances and bond lengths are given in Å. Angles in degrees for both the corresponding hydrogen bonds and the nucleophilic attack (Sub:**O**···Ace:C=O) are given in brackets.
[b] The atoms corresponding to the hydroxyl and amino group of propranolol (Sub) are marked in bold and italic respectively.
[c] Ace is the acetyl group which is transferred from the acetylated catalytic serine (SEA) to the alcohol oxygen of propranolol.

6.3.2.2. Details about the transformation of S-propranolol in binding mode II

As explained above the major problem of the transformation of *S*-propranolol in binding mode II is the thermodynamically unfavorable formation of the PDCs. Interestingly, in the gas-phase calculations no all formations of the PDCs of *S*-propranolol in binding mode II are endothermic. This is the case of the PDC of OSIII, whose formation in the gas-phase is exothermic by -3.6 kcal/mol (**Fig. 47a**). In addition the energies of the PDCs of OSII and OSIV are lower in the gas-phase. Thus the endothermic formation of these PDCs of *S*-propranolol is partly attributed to their electrostatic destabilization by the MM region, which is about 3-4 kcal/mol relative to the MCCs (see **Fig. 47b**). As shown in **Table 22**, the residues of the oxyanion hole are the major responsible for this destabilization energy, which is attributed to the weakening of the hydrogen bond interactions with these residues (**Table 24**). This is added to the fact that the MM energy is increased in these PDCs respect to their MCCs (see **Table 44** in **Appendix E**), which means that there is also a weakening of the van der Waals interactions between propranolol and CalB.

6.3.3. The TI-2 is not a TS analogue in the CalB-catalyzed acetylation of propranolol

An additional result of the QM/MM calculations which should be noted is that in contrast to what is commonly suggested for lipase-catalyzed reactions, the TI-2 is not a good representation of the TSs of the deacylation step in the CalB-catalyzed acetylation reaction of propranolol in toluene. It can be seen in **Fig. 43** and **Fig. 46** that in most of the computed reaction profiles TS1 and TS2 differ energetically from the TI-2 by more than 2.0 kcal/mol. Only in the reaction profiles of ORIV and OSIV, which belong to the less favorable reaction pathways, the TI-2 is both energetically and geometrically close to the TS1 and TS2, respectively. It can be particularly observed that in the most favorable reaction pathways (ORI, ORIII and OSI) the TI-2 differs energetically from the TS1 (rate-limiting step) by more than 6.5-14.0 kcal/mol. Thus these results show that for lipase-catalyzed reactions it should not be considered as a general rule that the TSs closely resemble (energetically and structurally) to the TIs.

The above of course does not invalidate the molecular modeling of the TIs as an approach for understanding the origin of the enantioselectivity of lipase-catalyzed reactions. Similarly to other studies it has been previously obtained from the molecular modeling of the TI-2 valuable qualitative information about the origin of the enantioselectivity of CalB catalyzing acetylation of propranolol (**Chapter 5**). However, there are factors contributing to the enantioselectivity of the reaction which are only visible by computing the reaction profiles. A good example are the variations of the hydrogen bond interactions with the oxyanion hole as the reaction proceeds, which have shown to have a

Table 24 Relevant interatomic distances and bond lengths[a] corresponding to the stationary points along the reaction profiles obtained at the B3LYP(TZVP)/CHARMM level for the transformation of *S*-propranolol[b] in binding mode II via the TI-2s OSII-OSIV[c]

Distance (Å)	OSII					OSIII					OSIV				
	MCC	**TS1**	**TI-2**	**TS2**	**PDC**	**MCC**	**TS1**	**TI-2**	**TS2**	**PDC**	**MCC**	**TS1**	**TI-2**	**TS2**	**PDC**
Asp187:O_D-His224:H_{ND}	1.81 (170)	1.62 (171)	1.52 (175)	1.59 (176)	1.66 (175)	1.98 (168)	1.75 (170)	1.58 (176)	1.63 (177)	1.70 (176)	1.82 (168)	1.68 (167)	1.54 (174)	1.58 (175)	1.66 (176)
His224:H_{ND}-His224:N_D	1.04	1.07	1.09	1.06	1.05	1.03	1.05	1.08	1.06	1.05	1.04	1.06	1.08	1.07	1.05
His224:**H**-Ser105:Oγ	-	-	1.76 (151)	1.20 (167)	1.02	-	-	1.67 (164)	1.33 (172)	1.02	-	-	1.66 (164)	1.41 (171)	1.02
Ace:C-Ser105:Oγ	1.33	1.38	1.52	1.96	2.33	1.33	1.36	1.55	1.99	2.52	1.34	1.39	1.57	1.92	2.44
His224:Nε-Sub:**H**	1.77 (168)	1.11 (171)	1.04	1.28 (167)	1.60 (168)	2.11 (147)	1.13 (170)	1.05	1.17 (172)	1.64 (176)	1.90 (173)	1.11 (176)	1.05	1.12 (171)	1.59 (173)
Sub:**H**-Sub:**O**	1.00	1.48	2.34 (130)	-	-	0.98	1.45	2.62 (132)	-	-	0.99	1.49	2.46 (128)	-	-
Ace:C-Sub:**O**	2.75 (100)	2.05 (109)	1.49 (118)	1.39 (122)	1.35 (124)	3.11 (101)	2.22 (107)	1.48 (118)	1.38 (122)	1.34 (124)	2.73 (94)	1.98 (108)	1.47 (118)	1.38 (122)	1.33 (124)
Ace:C-Ace:O	1.22	1.24	1.28	1.24	1.22	1.23	1.24	1.29	1.24	1.22	1.23	1.25	1.29	1.25	1.23
Ace:O-Gln106:NH	1.92 (149)	2.01 (155)	2.02 (160)	2.15 (153)	2.33 (143)	2.07 (148)	2.10 (151)	2.06 (160)	2.20 (152)	2.59 (137)	1.86 (154)	1.95 (163)	2.02 (167)	2.14 (162)	2.47 (155)
Ace:O-Thr40:NH	1.80 (170)	1.78 (169)	1.80 (168)	1.88 (164)	2.12 (158)	1.95 (168)	1.98 (168)	1.87 (170)	1.99 (166)	2.33 (158)	1.90 (165)	1.80 (168)	1.77 (168)	1.83 (164)	1.95 (157)
Ace:O-Thr40:OH	1.72 (170)	1.74 (169)	1.74 (170)	1.76 (168)	1.72 (168)	1.73 (174)	1.74 (172)	1.72 (175)	1.72 (177)	1.66 (179)	1.70 (171)	1.71 (169)	1.72 (171)	1.73 (168)	1.71 (164)
Sub:*H*-Sub:O	3.89	3.89	3.82	3.75	3.72	4.33	4.51	4.43	4.38	4.30	4.19	4.32	4.71	4.70	4.69

[a] Distances and bond lengths are given in Å. Angles in degrees for both the corresponding hydrogen bonds and the nucleophilic attack (Sub:**O**⋯Ace:C=O) are given in brackets.
[b] The atoms corresponding to the hydroxyl and amino group of propranolol (Sub) are marked in bold and italic respectively. The naphthoxy oxygen of propranolol is indicated as Sub:O.
[c] Ace is the acetyl group which is transferred from the acetylated catalytic serine (SEA) to the alcohol oxygen of propranolol.

significant effect on the thermodynamic and kinetic of the reaction. This is similar to the observed for the hydrolysis of acetylcholine catalyzed by acetylcholinesterase (a serine protease as lipases) [186]. Therefore the molecular modeling of the TIs alone must not be considered enough for understanding the origin of the enantioselectivity of lipase-catalyzed reactions.

6.3.4. Key enzyme residues for the enantioselectivity

As shown in **Fig. 42** there are several enzyme-substrate interactions that may contribute to the stabilization of the system along the reaction profile of ORI and thus facilitate the reaction via this TI-2. In addition to the residues of the oxyanion hole, the individual electrostatic contribution to the stabilization of the TI-2 ORI and its respective MCC of each residue around 7 Å from the substrate has been estimated (see **Fig. 48**). It has essentially been found that in addition to the residues of the oxyanion hole those residues participating in CH-π interactions with the naphthyl rings of propranolol (e.g. Ile89, Leu140 and Thr138) contribute significantly to the electrostatic stabilization of the system, particularly the residue Ile189. Thus the latter may be considered a very important residue for the observed faster transformation of *R*-propranolol. This reinforces the previous conclusions about the importance of these CH-π interactions for the enantioselectivity of the reaction given in the precedent chapters.

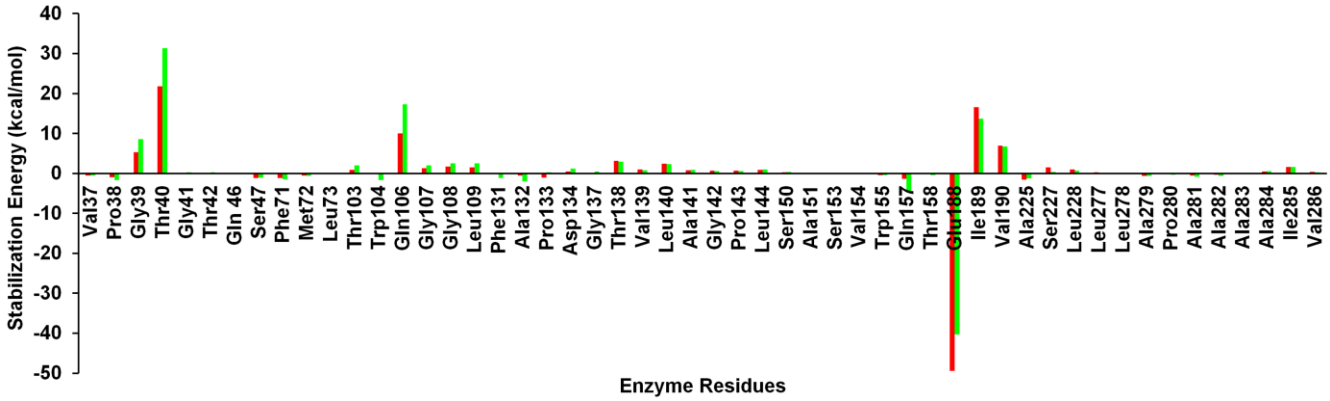

Fig. 48 Electrostatic contribution to the stabilization (positive values) or destabilization (negative values) of the QM system in the TI-2 ORI (green) and its respective MCC (red) by the residues around 7 Å from the substrate.

6.3.5. Other levels of theory

QM/MM single-point calculations were carried out for all stationary points along the computed B3LYP/CHARMM reaction profiles of *R*- and *S*-propranolol using different DFT methods. The influence of dispersion was checked at the B3LYP-D2/D3 level. In addition, the functionals M06,

M06-2X and wB97XD were tested for validation of the B3LYP results. On the other hand, it was also evaluated the accuracy of the semiempirical methods AM1, PM3, MNDO, OM2 and OM3, as well as of the SCC-DFTB method, for describing the thermochemistry and kinetic of the reaction. In this case the TI-2s ORI and ORIV were subjected to reaction path scans and TS search as it was done at the B3LYP level. This was done to figure out which of these methods is the most appropriate to be used in QM/MM free energy calculations, for which a QM method with low computational cost is required. Free energy calculations are important for analyzing the role of the entropy on the enantioselectivity of the reaction, which will be part of another investigation. The results with the different levels of theory mentioned above are discussed in the next sections.

6.3.5.1. QM/MM reaction profiles of R- and S-propranolol obtained with different DFT methods

Generally speaking, as observed at the B3LYP level, the other DFT methods used for computing the reaction profiles of *R*- and *S*-propranolol (see **Fig. 106** to **Fig. 107** in **Appendix E**) predict the transformation of *R*- and *S*-propranolol to be favored via ORI, ORIII and OSI, respectively. They also show that the transformation of *R*-propranolol is favored over that of *S*-propranolol either in binding mode I or II (see **Table 25**). However, there are some differences compared to the reaction profiles at the B3LYP level which should be highlighted. In most of the reaction profiles computed with the other DFT methods the relative energies of the TS1 and TI-2 are lower than those observed in the B3LYP calculations, while those of the TS2 and PDC are higher. Thus, in contrast to the observed at the B3LYP level, with the other DFT methods the transformation of *R*-propranolol via ORI and that of *S*-propranolol via OSI are practically thermoneutral, by -0.1 to 1.2 kcal/mol and -1.1 to 0.7 kcal/mol, respectively. In addition, the energy barriers involved in the formation of the PDCs from their respective TI-2s are higher respect to the B3LYP calculations, which may correct for the known general tendency of B3LYP to underestimate barriers. Interestingly, this changes the rate-determining step for the transformation of *R*-propranolol via ORI to the formation of the PDC from the TI-2.

6.3.5.2. Comparison of the semiempirical methods and the SCC-DFTB method

Firstly the semiempirical methods and the SCC-DFTB method were tested using the TI-2 ORI. The complete reaction profile for this TI-2 could be only computed with AM1, MNDO and SCC-DFTB. With the other methods (PM3, OM2 and OM3) the shape of the barriers obtained from the scans is flat or not very well defined, and attempts to locate the TSs (TS1 and TS2) failed. Among the computed reaction profiles the SCC-DFTB/CHARMM reaction profile is the most energetically close to those at the DFT/CHARMM level. In contrast, in the reaction profiles at the MNDO and AM1 level the relative

energies of most stationary points are notably higher or lower compared to the observed at the DFT level (e.g. the energy barrier for the formation of ORI is 18.2 kcal/mol, 32.1 kcal/mol and 4.6 kcal/mol, with AM1, MNDO and SCC-DFTB, respectively; see **Fig. 108** in **Appendix E**).

Table 25 QM/MM energy barriers (in kcal/mol) obtained for the rate-limiting step involved in the transformation of *R*-propranolol (via ORI and ORIII) and *S*-propranolol (via OSI) using different QM methods[a]

QM method	ORI	ORIII	OSI	OSI-ORI[b]	OSI-ORIII[b]
B3LYP	7.1	10.0	11.6	4.5	1.6
B3LYP-D2	7.5	7.5	8.8	1.3	1.3
B3LYP-D3	6.3	8.1	9.5	3.2	1.4
M06	10.1	11.3	12.2	2.1	0.9
M06-2X	11.4	9.7	11.8	0.4	2.1
Wb97XD	9.6	9.9	11.5	1.9	1.6

[a] The rate-limiting step is the formation of the TI-2, except for ORI at DFT levels different from B3LYP for which it is the formation of the PDC (see the text).
[b] Difference between the respective energy barriers of *S*- and *R*-propranolol.

Considering these results it was decided to test the semiempirical methods one more time using another TI-2 configuration (ORIV). The complete reaction profile for ORIV could be computed with AM1, MNDO and OM3. With PM3 only TS1 was located, while with OM2 it was not possible to locate any of the TSs. As observed for the TI-2 ORI, the reaction profiles obtained for ORIV using semiempirical methods are not energetically close to the DFT/CHARMM reaction profiles (see **Fig. 108** in **Appendix E**). Thus these results show that the SCC-DFTB method outperforms the studied semiempirical methods in accuracy for studying the thermochemistry and kinetic of the CalB-catalyzed acetylation of propranolol.

6.4. Conclusions

QM/MM calculations were performed to understand the origin of the enantioselectivity of the CalB-catalyzed acetylation of (*R*,*S*)-propranolol in toluene. These calculations were focused on the deacylation step of the reaction, from which the enantioselectivity is originated. The two characteristic binding modes of the substrate were taken into account. QM(B3LYP/TZVP)/CHARMM calculations show the transformation of *R*-propranolol to be thermodynamically favorable (exothermic) in both

binding mode I and II (by -2.6 and -8.8 kcal/mol, respectively), while for *S*-propranolol only in binding mode I (by -2.8 kcal/mol). On the other hand, these calculations show the formation of the second tetrahedral intermediate (TI-2) to be the rate-limiting step for the transformation of both propranolol enantiomers. The transformation of *R*-propranolol in binding mode I is predicted to be faster than in binding mode II, with an energy barrier for the formation of the TI-2 in binding mode I 2.9 kcal/mol lower relative to the binding mode II. Moreover, the transformation of *R*-propranolol in both binding mode I and II is predicted to be faster than that of *S*-propranolol in binding mode I. The activation barriers for the formation of the TI-2s of *R*-propranolol in binding mode I and II are 4.5 kcal/mol and 1.6 kcal/mol lower compared to the *S*-propranolol in binding mode I, respectively. This is in agreement with the faster transformation of *R*-propranolol observed in experiments. Furthermore, translation of the experimental enantioselectivity of the reaction predicts about 2.4 kcal/mol free energy difference that is in accordance with calculations.

The hydrogen bond interactions between the acetate oxygen (Ace:O) and the residues of the oxyanion hole are identified to be a determinant factor of the thermodynamic nature of the transformations of *R*- and *S*-propranolol. When the transformation of *S*-propranolol occurs in binding mode II a weakening of these hydrogen bond interactions as the reaction proceeds is observed. This leads to the electrostatic destabilization of the product complex (PDC) respect to the Michaelis complex (MCC), and thus to the endothermic formation of it. Similarly occurs for *R*-propranolol in binding mode I. However, a conformer of this enantiomer is identified, whose conformational changes as the reaction proceeds compensate (or outperform) the observed electrostatic destabilization of the PDC, which leads the overall reaction to be exothermic. Conversely, the interactions between the Ace:O atom and the residues of the oxyanion hole may be preserved or strengthened when the transformation of *R*- and *S*-propranolol proceed in binding mode II and I, respectively. In addition, in the latter cases, a displacement of the alcohol oxygen (Sub:**O**) toward the residues of the oxyanion hole is presented in the TI-2, which favors the formation of hydrogen bond interactions in the PDC which are not present in the MCC. These events contribute significantly to the electrostatic stabilization of the PDC and thus to the observed exothermic formation of it.

The CH-π interactions between the naphthyl rings of propranolol and the surrounding protein residues are the major source of the observed higher stabilization of the rate-limiting transition state (TS1) involved in the transformation of *R*-propranolol in binding mode II respect to the TS1 for *S*-propranolol in binding mode I. These interactions are also important for the stabilization of the TS1 involved in the

transformation of *R*-propranolol in binding mode I. However, the remarkably lower activation barrier observed in this case has another two important components: (i) in binding mode I the internal energy of *R*-propranolol in the TS1 is lower compared to the binding mode II and in turn to the observed for *S*-propranolol in binding mode I; (ii) in the MCC for *R*-propranolol in binding mode I the Sub:**O** atom is better positioned for executing the nucleophilic attack on the acetate group, with a distance (angle) of 2.46 Å (100°). Based on the strength of its interactions with the naphthyl rings of *R*-propranolol in both binding mode I and II, the residue Ile189 is identified as key for the enantioselectivity of the reaction.

On the other hand, in contrast to what is commonly suggested for lipase-catalyzed reactions, the QM/MM calculations show that the TI-2 is not a TS analogue in the CalB-catalyzed acetylation of (*R,S*)-propranolol in toluene, as it exhibits energies about 6.5-14.0 kcal/mol lower compared to the TS1. However, as it was described in **Chapter 5** valuable qualitative information about the molecular basis of the enantioselectivity of the reaction is obtained from MD simulations of the TI-2. Therefore the QM/MM calculations do not invalidate the latter as an approach for get a better understanding of lipase-catalyzed reactions, but show it must not be considered as a general rule that the TI-2 is a TS analogue in these reactions.

To summarize, the QM/MM calculations presented here provide detailed information about the origin of the enantioselectivity of the reaction, which may be helpful for improving the enantioselective acylation of (*R,S*)-propranolol catalyzed by CalB, through the rational redesign of CalB or the reaction conditions.

Chapter 7. Summary and general conclusions

In this thesis the kinetic resolution of (*R,S*)-propranolol via acetylation reaction catalyzed by *Candida antarctica lipase B* (CalB) in toluene was studied through an experimental and computational approach. The aim was to get a deep knowledge about the origin of the enantioselectivity of this reaction. Molecular modeling of the reaction gave valuable insights at molecular level which may be used for improving the enantioselective synthesis of propranolol via CalB catalyzed acylation reaction, either through a rational redesign of CalB or the reaction conditions.

It was experimentally found that CalB displays moderate enantioselectivity (E = 61-63) and exclusive chemoselectivity favoring the faster formation of *R*-*O*-acetyl-propranolol, which was obtained with an enantiomeric purity of 95-96 % at a conversion degree of 21-33 %. The chemo- and enantioselectivity of the reaction was independent of the reaction conditions evaluated here, that included the enzyme purification procedure, the ratio toluene/methanol and the concentration of propranolol.

From molecular modeling of the MCCs between AcCalB and *R*- or *S*-propranolol by using a docking protocol the chemoselectivity of the reaction was rationalised. Only productive MCCs leading to formation of *O*-acetyl-propranolol (*O*-AP) were identified for both propranolol enantiomers. Two events were found to be responsible for the observed chemoselectivity of CalB in favor of the formation of *O*-AP: i) a proper position of the amino group of propranolol for executing the nucleophilic attack at the acetylated catalytic serine involves unfavorable steric contacts with the enzyme ii) the amino group is not well positioned for a spontaneous *O*- to *N*-acyl migration in the propranolol conformers being *O*-acylated by CalB.

On the other hand, the rationalisation of the enantioselectivity involved MD simulations of the MCCs and TIs of the deacylation reaction as well as computing of the respective reaction profiles by QM/MM calculations. It was found that both the binding of propranolol to the acyl-enzyme and the subsequent acyl transfer contribute to the enantioselectivity of the reaction. In both the MD simulations of the MCCs and TI-2s different conformations of *R*- and *S*-propranolol were identified which in principle may be transformed to *O*-AP. Based on the analysis of the essential hydrogen bond interactions for the

catalytic process (those involving the catalytic triad and the oxyanion hole), the interactions between the enzyme and the side chains of propranolol, and the temporal stability of such conformations, the reactivities of *R*- and *S*-propranolol were qualitatively estimated. Several conformers of *R*-propranolol were identified which are expected to be more reactive than those of *S*-propranolol. In the MCCs and TI-2s of such conformers the CH-π interactions between the naphthyl group of propranolol and the surrounding protein residues are stronger than those observed for the *S*-propranolol conformers. Thus these interactions are considered to be important for the stabilization of the transition states involved in the transformation of *R*-propranolol. Based on the strength of their interactions with the naphthyl group of *R*-propranolol, Ile189, Ala282 and Leu278 were identified as key residues for the enantioselectivity of CalB.

The higher reactivity of *R*-propranolol respect to *S*-propranolol was quantitatively corroborated in the subsequent QM/MM calculations. The energy barrier involved in the transformation of *S*-propranolol was estimated to be 4.5 kcal/mol higher compared to *R*-propranolol. The important role that the CH-π interactions between the naphthyl group of propranolol and the surrounding protein residues play for the enantioselectivity was also corroborated. Moreover, the QM/MM calculations revealed that the hydrogen bond patterns with the residues of the oxyanion hole as the reaction proceeds from the MCC to the product complex (PDC) are also important for the enantioselectivity of the reaction. A weakening of these interactions as the reaction proceeds leads to the endothermic formation of the product (i.e. to a thermodynamically unfavorable reaction). On the other hand, in contrast to what is commonly suggested for lipase-catalyzed reactions, the QM/MM calculations showed that the TI-2 is not a TS analogue in the CalB-catalyzed acetylation of (*R*,*S*)-propranolol in toluene. The TI-2 exhibits energies about 6.5-14.0 kcal/mol lower compared to the rate-limiting TS.

Appendix A

Supplementary information for Chapter 2

NMR analysis of the chemical acetylation of (*R,S*)-propranolol

Once the chemical acetylation reaction of propranolol was completed, the reaction mixture was analyzed by ^{1}H- and ^{13}C-NMR spectroscopy. The ^{1}H-NMR spectrum resulted to be complex because of overlapping signals, especially in the chemical shift ranges 7.3-7.5 and 3.7-4.4 ppm (**Fig. 49**). The composition of the reaction mixture was then principally determined by ^{13}C-NMR and by using DEPT135° as well as HMBC and HSQC heteronuclear correlation techniques. DEPT135° was used for determining the carbon type (i.e. C, CH, etc.). Assignments of the protonated carbons were made applying the HSQC method using delay values which correspond to the ^{1}J(C,H) coupling. The non-protonated carbons were determined using delays in the HMBC experiment to emphasize the long range coupling, either ^{2}J(C,H) or ^{3}J(C,H).

It was possible to identify easily the ^{13}C-NMR signals (**Fig. 50**) corresponding to the non-protonated carbon atoms (chemical shift range 134-180 ppm) in the DEPT135° spectrum (**Fig. 51**), in which the signal intensity is zero for this type of carbon atoms.

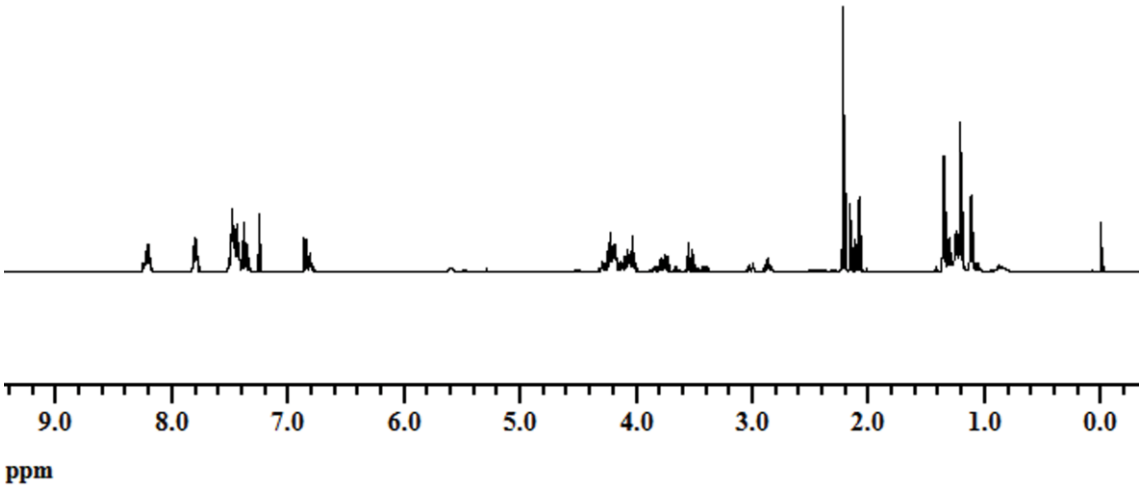

Fig. 49 ^{1}H-NMR spectrum of the reaction mixture of the chemical acetylation of propranolol

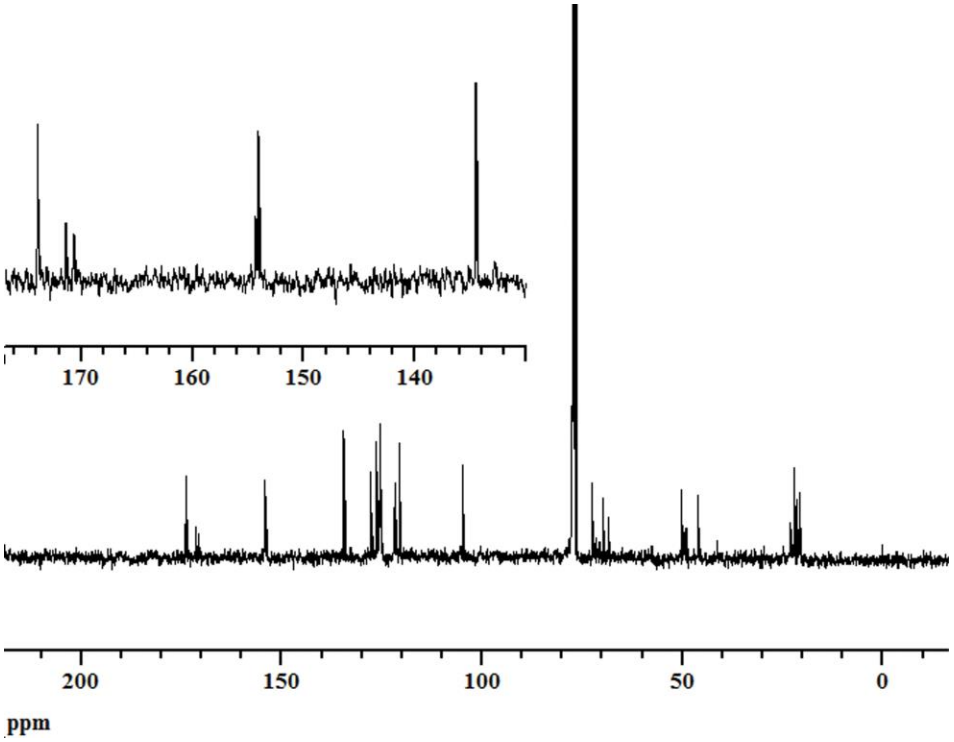

Fig. 50 ^{13}C-NMR spectrum of the reaction mixture of the chemical acetylation of propranolol.

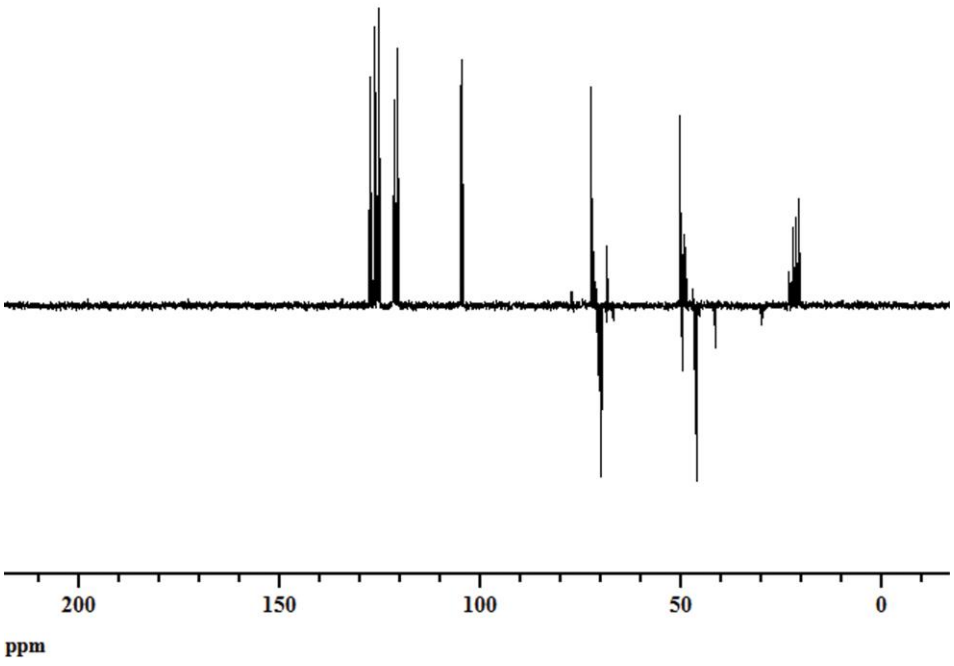

Fig. 51 DEPT135° spectrum of the reaction mixture of the chemical acetylation of propranolol.

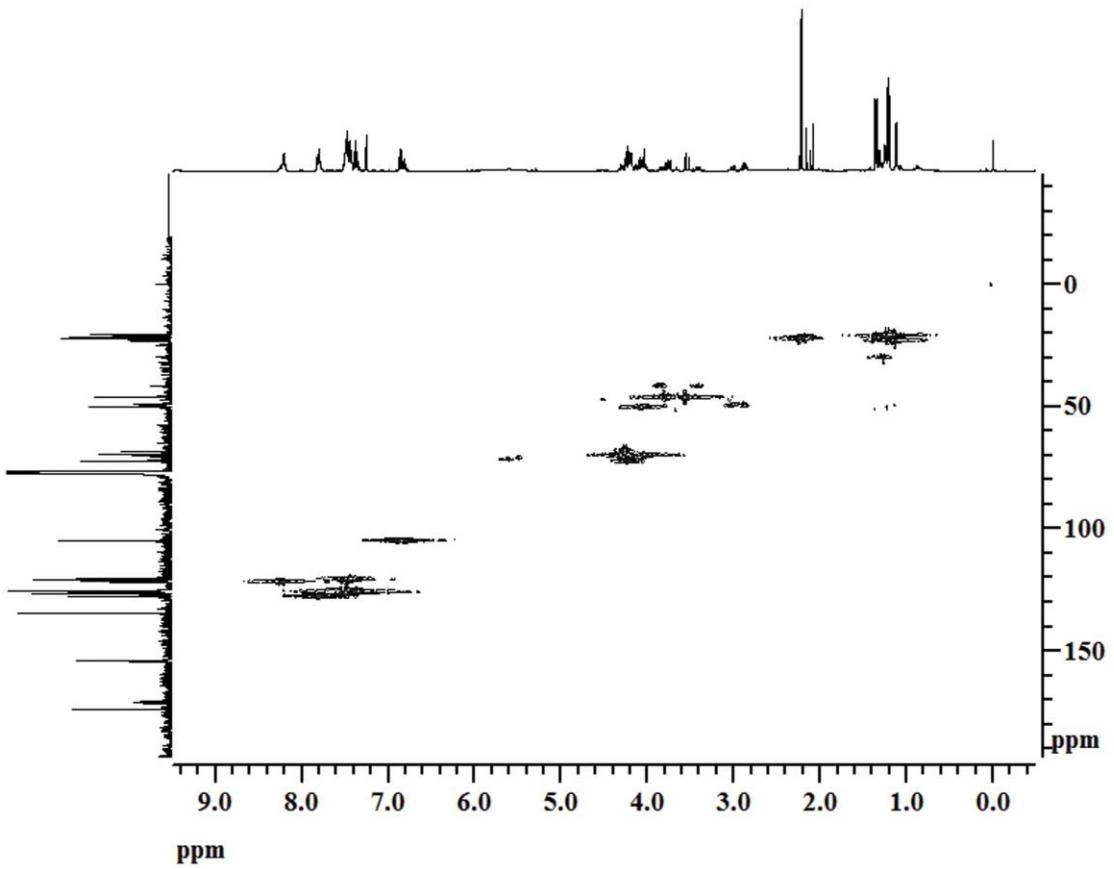

Fig. 52 HSQC spectrum of the reaction mixture of the chemical acetylation of propranolol.

The HSQC spectrum of the reaction mixture is shown in **Fig. 52**. Using the HSQC experiment it was possible to identify the protonated carbon atoms and to verify the ^{13}C-NMR signals assigned to the non-protonated carbon atoms. The ^{13}C-NMR chemical shifts of the protonated carbons are distributed in the ranges 104-130 ppm for CH aromatic carbons, 40-73 ppm for CH and CH_2 non-aromatic carbons, and 20-30 ppm for methyl groups. Nine signals were identified corresponding to non-protonated carbon atoms. According to the reaction scheme (**Fig. 53**), it can be noted that the signals for non-protonated carbon atoms correspond to the carbonylic carbon of the acetylated compounds (*N*-AP, *O*-AP and acetyl chloride), and to the aromatic carbons in propranolol and its acetylated derivatives, which are not bound to hydrogen.

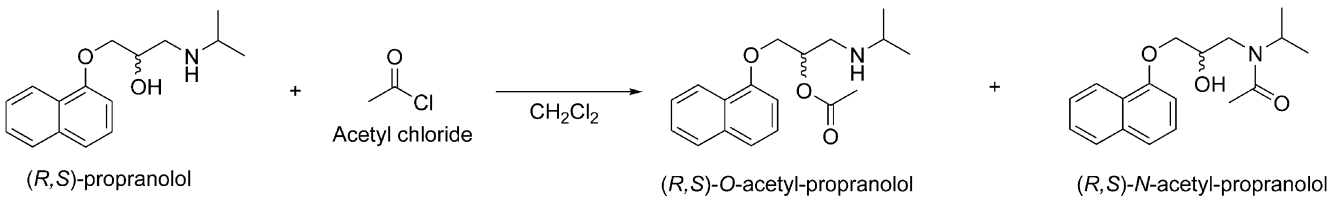

Fig. 53 Chemical acetylation of (*R*,*S*)-propranolol.

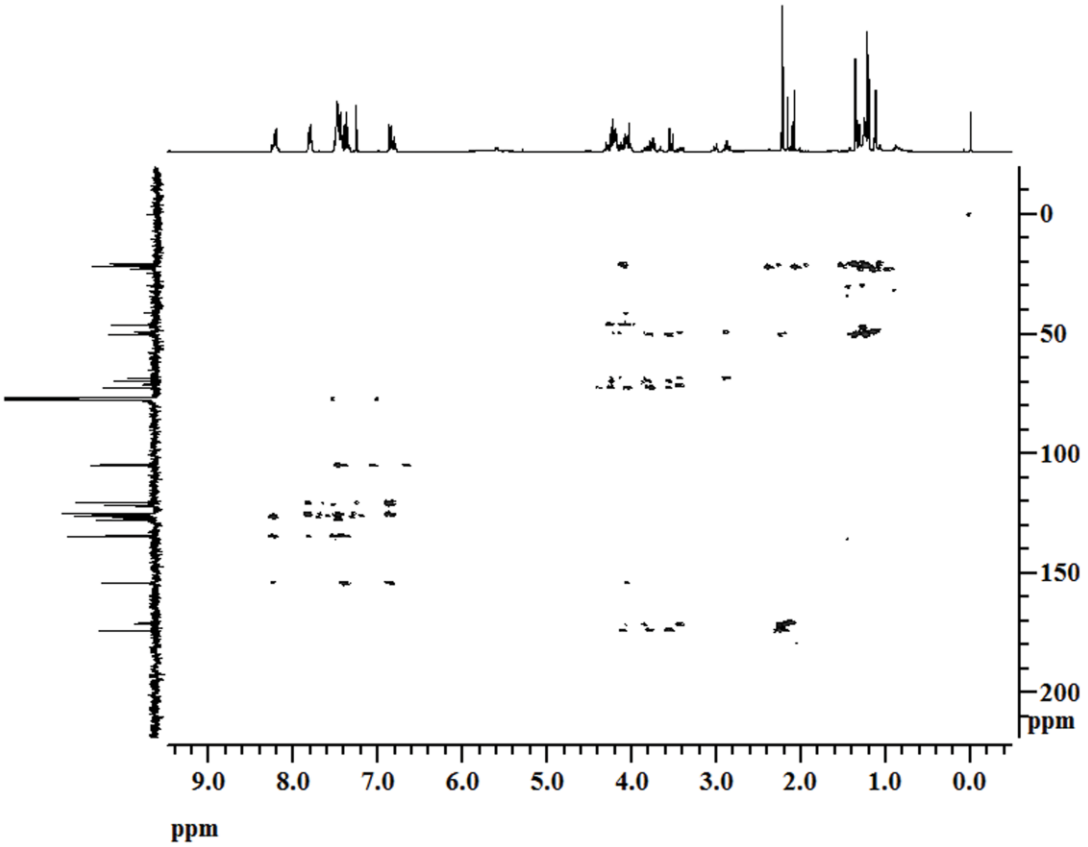

Fig. 54 HMBC spectrum of the reaction mixture of the chemical acetylation of propranolol.

For a full assignment of the chemical shifts of the chemical compounds in the reaction mixture, both HSQC and HMBC spectra were used. The HMBC spectrum is shown in **Fig. 54**. The heteronuclear long range interactions between the ^{13}C-NMR signals in the range 170-175 ppm (at 170.6, 171.4 and 173.9 ppm) and methyl groups (^{1}H-NMR chemical shift range 2.0-2.5 ppm) confirmed that these ^{13}C-NMR chemical shifts correspond to the carbonylic carbons. The signals at 171.4 and 173.9 ppm present also long range interactions with CH and CH_2 groups. Therefore these signals were attributed to the acetylated derivatives of propranolol, and the signal at 170.6 to the remaining acetyl chloride (**Fig. 55**). According to the number, type and intensity of the ^{1}H-^{13}C couplings of the ^{13}C-NMR signals of the carbonylic carbons of the acetylated products of propranolol, the signal at 171.4 ppm was attributed to *O*-AP and 173.9 to *N*-AP. Verification of the full assignment of the chemical shifts was done following the general strategy described by Yoshimoto et al. [224] for identifying acylated products (obtained from alcohols) by ^{13}C-NMR, and by comparing with the ^{13}C-NMR chemical shifts reported for acetylated vinyl derivatives of propranolol [40]. In particular, the strategy described by Yoshimoto et al. [224] was taken into account for identifying *O*-acetyl-propranolol (*O*-AP). According to this study, acylation of a hydroxyl group of the substrate results in a downfield shift of the peak

corresponding to the neighboring carbon. This strategy has also been successfully used for identifying *O*-acyl-propranolol vinyl derivatives obtained in lipase-catalyzed acylation reactions [40]. It can be noted in **Table 1** that the chemical shift for the CH carbon in –OCH$_2$**C**H- of *O*-AP is downfield shifted from 68.40 ppm in the non-acetylated product to 71.63 ppm. The signals of the –O**C**H$_2$- and -**C**H$_2$N- carbons of *O*-AP are upfield shifted from 70.65 to 68.20 ppm and from 49.46 to 45.40 ppm, respectively. Finally, integration of the ^{13}C-NMR signals of the carbonylic carbons and the methyl groups of the acetate group, and of the ^{1}H-NMR signal for these methyl groups (at 2.16 ppm and 2.22 ppm for *O*-AP and *N*-AP, respectively), was used for quantifying the chemoselectivity of the chemical acetylation of propranolol, obtaining the same ratio with any of these NMR signals used.

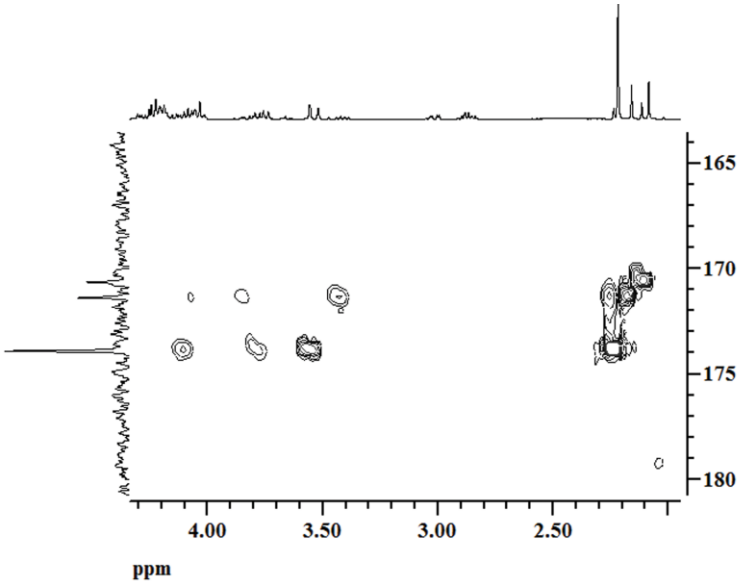

Fig. 55 Expanded HMBC spectrum of the reaction mixture of the chemical acetylation of propranolol in the region of ^{13}C-NMR chemical shifts of carboxylic carbon atoms.

NMR analysis of the CalB-catalyzed acetylation of (*R,S*)-propranolol

As shown in **Fig. 56**, the ^{1}H-NMR spectrum of the reaction mixture of the CalB-catalyzed acetylation of propranolol presented many overlapping signals. However, the following chemical compounds were clearly identified: acetaldehyde (aldehyde proton resonance at 9.2 ppm), acetic acid (acid proton resonance at 9.98 ppm), methyl acetate (acetyl protons resonance at 2.04 ppm), vinyl acetate (vinyl protons resonances at 4.2 and 4.7 ppm) and *O*-acetyl-propranolol (acetyl protons resonance at 2.18 ppm). The signals given in brackets correspond to those which were not in regions with overlapping signals and therefore were easy to identify. Compounds different from *O*-acetyl-propranolol were easily identified because they do not appear in the spectrum of the chemical

acetylation and their ^{1}H-NMR spectra are widely known. The signal at 2.18 ppm was attributed to *O*-AP according to the NMR data obtained from the analysis of the chemical acetylation. All acetylated compounds mentioned above were also identified in the ^{13}C-NMR spectrum. DEPT135° was successfully used to identify the ^{13}C-NMR signals corresponding to the carbonyl carbon in these compounds because in the DEPT135° spectrum the signal intensity is zero for this type of carbon atoms. A full assignment of the chemical shifts for these compounds was done by using HSQC and HMBC experiments. These experiments corroborated that only *O*-AP is formed from the acetylation of propranolol as the corresponding ^{1}H-^{13}C couplings for this compound were observed and not those for *N*-AP. Both the ^{13}C-NMR and ^{1}H-NMR signals obtained for these compounds showed that the amount of acetaldehyde, methyl acetate and acetic acid increased faster than the amount of *O*-AP, which indicates that the major reactions were the hydrolysis and alcoholysis of vinyl acetate and not the desired acetylation of propranolol.

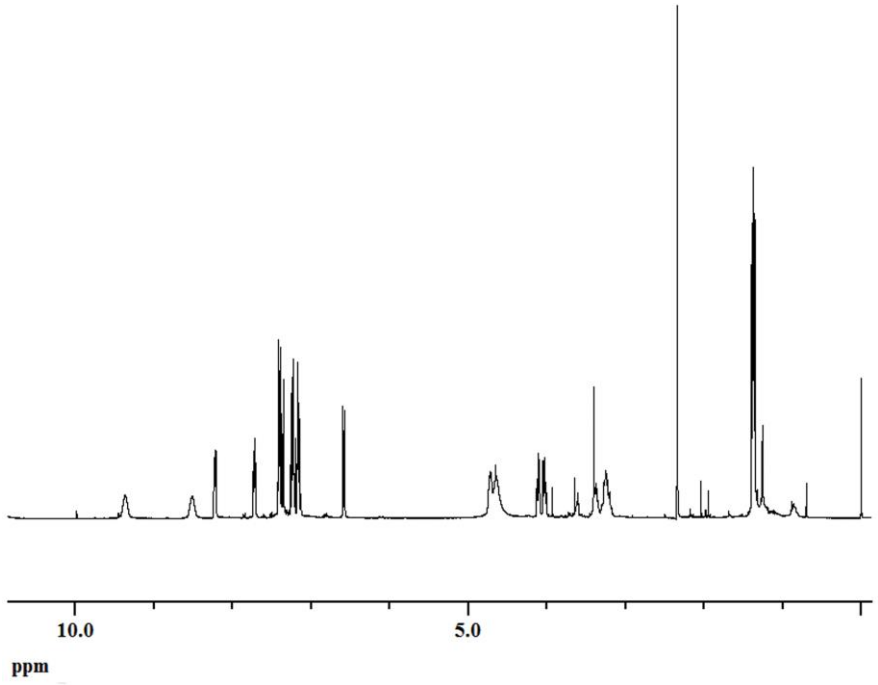

Fig. 56 ^{1}H-NMR spectrum of the reaction mixture corresponding to the acetylation of propranolol catalyzed by CalB-I.

Appendix B

Supplementary information for Chapter 3

Computational details

CHARMM parameters for the acetylated serine (SEA)

The topology for the SEA residue (see below) was created by removing a hydrogen atom from the methyl group of methyl acetate (toppar_all22_prot_model.str, MAS) and replacement of the side chain of the serine residue (top_all27_prot_lipid.rtf, SER) by the rest of MAS. For a correct description of the SEA residue the name of some atoms belonging to MAS with the same name of atoms in the preserved part of the serine residue were modified (**C** by **CE**, **O** by **OE**). The charge of the **C2** carbon atom in MAS was adjusted from -0.14 to -0.05 (this value was obtained by adding the charge (0.09) of the hydrogen atom which was removed from MAS). The **C2** atom was assigned to be a **CT2** (CH_2) atom type instead of **CT3** (CH_3). The relevant sections of the topology file are shown below.

!!!!!!!!!!!!!!!!!!!! MAS TOPOLOGY !!!!!!!!!!!!!!!!!!!!!!!!

```
RESI MAS              0.00 !
GROUP
ATOM   C1     CT3   -0.17 !            H22
ATOM   C      CD     0.63 !            |
ATOM   OM     OS    -0.34 !      H21-C2-H23
ATOM   C2     CT3   -0.14 !            \
ATOM   O      OB    -0.52 !            OM
ATOM   H11  HA      0.09 !            /
ATOM   H12  HA      0.09 !       O=C
ATOM   H13  HA      0.09 !           |
ATOM   H21  HA      0.09 !     H11-C1-H13
ATOM   H22  HA      0.09 !           |
ATOM   H23  HA      0.09 !          H12
BOND   C1   C       C    OM      OM    C2
DOUBLE   C   O
```

```
BOND   C1   H11    C1   H12    C1   H13
BOND   C2   H21    C2   H22    C2   H23
IMPR    C C1 OM O
```

!!!!!!!!!!!!!!!!!!!!!!!!SERINE TOPOLOGY!!!!!!!!!!!!!!!!!!!!!!!!

```
RESI SER                0.00
GROUP
ATOM   N     NH1   -0.47    !
ATOM   HN    H      0.31    !          |
ATOM   CA    CT1    0.07    !    HN-N      HB1
ATOM   HA    HB     0.09    !          |      |
GROUP                       !    HA-CA--CB--OG
ATOM   CB    CT2    0.05    !          |      |     \
ATOM   HB1   HA     0.09    !      O=C      HB2  HG1
ATOM   HB2   HA     0.09    !          |
ATOM   OG    OH1   -0.66
ATOM   HG1   H      0.43
GROUP
ATOM   C     C      0.51
ATOM   O     O     -0.51
BOND   CB CA   OG CB   N HN   N  CA
BOND   C  CA   C +N   CA HA   CB HB1
BOND   CB HB2   OG HG1
DOUBLE   O  C
IMPR   N -C CA HN   C CA +N O
CMAP   -C  N  CA  C   N  CA  C  +N
DONOR   HN N
DONOR   HG1 OG
ACCEPTOR   OG
ACCEPTOR   O C
```

!!!!!!!!!!!!!!!!!!!!!!!!SEA TOPOLOGY!!!!!!!!!!!!!!!!!!!!!!!!

```
RESI SEA                0.00
GROUP
```

```
ATOM   N      NH1   -0.47
ATOM   HN   H        0.31    !           |
ATOM   CA   CT1     0.07    !     HN-N     H21      OE   H11
ATOM   HA   HB      0.09    !          |      |          ||     |
GROUP                       !     HA-CA--C2--OM-CE--C1-H12
ATOM   C1    CT3    -0.17   !          |      |                |
ATOM   CE   CD       0.63   !      O=C     H23             H13
ATOM   OM  OS      -0.34   !           |
ATOM   C2    CT2   -0.05
ATOM   OE   OB     -0.52
ATOM   H11  HA     0.09
ATOM   H12  HA     0.09
ATOM   H13  HA     0.09
ATOM   H21  HA     0.09
ATOM   H23  HA     0.09
GROUP
ATOM   C    C         0.51
ATOM   O    O        -0.51
BOND   C2 CA   OM C2   N HN   N  CA
BOND   C  CA   C +N   CA HA   C2 H21
BOND   C2 H23   OM CE   C1 CE
BOND   C1 H11   C1 H12   C1 H13
DOUBLE   O  C   CE  OE
IMPR   N -C CA HN   C CA +N O   CE C1 OM OE
CMAP   -C  N  CA  C   N  CA  C  +N
DONOR   HN N
ACCEPTOR   OM
ACCEPTOR   O C
ACCEPTOR   OE CE
```

The parameters missing for describing the bond OS-CT2 and the angle bending OS-CT2-CT1 in SEA were assigned in analogy to the parameters for OSL-CTL2-CTL1 and OSL-CTL2 in lipids (par_all27_prot_lipid.prm).

Solvation cycles in the MD simulations

Information about the solvation cycles used in the MD simulations is listed below. Almost all residues of the protein were in the active region; only 80 atoms corresponding to some of the surface residues of the protein were fixed. Crystal waters and all toluene molecules were also active.

Solvation cycles

Run	Number of toluene molecules added[a]	k (mol/Å^2)*
1	860	fixed
2	100	50
3	19	45
4	12	40
5	26	35
6	14	30
7	8	25
8	10	20
9	7	15
10	13	10
11	9	5
12	11	3
13	9	1

[a]MD simulation of ACE03

*force constant of harmonic constraints on all residues within 30 Å around CA (SEA) –active region-, toluene and crystal water molecules are free to move, all other residues are fixed.

Docking of propranolol

Most of the complexes selected from the docking procedure to be optimized involved ACE03 and ACE01 as targets. Only three complexes with ACE02 were selected. In ACE02 the SEA:C atom is not exposed to the front of the binding pocket (**Fig. 17**), therefore the nucleophilic groups of propranolol are not able to be well positioned to be acetylated by ACE02 due to the size of the propranolol molecule, which has to be fitted into the binding pocket without unfavorable steric contacts. The binding affinity for these complexes and the distances used as a selection criterion are given in **Table 26**. The selected complexes (**Fig. 57** to **Fig. 61**) are characteristic for the two binding modes observed for *R*- and *S*-propranolol.

Table 26 Interatomic distances between nucleophilic groups[a] of propranolol and the carbonyl carbon of the acetylated serine (SEA:C) and the N atom of the catalytic histidine (His224:Nε) in the complexes selected from the docking procedure.

NAME[b]	TARGET	Affinity (Kcal/mol)	SEA:C-Sub:*N* (Å)	His224:Nε-Sub:*H* (Å)	SEA:C-Sub:**O** (Å)	His224:Nε-Sub:**H** (Å)
OR1	ACE03	-7.0	6.19	5.45	3.54	2.96
OR2	ACE01	-6.7	6.37	5.76	3.67	4.56
OR3	ACE01	-6.6	7.31	7.21	4.63	5.43
OR4	ACE03	-6.3	4.32	4.76	3.35	4.32
OR5	ACE01	-6.2	7.58	7.06	4.86	5.42
OR6	ACE03	-6.1	6.11	6.84	4.05	5.98
OR7	ACE03	-6.0	7.71	5.39	5.40	4.00
OR8	ACE03	-6.0	8.84	6.61	5.75	4.02
OR9	ACE01	-5.9	7.76	7.68	4.69	3.81
OR10	ACE02	-5.7	8.37	8.86	5.17	4.38
OR11	ACE01	-5.6	9.70	8.54	6.33	6.18
OR12	ACE02	-5.6	7.54	7.35	4.52	3.66
OS1	ACE03	-7.1	6.24	5.17	3.46	2.88
OS2	ACE01	-6.4	6.84	6.39	3.79	2.61
OS3	ACE03	-6.0	8.85	6.96	5.98	4.48
OS4	ACE03	-6.0	4.97	6.41	3.31	2.79
OS5	ACE02	-5.9	7.91	6.29	5.35	5.10
OS6	ACE03	-5.7	6.49	5.39	3.84	2.68
OS7	ACE02	-6.2	6.74	6.50	4.58	5.38

[a] The atoms corresponding to the amino and hydroxyl group are shown in italic and bold respectively.
[b] The complexes were named as OR or OS to emphasize the tendency of the hydroxyl group to be acetylated and according to if it is the *R* or *S* enantiomer, followed by 1, 2, 3, … according to the binding affinity value.

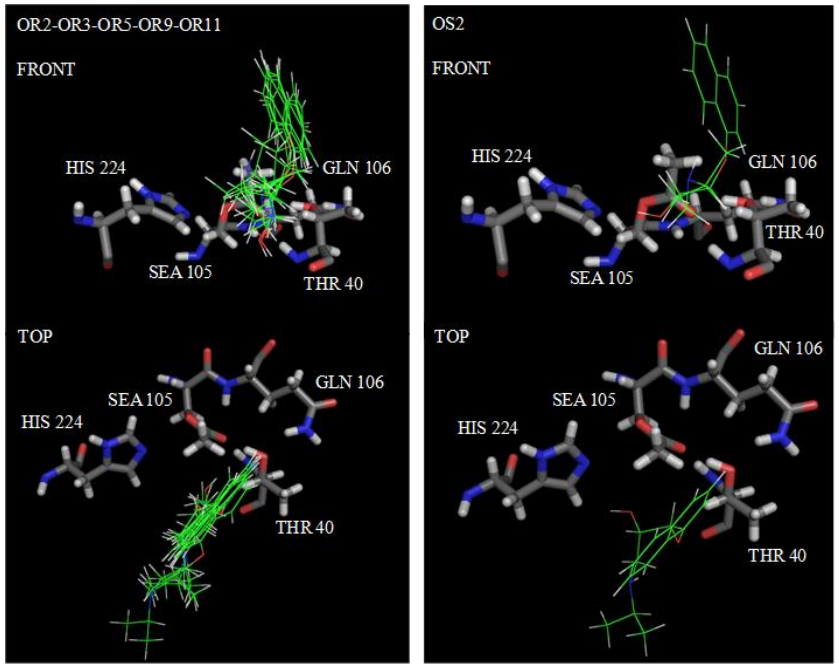

Fig. 57 Complexes between *R*- or *S*-propranolol and ACE01 selected for optimization. A top and a front view are shown.

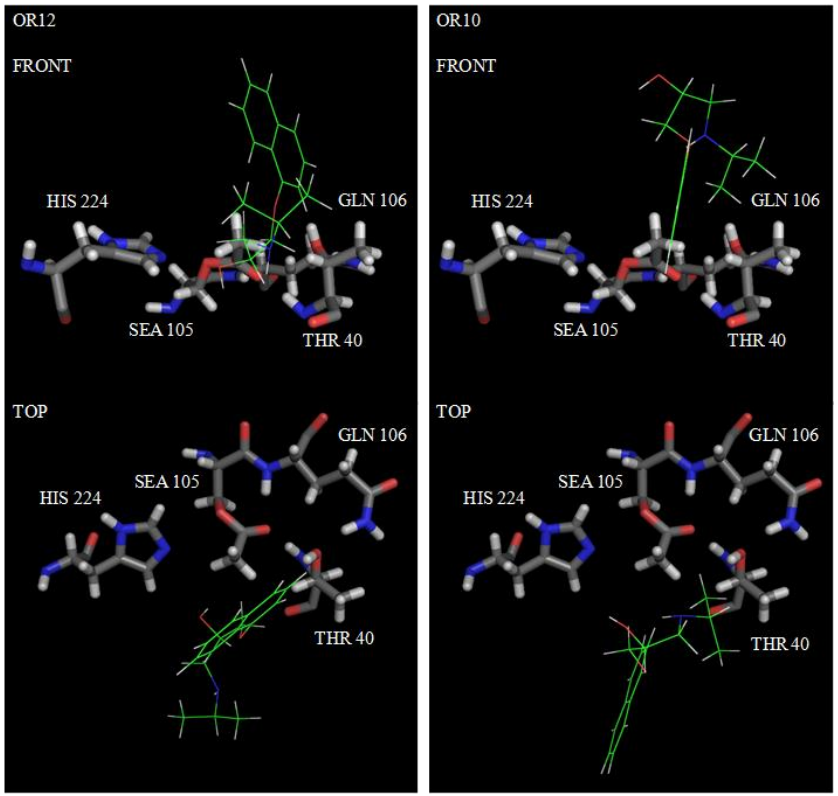

Fig. 58 Complexes between *R*-propranolol and ACE02 selected for optimization. A top and a front view are shown.

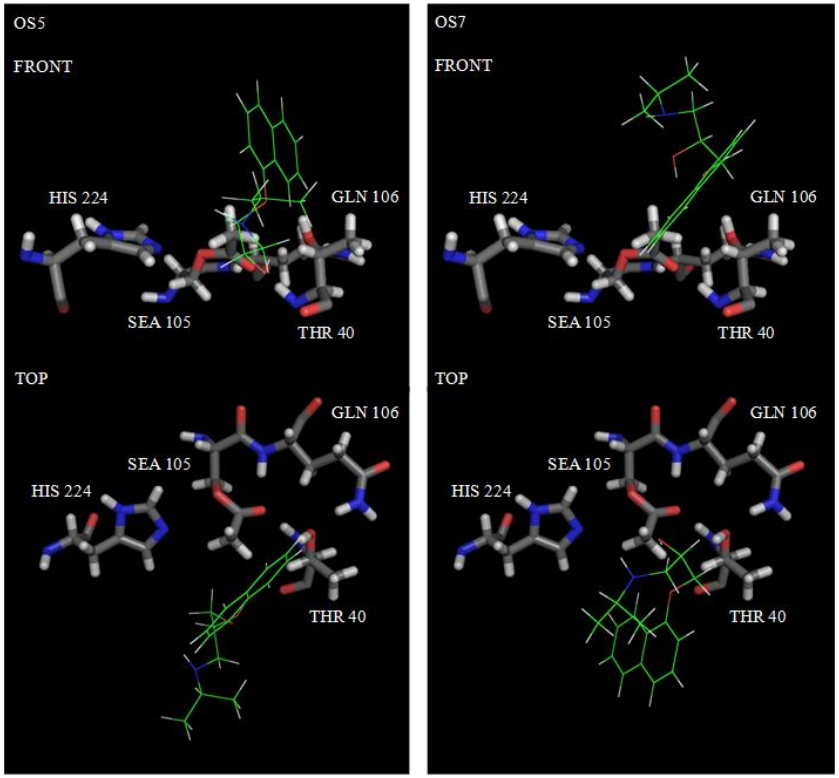

Fig. 59 Complexes between *S*-propranolol and ACE02 selected for optimization. A top and a front view are shown.

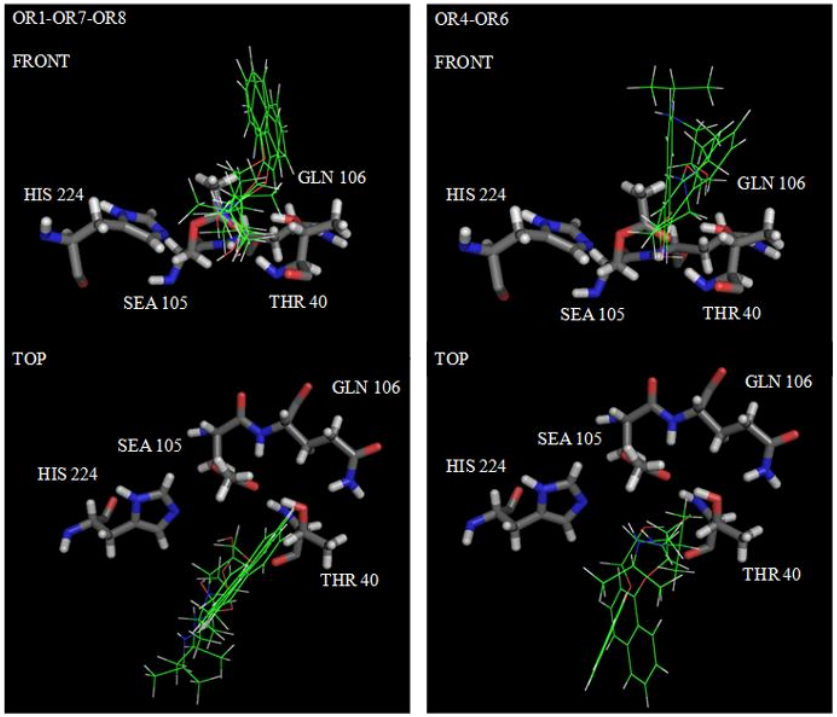

Fig. 60 Complexes between *R*-propranolol and ACE03 selected for optimization. A top and a front view are shown.

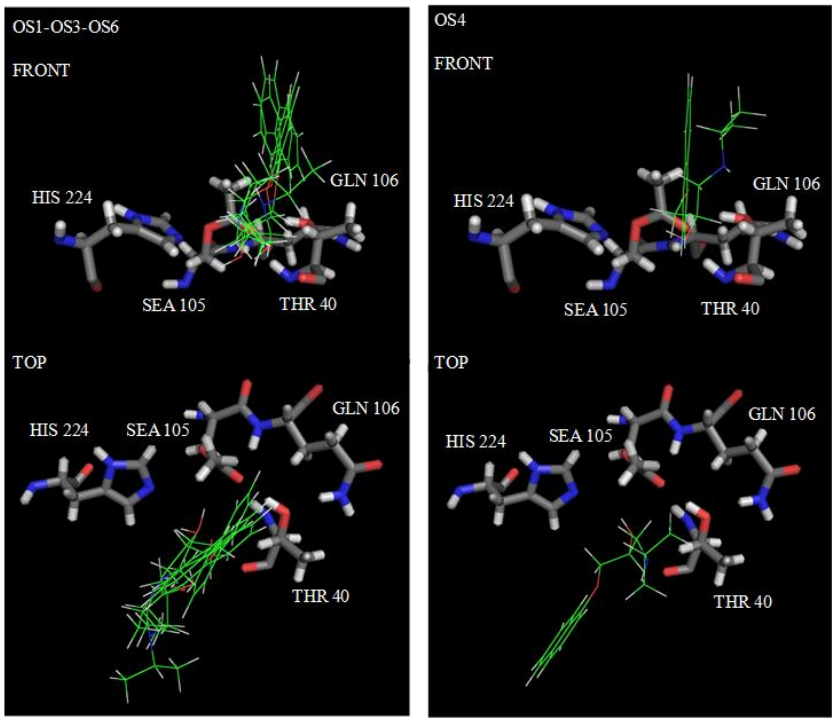

Fig. 61 Complexes between ACE03 and *S*-propranolol selected for optimization. A top and a front view are shown.

Table 27 Hydrogen bond distances[a] and angles[b] involving *R*- and *S*-propranolol in the complexes after optimization.

COMPLEX[c]	SEA:O-Gln106:NH	SEA:O-Thr40:NH	SEA:O-Thr40:OH	Gln106:H2N-Thr40:Oγ	Asp187:O_D-His224:H_{ND}	Sub:H[d]-Thr40:O
ORI	2.09 (148.86)	2.05 (160.88)	1.86 (168.77)	1.98 (164.99)	1.87 (167.76)	4.44
ORII	2.31 (136.64)	1.92 (164.02)	1.65 (172.25)	2.05 (158.38)	1.84 (166.88)	2.43 (149.42)
ORIII	2.32 (136.20)	1.93 (163.80)	1.65 (172.30)	2.04 (158.46)	1.84 (166.98)	2.29 (154.00)
ORIV	2.03 (150.85)	1.97 (160.19)	1.83 (167.31)	1.99 (164.61)	1.78 (170.89)	1.86 (153.83)
ORV	2.29 (137.79)	1.87 (164.53)	1.65 (172.24)	2.06 (157.95)	1.84 (166.57)	2.54 (163.29)
ORVI	2.13 (151.98)	1.95 (162.34)	1.84 (170.54)	2.00 (164.04)	1.79 (171.07)	6.50
ORVII	2.14 (153.13)	1.91 (162.93)	1.85 (167.53)	1.98 (165.37)	1.79 (170.90)	1.74 (175.32)
ORVIII	2.10 (153.62)	1.88 (162.28)	1.85 (167.68)	1.97 (165.13)	1.78 (170.38)	6.51
ORIX	2.31 (138.20)	1.86 (164.84)	1.66 (171.54)	2.04 (159.28)	1.88 (165.06)	4.62
ORX	1.93 (168.75)	1.82 (173.23)	1.89 (161.17)	1.90 (168.24)	1.81 (170.43)	10.07
ORXI	2.36 (138.36)	1.86 (174.65)	1.66 (176.34)	2.05 (158.56)	1.85 (166.80)	4.52
ORXII	1.98 (164.59)	1.94 (173.11)	1.83 (162.81)	1.91 (168.21)	1.80 (171.38)	2.04 (177.72)
OSI	2.11 (151.65)	1.96 (161.91)	1.85 (168.99)	1.98 (165.29)	1.85 (167.72)	4.49
OSII	2.29 (136.99)	1.90 (164.17)	1.65 (173.17)	2.06 (158.27)	1.93 (164.28)	4.18
OSIII	2.11 (153.71)	1.88 (162.54)	1.85 (167.52)	1.97 (164.89)	1.80 (170.05)	2.19 (130.18)
OSIV	2.08 (146.93)	2.12 (160.40)	1.89 (165.88)	1.99 (163.94)	1.89 (167.95)	4.33
OSV	1.98 (165.97)	1.90 (172.77)	1.87 (161.26)	1.90 (168.43)	1.84 (169.62)	4.54
OSVI	2.15 (151.94)	1.96 (162.92)	1.87 (165.87)	1.98 (164.96)	1.83 (165.79)	4.67
OSVII	1.96 (167.68)	1.85 (172.79)	1.88 (160.85)	1.90 (168.37)	1.81 (170.29)	7.34

[a] Distances are given in Å. [b] Angles are in degrees (º) and given in brackets. [c] The name of the optimized complexes was slightly changed to differentiate from the non-optimized complexes. [d] Hydrogen atom of the hydroxyl group of propranolol.

Table 28 Interatomic distances between nucleophile groups[a] of propranolol and the carbonyl carbon of the acetylated serine (SEA:C) and the catalytic histidine (His224:Nε) in the complexes after optimization.

COMPLEX	SEA:C-Sub:*N* (Å)	His224:Nε-Sub:*H* (Å)	SEA:C-Sub:**O** (Å)	His224:Nε-Sub:**H** (Å)	Attack angle[b] (º)
ORI	6.59	5.89	3.99	1.98 (172.89)	98.09
ORII	7.33	7.31	4.97	4.74	104.99
ORIII	7.30	7.45	4.88	4.85	105.61
ORIV	4.88	4.71	3.50	4.78	120.20
ORV	8.29	7.45	5.55	5.05	107.70
ORVI	6.67	6.12	5.13	6.98	146.61
ORVII	7.34	5.64	5.42	5.25	114.19
ORVIII	9.96	8.40	7.36	6.01	117.14
ORIX	7.90	7.85	4.65	3.18 (134.92)	108.37
ORX	6.24	6.29	8.48	7.55	107.54
ORXI	10.03	9.51	6.52	5.79	120.57
ORXII	7.70	6.96	4.99	5.71	114.35
OSI	6.73	6.20	3.90	1.96 (169.29)	101.25
OSII	7.33	5.83	4.67	2.78 (162.38)	101.50
OSIII	6.98	6.75	6.29	5.45	129.08
OSIV	4.87	5.66	3.68	2.09 (167.03)	104.81
OSV	8.69	7.40	5.51	3.95 (178.34)	110.49
OSVI	6.73	5.14	4.03	1.92 (169.48)	98.75
OSVII	7.05	6.59	4.66	5.37	115.43

[a] The atoms corresponding to the amino and hydroxyl group are shown in italic and bold respectively.
[b] Attack angle refers to the angle involved in the nucleophilic attack of the hydroxyl group of propranolol on the carbonyl carbon of SEA (**O**···C=O).

Appendix C

Supplementary information for Chapter 4

Supplementary figures and tables for **Chapter 4** are presented below after the discussion associated to the dynamic behaviour of *R*- and *S*-propranolol during the MD simulations of the AcCalB-propranolol complexes given in the next sections. The latter contain a more detailed analysis of the information provided in section **4.3.1.3** about the temporal stability of the productive complexes and the influence of the solvent on it.

Dynamic behaviour of *R*-propranolol during the MD simulations of the MCCs in binding mode I

The stabilization of propranolol with its hydroxyl group positioned near to the catalytic residues in the MD simulations of the complexes R1 and R2 can be judged from the variations of the interatomic distances **b** and **c** during the simulations (**Fig. 69**). Propranolol is stabilized close to the catalytic residues during the first 544 ps, 454 ps and 235 ps, of the corresponding three MD simulations of the system R1 with different initial velocities. Then propranolol adopts non-productive conformations. In case of the system R2, propranolol has the tendency to stay positioned far from the catalytic residues and in some cases leaves the binding pocket at the end of the simulation. Only in one of the simulations of the system R2 (R2*), propranolol is stabilized relatively close to the catalytic residues throughout the simulation, but it does not satisfy completely the distance criteria to react. There are only a few time intervals in which the distance **b** is less than 4 Å. This behavior may be explained by the better ability of the solvent to interact with the isopropyl side chain of propranolol in the system R2, as this isopropyl group is more exposed toward the exterior of the binding pocket in this system (**Fig. 70**).

Dynamic behaviour of *S*-propranolol during the MD simulations of the MCCs in binding mode I

The time evolution of the interatomic distances **b** and **c** in the MD simulations of the *S*-propranolol complexes in binding mode I is shown in **Fig. 71** and **Fig. 72**. In general, it can be noted that propranolol is stabilized near to the catalytic residues for a longer time in the system in which its naphthyl group is oriented pointing toward the interior of the binding pocket (S3). Only in two of the MD simulations of S3 (S3* and S3**) the substrate is positioned far from the catalytic residues, but this for only about 100 ps (S3*) and 200 ps (S3**). This means that in the MD simulations of S3 the

substrate is stabilized near to the catalytic residues for more than 1300 ps. During this time a fluctuation of the distance **b** leading to the breaking of the hydrogen bond interaction is observed in some cases (see S3 and S3** MD simulations). This fluctuation leads in turn to the formation of non-productive complexes of the *S*-propranolol in binding mode I. In contrast, in most of the MD simulations of S1 and S2, systems in which the naphthyl group of the substrate is oriented pointing toward the exterior of the binding pocket, propranolol is stabilized near to the catalytic residues for about 300 ps to 600 ps. Then propranolol adopts non-productive conformations and finally leaves the binding pocket. There is only one particular case (S2**) in which propranolol is stabilized close to the catalytic residues almost all the time of the MD.

This behavior observed for *S*-propranolol in binding mode I differs from that of *R*-propranolol, which is stabilized close to the catalytic residues for a longer time in the system in which its naphthyl group is oriented pointing toward the exterior of the binding pocket (R1). This is explained by a better exposition of the isopropyl side chain of propranolol toward the exterior of the binding pocket in the systems S1 and S2 than in the system S3 (**Fig. 73**). In other words, the better exposition of the isopropyl group of propranolol toward the entrance of the binding pocket the shorter the temporal stability of the productive complexes in binding mode I.

Dynamic behaviour of *R*- and *S*-propranolol during the MD simulations of the MCCs in binding mode II

The time evolution of the interatomic distances **b** and **c** in the MD simulations of the *R*- and *S*-propranolol complexes in binding mode II is shown in **Fig. 74**. In the MD simulations of *R*-propranolol different reactive conformers are identified (namely, **R3a-R3f**; **Fig. 75**). **R3a** and **R3b** are observed in all MD simulations (R3: during the first 300 ps, R3*: during the first 124 ps, R3**: during the first 44 ps). **R3c** and **R3d** are observed in the MD simulations with the second and third seed velocity (R3*: between 124-549 ps, R3**: between 44-300 ps). **R3e** and **R3f** are only observed in the MD simulation with the third initial velocity distribution (R3**: after 300 ps). These reactive conformations of *R*-propranolol differ mainly in the orientation of the naphthyl group of propranolol in the medium pocket of CalB, where it is stabilized through CH-π interactions by the residues of the surrounding protein (see **Fig. 75** and **Table 9**). Thus temporal stabilization of *R*-propranolol close to the catalytic residues is strongly dependent on the orientation of its naphthyl group. The better the exposition of its naphthyl group to the solvent, the shorter temporal stability of the *R*-propranolol productive complexes in binding mode II. Thus *R*-propranolol is stabilized close to the catalytic

residues for a longer time in the MD simulation with the third seed velocity (R3**), in which the **R3e** and **R3f** complexes are formed, as in these complexes the naphthyl group of propranolol is more hindered (see **Fig. 75**).

In most of the MD simulations of *S*-propranolol in binding mode II, propranolol is stabilized close to the catalytic residues throughout the MD trajectory (**Fig. 74**). The identified *S*-propranolol productive complexes (namely, **S4a** and **S4b**) are specular binding modes of **R3c** and **R3d**. The exposition of the naphthyl group of propranolol to the solvent in **S4a** and **S4b** is similar to that observed in **R3c** and **R3d** (see **Fig. 76**). This explain the similar temporal stability observed for these productive complexes of *R*- and *S*-propranolol in the MD simulation with the second initial velocity (R3* and S4*).

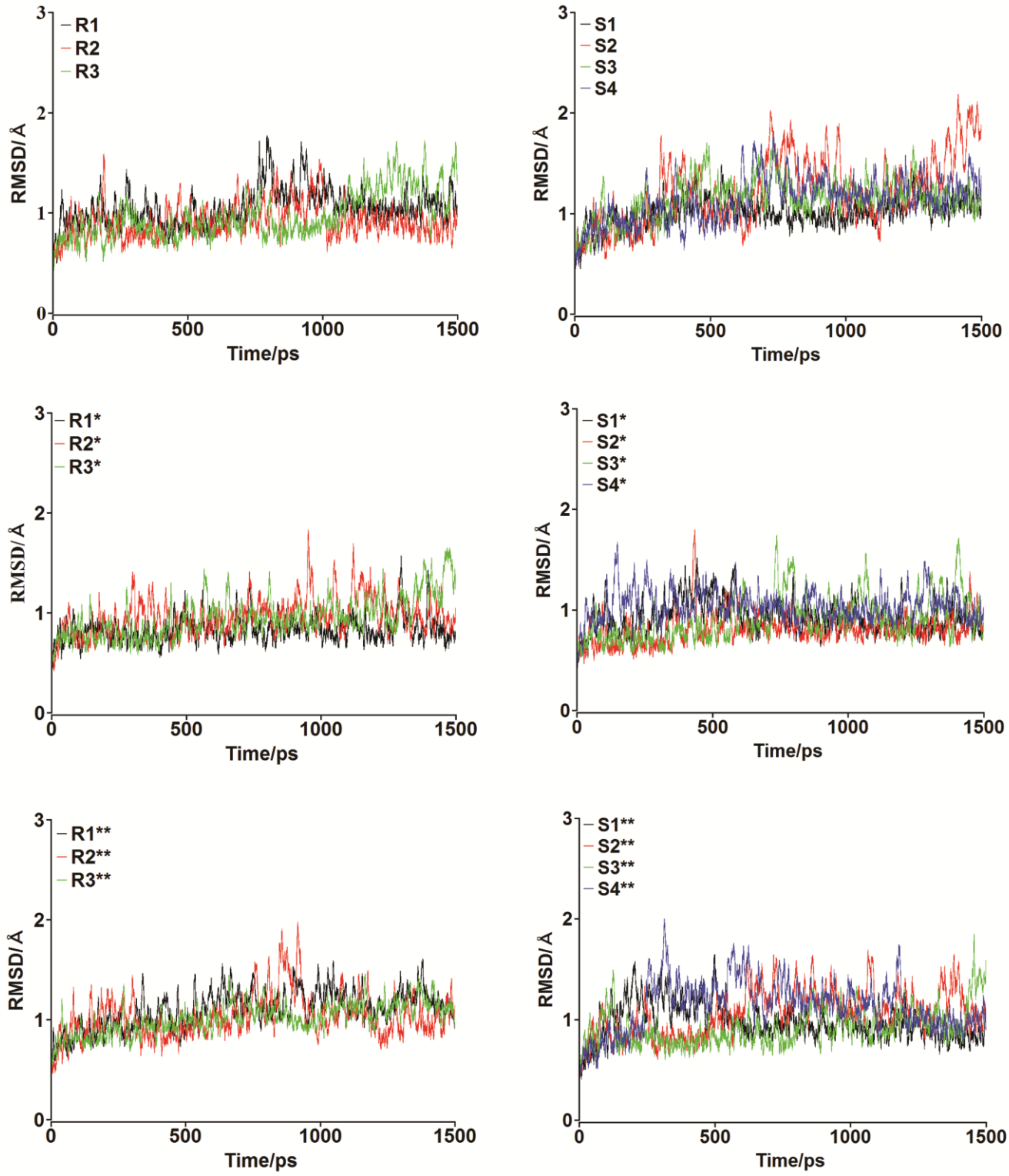

Fig. 62. Time evolution of the root mean square deviation (RMSD) for the protein backbone in the MD simulations of the Michaelis complexes between AcCalB and *R*- or *S*-propranolol. Three MD simulations of each complex using different initial velocity distributions are shown (indicated by *).

Table 29 Average RMSD (respect to the CalB crystal structure) for all heavy atoms of the protein backbone in the MD simulations of the AcCalB-propranolol complexes[a]

COMPLEX	RMSD	RMSD*	RMSD**
R1	1.05 ± 0.18	0.83 ± 0.12	1.10 ± 0.18
R2	0.91 ± 0.16	0.95 ± 0.18	1.02 ± 0.21
R3	0.97 ± 0.22	0.95 ± 0.20	1.01 ± 0.15
S1	1.01 ± 0.13	0.92 ± 0.15	0.97 ± 0.17
S2	1.22 ± 0.34	0.80 ± 0.14	1.06 ± 0.22
S3	1.15 ± 0.19	0.90 ± 0.21	0.91 ± 0.17
S4	1.13 ± 0.22	1.03 ± 0.14	1.13 ± 0.24

[a] RMSD values (in Å) are given for the three MD simulations with different initial velocity distribution as indicated by *.

Table 30 Average distances[a] (in Å) between the His224:Nε – SEA:Oγ atoms during the MD simulations of the AcCalB-propranolol complexes[b]

COMPLEX	His224:Nε – SEA:Oγ	His224:Nε – SEA:Oγ*	His224:Nε – SEA:Oγ**
R1	3.27 (0.20)	3.27 (0.21)	3.23 (0.18)
R2	3.22 (0.18)	3.24 (0.18)	3.23 (0.19)
R3	3.26 (0.19)	3.28 (0.19)	3.30 (0.20)
S1	3.21 (0.17)	3.30 (0.20)	3.26 (0.20)
S2	3.26 (0.19)	3.29 (0.20)	3.36 (0.23)
S3	3.26 (0.19)	3.31 (0.21)	3.22 (0.18)
S4	3.28 (0.19)	3.26 (0.19)	3.26 (0.19)

[a] Numbers in brackets correspond to standard deviations from average values.
[b] Three MD simulations of each complex were carried out using a different initial velocity distribution as indicated by *

Table 31 Essential hydrogen bond distances[a] (in Å) for the catalytic activity of CalB in the Michaelis complexes between AcCalB and *R*- or *S*-propranolol averaged throughout the 1.5 ns MD simulations[b].

Complex	Distance a	Distance d	Distance e	Distance f
R1	1.91 (0.17)	2.24 (0.23)	1.80 (0.15)	2.21 (0.40)
R1*	1.93 (0.18)	2.17 (0.21)	1.79 (0.15)	2.10 (0.29)
R1**	1.92 (0.17)	2.26 (0.24)	1.81 (0.15)	2.11 (0.26)
R2	1.91 (0.17)	2.22 (0.23)	1.80 (0.14)	2.08 (0.24)
R2*	1.93 (0.17)	2.22 (0.23)	1.83 (0.19)	2.11 (0.29)
R2**	1.92 (0.17)	2.24 (0.24)	1.78 (0.14)	2.31 (0.51)
R3	1.93 (0.16)	2.23 (0.24)	1.78 (0.16)	2.06 (0.31)
R3*	1.91 (0.17)	2.20 (0.22)	1.80 (0.15)	2.03 (0.23)
R3**	1.95 (0.17)	2.14 (0.21)	1.79 (0.14)	2.09 (0.23)
S1	1.90 (0.16)	2.23 (0.24)	1.79 (0.14)	2.07 (0.28)
S1*	1.92 (0.17)	2.23 (0.23)	1.82 (0.16)	2.19 (0.36)
S1**	1.94 (0.17)	2.25 (0.24)	1.81 (0.15)	2.39 (0.50)
S2	1.92 (0.17)	2.22 (0.23)	1.81 (0.16)	2.12 (0.30)
S2*	1.92 (0.17)	2.22 (0.24)	1.80 (0.16)	2.15 (0.33)
S2**	1.96 (0.18)	2.16 (0.21)	1.81 (0.15)	2.44 (0.51)
S3	1.94 (0.18)	2.13 (0.20)	1.80 (0.14)	2.30 (0.40)
S3*	1.94 (0.18)	2.16 (0.22)	1.82 (0.18)	2.07 (0.26)
S3**	1.93 (0.17)	2.12 (0.20)	1.80 (0.15)	2.11 (0.26)
S4	1.92 (0.17)	2.24 (0.24)	1.82 (0.16)	2.05 (0.24)
S4*	2.06 (0.18)	2.22 (0.23)	1.80 (0.16)	2.02 (0.21)
S4**	1.92 (0.17)	2.25 (0.24)	1.83 (0.17)	2.11 (0.32)

[a] Distances **a-f** correspond to those shown in **Fig. 24**. Numbers in brackets correspond to standard deviations from average values.
[b] Three MD simulations of each complex were carried out using a different initial velocity distribution as indicated by *

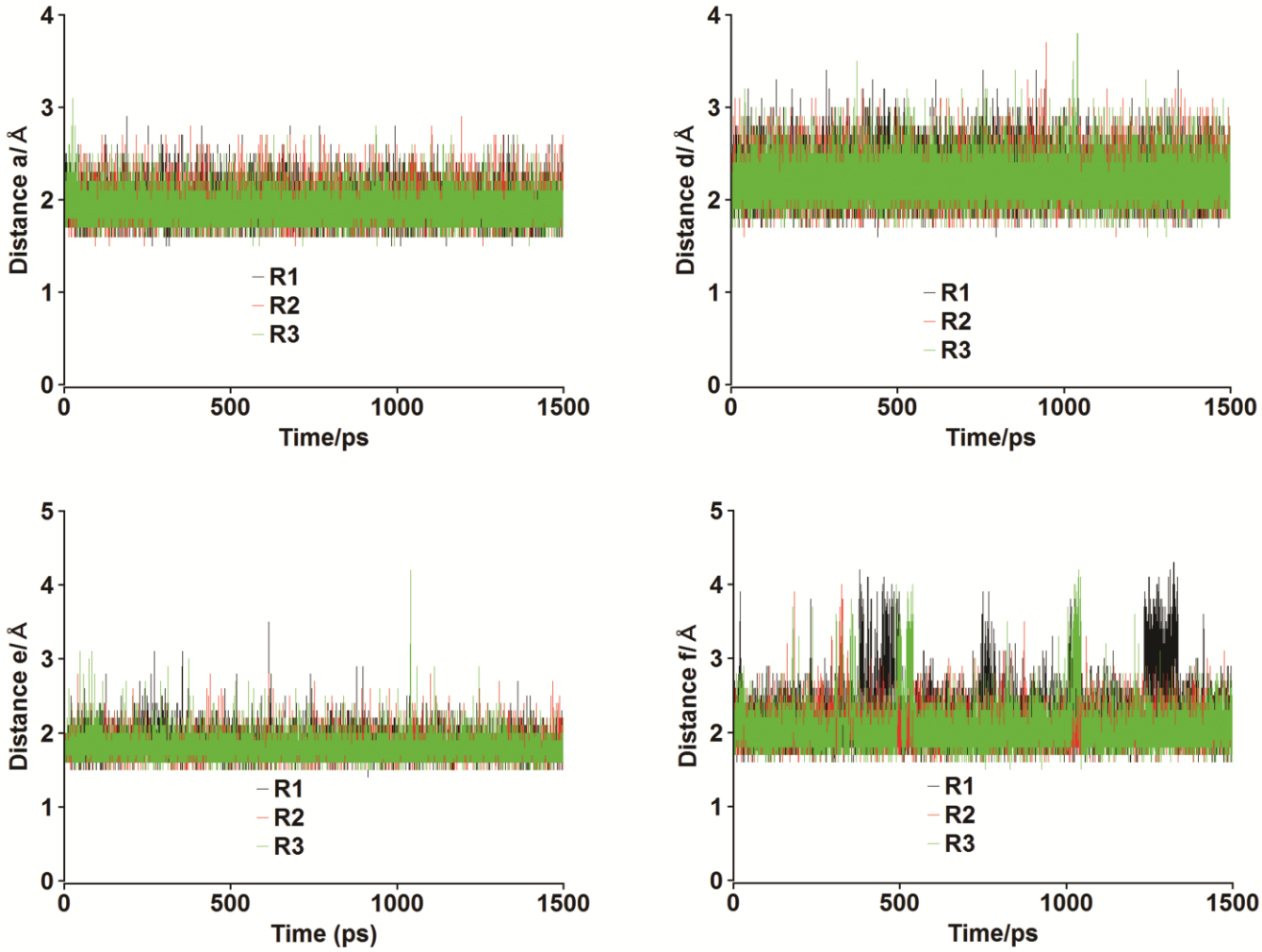

Fig. 63 Time evolution of the hydrogen bonds which are essential for the catalytic activity of CalB in the Michaelis complexes between *R*-propranolol and AcCalB in the MD simulations with the first initial velocity distribution. Distances **a-f** correspond to those shown in **Fig. 24**.

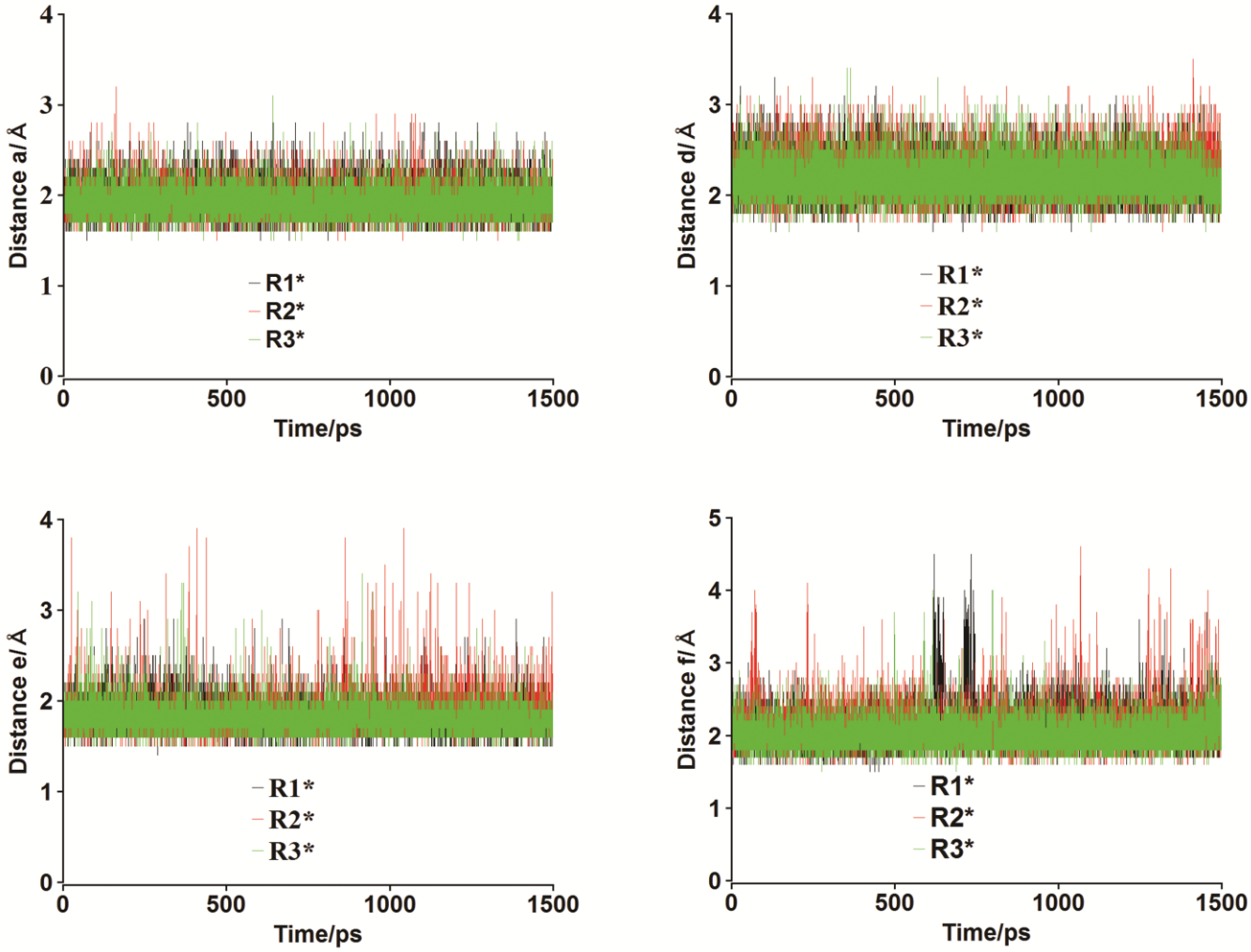

Fig. 64 Time evolution of the hydrogen bonds which are essential for the catalytic activity of CalB in the Michaelis complexes between *R*-propranolol and AcCalB in the MD simulations with the second initial velocity distribution (indicated by *). Distances **a-f** correspond to those shown in **Fig. 24**.

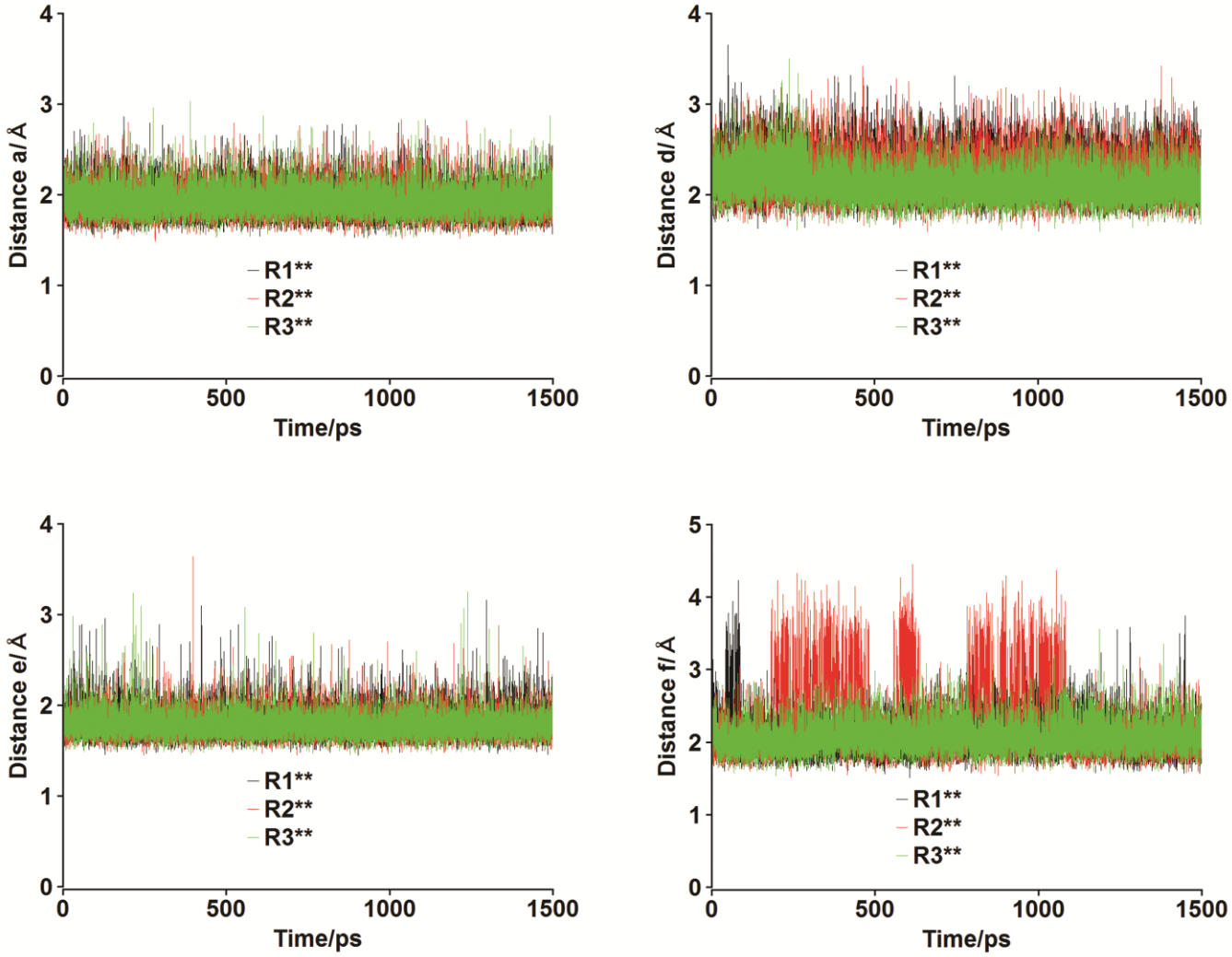

Fig. 65 Time evolution of the hydrogen bonds which are essential for the catalytic activity of CalB in the Michaelis complexes between *R*-propranolol and AcCalB in the MD simulations with the third initial velocity distribution (indicated by **). Distances **a-f** correspond to those shown in **Fig. 24**.

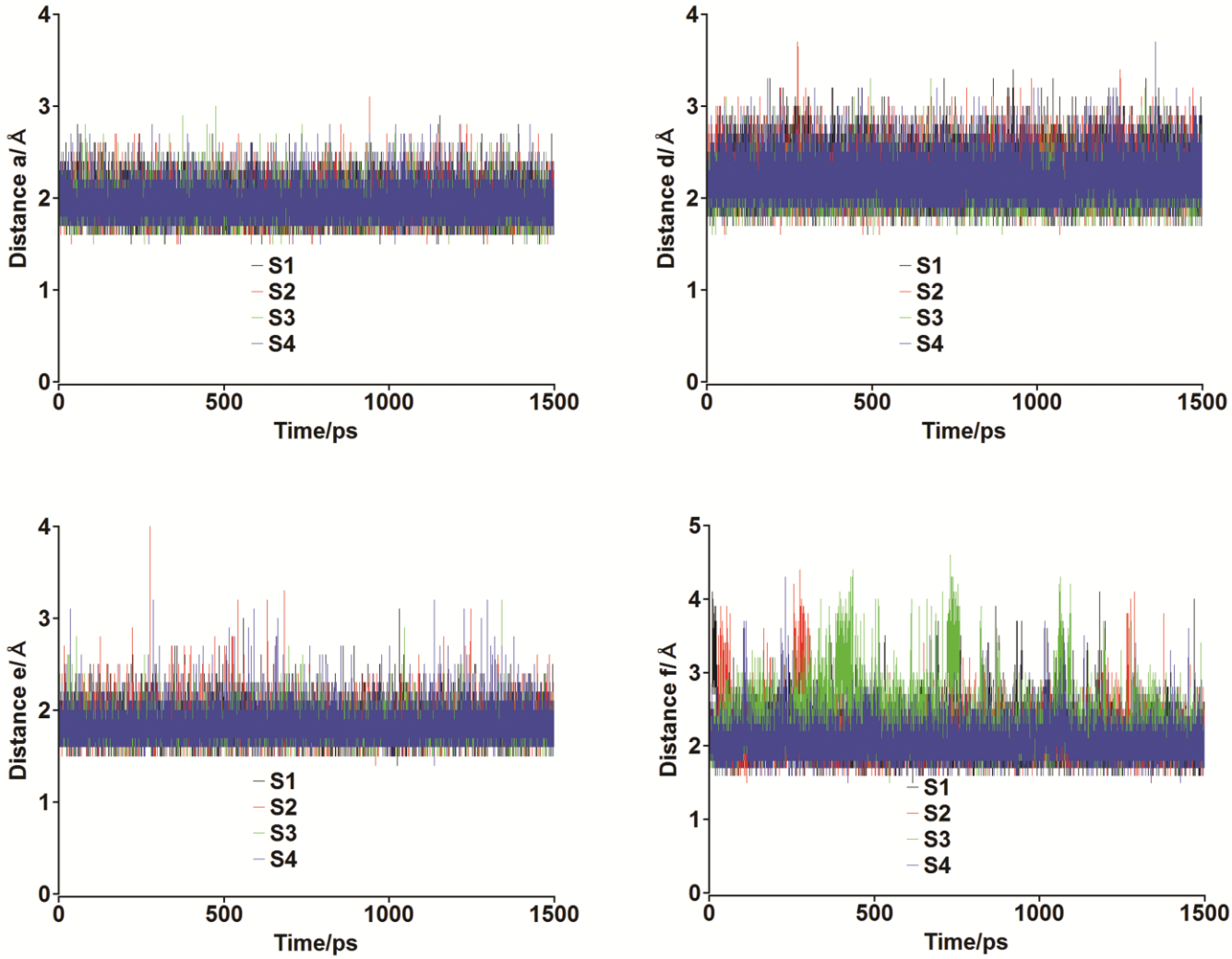

Fig. 66 Time evolution of the hydrogen bonds which are essential for the catalytic activity of CalB in the Michaelis complexes between *S*-propranolol and AcCalB in the MD simulations with the first initial velocity distribution. Distances **a-f** correspond to those shown in **Fig. 24**.

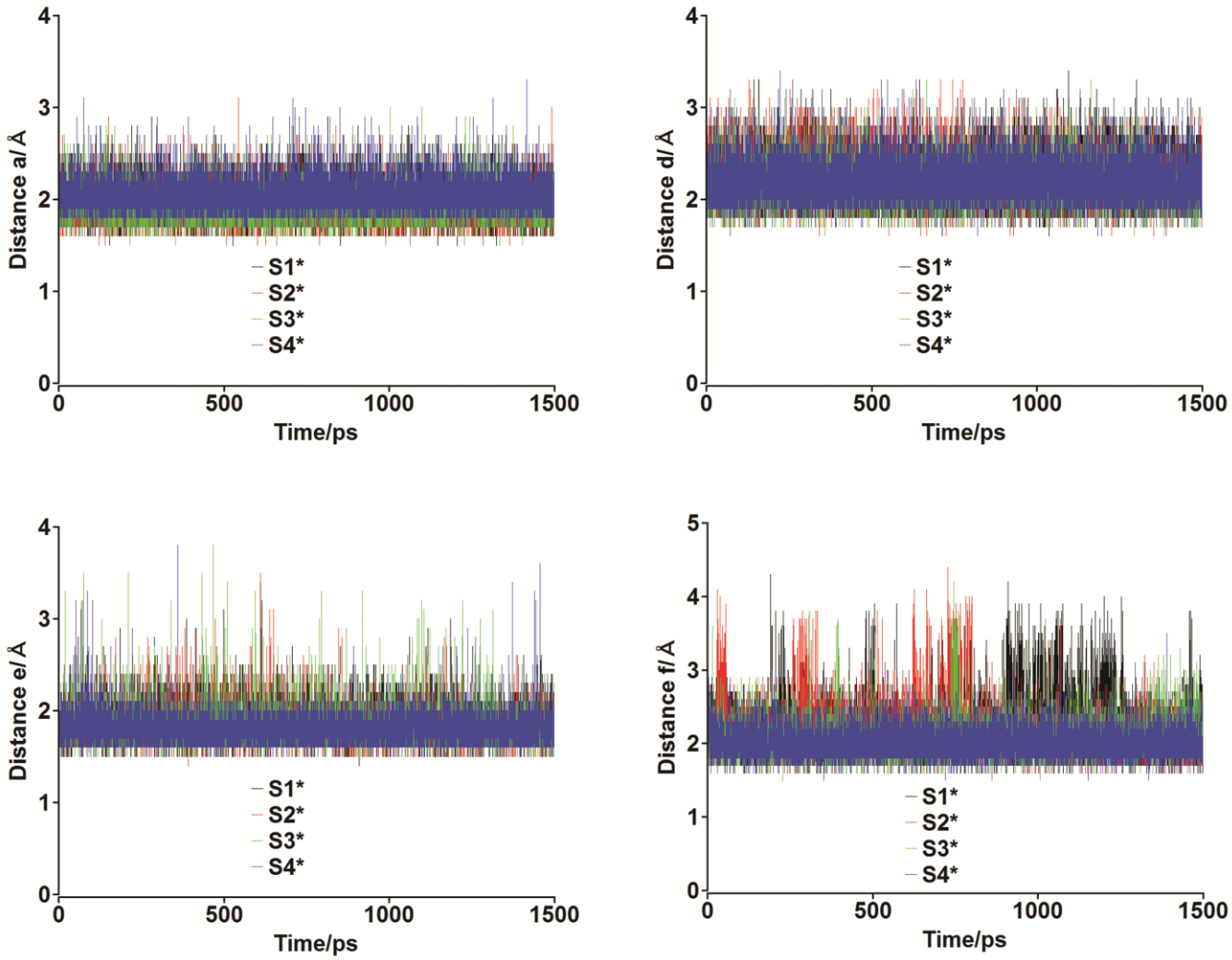

Fig. 67 Time evolution of the hydrogen bonds which are essential for the catalytic activity of CalB in the Michaelis complexes between *S*-propranolol and AcCalB in the MD simulations with the second initial velocity distribution (indicated by *). Distances **a-f** correspond to those shown in **Fig. 24**.

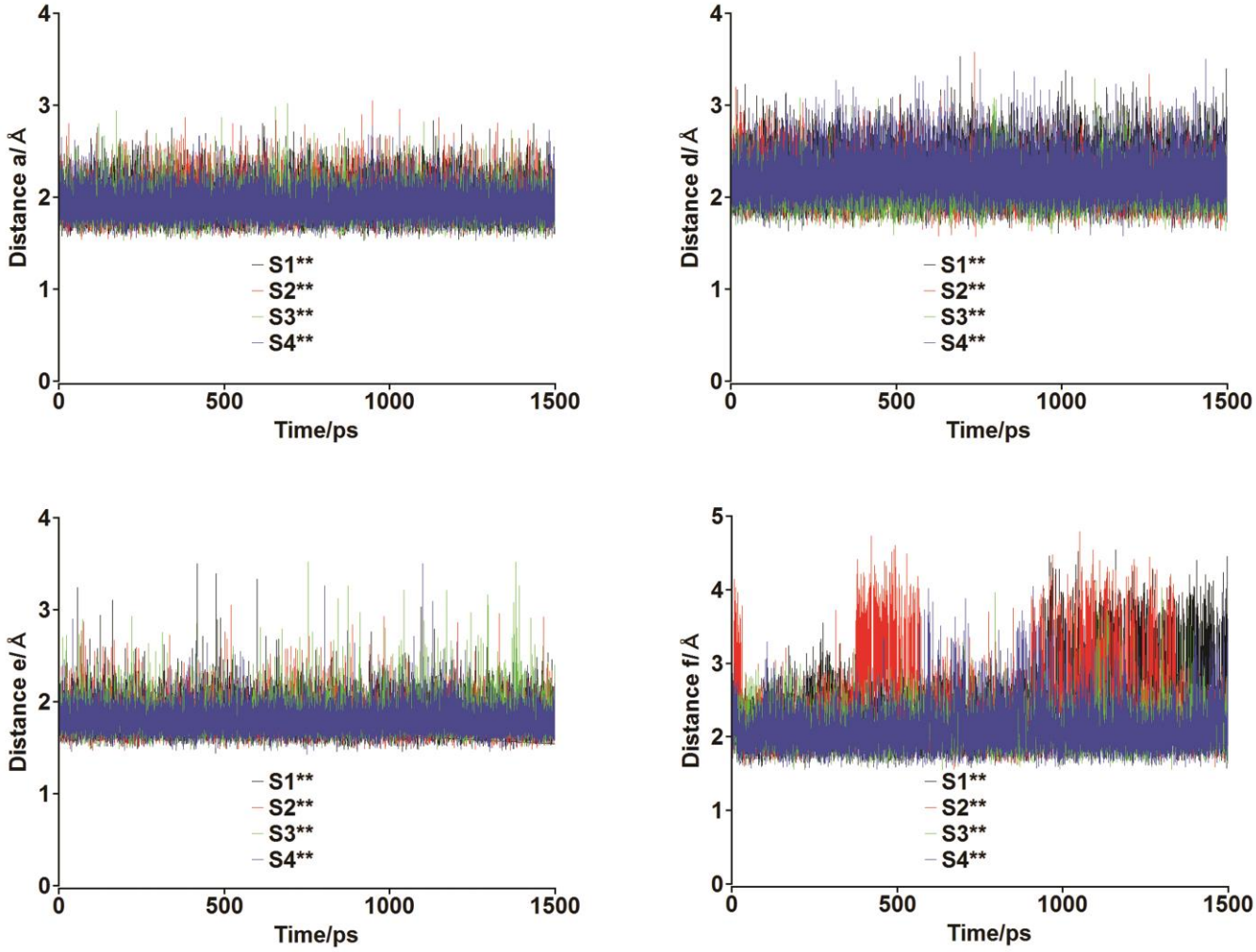

Fig. 68 Time evolution of the hydrogen bonds which are essential for the catalytic activity of CalB in the Michaelis complexes between *S*-propranolol and AcCalB in the MD simulations with the third initial velocity distribution (indicated by **). Distances **a-f** correspond to those shown in **Fig. 24**.

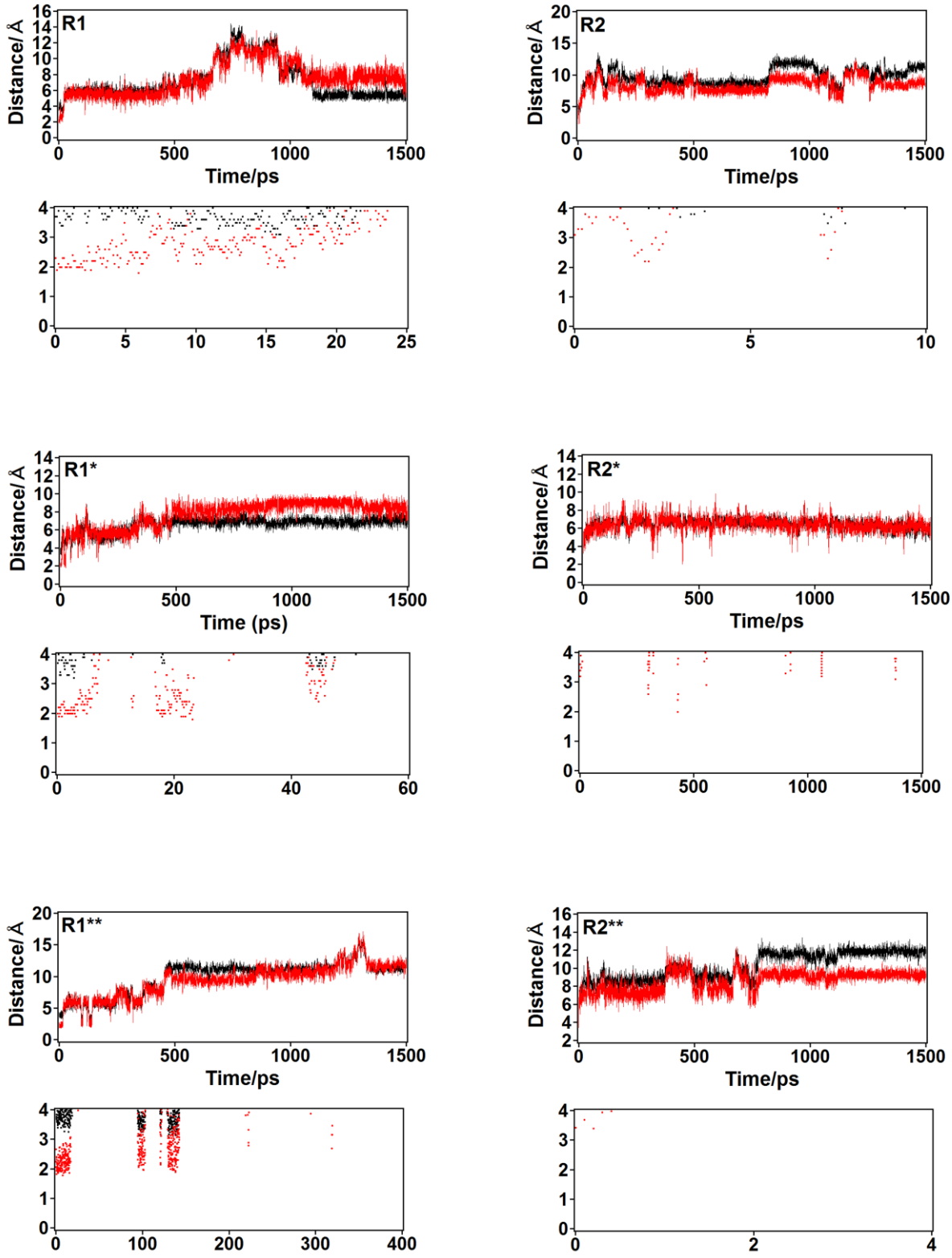

Fig. 69 Time evolution of the distances b (red) and c (black) in the MD simulations of the Michaelis complexes between *R*-propranolol and AcCalB in binding mode I. An expanded version of the times in which productive complexes are formed during the simulation is shown below each figure. Simulations with different initial velocitty distributions are indicated by *. Distances **b** and **c** correspond to those shown in **Fig. 24.**

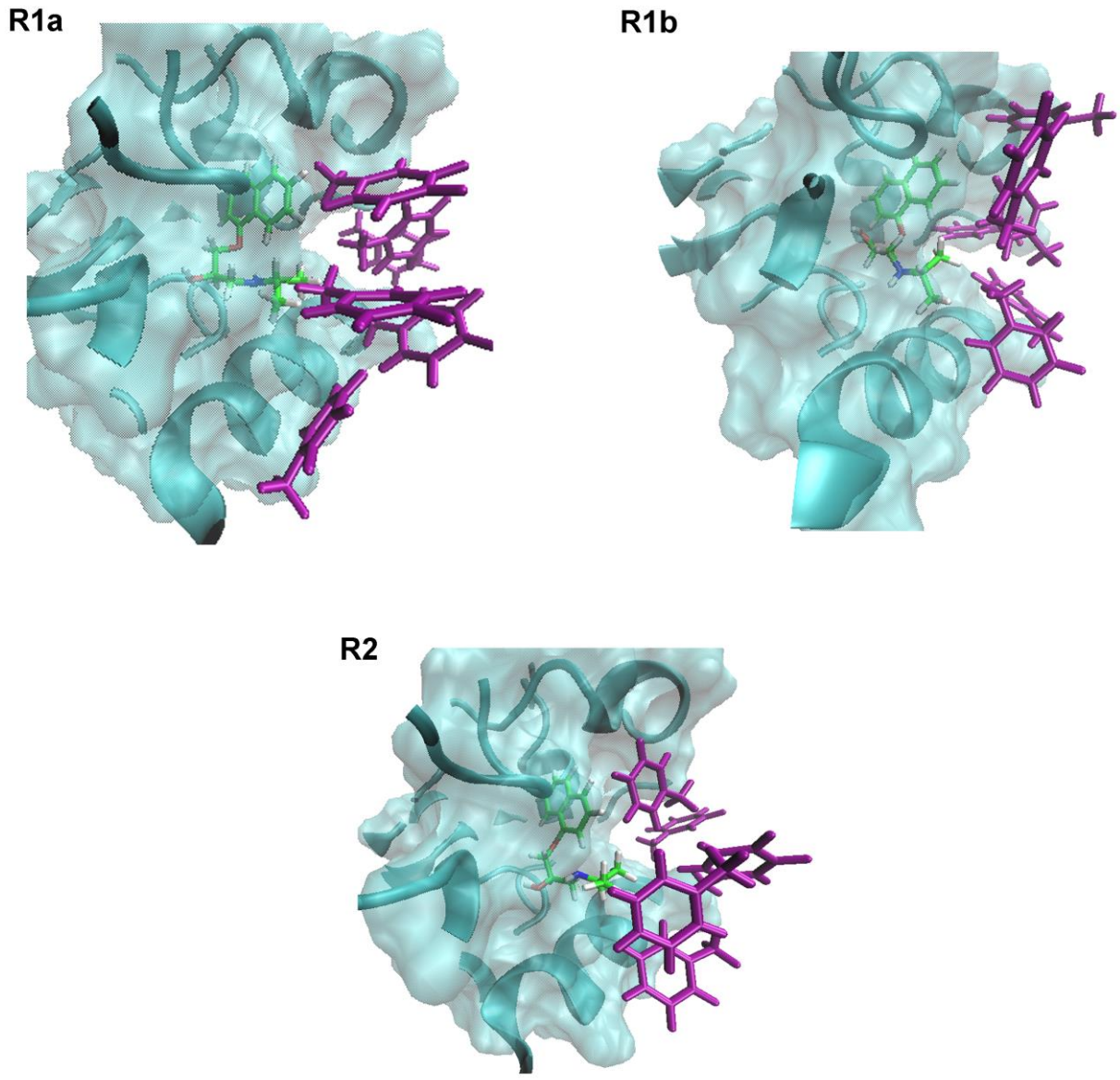

Fig. 70 Predominant conformations of *R*-propranolol in the MD simulations of the Michaelis complexes between AcCalB and *R*-propranolol in binding mode I. Solvent molecules around 5 Å from the substrate are shown in licorice (purple). Protein residues around 8 Å from the substrate are shown in cartoon and surface (cyan). It can be noted that in the system R2 the isopropyl side chain of propranolol is more exposed to the solvent.

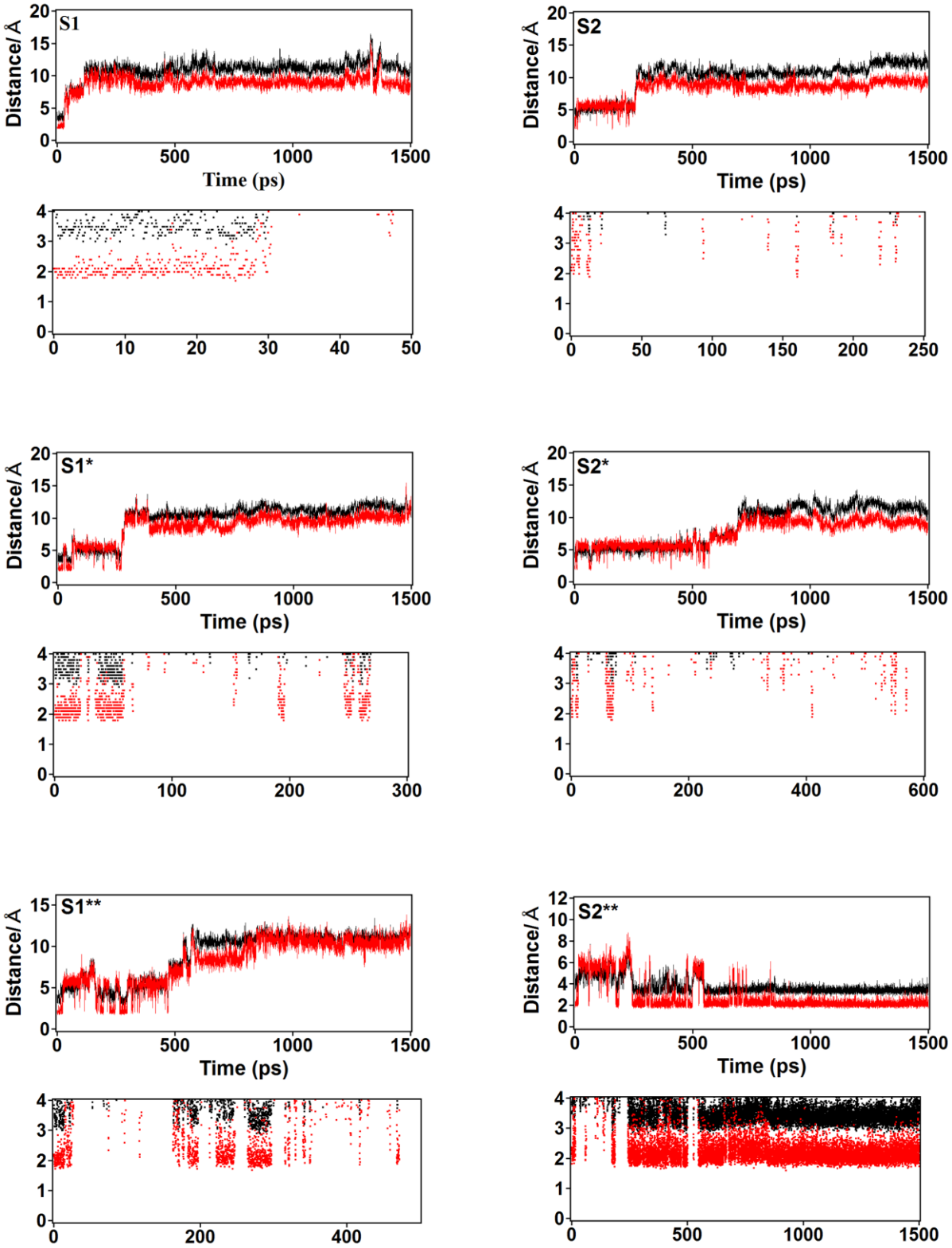

Fig. 71 Time evolution of the distances b (red) and c (black) in the MD simulations of the Michaelis complexes between *S*-propranolol and AcCalB in binding mode I (S1 and S2). An expanded version of the times in which productive complexes are formed during the simulation is shown below each figure. Simulations with different initial velocity distributions are indicated by *. Distances **b** and **c** correspond to those shown in **Fig. 24.**

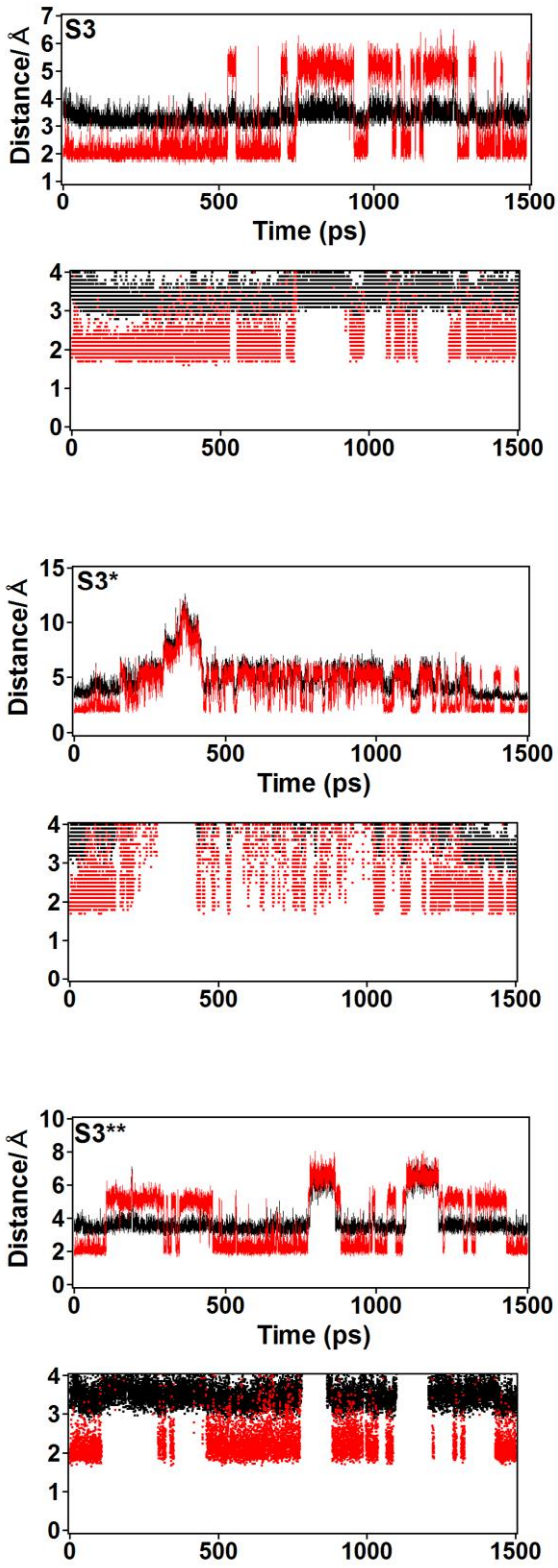

Fig. 72 Time evolution of the distances b (red) and c (black) in the MD simulations of the Michaelis complexes between *S*-propranolol and AcCalB in binding mode I (S3). An expanded version of the times in which productive complexes are formed during the simulation is shown below each figure. Simulations with different initial velocity distributions are indicated by *. Distances **b** and **c** correspond to those shown in **Fig. 24.**

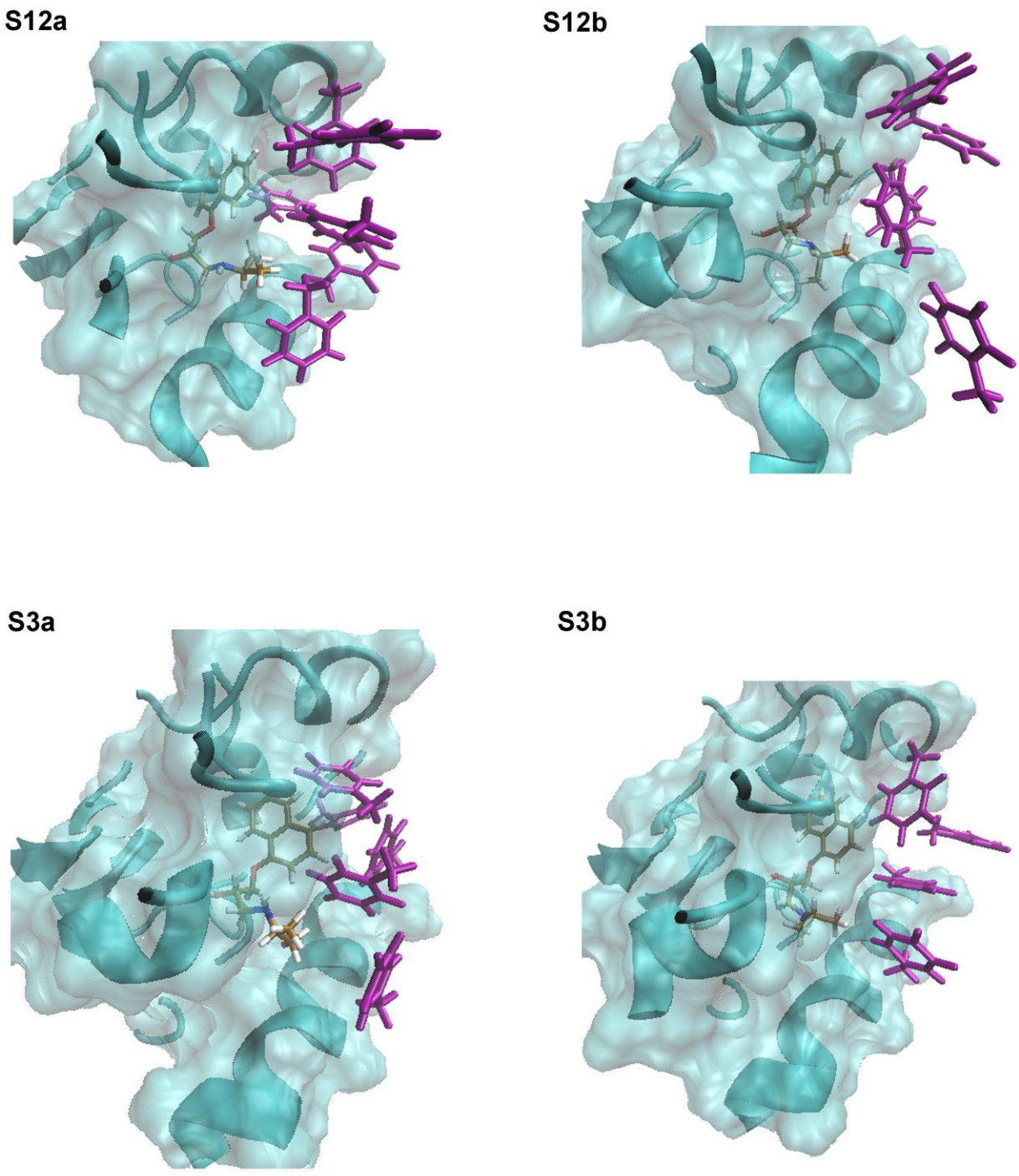

Fig. 73 Predominant conformations of *S*-propranolol in the MD simulations of the Michaelis complexes between AcCalB and *S*-propranolol in binding mode I. Solvent molecules around 5 Å from the substrate are shown in licorice (purple). Protein residues around 8 Å from the substrate are shown in cartoon and surface (cyan). It can be noted that in the system S3 the isopropyl side chain of propranolol is more hindered than in the systems S1 and S2.

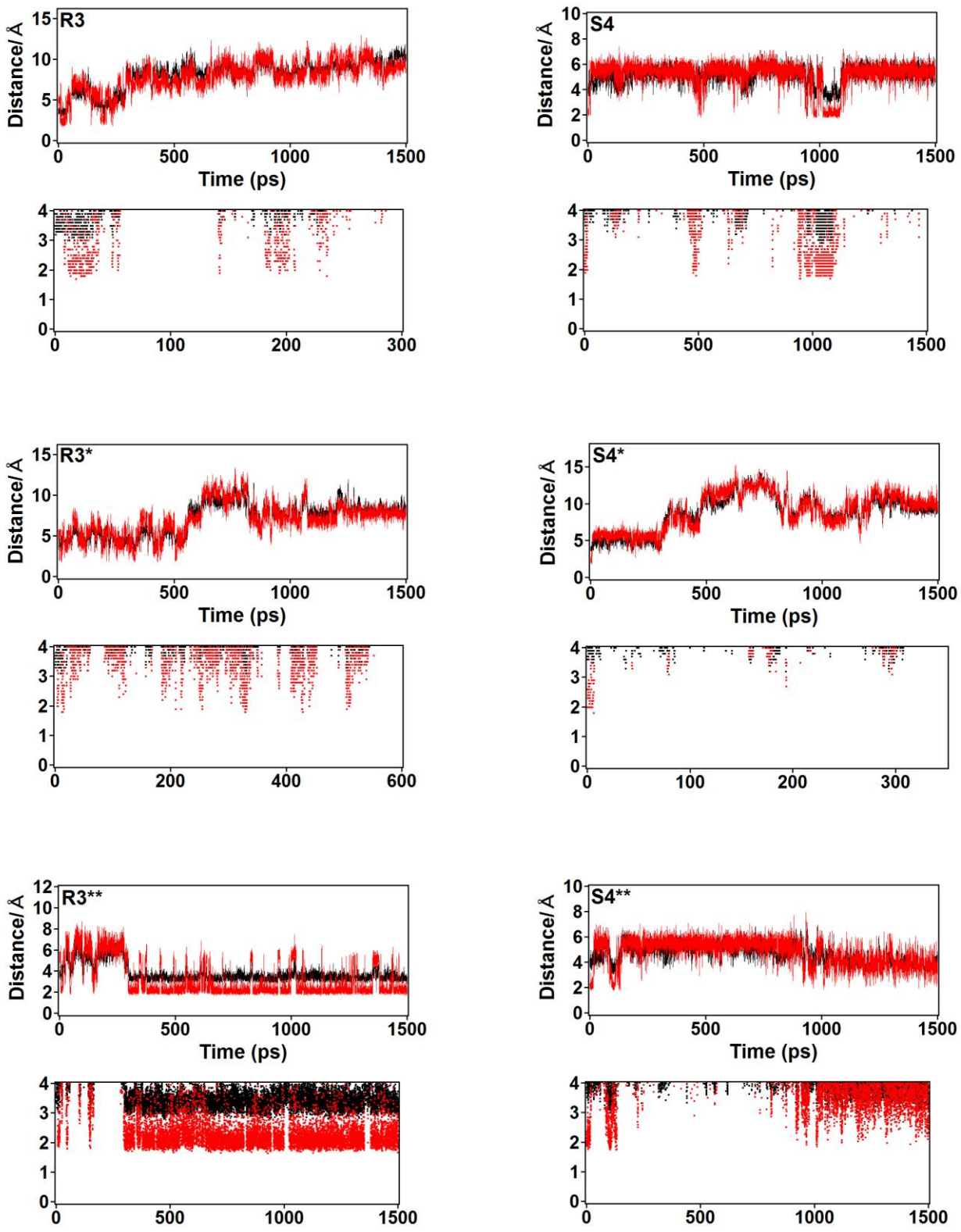

Fig. 74 Time evolution of the distances b (red) and c (black) in the MD simulations of the Michaelis complexes between *R*- or *S*-propranolol and AcCalB in binding mode II. An expanded version of the times in which productive complexes are formed during the simulation is shown below each figure. Simulations with different initial velocity distributions are indicated by *. Distances **b** and **c** correspond to those shown in **Fig. 24.**

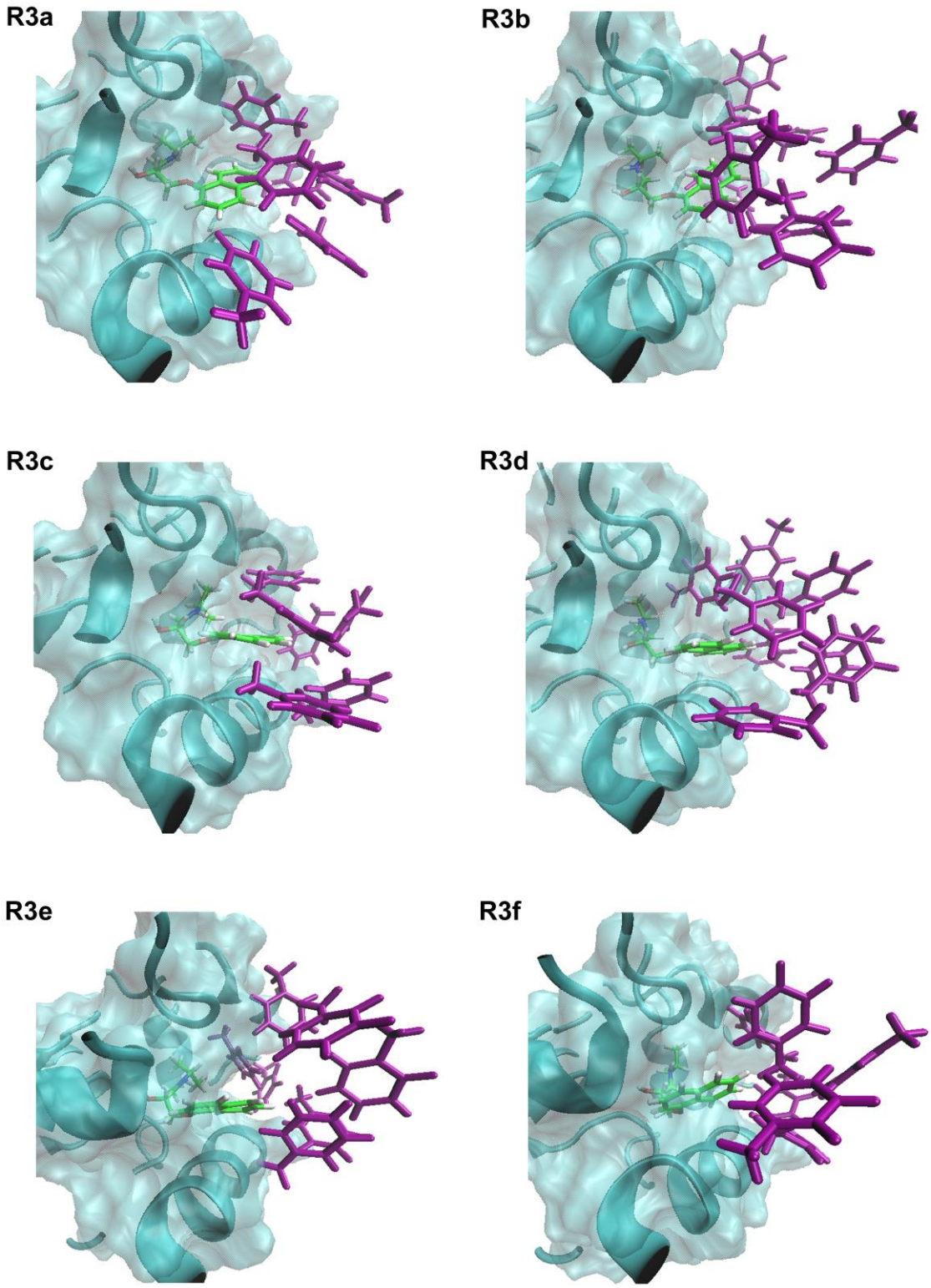

Fig. 75 Predominant conformations of *R*-propranolol in the MD simulations of the Michaelis complexes between AcCalB and *R*-propranolol in binding mode II. Solvent molecules around 5 Å from the substrate are shown in licorice (purple). Protein residues around 8 Å from the substrate are shown in cartoon and surface (cyan). It can be noted that in the R3e and R3f complexes the naphthyl group of propranolol is more hindered to interact with the solvent.

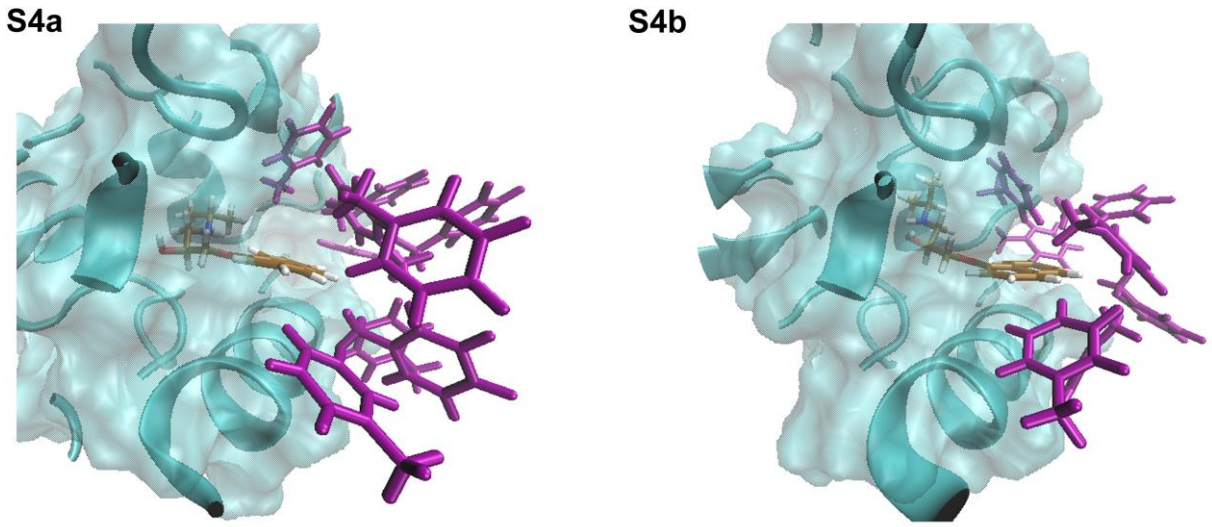

Fig. 76 Predominant conformations of *S*-propranolol in the MD simulations of the Michaelis complexes between AcCalB and *S*-propranolol in binding mode II. Solvent molecules around 5 Å from the substrate are shown in licorice (purple). Protein residues around 8 Å from the substrate are shown in cartoon and surface (cyan).

Table 32 Lifetime and percentage of NACs[a] of each reactive conformer of *R*- and *S*-propranolol in the MD simulations of the AcCalB-propranolol complexes carried out with the first initial velocity distribution.

Binding Mode I			Binding Mode II		
Conformer	Lifetime (ps)	NACs (%)	Conformer	Lifetime (ps)	NACs (%)
R1a	382.2	0.00	R3a	36.5	1.10
R1b	161.9	0.31	R3b	199.2	0.05
S12a[b]	105.2	6.71	S4a	1073.0	0.98
S12b[b]	42.4	1.94	S4b	417.0	2.88
S3a	844.6	37.24			
S3b	645.4	38.39			

[a] The percentage of NACs formation is given related to the lifetime of each reactive conformer.
[b] Averages have been performed over the MD simulations of S1 and S2.

Table 33 Lifetime and percentage of NACs[a] of each reactive conformer of *R*- and *S*-propranolol in the MD simulations of the AcCalB-propranolol complexes carried out with the second initial velocity distribution.

Binding Mode I			Binding Mode II		
Confomer	Lifetime* (ps)	NACs* (%)	Conformer	Lifetime* (ps)	NACs* (%)
R1a	274.4	0.07	R3a	28.0	0.71
R1b	179.7	0.00	R3b	86.3	0.00
S12a[b]	370.4	1.30	R3c	55.1	0.18
S12b[b]	158.4	1.87	R3d	370.6	0.05
S3a	1126.0	1.84	S4a	197.5	0.80
S3b	364.0	21.51	S4b	95.9	1.20

[a] The percentage of NACs formation is given related to the lifetime of each reactive conformer.
[b] Averages have been performed over the MD simulations of S1 and S2.

Table 34 Relevant interatomic distances, bond lengths and angles in the reactant states (RS) and the intermediates (TI-2) for the optimized small model systems of the complexes between AcCalB and *R*-propranolol[a].

Distance (Å)	*Binding Mode I*		*Binding Mode II*							
	R1a		R3b		R3d		R3e		R3f	
	RS	TI-2	RS	TI-2	RS	TI-2	RS	TI-2	RS	TI-2
Asp187:O_D-His224:H_{ND}	1.45 (173)	1.01	1.43 (175)	1.01	1.55 (177)	1.01	1.53 (175)	1.01	1.52 (175)	1.01
His224:N_D-His224:H_{ND}	1.13	1.85 (159)	1.14	1.86 (170)	1.10	1.83 (172)	1.10	1.83 (174)	1.10	1.83 (175)
His224:**H**-SEA:Oγ	-	2.45 (121)	-	2.63 (128)	-	2.59 (118)	-	2.49 (117)	-	2.45 (117)
His224:Nε-Sub:***H***	1.90 (162)	1.06	1.92 (180)	1.06	1.85 (163)	1.06	1.88 (177)	1.06	1.88 (172)	1.06
Sub:**O**-Sub:***H***	1.00	1.73 (172)	1.00	1.80 (158)	1.01	1.75 (168)	1.00	1.78 (166)	1.00	1.75 (166)
SEA:C-Sub:**O**	2.60 (100)	1.61	3.68 (99)	1.66	3.69 (105)	1.64	2.52 (97)	1.65	2.73 (94)	1.64
SEA:C-SEA:Oγ	1.37	1.50	1.38	1.52	1.38	1.54	1.37	1.51	1.38	1.53
SEA:C-SEA:O	1.24	1.33	1.24	1.31	1.24	1.31	1.24	1.32	1.24	1.31
SEA:O-Gln106:NH	1.83 (162)	1.73 (173)	1.89 (162)	1.80 (169)	1.90 (160)	1.69 (174)	1.92 (148)	1.76 (168)	1.99 (136)	1.76 (162)
SEA:O-Thr40:NH	2.14 (144)	1.91 (148)	2.61 (110)	2.30 (111)	2.60 (96)	2.98 (98)	2.20 (134)	2.15 (139)	2.29 (120)	2.30 (125)
SEA:O-Thr40:OH	1.82 (161)	1.65 (166)	1.83 (164)	1.62 (172)	1.87 (163)	1.77 (168)	1.83 (163)	1.66 (175)	1.78 (172)	1.66 (175)
Sub:*H*-Sub:O	2.10 (135)	2.36 (119)	4.64	4.72	4.78	4.64	2.08 (134)	2.64 (121)	4.13	2.39 (126)
Sub:*H*-Thr40:O	3.79	2.09 (156)	-	-	-	-	-	-	-	-

[a] The atoms corresponding to the hydroxyl and amino group of the substrate (Sub) are marked in bold and italic respectively. The Oxygen of the naphthoxy group of propranolol is indicated as Sub:O. Angles in degrees for both the corresponding hydrogen bonds and the nucleophilic attack (Sub:**O**···SEA:C=O) are given in brackets. SEA is the acetylated serine of CalB.

Table 35 Relevant Mulliken atomic charges in the reactant states (RS) and the intermediates (TI-2) for the optimized small model systems of the complexes between AcCalB and *R*-propranolol[a].

Atom	*Binding Mode I*		*Binding Mode II*							
	R1a		R3b		R3d		R3e		R3f	
	RS	TI-2	RS	TI-2	RS	TI-2	RS	TI-2	RS	TI-2
Asp187:O_D	-0.676	-0.458	-0.670	-0.463	-0.677	-0.468	-0.677	-0.466	-0.677	-0.467
His224:H_{ND}	+0.277	+0.355	+0.280	+0.356	+0.268	+0.353	+0.270	+0.352	+0.270	+0.352
His224:Nε	-0.399	-0.044	-0.393	-0.040	-0.387	-0.048	-0.392	-0.048	-0.392	-0.048
SEA:Oγ	-0.317	-0.466	-0.321	-0.474	-0.327	-0.478	-0.322	-0.465	-0.322	-0.474
Sub:**H**	+0.329	+0.243	+0.332	+0.242	+0.329	+0.245	+0.331	+0.243	+0.330	+0.245
Sub:**O**	-0.533	-0.528	-0.531	-0.537	-0.518	-0.527	-0.527	-0.532	-0.524	-0.526
SEA:C	+0.684	+0.757	+0.654	+0.744	+0.650	+0.752	+0.677	+0.748	+0.671	+0.745
SEA:O	-0.575	-0.802	-0.565	-0.766	-0.554	-0.782	-0.564	-0.782	-0.562	-0.776
Gln106:NH	+0.220	+0.245	+0.219	+0.244	+0.213	+0.249	+0.206	+0.236	+0.210	+0.241
Thr40:NH	+0.201	+0.233	+0.197	+0.215	+0.195	+0.196	+0.202	+0.222	+0.206	+0.219
Thr40:OH	+0.335	+0.353	+0.335	+0.354	+0.334	+0.361	+0.333	+0.357	+0.335	+0.358

[a] The atoms corresponding to the hydroxyl group of the substrate (Sub) are marked in bold. SEA is the acetylated serine of CalB.

Table 36 Relevant interatomic distances, bond lengths and angles in the reactant states (RS) and the intermediates (TI-2) for the optimized small model systems of the complexes between AcCalB and *S*-propranolol[a].

Distance (Å)	*Binding Mode I*						*Binding Mode II*			
	S12b		S3a		S3b		S4a		S4b	
	RS	TI-2	RS	TI-2	RS	TI-2	RS	TI-2	RS	TI-2
Asp187:O_D-His224:H_{ND}	1.52 (177)	1.01	1.46 (174)	1.01	1.52 (178)	1.01	1.53 (177)	1.01	1.62 (175)	1.01
His224:N_D-His224:H_{ND}	1.11	1.84 (175)	1.12	1.83 (177)	1.10	1.83 (173)	1.11	1.86 (169)	1.10	1.84 (168)
His224:**H**-SEA:Oγ	-	2.72 (117)	-	2.90 (125)	-	2.64 (118)	-	3.16 (121)	-	2.41 (115)
His224:Nε-Sub:***H***	1.85 (172)	1.05	1.88 (177)	1.06	1.85 (165)	1.06	1.87 (164)	1.04	1.87 (177)	1.06
Sub:**O**-Sub:***H***	1.01	1.89 (168)	1.00	1.71 (165)	1.01	1.79 (169)	1.01	2.17 (151)	1.01	1.73 (175)
SEA:C-Sub:**O**	3.14 (98)	1.61	2.66 (94)	1.76	3.69 (108)	1.64	3.52 (104)	1.56	2.55 (104)	1.61
SEA:C-SEA:Oγ	1.37	1.51	1.38	1.50	1.38	1.51	1.38	1.52	1.37	1.54
SEA:C-SEA:O	1.24	1.33	1.24	1.29	1.24	1.32	1.24	1.34	1.24	1.31
SEA:O-Gln106:NH	1.83 (152)	1.72 (171)	1.92 (155)	1.92 (169)	1.88 (154)	1.69 (169)	1.88 (148)	1.70 (168)	1.93 (140)	2.24 (151)
SEA:O-Thr40:NH	2.08 (153)	2.27 (154)	2.98 (109)	2.93 (111)	2.40 (116)	2.87 (117)	2.07 (172)	1.83 (178)	2.17 (119)	1.90 (136)
SEA:O-Thr40:OH	1.79 (165)	1.63 (178)	1.86 (167)	1.71 (169)	1.83 (154)	1.66 (172)	1.80 (172)	1.66 (175)	1.84 (155)	1.67 (165)
Sub:*H*-Sub:O	3.03 (73)	2.67 (100)	4.30	4.19	4.70	4.69	2.05 (135)	2.18 (132)	4.67	4.70
Sub:*H*-Thr40:O	4.99	7.15	7.77	8.58	9.69	7.14	-	-	-	-

[a] The atoms corresponding to the hydroxyl and amino group of the substrate (Sub) are marked in bold and italic respectively. The Oxygen of the naphthoxy group of propranolol is indicated as Sub:O. Angles in degrees for both the corresponding hydrogen bonds and the nucleophilic attack (Sub:**O**···SEA:C=O) are given in brackets. SEA is the acetylated serine of CalB.

Table 37 Relevant Mulliken atomic charges in the reactant states (RS) and the intermediates (TI-2) for the optimized small model systems of the complexes between AcCalB and *S*-propranolol[a].

Atom	*Binding Mode I*						*Binding Mode II*			
	S12b		S3a		S3b		S4a		S4b	
	RS	TI-2	RS	TI-2	RS	TI-2	RS	TI-2	RS	TI-2
Asp187:O_D	-0.686	-0.463	-0.676	-0.465	-0.677	-0.468	-0.674	-0.460	-0.701	-0.467
His224:H_{ND}	+0.270	+0.354	+0.276	+0.354	+0.269	+0.353	+0.270	+0.352	+0.274	+0.354
His224:Nε	-0.391	-0.033	-0.396	-0.050	-0.385	-0.040	-0.388	-0.030	-0.387	-0.044
SEA:Oγ	-0.312	-0.462	-0.325	-0.446	-0.325	-0.467	-0.317	-0.477	-0.304	-0.486
Sub:**H**	+0.332	+0.237	+0.336	+0.251	+0.333	+0.244	+0.333	+0.227	+0.332	+0.243
Sub:**O**	-0.545	-0.513	-0.525	-0.580	-0.516	-0.529	-0.522	-0.502	-0.543	-0.519
SEA:C	+0.667	+0.754	+0.672	+0.732	+0.649	+0.752	+0.660	+0.757	+0.676	+0.744
SEA:O	-0.565	-0.806	-0.556	-0.746	-0.561	-0.787	-0.567	-0.800	-0.570	-0.799
Gln106:NH	+0.218	+0.248	+0.214	+0.236	+0.222	+0.254	+0.212	+0.245	+0.216	+0.225
Thr40:NH	+0.199	+0.217	+0.197	+0.199	+0.195	+0.198	+0.200	+0.240	+0.205	+0.229
Thr40:OH	+0.331	+0.360	+0.337	+0.359	+0.330	+0.360	+0.328	+0.351	+0.333	+0.352

[a] The atoms corresponding to the hydroxyl group of the substrate (Sub) are marked in bold. SEA is the acetylated serine of CalB.

Appendix D

Supplementary information for Chapter 5

Table 38 RMSD values for all heavy atoms of the protein in the optimized TI-2s respect to the CalB crystal structure.

R-propranolol		*S*-propranolol	
TI-2	RMSD (Å)	TI-2	RMSD (Å)
TI-R1	0.555	TI-S1	0.554
TI-R2	0.553	TI-S2	0.554
TI-R3	0.554	TI-S3	0.558
TI-R4	0.552	TI-S4	0.553
TI-R5	0.553	TI-S5	0.553
TI-R6	0.554	TI-S6	0.554

Table 39 Average RMSD (respect to the CalB crystal structure) for all heavy atoms of the protein backbone in the MD simulations of the TI-2s[a]

TI-2	RMSD	RMSD*
TI-R1	0.95 ± 0.21	0.99 ± 0.15
TI-R2	0.98 ± 0.16	1.03 ± 0.20
TI-R3	1.08 ± 0.17	0.83 ± 0.10
TI-R4	1.00 ± 0.14	0.85 ± 0.12
TI-R5	0.90 ± 0.12	1.02 ± 0.20
TI-R6	0.85 ± 0.11	1.02 ± 0.21
TI-S1	1.00 ± 0.21	1.08 ± 0.16
TI-S2	0.88 ± 0.11	1.10 ± 0.17
TI-S3	0.92 ± 0.14	1.14 ± 0.22
TI-S4	1.02 ± 0.17	0.96 ± 0.13
TI-S5	1.01 ± 0.18	1.08 ± 0.23
TI-S6	0.94 ± 0.17	0.91 ± 0.17

[a] RMSD values are given (in Å) for the two MD simulations with different initial velocity distribution as indicated by *.

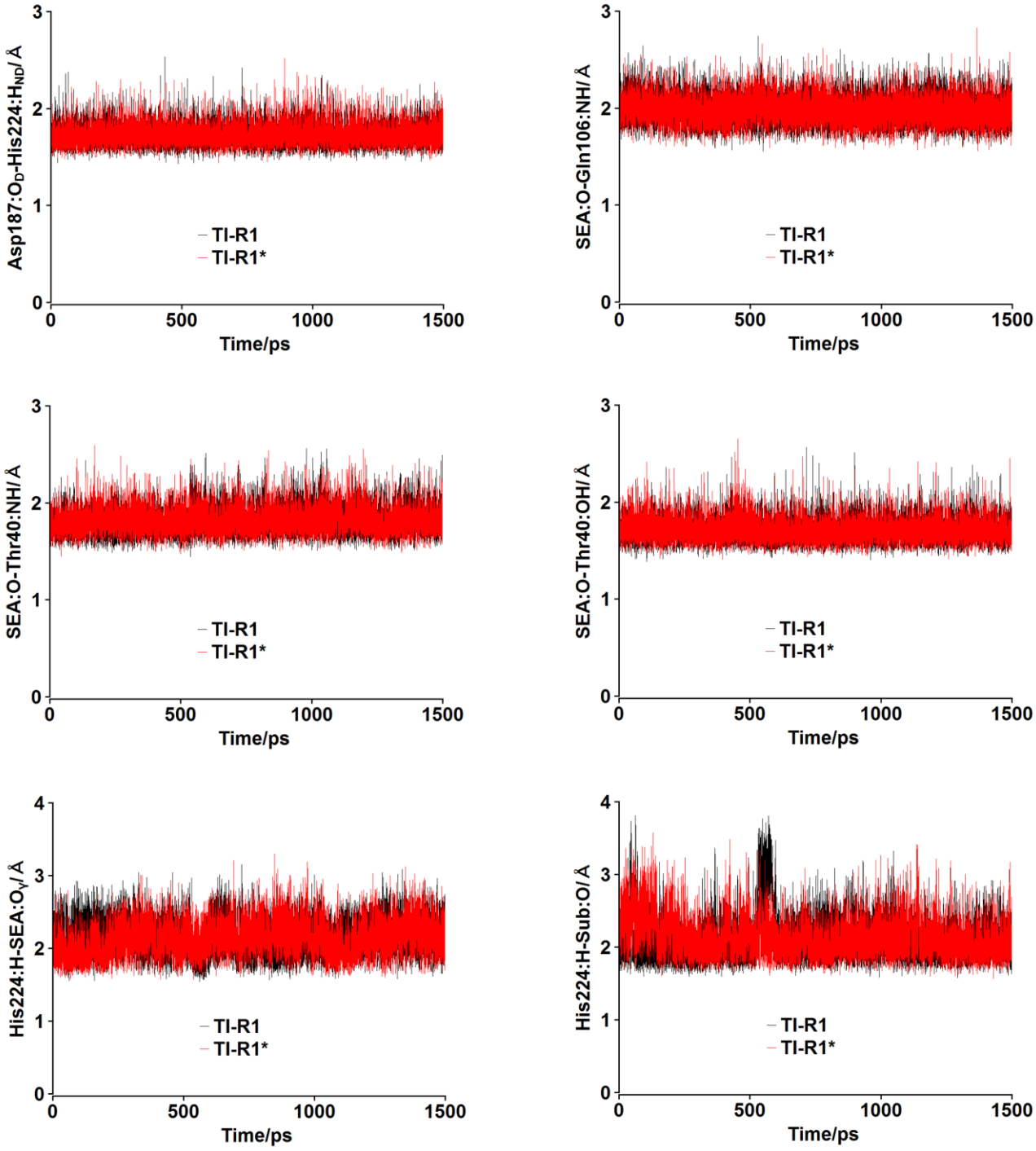

Fig. 77 Time evolution of the essential hydrogen bonds for the catalytic activity of CalB in the MD simulations of TI-R1. The simulation with different seed velocity is indicated by *.

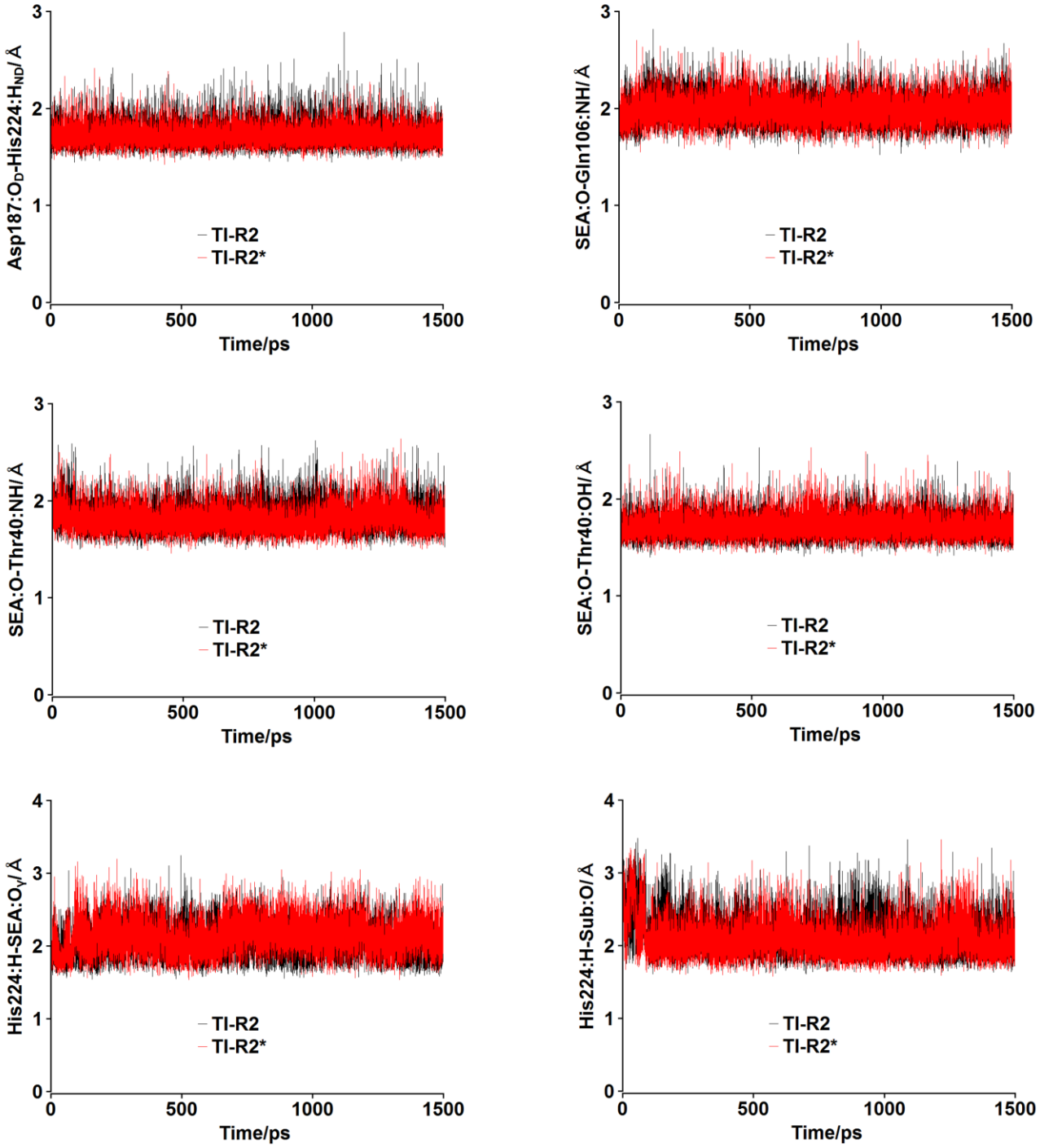

Fig. 78 Time evolution of the essential hydrogen bonds for the catalytic activity of CalB in the MD simulations of TI-R2. The simulation with different seed velocity is indicated by *.

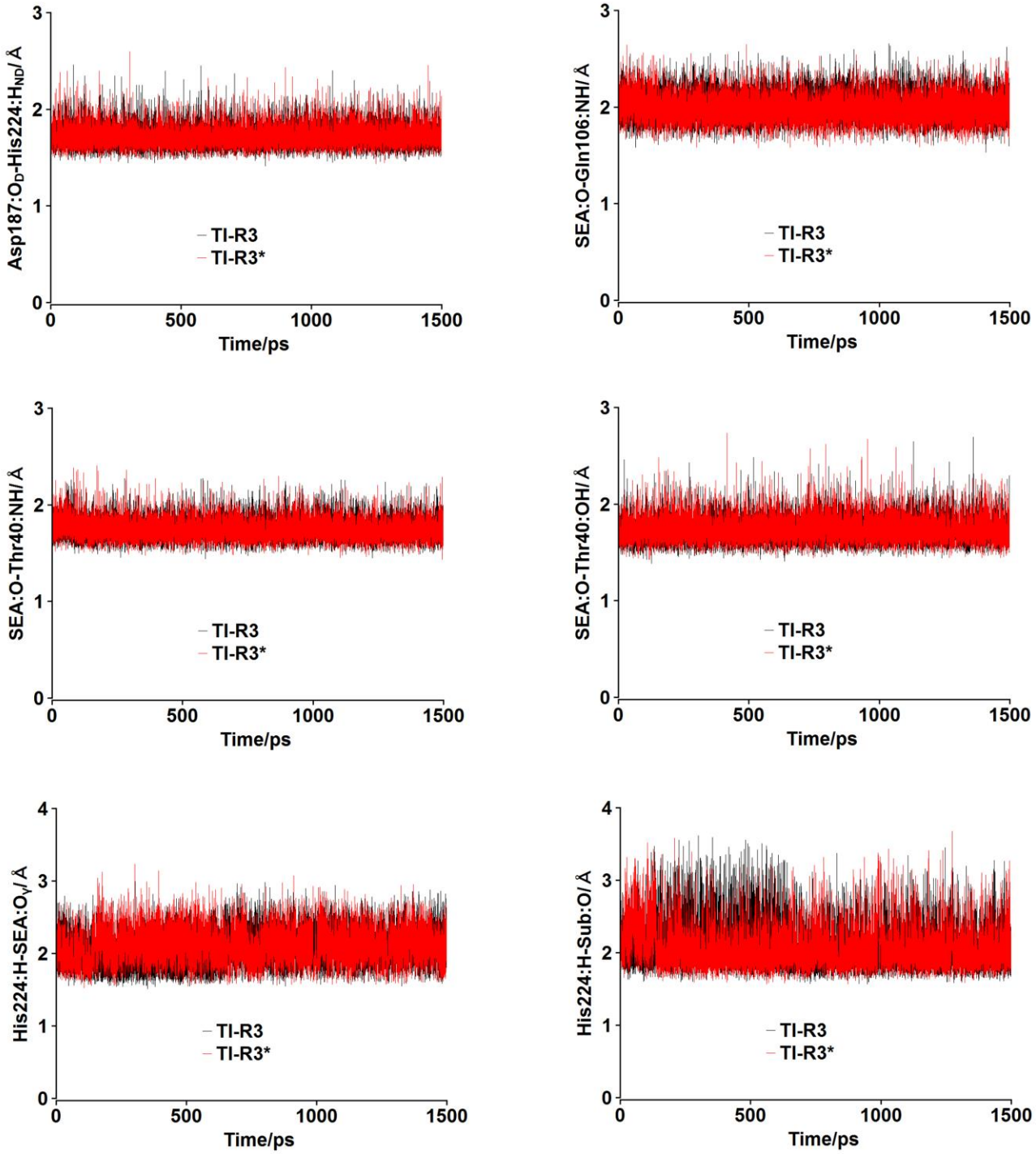

Fig. 79 Time evolution of the essential hydrogen bonds for the catalytic activity of CalB in the MD simulations of TI-R3. The simulation with different seed velocity is indicated by *.

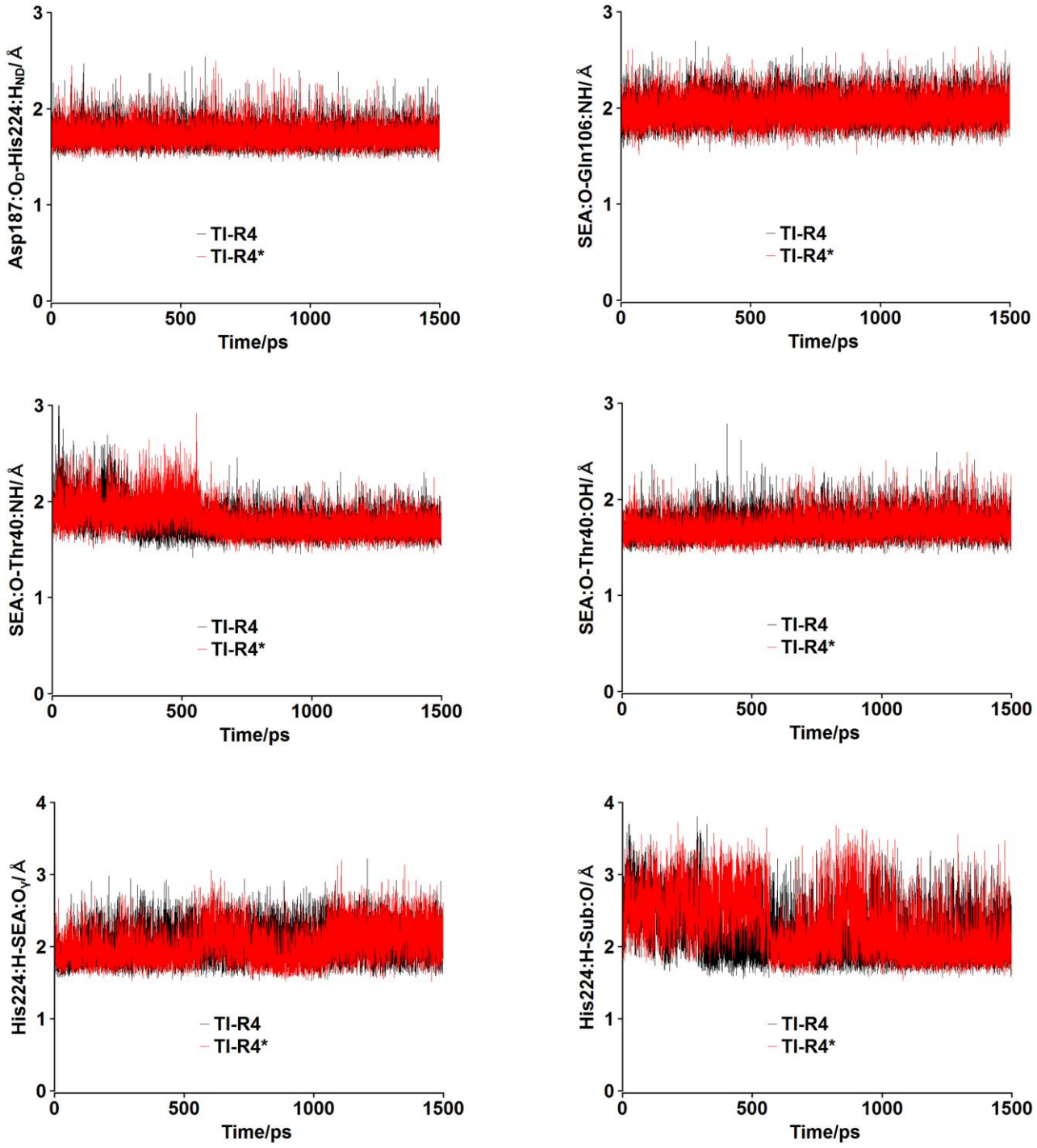

Fig. 80 Time evolution of the essential hydrogen bonds for the catalytic activity of CalB in the MD simulations of TI-R4. The simulation with different seed velocity is indicated by *.

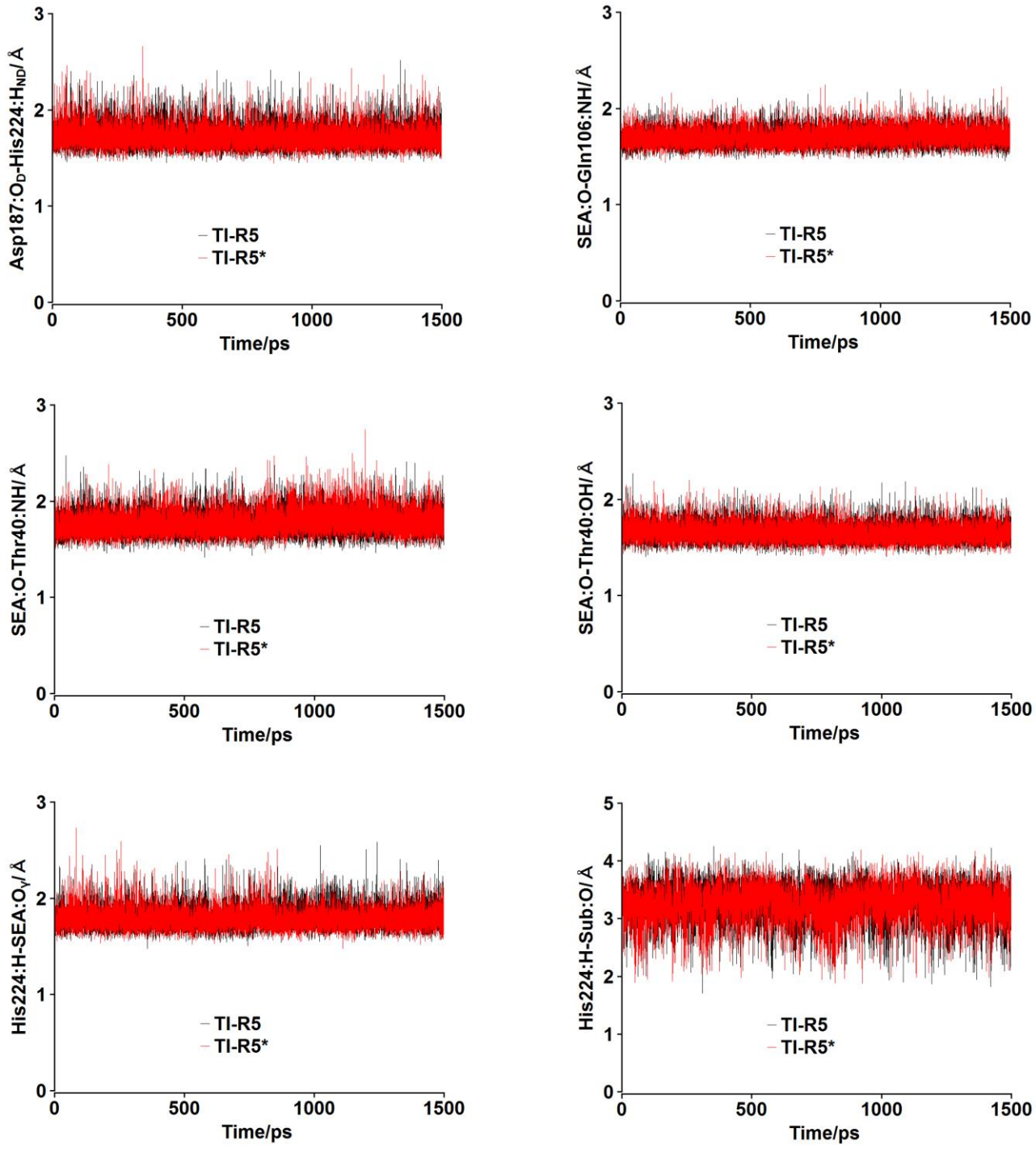

Fig. 81 Time evolution of the essential hydrogen bonds for the catalytic activity of CalB in the MD simulations of TI-R5. The simulation with different seed velocity is indicated by *. The movement of Sub:**O** atom toward the oxyanion hole leads to the disruption of the His224:**H**-Sub:**O** hydrogen bond.

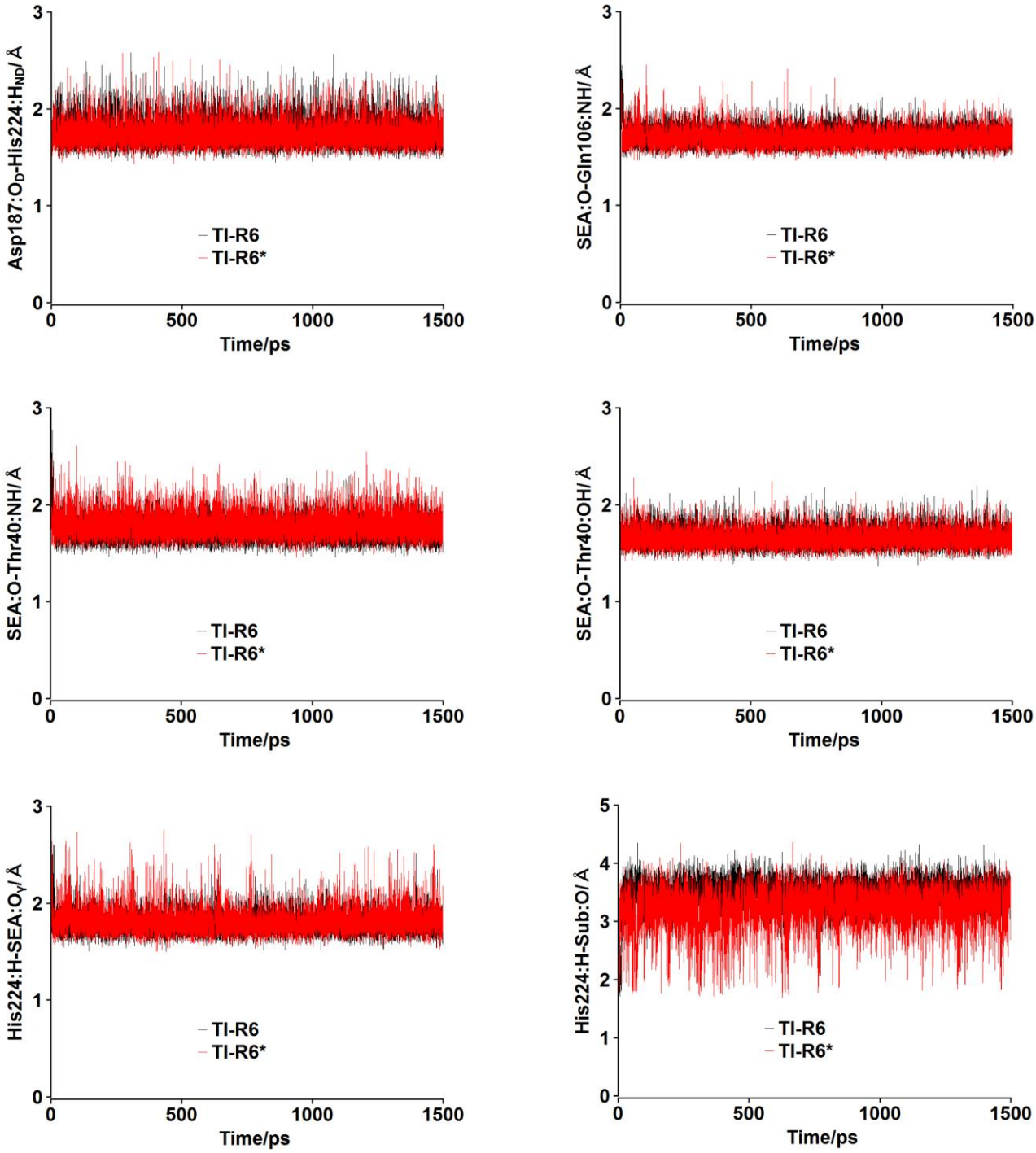

Fig. 82 Time evolution of the essential hydrogen bonds for the catalytic activity of CalB in the MD simulations of TI-R6. The simulation with different seed velocity is indicated by *. The movement of Sub:**O** atom toward the oxyanion hole leads to the disruption of the His224:**H**-Sub:**O** hydrogen bond.

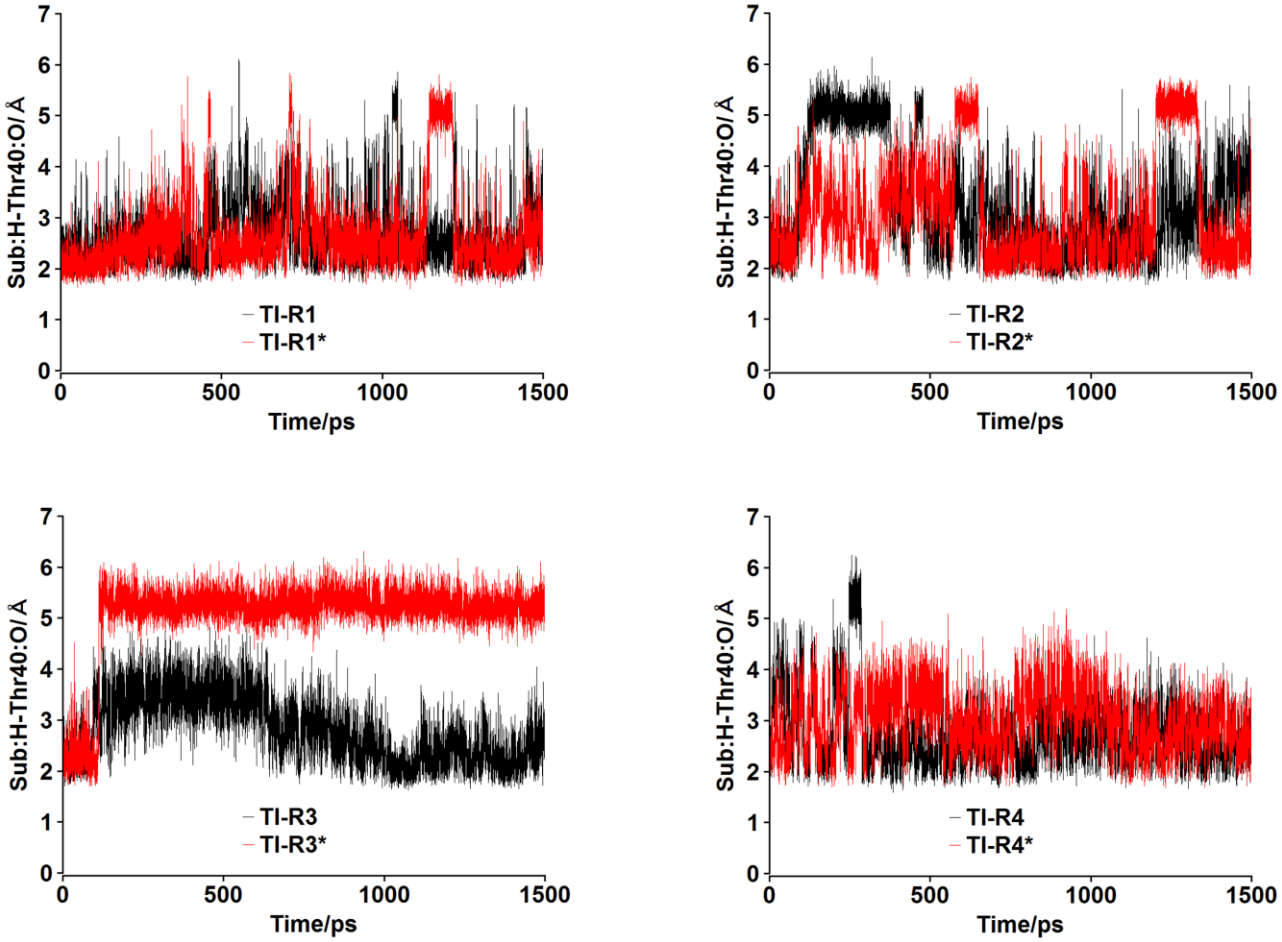

Fig. 83 Time evolution of the Sub:*H*-Thr40:O hydrogen bond in the MD simulations of the TI2s of *R*-propranolol in binding mode I. The simulation with different seed velocity is indicated by *. The Sub:*H*-Thr40:O hydrogen bond is formed during 1175.5 ps, 1204.5 ps, 777.8 ps, 862.2 ps, 925.6 ps, 96 ps, 1113.4 ps and 750 ps in the MD simulations of TI-R1, TI-R1*, TI-R2, TI-R2*, TI-R3, TI-R3*, TI-R4 and TI-R4*, respectively.

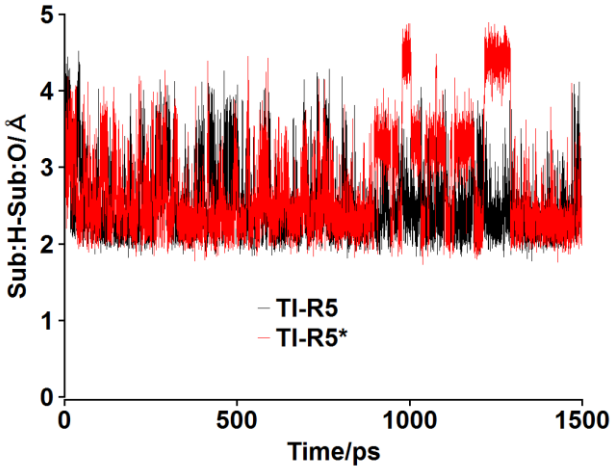

Fig. 84 Time evolution of the intramolecular hydrogen bond between the amino and naphthoxy groups of propranolol (Sub:*H*-Sub:O) in the MD simulations of TI-R5. The simulation with different seed velocity is indicated by *. This hydrogen bond is formed during 1215.5 ps and 995.2 ps in the MD simulations of TI-R5 and TI-R5*, respectively.

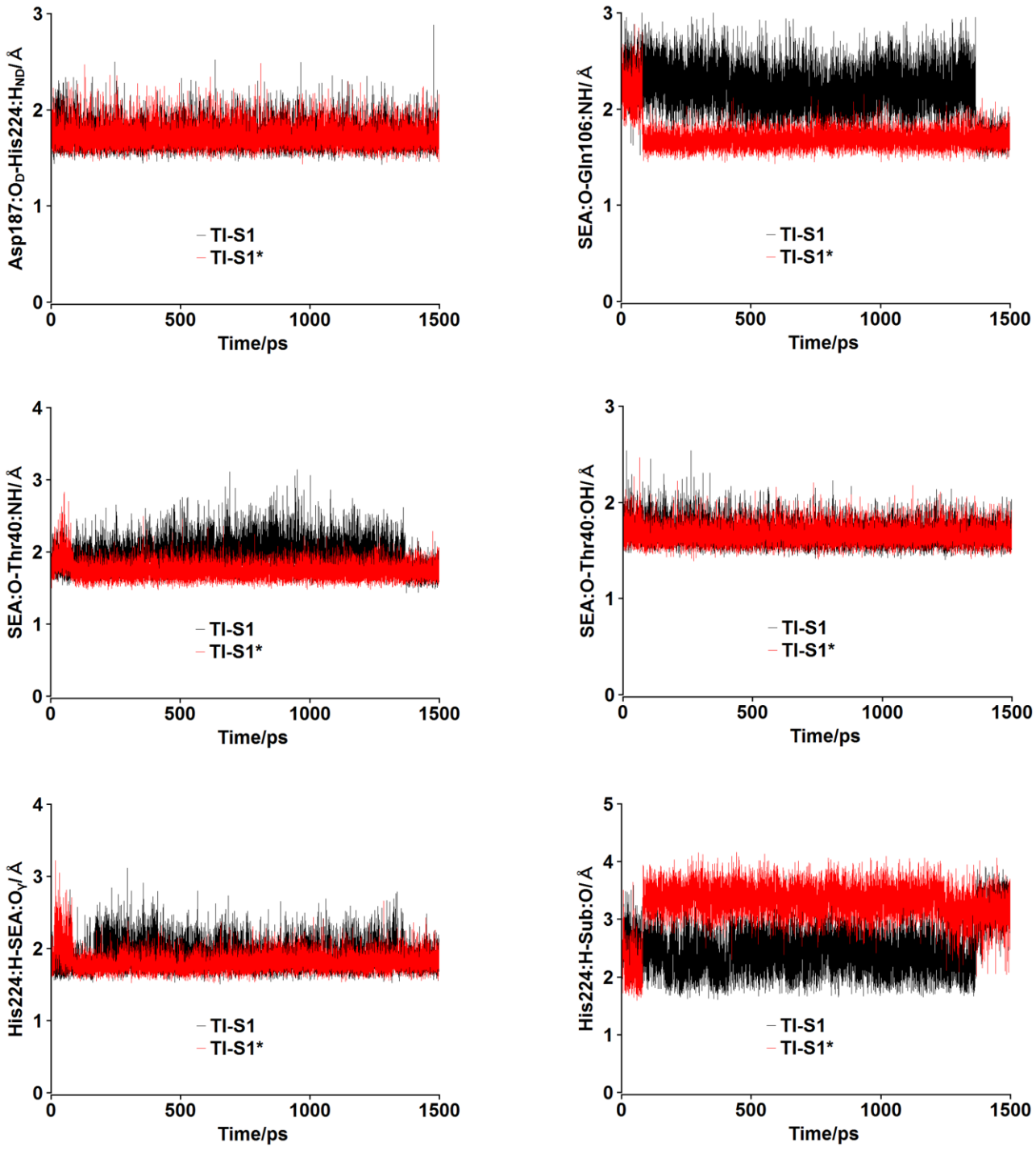

Fig. 85 Time evolution of the essential hydrogen bonds for the catalytic activity of CalB in the MD simulations of TI-S1. The simulation with different seed velocity is indicated by *. The movement of Sub:**O** atom toward the oxyanion hole leads to the disruption of the His224:**H**-Sub:**O** hydrogen bond.

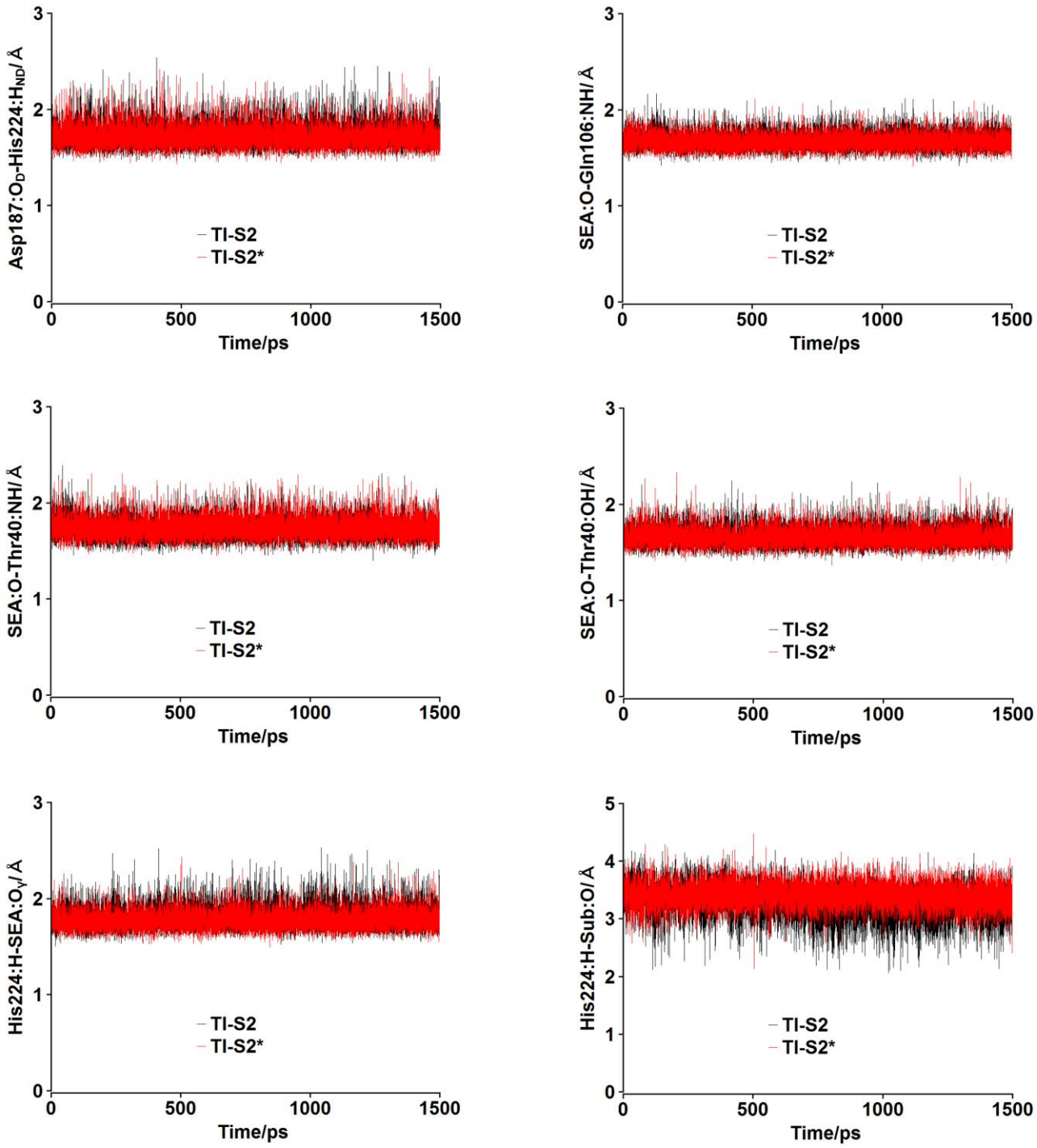

Fig. 86 Time evolution of the essential hydrogen bonds for the catalytic activity of CalB in the MD simulations of TI-S2. The simulation with different seed velocity is indicated by *. The movement of Sub:**O** atom toward the oxyanion hole leads to the disruption of the His224:**H**-Sub:**O** hydrogen bond.

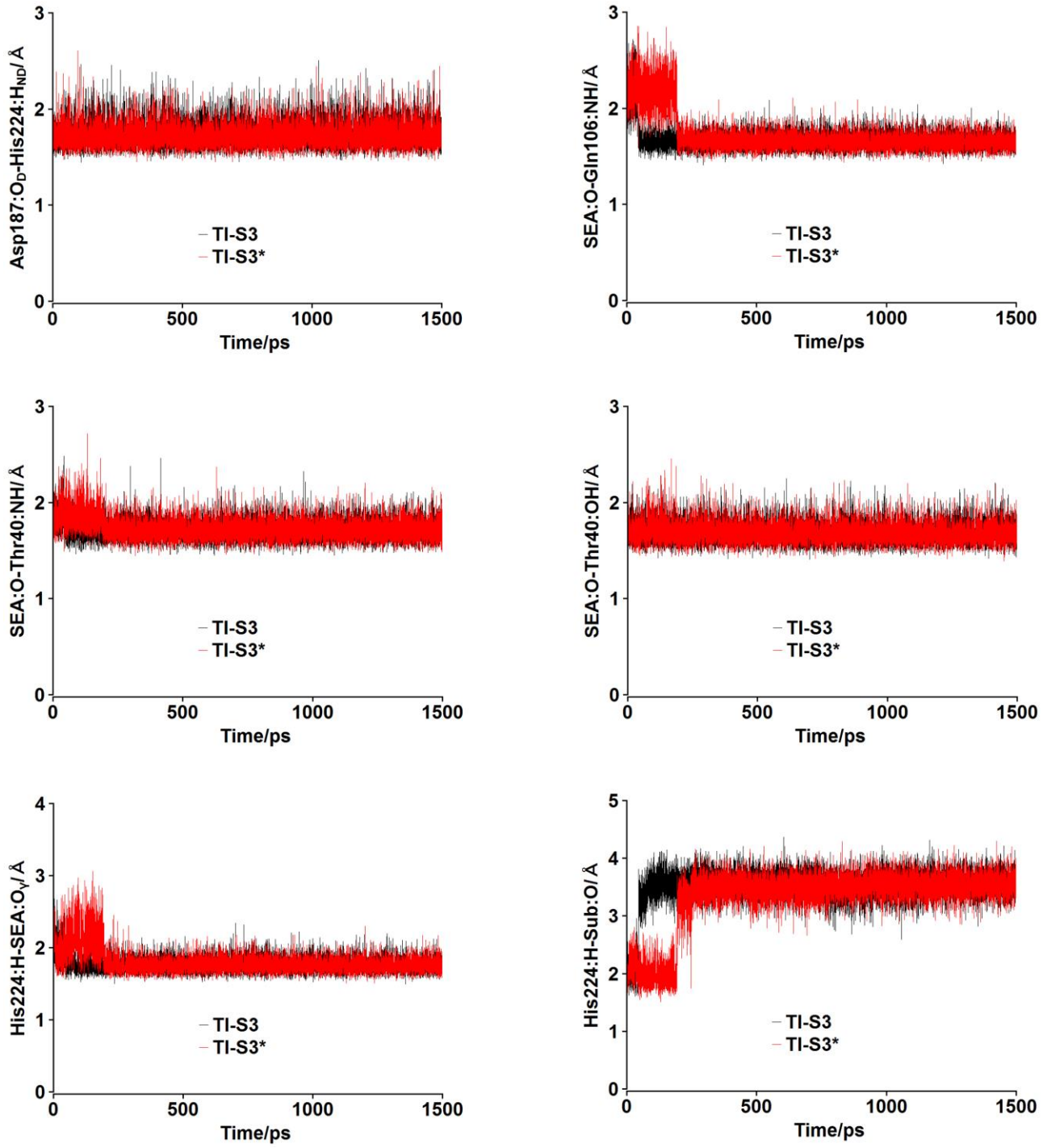

Fig. 87 Time evolution of the essential hydrogen bonds for the catalytic activity of CalB in the MD simulations of TI-S3. The simulation with different seed velocity is indicated by *. The movement of Sub:**O** atom toward the oxyanion hole leads to the disruption of the His224:**H**-Sub:**O** hydrogen bond.

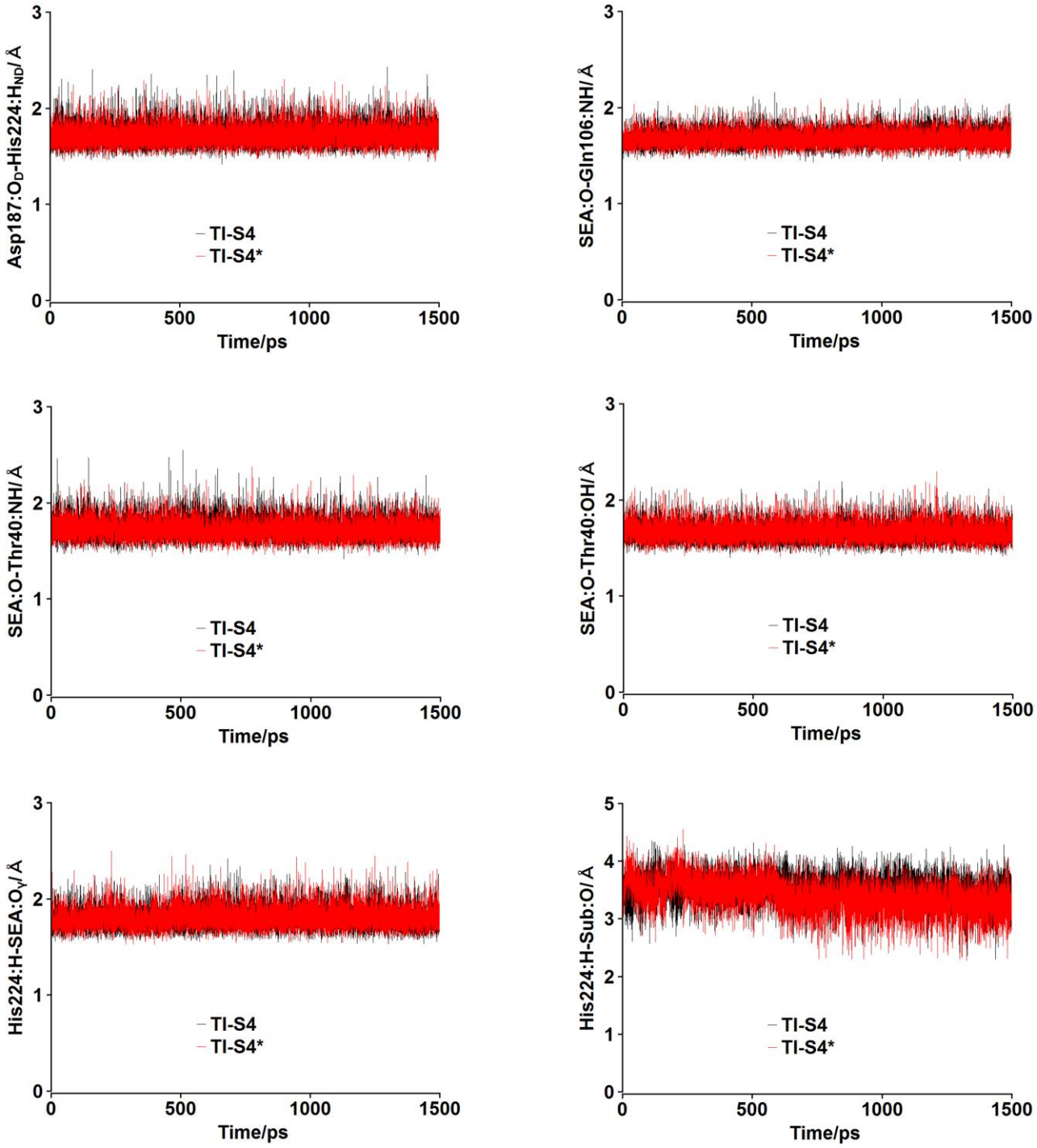

Fig. 88 Time evolution of the essential hydrogen bonds for the catalytic activity of CalB in the MD simulations of TI-S4. The simulation with different seed velocity is indicated by *. The movement of Sub:**O** atom toward the oxyanion hole leads to the disruption of the His224:**H**-Sub:**O** hydrogen bond.

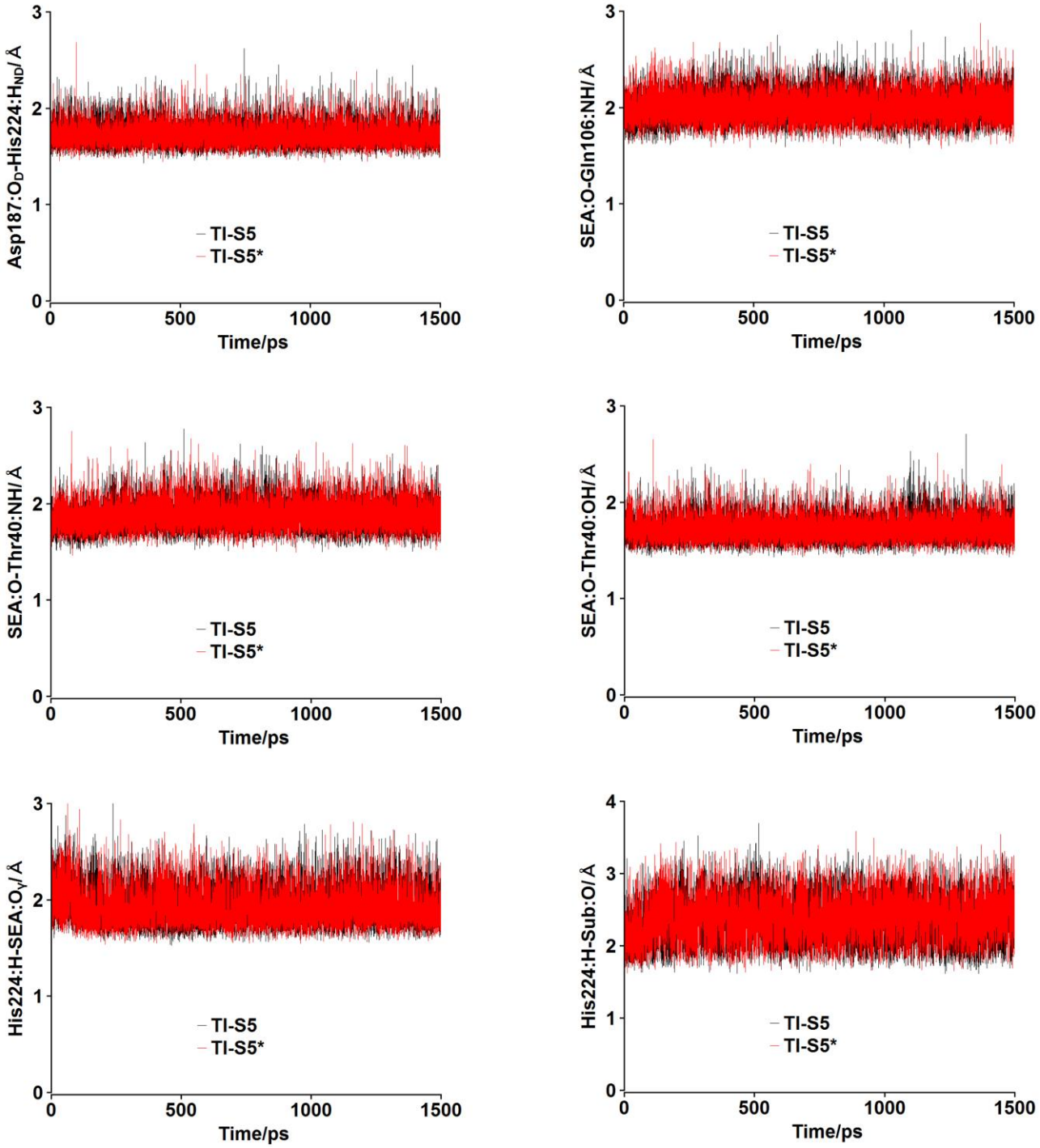

Fig. 89 Time evolution of the essential hydrogen bonds for the catalytic activity of CalB in the MD simulations of TI-S5. The simulation with different seed velocity is indicated by *.

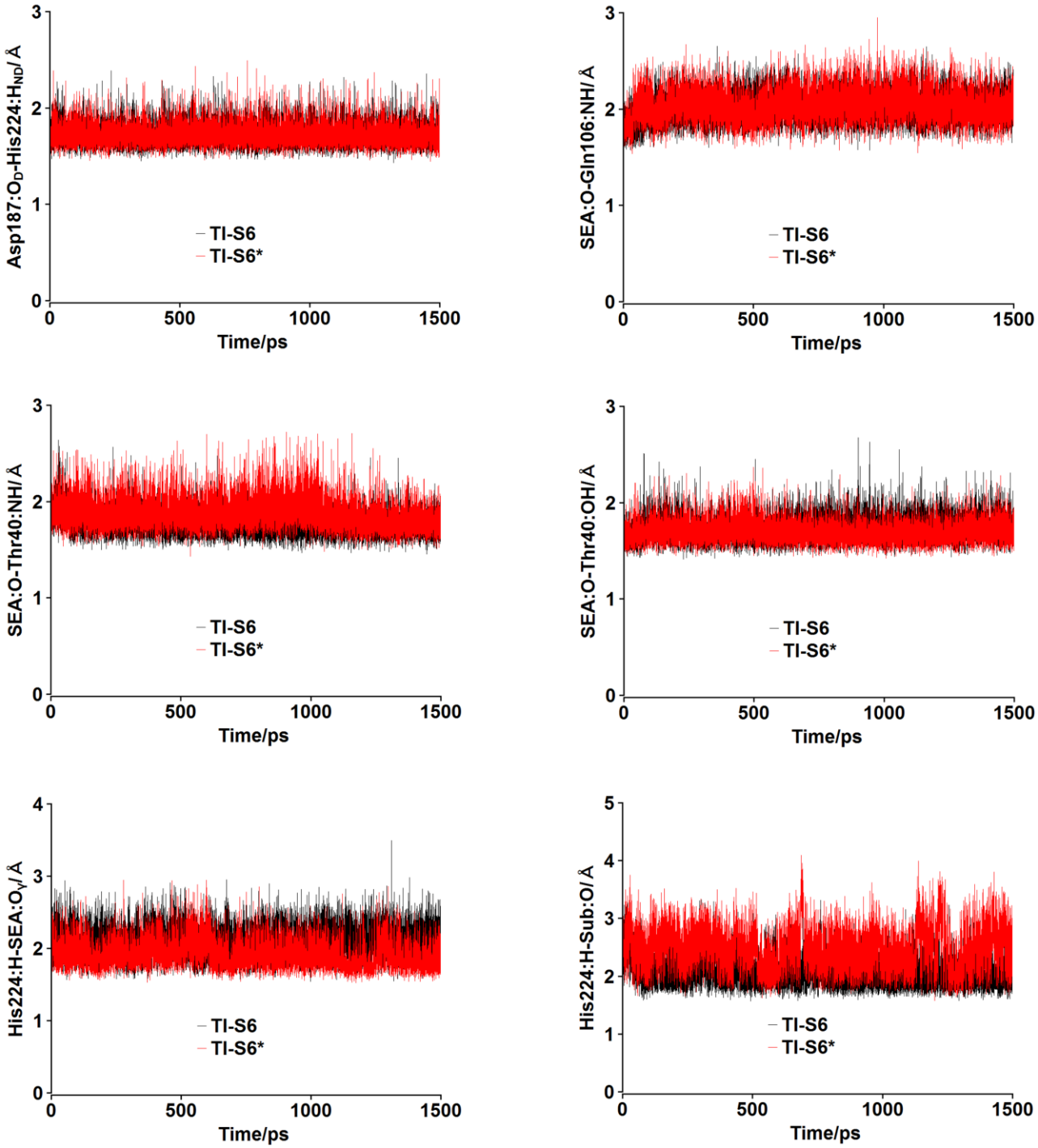

Fig. 90 Time evolution of the essential hydrogen bonds for the catalytic activity of CalB in the MD simulations of TI-S6. The simulation with different seed velocity is indicated by *.

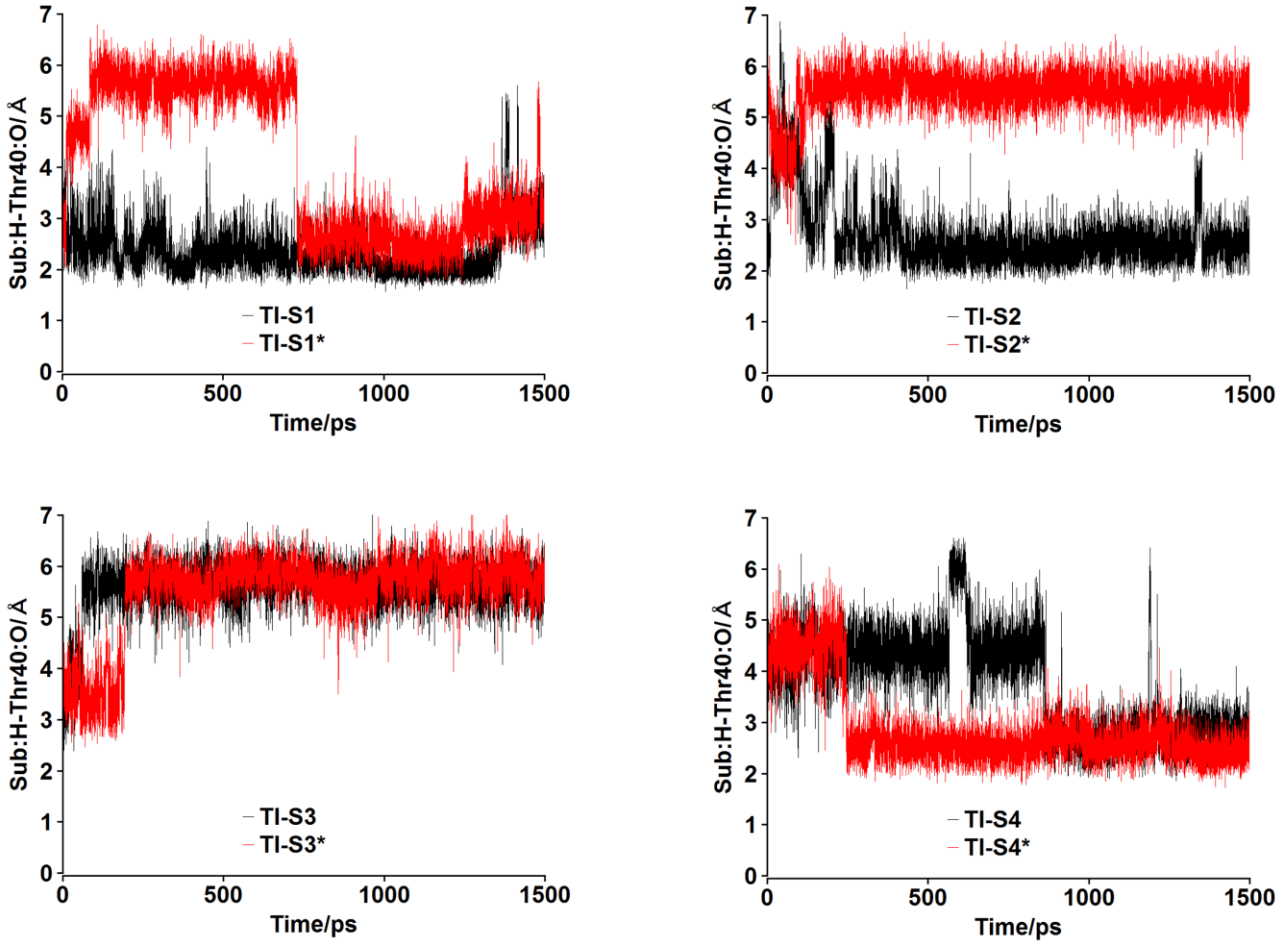

Fig. 91 Time evolution of the Sub:*H*-Thr40:O hydrogen bond in the MD simulations of the TI2s of *S*-propranolol in binding mode I. The simulation with different seed velocity is indicated by *. The Sub:*H*-Thr40:O hydrogen bond is formed during 1346.7 ps, 584.2 ps, 1225.5 ps, 1 ps, 3.4 ps, 21.4 ps, 504.3 ps and 1162.8 ps in the MD simulations of TI-S1, TI-S1*, TI-S2, TI-S2*, TI-S3, TI-S3*, TI-S4 and TI-S4*, respectively.

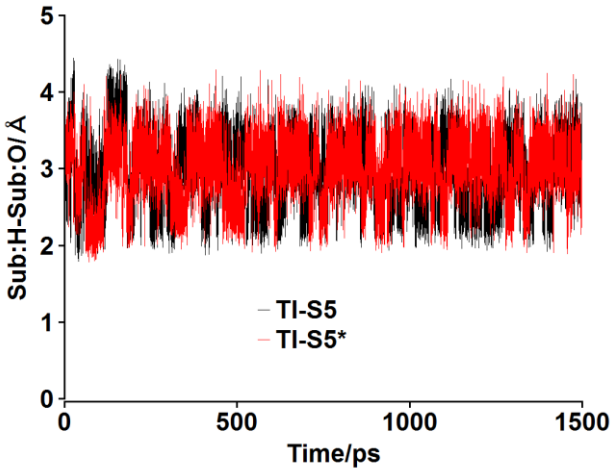

Fig. 92 Time evolution of the intramolecular hydrogen bond between the amino and naphthoxy groups of propranolol (Sub:*H*-Sub:O) in the MD simulations of TI-S5. The simulation with different seed velocity is indicated by *. This hydrogen bond is formed during 616.3 ps and 491.5 ps in the MD simulations of TI-S5 and TI-S5*, respectively.

Appendix E

Supplementary information for Chapter 6

Supplementary information for **Chapter 6** is given below. This includes optimized geometries and geometry descriptors of the stationary points, QM and MM energies, and QM/MM energy profiles at different levels of theory.

B3LYP(TZVP)/CHARMM results for the conversion of *R*-propranolol in binding mode I

Table 40 QM(B3LYP/TZVP) and MM(CHARMM) energies in kcal/mol (relative to the MCC) for the transformation of *R*-propranolol in binding mode I via the TI-2s ORI and ORII[a]

Stationary Point	ORI				ORII			
	QM energy		MM energy		QM energy		MM energy	
MCC	0		0		0		0	
TS1	9.4	(9.4)	-2.3	(-2.3)	7.1	(7.1)	-0.6	(-0.6)
TI-2	3.6		-3.1		2.3		0.9	
TS2	6.8	(3.2)	-2.2	(0.9)	6.7	(4.4)	-0.5	(-1.4)
PDC	-1.8		-0.8		0.1		0.8	

[a] Activation barriers relative to the preceding minima are given in parentheses

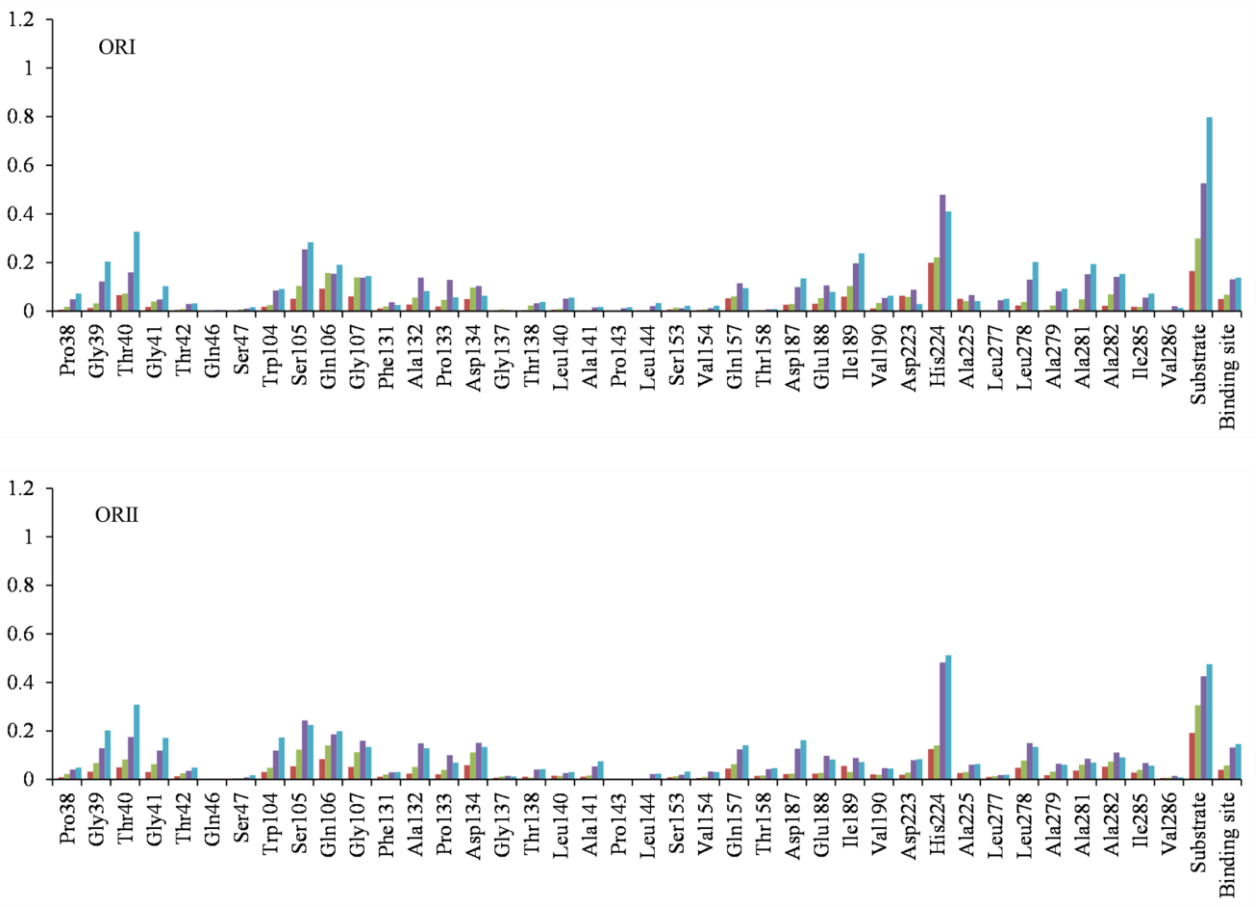

Fig. 93 RMSD (respect to the MCC) of all heavy atoms of the residues around 5 Å from the substrate at the stationary points along the energy profiles obtained for the transformation of *R*-propranolol in binding mode I via the TI-2s ORI and ORII: TS1 (red), TI-2 (green), TS2 (violet) and PDC (blue). Binding side correspond to all residues considered. The acyl group has been considered as part of the substrate.

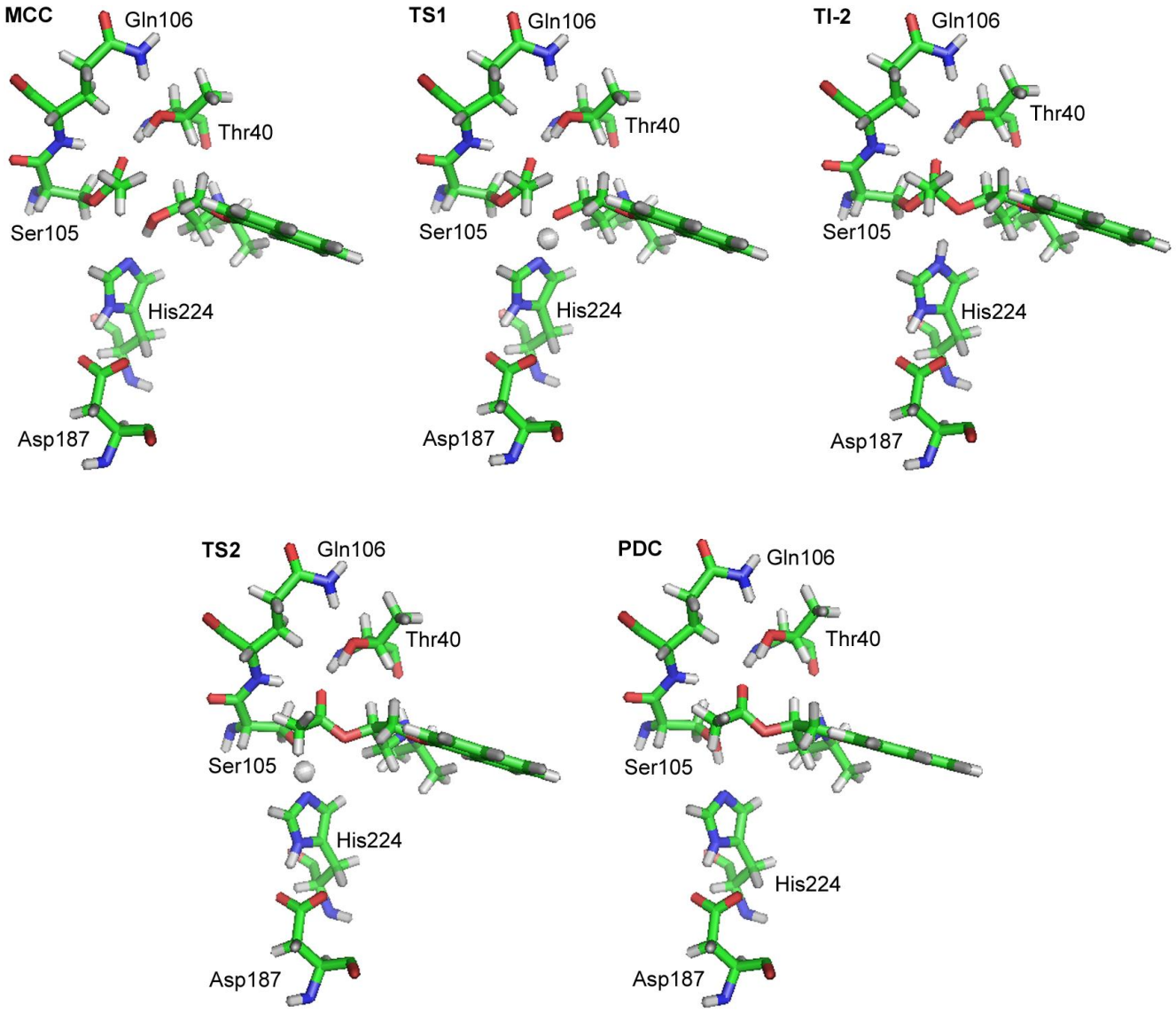

Fig. 94 Stationary points along the energy profile for the conversion of *R*-propranolol to *R*-acetyl-propranolol via the TI-2 ORI.

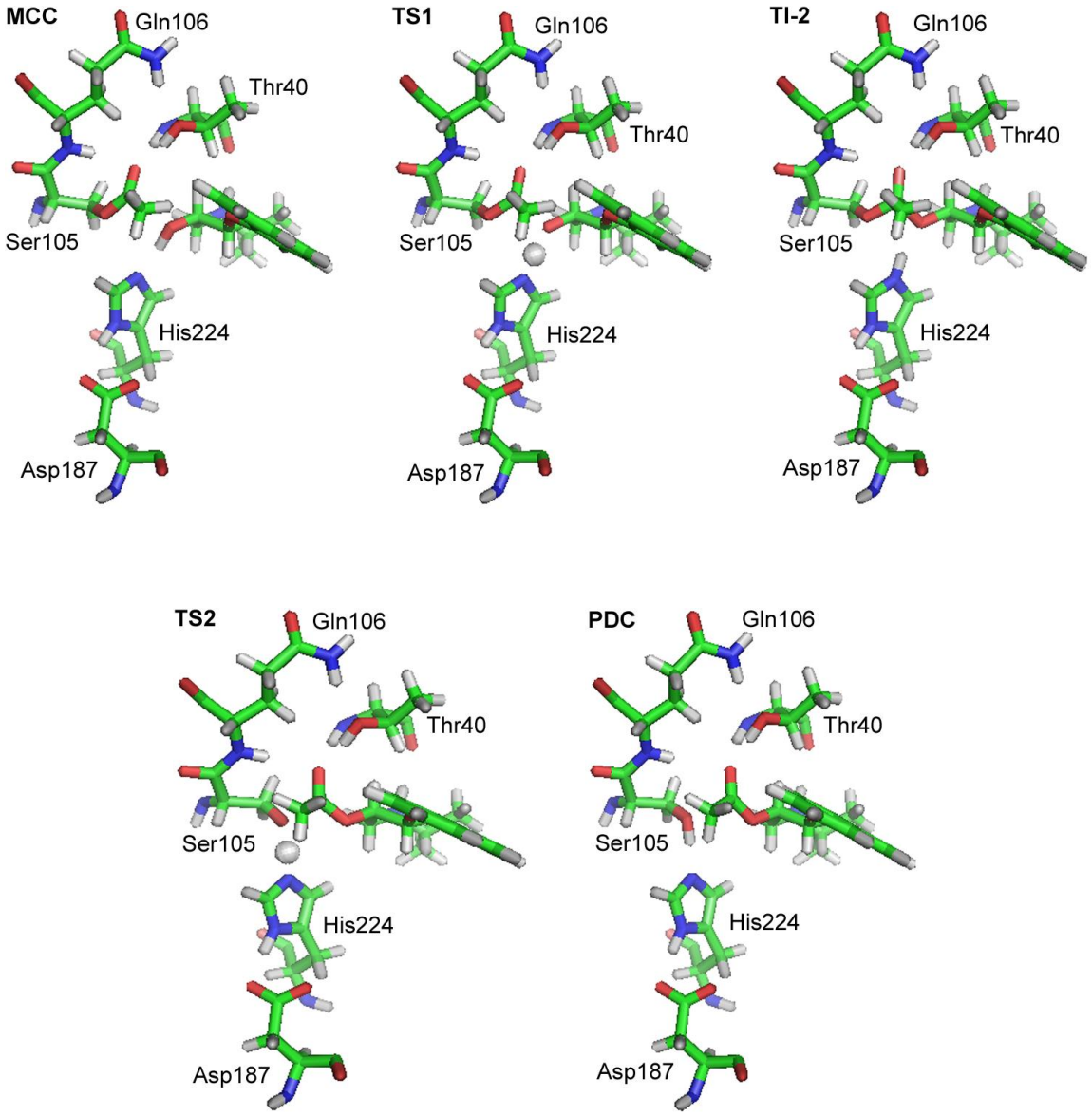

Fig. 95 Stationary points along the energy profile for the conversion of *R*-propranolol to *R*-acetyl-propranolol via the TI-2 ORII.

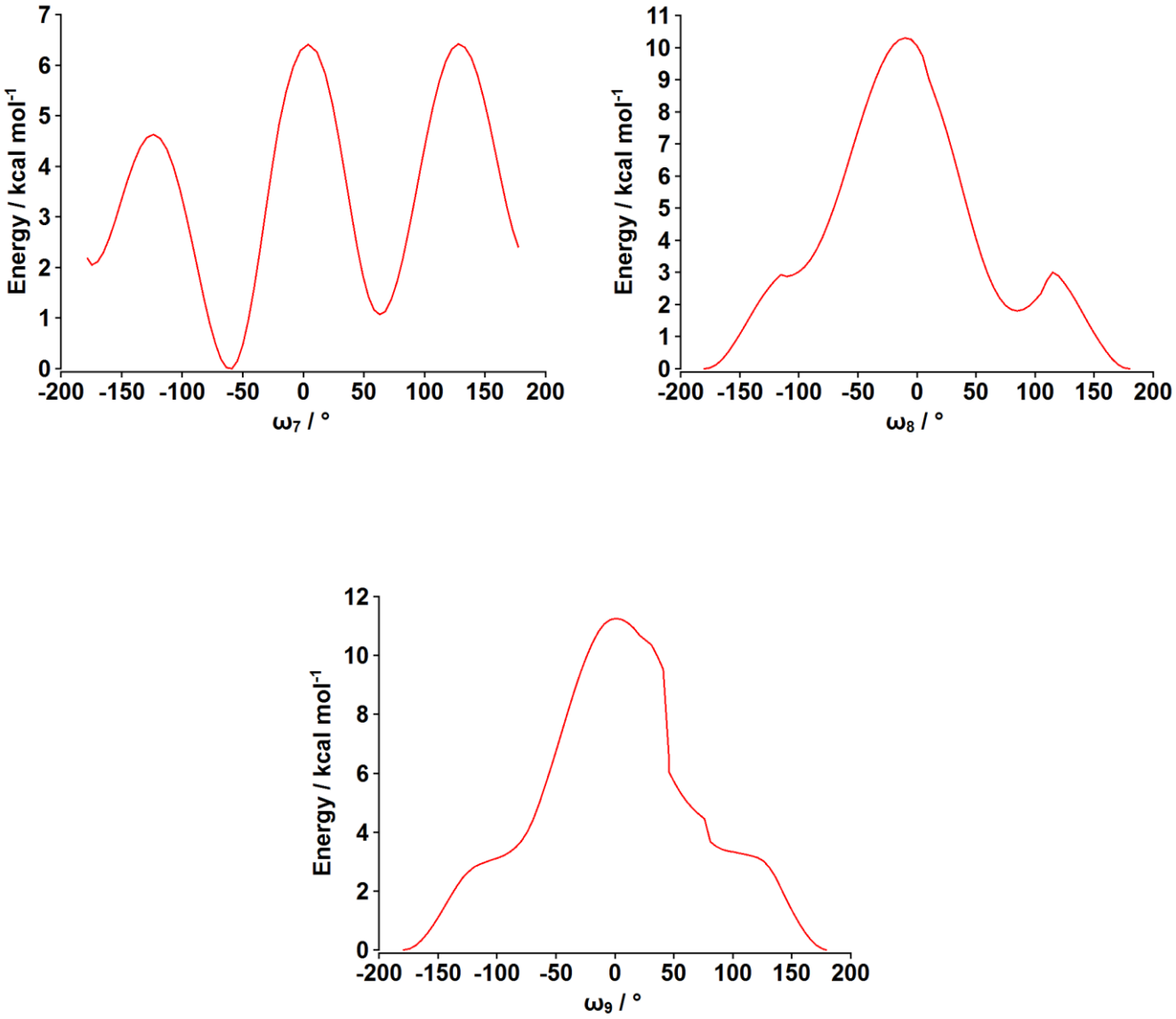

Fig. 96 PES scans along the dihedral angles of *R*-1-methyl-3-(1-naphthoxy)-2-propanol.

B3LYP(TZVP)/CHARMM results for the conversion of *R*-propranolol in binding mode II

Table 41 QM(B3LYP/TZVP) and MM(CHARMM) energies in kcal/mol (relative to the MCC) for the transformation of *R*-propranolol in binding mode II via the TI-2s ORIII and ORIV[a]

Stationary Point	ORIII				ORIV			
	QM energy		MM energy		QM energy		MM energy	
MCC	0		0		0		0	
TS1	13.3	(13.3)	-3.3	(-3.3)	17.5	(17.5)	-1.3	(-1.3)
TI-2	0.1		-3.9		16.4		-1.7	
TS2	2.0	(1.9)	-3.8	(0.1)	21.6	(5.2)	-3.3	(-1.6)
PDC	-5.7		-3.1		9.7		-1.1	

[a] Activation barriers relative to the preceding minima are given in parentheses

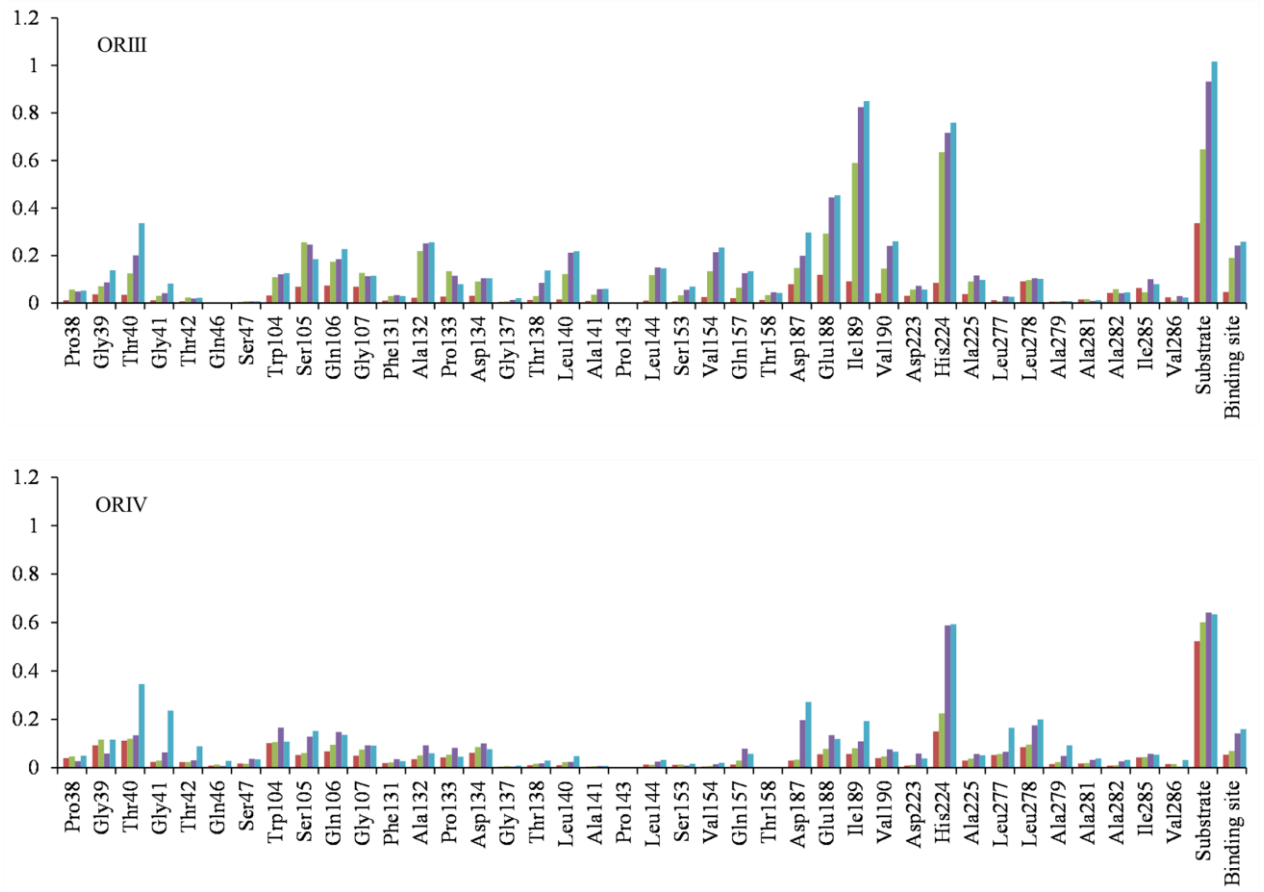

Fig. 97 RMSD (respect to the MCC) of all heavy atoms of the residues around 5 Å from the substrate at the stationary points along the energy profiles obtained for the transformation of *R*-propranolol in binding mode II via the TI-2s ORIII and ORIV: TS1 (red), TI-2 (green), TS2 (violet) and PDC (blue). Binding side correspond to all residues considered. The acyl group has been considered as part of the substrate.

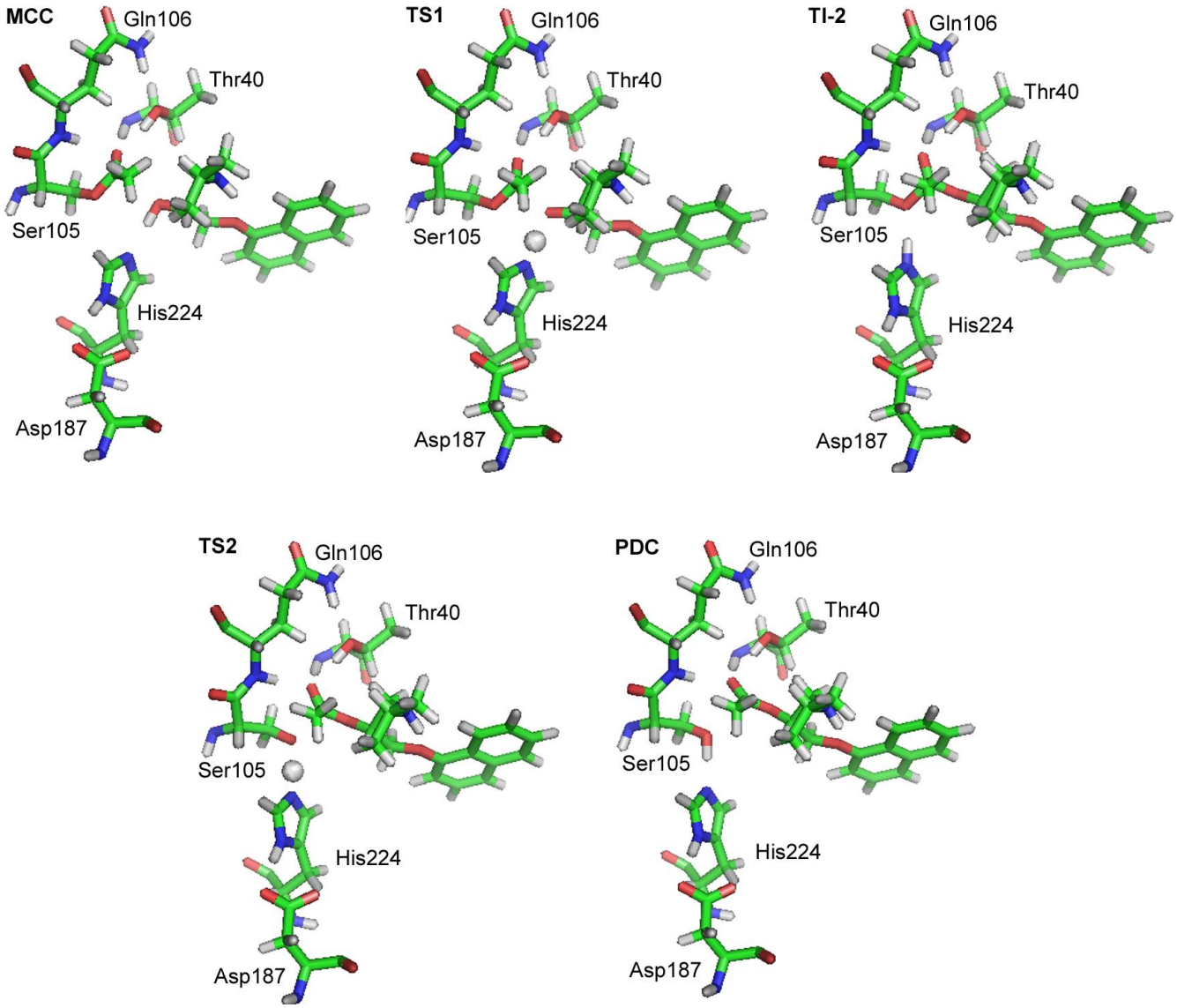

Fig. 98 Stationary points along the energy profile for the conversion of *R*-propranolol to *R*-acetyl-propranolol via ORIII. The formation of the TI-2 is accompanied by the displacement of the alcohol oxygen toward the oxyanion hole.

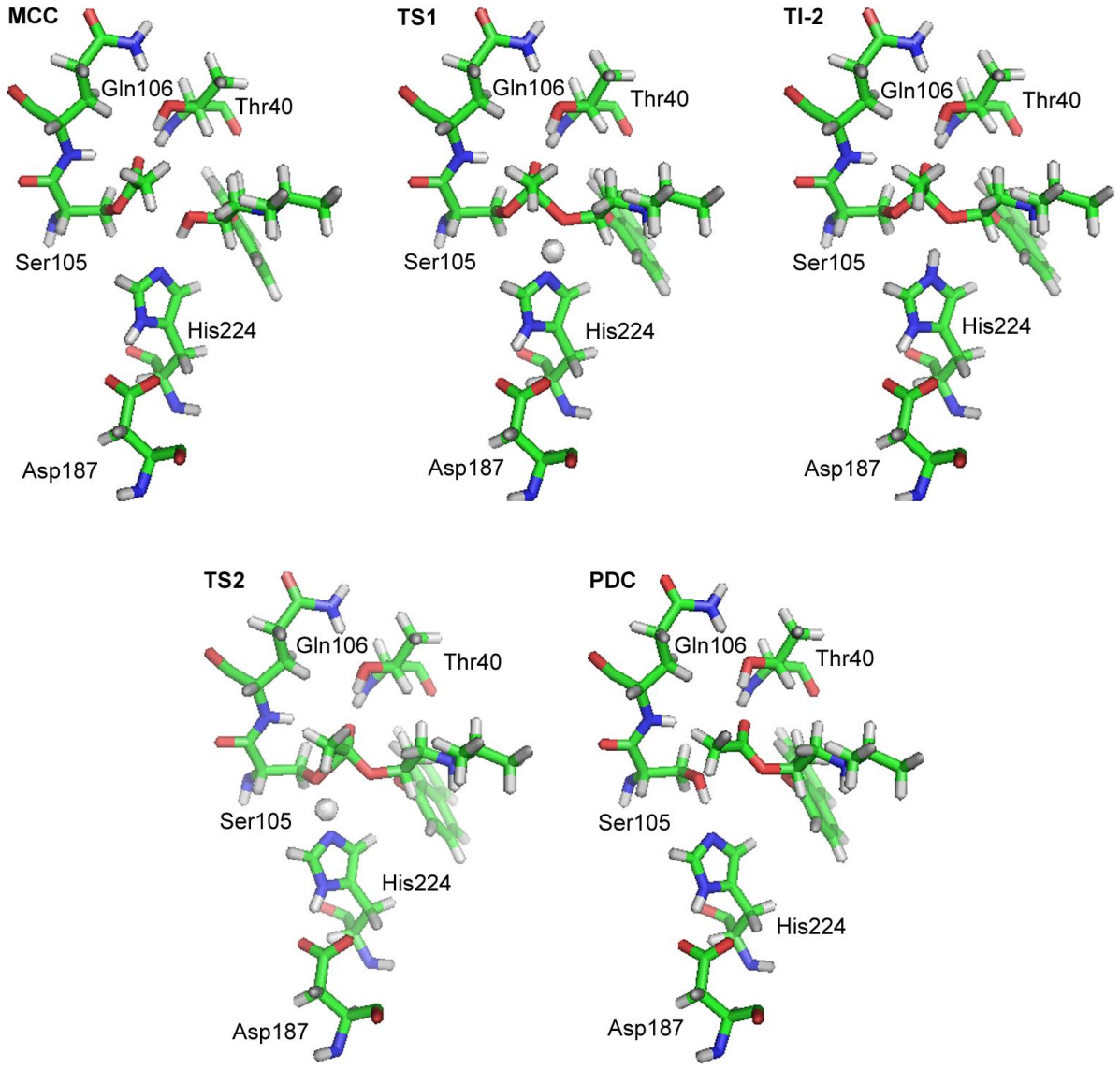

Fig. 99 Stationary points along the energy profile for the conversion of *R*-propranolol to *R*-acetyl-propranolol via ORIV.

B3LYP(TZVP)/CHARMM results for the conversion of *S*-propranolol in binding mode I

Table 42 QM(B3LYP/TZVP) and MM(CHARMM) energies in kcal/mol (relative to the MCC) for the transformation of *S*-propranolol in binding mode I via the TI-2 OSI[a]

Stationary point	**OSI**			
	QM energy		**MM energy**	
MCC	0		0	
TS1	13.2	(13.2)	-1.6	(-1.6)
TI-2	-2.1		2.3	
TS2	1.2	(3.3)	1.1	(-1.2)
PDC	-4.0		1.2	

[a] Activation barriers relative to the preceding minima are given in parentheses

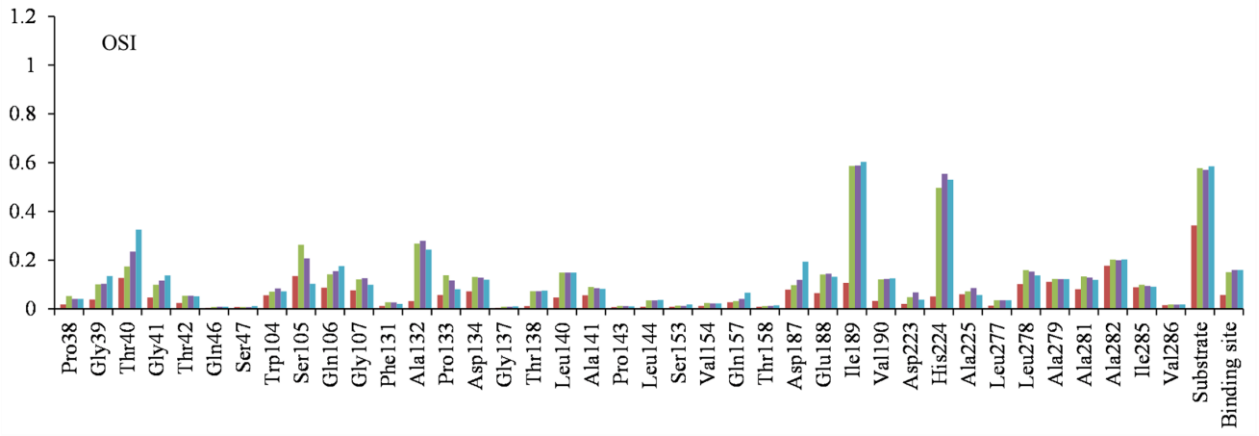

Fig. 100 RMSD (respect to the MCC) of all heavy atoms of the residues around 5 Å from the substrate at the stationary points along the energy profile obtained for the transformation of *S*-propranolol in binding mode I via the TI-2 OSI: TS1 (red), TI-2 (green), TS2 (violet) and PDC (blue). Binding side correspond to all residues considered. The acyl group has been considered as part of the substrate.

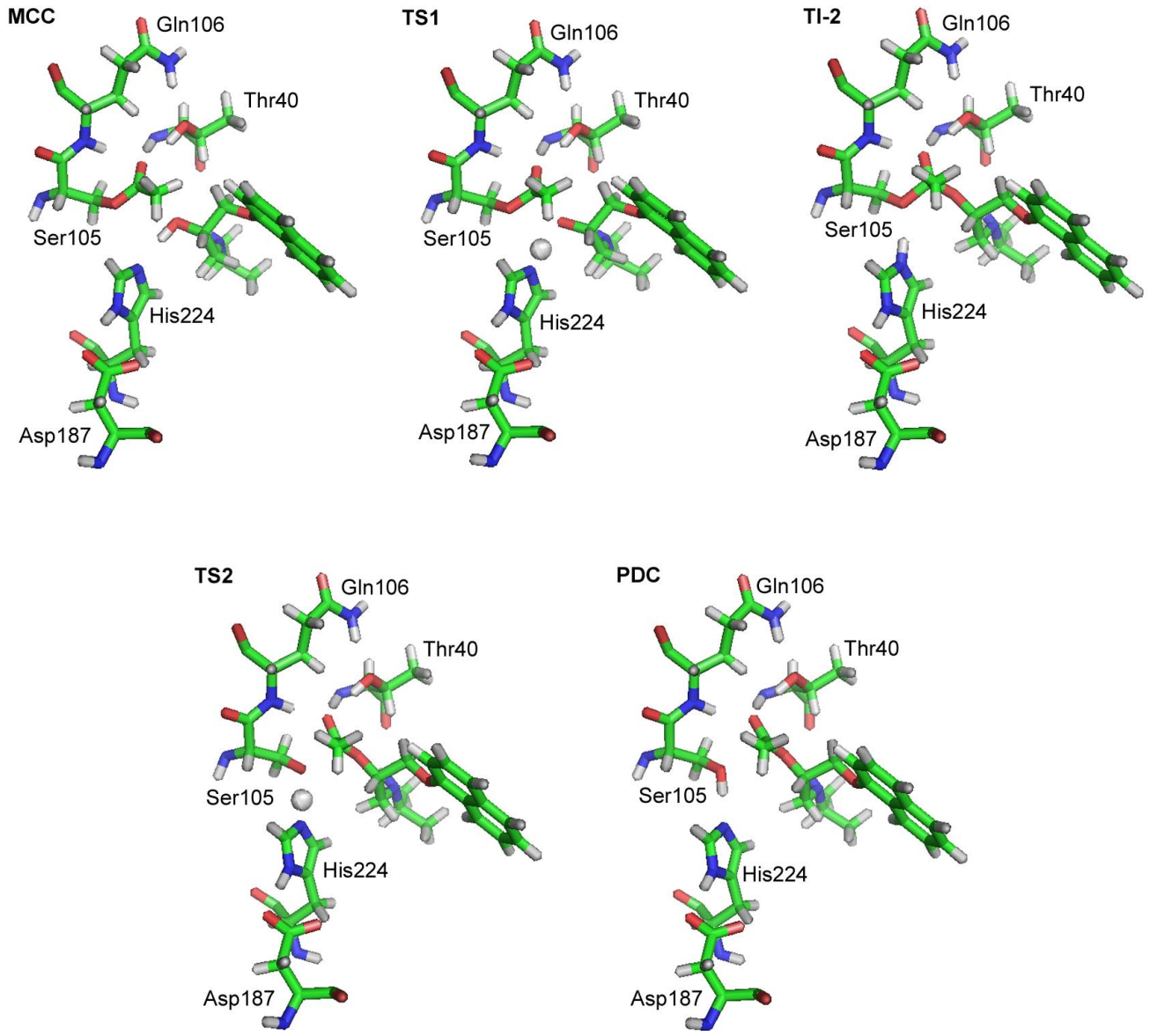

Fig. 101 Stationary points along the energy profile for the conversion of *S*-propranolol to *S*-acetyl-propranolol via the TI-2 OSI. The formation of the TI-2 is accompanied by the displacement of the alcohol oxygen toward the oxyanion hole.

Table 43 Distribution of dihedral angles characterizing TI-2[a] at the stationary points along the reaction profile obtained at the B3LYP(TZVP)/CHARMM level for the transformation of *S*-propranolol in binding mode I via the TI-2 OSI

Dihedral (°)	OSI				
	MCC	**TS1**	**TI-2**	**TS2**	**PDC**
ω_1	4	8	9	11	19
ω_2	113	102	153	162	170
ω_3	172	-178	141	143	144
ω_4	62	64	66	67	67
ω_5	-167	-170	177	174	171
ω_6	-65	-62	-79	-79	-79
ω_7	176	176	-180	179	177
ω_8	-88	-89	-116	-113	-108
ω_9	157	159	-172	-172	-173

[a] ω_1-ω_3 are the dihedral angles directly involved in the formation of TI-2. ω_4-ω_9 are the dihedral angles involving the propranolol molecule. See **Fig. 40b**.

B3LYP(TZVP)/CHARMM results for the conversion of *S*-propranolol in binding mode II

Table 44 QM(B3LYP/TZVP) and MM(CHARMM) energies in kcal/mol (relative to the MCC) for the transformation of *S*-propranolol in binding mode II via the TI-2s OSII-OSIV[a]

Stationary point	OSII				OSIII				OSIV			
	QM energy		**MM energy**		**QM energy**		**MM energy**		**QM energy**		**MM energy**	
MCC	0		0		0		0		0		0	
TS1	14.2	(14.2)	-3.1	(-3.1)	12.4	(12.4)	2.0	(2.0)	18.0	(18.0)	-2.3	(-2.3)
TI-2	7.9		-2.7		3.1		1.7		12.7		-0.6	
TS2	14.2	(6.3)	-1.8	(0.9)	7.2	(4.2)	1.2	(-0.5)	14.2	(1.5)	-0.6	(0.0)
PDC	9.2		0.7		-0.4		2.2		6.0		0.9	

[a] Activation barriers relative to the preceding minima are given in parentheses

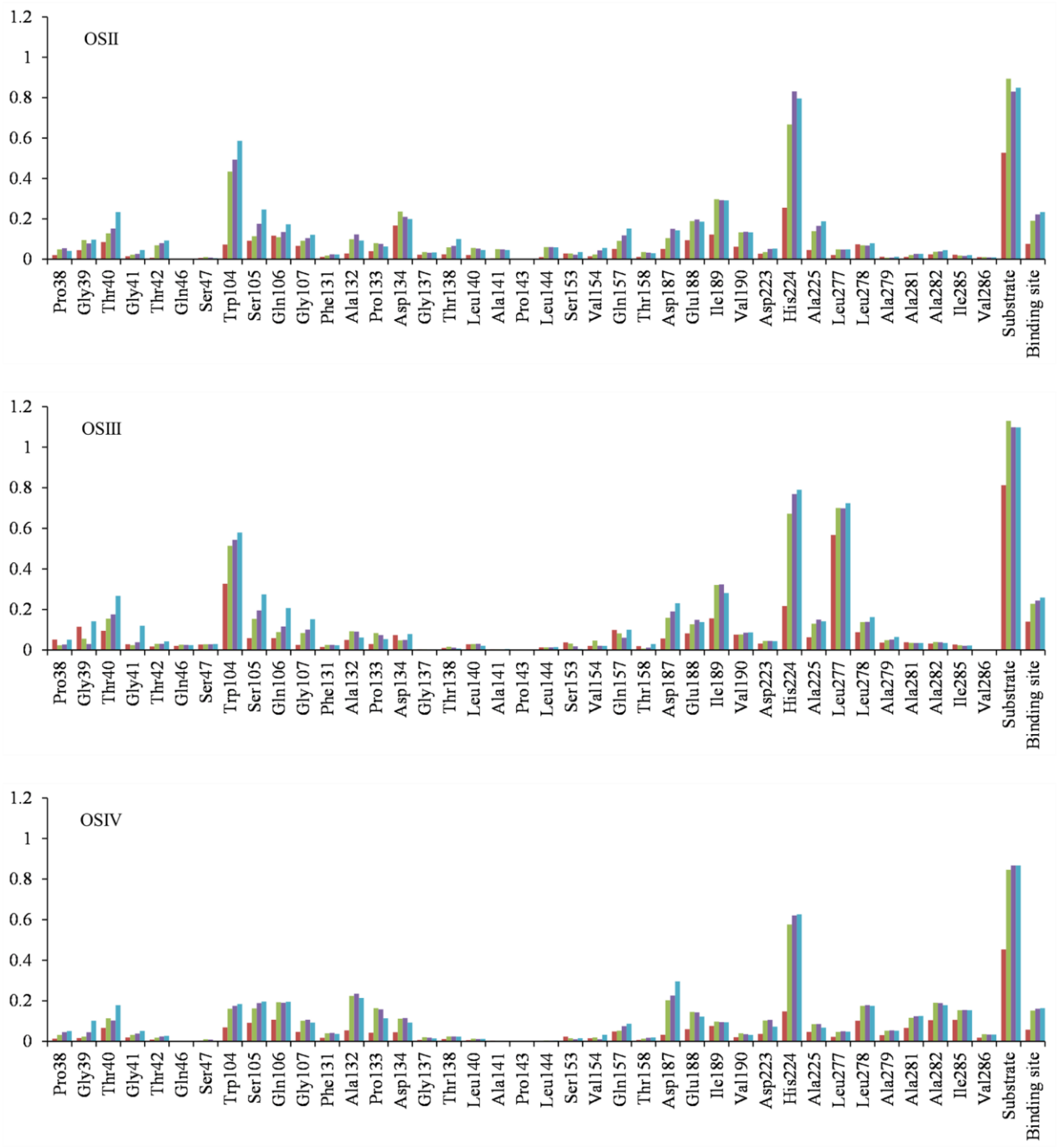

Fig. 102 RMSD (respect to the MCC) of all heavy atoms of the residues around 5 Å from the substrate at the stationary points along the energy profiles obtained for the transformation of *S*-propranolol in binding mode II via the TI-2s OSII-OSIV: TS1 (red), TI-2 (green), TS2 (violet) and PDC (blue). Binding side correspond to all residues considered. The acyl group has been considered as part of the substrate.

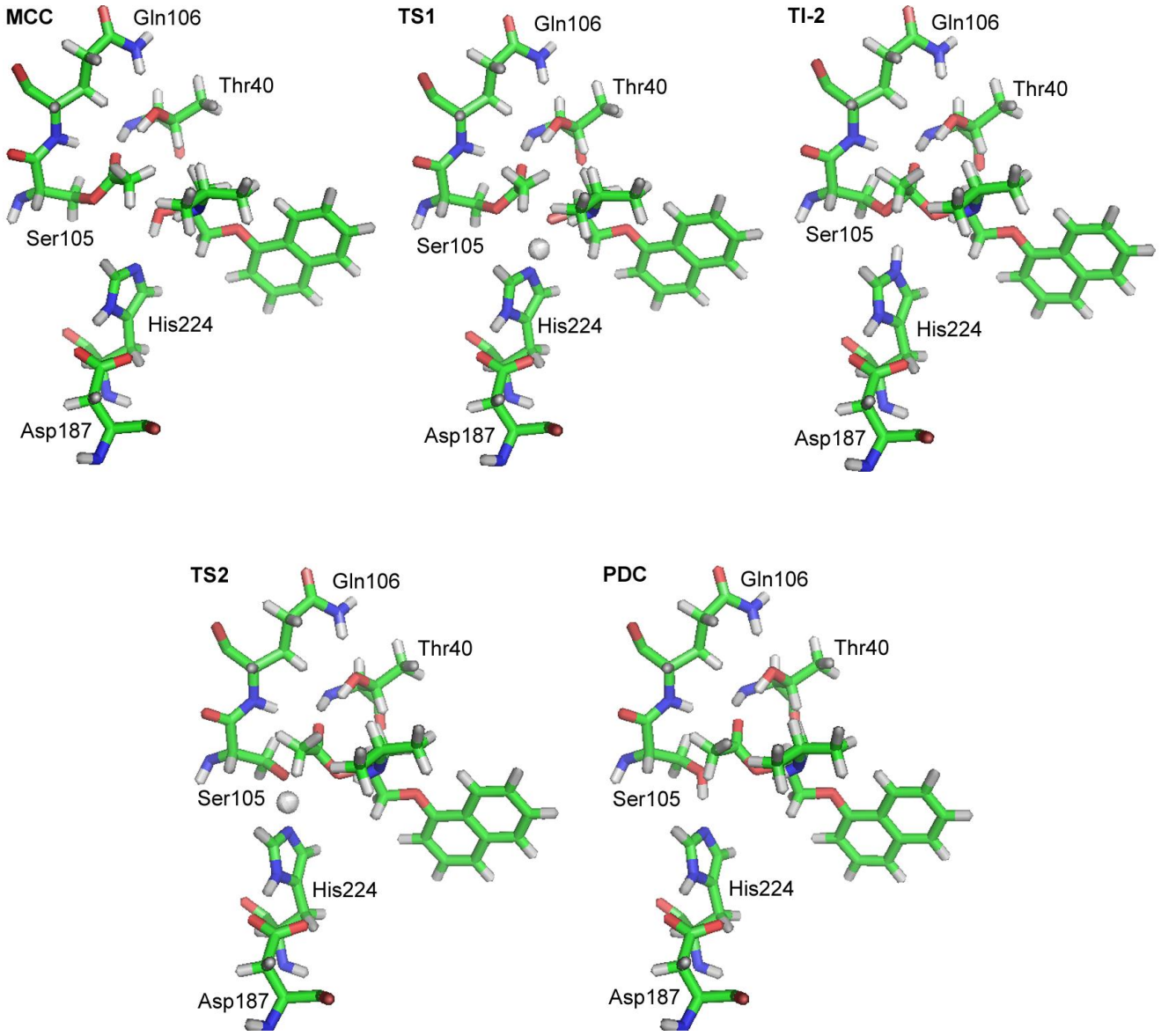

Fig. 103 Stationary points along the energy profile for the conversion of *S*-propranolol to *S*-acetyl-propranolol via the TI-2 OSII.

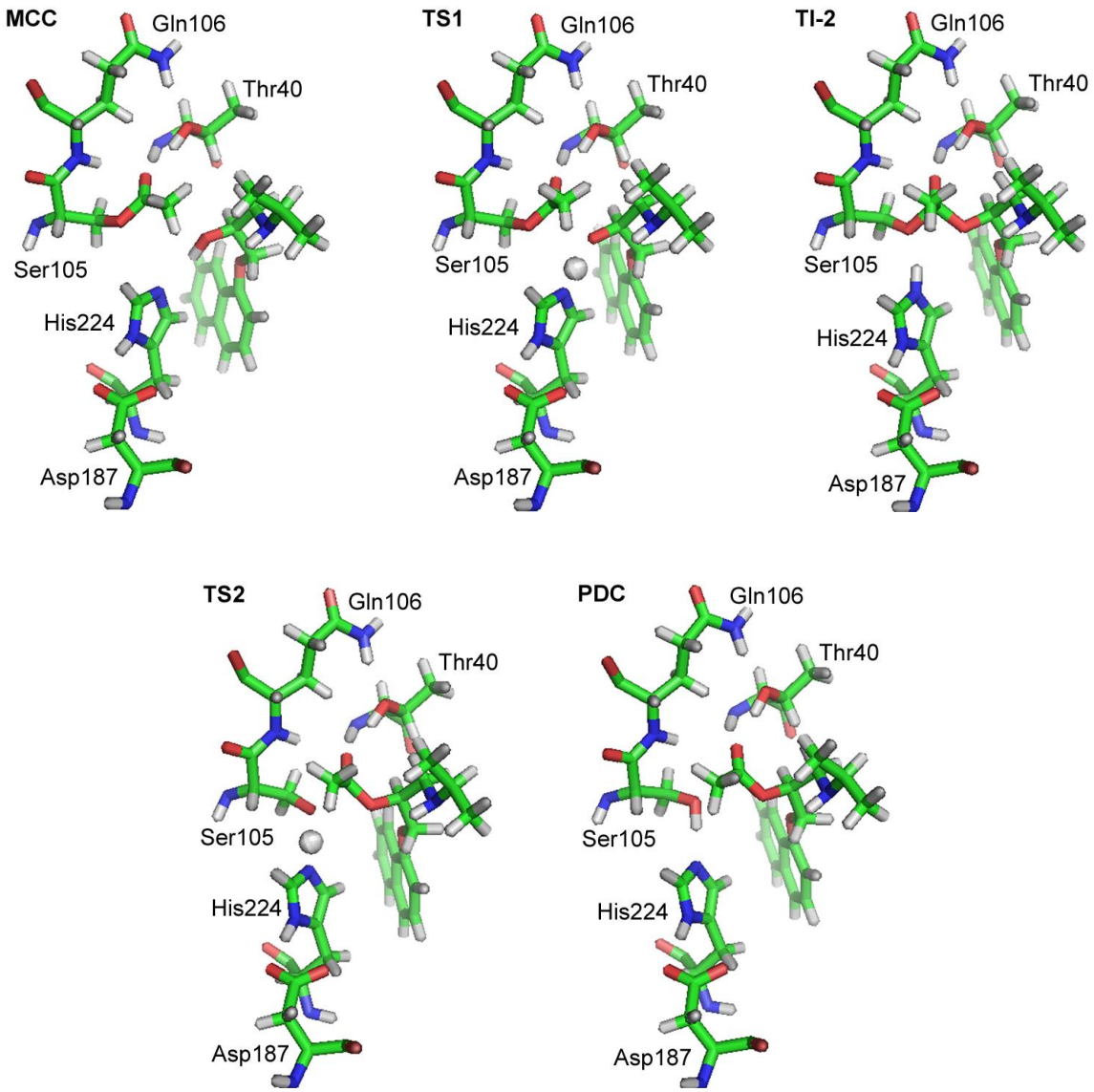

Fig. 104 Stationary points along the energy profile for the conversion of *S*-propranolol to *S*-acetyl-propranolol via the TI-2 OSIII.

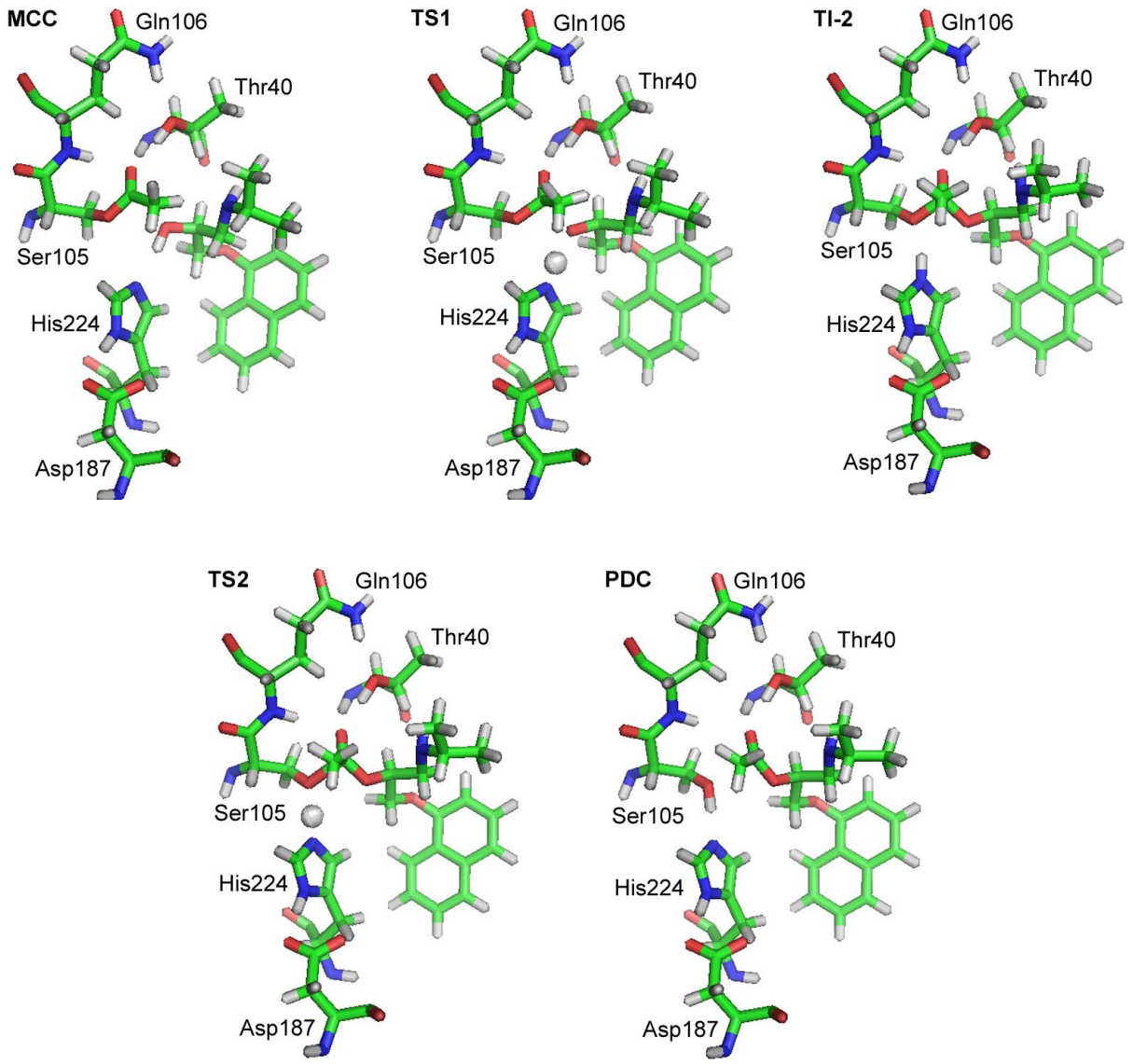

Fig. 105 Stationary points along the energy profile for the conversion of *S*-propranolol to *S*-acetyl-propranolol via the TI-2 OSIV.

Table 45 Distribution of dihedral angles characterizing TI-2[a] at the stationary points along the reaction profiles obtained at the B3LYP(TZVP)/CHARMM level for the transformation of *S*-propranolol in binding mode II via the TI-2s OSII-OSIV

Dihedral (°)	OSII					OSIII					OSIV				
	MCC	**TS1**	**TI-2**	**TS2**	**PDC**	**MCC**	**TS1**	**TI-2**	**TS2**	**PDC**	**MCC**	**TS1**	**TI-2**	**TS2**	**PDC**
ω_1	-3	-3	-21	-20	-34	2	-4	-17	-20	-36	12	21	4	-7	-1
ω_2	59	39	30	34	26	24	27	22	17	13	74	40	17	8	20
ω_3	43	66	73	73	76	72	71	80	85	85	54	89	105	113	106
ω_4	58	48	48	48	47	68	63	64	62	62	-77	-79	-60	-59	-59
ω_5	-169	-163	-158	-156	-153	-166	-172	-173	-166	-157	173	161	164	157	153
ω_6	-86	-87	-82	-83	-88	-163	-167	-166	-166	-165	-177	-177	-172	-170	-167
ω_7	-167	-163	-160	-158	-156	87	94	88	96	103	166	178	-180	-180	179
ω_8	-177	177	-178	-177	-176	-145	-152	-160	-166	-169	91	94	101	98	96
ω_9	-168	-159	-165	-165	-167	176	179	-175	-174	-177	62	60	63	67	70

[a] ω_1-ω_3 are the dihedral angles directly involved in the formation of TI-2. ω_4-ω_9 are the dihedral angles involving the propranolol molecule. See **Fig. 40b**.

QM/MM at different levels of theory

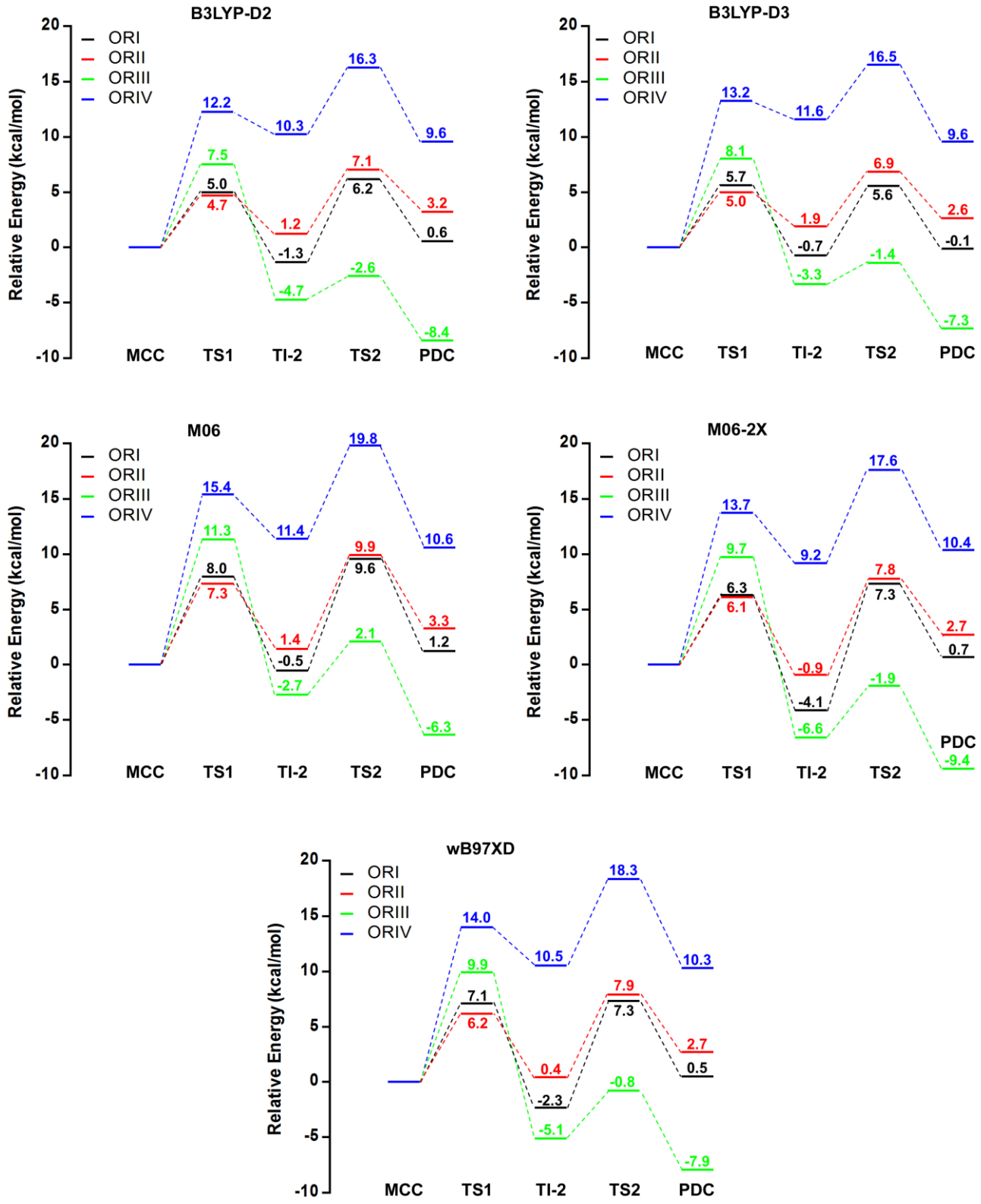

Fig. 106 QM/MM energies for the stationary points along the reaction profiles of *R*-propranolol evaluated with different DFT methods in single-point calculations.

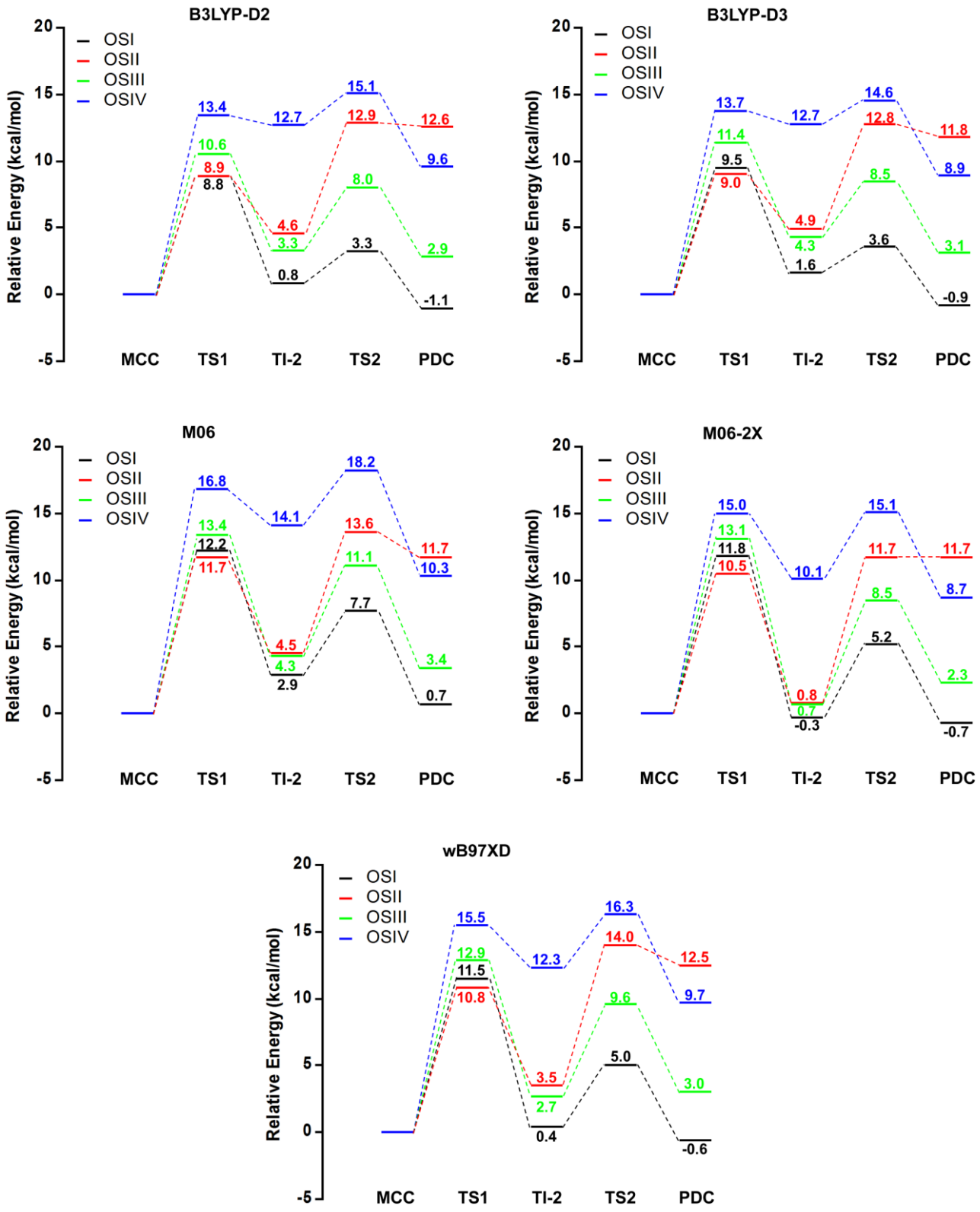

Fig. 107 QM/MM energies for the stationary points along the reaction profiles of *S*-propranolol evaluated with different DFT methods in single-point calculations.

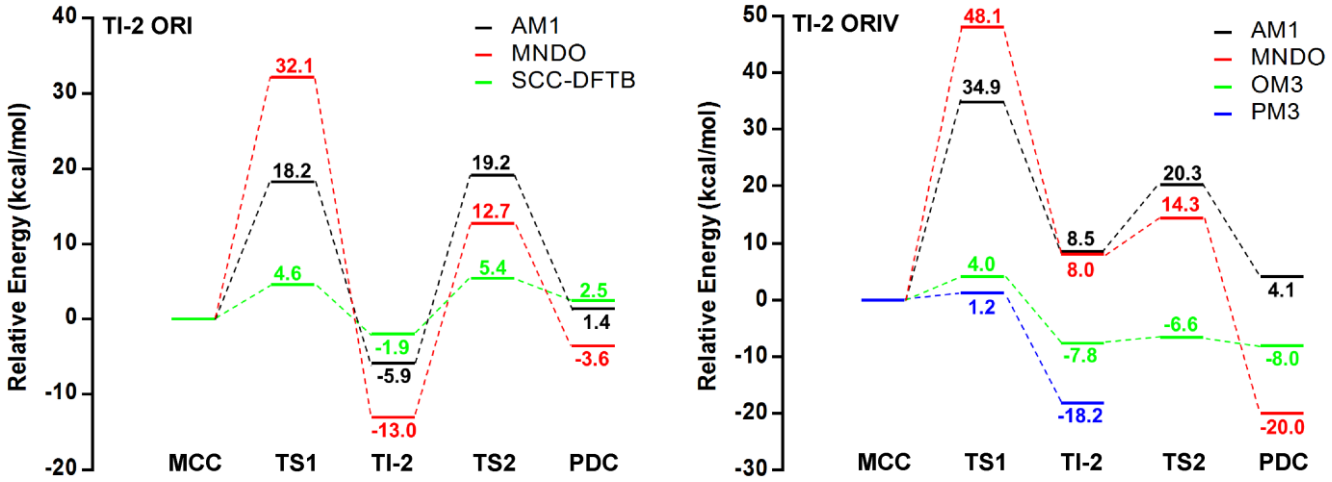

Fig. 108 QM/MM reaction profiles obtained for the TI-2s ORI and ORIV using semiempirical methods and the SCC-DFTB method. For the TI-2 ORI was not possible to locate any of the TSs (TS1 and TS2) using PM3, OM2 and OM3. The same occurred for the TI-2 ORIV using OM2, while with PM3 at least TS1 was located. For ORIV only semimpirical methods were tested (see the text).

References

[1] A.M. Barrett, Cardiac beta-adrenoceptor blockade: the quest for selectivity, J. Pharmacol., 16 Suppl 2 (1985) 95–108.

[2] R. Rabkin, D.P. Stables, N.W. Levin, M.M. Suzman, The prophylactic value of propranolol in angina pectoris, Am. J. Cardiol., 18 (1966) 370–380.

[3] E.M. Besterman, D.H. Friedlander, Clinical experiences with propranolol, Postgrad. Med. J., 41 (1965) 526–535.

[4] C.V.S. Ram, Risk of New-Onset Diabetes Mellitus in Patients With Hypertension Treated With Beta Blockers, Am. J. Cardiol., 102 (2008) 242–244.

[5] S. Belknap, Review: beta-blockers for hypertension increase risk of new onset diabetes, Evid. Based Med., 13 (2008) 50.

[6] D. Patakas, V. Argiropoulou, G. Louridas, V. Tsara, Beta-blockers in bronchial asthma: effect of propranolol and pindolol on large and small airways, Thorax, 38 (1983) 108–112.

[7] H.S. Bevinakatti, A.A. Banerji, Practical chemoenzymic synthesis of both enantiomers of propranolol, J Org Chem, 56 (1991) 5372–5375.

[8] S.V. Darnle, P.N. Patil, M.M. Salunkhe, Chemoenzymatic Synthesis of (R) - and (S) - Atenolol and Propranolol employing Lipase Catalyzed Enantioselective Esterification and Hydrolysis, Synth. Commun., 29 (1999) 3855–3862.

[9] A. Kamal, M. Sandbhor, A. Ali Shaik, Chemoenzymatic synthesis of (S) and (R)-propranolol and sotalol employing one-pot lipase resolution protocol, Bioorg. Med. Chem. Lett., 14 (2004) 4581–4583.

[10] R.A. Veloo, G.-J. Koomen, Synthesis of enantiomerically pure (S)-(−)-propranolol from sorbitol, Tetrahedron Asymmetry, 4 (1993) 2401–2404.

[11] H. Sasai, N. Itoh, T. Suzuki, M. Shibasaki, Catalytic asymmetric nitroaldol reaction: An efficient synthesis of (S) propranolol using the lanthanum binaphthol complex, Tetrahedron Lett., 34 (1993) 855–858.

[12] Y.-F. Wang, S.-T. Chen, K.K.-C. Liu, C.-H. Wong, Lipase-catalyzed irreversible transesterification using enol esters: Resolution of cyanohydrins and syntheses of ethyl (R)-2-hydroxy-4-phenylbutyrate and (S)-propranolol, Tetrahedron Lett., 30 (1989) 1917–1920.

[13] O. Barbosa, C. Ariza, C. Ortiz, R. Torres, Kinetic resolution of (R/S)-propranolol (1-isopropylamino-3-(1-naphtoxy)-2-propanolol) catalyzed by immobilized preparations of Candida antarctica lipase B (CAL-B), New Biotechnol., 27 (2010) 844–850.

[14] T.-W. Chiou, C.-C. Chang, C.-T. Lai, D.-F. Tai, Kinetic resolution of propranolol by a lipase-catalyzed N-acetylation, Bioorg. Med. Chem. Lett., 7 (1997) 433–436.

[15] R. Ávila, R. Ruiz, D. Amaro-González, O. Díaz, J.A. González, A.J. Núñez, Increased racemate resolution of propranolol esters by lipase immobilized catalysis, Lat. Am. Appl. Res., 35 (2005) 307–311.

[16] R. Ávila-González, M. Pérez-Gilabert, F. García-Carmona, Lipase-catalyzed preparation of S-propranolol in presence of hydroxypropyl β-cyclodextrins, J. Biosci. Bioeng., 100 (2005) 423–428.

[17] V. Gotor-Fernández, R. Brieva, V. Gotor, Lipases: Useful biocatalysts for the preparation of pharmaceuticals, J. Mol. Catal. B Enzym., 40 (2006) 111–120.

[18] A. Ghanem, H.Y. Aboul-Enein, Lipase-mediated chiral resolution of racemates in organic solvents, Tetrahedron Asymmetry, 15 (2004) 3331–3351.

[19] A. Ghanem, Trends in lipase-catalyzed asymmetric access to enantiomerically pure/enriched compounds, Tetrahedron, 63 (2007) 1721–1754.

[20] M.T. Reetz, Lipases as practical biocatalysts, Curr. Opin. Chem. Biol., 6 (2002) 145–150.
[21] M. Romero, J. Gomez, B. Diaz-Suelto, A. Garcia-Sanz, N. Baster, Kinetic Resolution of (*R,S*)-2-Butanol Using Enzymatic Synthesis of Esters, Appl. Biochem. Biotechnol., 165 (2011) 1129–1140.
[22] M. Rodríguez-Mata, V. Gotor-Fernández, J. González-Sabín, F. Rebolledo, V. Gotor, Straightforward preparation of biologically active 1-aryl- and 1-heteroarylpropan-2-amines in enantioenriched form, Org. Biomol. Chem., 9 (2011) 2274–2278.
[23] D. Brady, S. Reddy, B. Mboniswa, L.H. Steenkamp, A.L. Rousseau, C.J. Parkinson, J. Chaplin, R.K. Mitra, T. Moutlana, S.F. Marais, N.S. Gardiner, Biocatalytic enantiomeric resolution of l-menthol from an eight isomeric menthol mixture through transesterification, J. Mol. Catal. B Enzym., 75 (2012) 1–10.
[24] O. Barbosa, C. Ortiz, R. Torres, R. Fernandez-Lafuente, Effect of the immobilization protocol on the properties of lipase B from Candida antarctica in organic media: Enantiospecifc production of atenolol acetate, J. Mol. Catal. B Enzym., 71 (2011) 124–132.
[25] V. Léonard-Nevers, Z. Marton, S. Lamare, K. Hult, M. Graber, Understanding water effect on Candida antarctica lipase B activity and enantioselectivity towards secondary alcohols, J. Mol. Catal. B Enzym., 59 (2009) 90–95.
[26] B. Gao, T. Xu, J. Lin, L. Zhang, E. Su, Z. Jiang, D. Wei, Improving the catalytic activity of lipase LipK107 from Proteus sp by site-directed mutagenesis in the lid domain based on computer simulation, J. Mol. Catal. B Enzym., 68 (2011) 286–291.
[27] A. ESCORCIA, J. CRUZ, R. TORRES, C. ORTIZ, KINETIC RESOLUTION OF (R,S)-METHYL MANDELATE BY IMMOBILIZED LIPASE PREPARATIONS FROM Candida antarctica B, Vitae, 18 (2011) 33–41.
[28] J. Nyhlén, B. Martín-Matute, A.G. Sandström, M. Bocola, J. Bäckvall, Influence of δ-Functional Groups on the Enantiorecognition of Secondary Alcohols by Candida antarctica Lipase B, ChemBioChem, 9 (2008) 1968–1974.
[29] M.T. Reetz, M. Puls, J.D. Carballeira, A. Vogel, K. Jaeger, T. Eggert, W. Thiel, M. Bocola, N. Otte, Learning from Directed Evolution: Further Lessons from Theoretical Investigations into Cooperative Mutations in Lipase Enantioselectivity, ChemBioChem, 8 (2007) 106–112.
[30] S.A. Funke, N. Otte, T. Eggert, M. Bocola, K.-E. Jaeger, W. Thiel, Combination of Computational Prescreening and Experimental Library Construction Can Accelerate Enzyme Optimization by Directed Evolution, Protein Eng. Des. Sel., 18 (2005) 509–514.
[31] M. Bocola, N. Otte, K. Jaeger, M.T. Reetz, W. Thiel, Learning from Directed Evolution: Theoretical Investigations into Cooperative Mutations in Lipase Enantioselectivity, ChemBioChem, 5 (2004) 214–223.
[32] E.B. De Oliveira, C. Humeau, E.R. Maia, L. Chebil, E. Ronat, G. Monard, M.F. Ruiz-Lopez, M. Ghoul, J.-M. Engasser, An approach based on Density Functional Theory (DFT) calculations to assess the Candida antarctica lipase B selectivity in rutin, isoquercitrin and quercetin acetylation, J. Mol. Catal. B Enzym., 66 (2010) 325–331.
[33] M. Luić, Z. Stefanić, I. Ceilinger, M. Hodoscek, D. Janezic, T. Lenac, I.L. Asler, D. Sepac, S. Tomić, Combined X-ray diffraction and QM/MM study of the Burkholderia cepacia lipase-catalyzed secondary alcohol esterification, J. Phys. Chem. B, 112 (2008) 4876–4883.
[34] I. Baum, B. Elsässer, L.W. Schwab, K. Loos, G. Fels, Atomistic Model for the Polyamide Formation from β-Lactam Catalyzed by Candida antarctica Lipase B, ACS Catal., 1 (2011) 323–336.
[35] P.B. Juhl, P. Trodler, S. Tyagi, J. Pleiss, Modelling substrate specificity and enantioselectivity for lipases and esterases by substrate-imprinted docking, BMC Struct. Biol., 9 (2009) 39.

[36] E. García-Urdiales, N. Ríos-Lombardía, J. Mangas-Sánchez, V. Gotor-Fernández, V. Gotor, Influence of the nucleophile on the Candida antarctica lipase B-catalysed resolution of a chiral acyl donor, Chembiochem Eur. J. Chem. Biol., 10 (2009) 1830–1838.
[37] B. Christelle, B.D.O. Eduardo, C. Latifa, M. Elaine-Rose, M. Bernard, R.-H. Evelyne, G. Mohamed, E. Jean-Marc, H. Catherine, Combined docking and molecular dynamics simulations to enlighten the capacity of Pseudomonas cepacia and Candida antarctica lipases to catalyze quercetin acetylation, J. Biotechnol., 156 (2011) 203–210.
[38] M.A.J. Veld, L. Fransson, A.R.A. Palmans, E.W. Meijer, K. Hult, Lactone Size Dependent Reactivity in Candida Antarctica Lipase B: A Molecular Dynamics and Docking Study, ChemBioChem, 10 (2009) 1330–1334.
[39] S. Raza, L. Fransson, K. Hult, Enantioselectivity in Candida antarctica lipase B: A molecular dynamics study, Protein Sci., 10 (2001) 329–338.
[40] J. Quan, N. Wang, X.-Q. Cai, Q. Wu, X.-F. Lin, Controllable selective enzymatic synthesis of N-acyl and O-acylpropranolol vinyl esters and preparation of polymeric prodrug of propranolol, J. Mol. Catal. B Enzym., 44 (2007) 1–7.
[41] A.M. Escorcia, D. Molina, M.C. Daza, M. Doerr, Acetylation of (R,S)-propranolol catalyzed by Candida antarctica lipase B: An experimental and computational study, J. Mol. Catal. B Enzym., 98 (2013) 21–29.
[42] L. Hedstrom, Serine Protease Mechanism and Specificity, Chem. Rev., 102 (2002) 4501–4524.
[43] A.M. Escorcia, M.C. Daza, M. Doerr, Computational study of the enantioselectivity of the O-acetylation of (R,S)-propranolol catalyzed by Candida antarctica lipase B, J. Mol. Catal. B Enzym., 108 (2014) 21–31.
[44] G.P. Moss, Basic terminology of stereochemistry (IUPAC Recommendations 1996), Pure Appl. Chem., 68 (2009) 2193–2222.
[45] R.S. Cahn, C. Ingold, V. Prelog, Specification of Molecular Chirality, Angew. Chem. Int. Ed. Engl., 5 (1966) 385–415.
[46] M. Quack, Structure and Dynamics of Chiral Molecules, Angew. Chem. Int. Ed. Engl., 28 (1989) 571–586.
[47] L.A. Nguyen, H. He, C. Pham-Huy, Chiral Drugs: An Overview, Int. J. Biomed. Sci. IJBS, 2 (2006) 85–100.
[48] J.H. Kim, A.R. Scialli, Thalidomide: The Tragedy of Birth Defects and the Effective Treatment of Disease, Toxicol. Sci., 122 (2011) 1–6.
[49] G.W. Muller, ChemInform Abstract: Thalidomide: From Tragedy to New Drug Discovery, ChemInform, 28 (1997) no–no.
[50] W.H. Brooks, W.C. Guida, K.G. Daniel, The Significance of Chirality in Drug Design and Development, Curr. Top. Med. Chem., 11 (2011) 760–770.
[51] N.M. Maier, P. Franco, W. Lindner, Separation of enantiomers: needs, challenges, perspectives, J. Chromatogr. A, 906 (2001) 3–33.
[52] S.C. Stinson, Chiral drugs, Chem. Eng. News, 78 (2000) 55–78.
[53] S.C. Stinson, Counting on chiral drugs, 76 (1998).
[54] J. Ottosson, Enthalpy and Entropy in Enzyme Catalysis - A study of Lipase Enantioselectivity, Department of Biotechnology, Royal Institute of Technology, Stockholm, Sweden, 2001.
[55] R.A. Sheldon, Chirotechnology: Industrial Synthesis of Optically Active Compounds, CRC Press, 1993.
[56] R.A. Aitken, S.N. Kilényi, Asymmetric Synthesis, Softcover reprint of the original 1st ed. 1992 edition, Springer, Dordrecht, 2012.
[57] E. Eliel, S.H. Wilen, L.N. Mander, Stereochemistry of Organic Compounds, Edición: 1, John Wiley & Sons, New York, 1994.

[58] S.C. STINSON, SYNTHETIC ORGANIC CHEMISTRY ADVANCES, Chem. Eng. News Arch., 79 (2001) 31–34.
[59] R.S. Atkinson, Stereoselective Synthesis, Wiley, Chichester England ; New York, 1995.
[60] A.J. Carnell, Desymmetrisation of prochiral ketones using lipases, J. Mol. Catal. B Enzym., 19–20 (2002) 83–92.
[61] A.S. Bommarius, B. Riebel, Biocatalysis: Fundamentals and Applications, Edición: 1, Wiley Vch Verlag Gmbh, Weinheim ; Cambridge, 2004.
[62] C.J. Sih, S.-H. Wu, Resolution of Enantiomers via Biocatalysis, in: E.L. Eliel, S.H. Wilen (Eds.), Top. Stereochem., John Wiley & Sons, Inc., 1989: pp. 63–125.
[63] G.G. Haraldsson, The application of lipases in organic synthesis, in: S. Patai (Ed.), Acid Deriv. 1992, John Wiley & Sons, Inc., 1992: pp. 1395–1473.
[64] C.-H. Wong, G.M. Whitesides, Enzymes in Synthetic Organic Chemistry, Academic Press, 1994.
[65] R.N. Patel, Stereoselective Biocatalysis, 1 edition, CRC Press, New York, 2000.
[66] Biotransformations in Organic Chemistry - A Textbook, n.d.
[67] S.M. Roberts, G. Casy, M.-B. Nielsen, S. Phythian, C. Todd, K. Wiggins, Biocatalysts for Fine Chemicals Synthesis, Edición: 1, John Wiley & Sons Ltd, Chichester ; New York, 1999.
[68] U.T. Bornscheuer, R.J. Kazlauskas, Hydrolases in Organic Synthesis: Regio- and Stereoselective Biotransformations, Edición: 2nd Revised edition, Wiley-VCH Verlag GmbH, Weinheim, 2005.
[69] K.M. Koeller, C.-H. Wong, Enzymes for chemical synthesis, Nature, 409 (2001) 232–240.
[70] H.M.C. Ferraz, G.G. Bianco, C.C. Teixeira, L.H. Andrade, A.L.M. Porto, Enzymatic resolution of α-tetralols by CALB-catalyzed acetylation, Tetrahedron Asymmetry, 18 (2007) 1070–1076.
[71] P.-Y. Wang, S.-W. Tsai, Enzymatic hydrolytic resolution of (R,S)-tropic acid esters and (R,S)-ethyl α-methoxyphenyl acetate in biphasic media, J. Mol. Catal. B Enzym., 57 (2009) 158–163.
[72] A.Z. Abdullah, N.S. Sulaiman, A.H. Kamaruddin, Biocatalytic esterification of citronellol with lauric acid by immobilized lipase on aminopropyl-grafted mesoporous SBA-15, Biochem. Eng. J., 44 (2009) 263–270.
[73] A. Kamal, T. Krishnaji, M.N.A. Khan, Lipase-catalyzed resolution of 1-chloro-3-[(4-morpholin-4-yl-1,2,5-thiadiazole-3-yl)oxy]propan-2-ol: Synthesis of (R)- and (S)-timolol, J. Mol. Catal. B Enzym., 54 (2008) 55–59.
[74] D. Acetti, E. Brenna, C. Fuganti, F.G. Gatti, S. Serra, Lipase-catalysed synthesis of homotartaric acid enantiomers, Tetrahedron Lett., 50 (2009) 2249–2251.
[75] A. Sobolev, M.C.R. Franssen, J. Poikans, G. Duburs, A. de Groot, Enantioselective lipase-catalysed kinetic resolution of acyloxymethyl and ethoxycarbonylmethyl esters of 1,4-dihydroisonicotinic acid derivatives, Tetrahedron Asymmetry, 13 (2002) 2389–2397.
[76] J. González-Sabín, V. Gotor, F. Rebolledo, CAL-B-catalyzed resolution of some pharmacologically interesting β–substituted isopropylamines, Tetrahedron Asymmetry, 13 (2002) 1315–1320.
[77] F. Berti, C. Forzato, P. Nitti, G. Pitacco, E. Valentin, A study of the enantiopreference of lipase PS (Pseudomonas cepacia) towards diastereomeric dihydro-5-alkyl-4-hydroxymethyl-2(3H)-furanones, Tetrahedron Asymmetry, 16 (2005) 1091–1102.
[78] M. Habulin, Ž. Knez, Optimization of (R,S)-1-phenylethanol kinetic resolution over Candida antarctica lipase B in ionic liquids, J. Mol. Catal. B Enzym., 58 (2009) 24–28.
[79] T. Miyazawa, T. Yukawa, T. Koshiba, H. Sakamoto, S. Ueji, R. Yanagihara, T. Yamada, Resolution of 2-aryloxy-1-propanols via lipase-catalyzed enantioselective acylation in organic media, Tetrahedron Asymmetry, 12 (2001) 1595–1602.
[80] P. Berglund, Controlling lipase enantioselectivity for organic synthesis, Biomol. Eng., 18 (2001) 13–22.
[81] F. van Rantwijk, R.A. Sheldon, Enantioselective acylation of chiral amines catalysed by serine hydrolases, Tetrahedron, 60 (2004) 501–519.

[82] O. Jurček, M. Wimmerová, Z. Wimmer, Selected chiral alcohols: Enzymic resolution and reduction of convenient substrates, Coord. Chem. Rev., 252 (2008) 767–781.
[83] C.S. Chen, S.H. Wu, G. Girdaukas, C.J. Sih, Quantitative analyses of biochemical kinetic resolution of enantiomers 2 Enzyme-catalyzed esterifications in water-organic solvent biphasic systems, J. Am. Chem. Soc., 109 (1987) 2812–2817.
[84] W.W. Bachovchin, Review: Contributions of NMR spectroscopy to the study of hydrogen bonds in serine protease active sites, Magn. Reson. Chem., 39 (2001) S199–S213.
[85] M.L. Bender, F.J. Kezdy, The Current Status of the -Chymotrypsin Mechanism, J. Am. Chem. Soc., 86 (1964) 3704–3714.
[86] J.C. Powers, [16] Reaction of serine proteases with halomethyl ketones, in: M.W. William B. Jakoby (Ed.), Methods Enzymol., Academic Press, 1977: pp. 197–208.
[87] R. Bone, D. Frank, C.A. Kettner, D.A. Agard, Structural analysis of specificity: .alpha-lytic protease complexes with analogs of reaction intermediates, Biochemistry (Mosc.), 28 (1989) 7600–7609.
[88] P.R. Carey, P.J. Tonge, Unlocking the Secrets of Enzyme Power Using Raman Spectroscopy, Acc. Chem. Res., 28 (1995) 8–13.
[89] G.P. Hess, J. McConn, E. Ku, G. McConkey, Studies of the activity of chymotrypsin, Philos. Trans. R. Soc. Lond. B. Biol. Sci., 257 (1970) 89–104.
[90] M.L. Bender, J.V. Killheffer, Chymotrypsins, CRC Crit. Rev. Biochem., 1 (1973) 149–199.
[91] T.A. Steitz, R.G. Shulman, Crystallographic and NMR Studies of the Serine Proteases, Annu. Rev. Biophys. Bioeng., 11 (1982) 419–444.
[92] S. Tomić, M. Ramek, Quantum mechanical study of Burkholderia cepacia lipase enantioselectivity, J. Mol. Catal. B Enzym., 38 (2006) 139–147.
[93] V. Daggett, S. Schroeder, P. Kollman, Catalytic pathway of serine proteases: classical and quantum mechanical calculations, J. Am. Chem. Soc., 113 (1991) 8926–8935.
[94] M. Topf, P. Várnai, W.G. Richards, Ab Initio QM/MM Dynamics Simulation of the Tetrahedral Intermediate of Serine Proteases: Insights into the Active Site Hydrogen-Bonding Network, J. Am. Chem. Soc., 124 (2002) 14780–14788.
[95] T. Xu, L. Zhang, E. Su, D. Cui, X. Wang, D. Wei, Disparity in productive binding mode of the slow-reacting enantiomer determines the novel catalytic behavior of Candida antarctica lipase B, J. Mol. Catal. B Enzym., 62 (2010) 288–296.
[96] M. Maciejewski, K. Półtorak, J.E. Kamińska, Lipase resolution of new (±)-3-aryloxy-1-halogenopropan-2-ols: Versatile building blocks for β-adrenergic receptor antagonists, J. Mol. Catal. B Enzym., 62 (2010) 248–256.
[97] S. Serra, Lipase-mediated resolution of substituted 2-aryl-propanols: application to the enantioselective synthesis of phenolic sesquiterpenes, Tetrahedron Asymmetry, 22 (2011) 619–628.
[98] N. Li, S.-B. Hu, G.-Y. Feng, Resolution of 2-nitroalcohols by Burkholderia cepacia lipase-catalyzed enantioselective acylation, Biotechnol. Lett., 34 (2012) 153–158.
[99] L. Piovan, M.D. Pasquini, L.H. Andrade, Enzymatic kinetic resolution of tert-butyl 2-(1-hydroxyethyl)phenylcarbamate, a key intermediate to chiral organoselenanes and organotelluranes, Mol. Basel Switz., 16 (2011) 8098–8109.
[100] C. Pilissão, P. de O. Carvalho, M. da G. Nascimento, Enantioselective acylation of (RS)-phenylethylamine catalysed by lipases, Process Biochem., 44 (2009) 1352–1357.
[101] J.B. Sontakke, G.D. Yadav, Optimization and kinetic modeling of lipase catalyzed enantioselective N-acetylation of (±)-1-phenylethylamine under microwave irradiation, J. Chem. Technol. Biotechnol., 86 (2011) 739–748.

[102] J.A. Rodríguez-Rodríguez, F.J. Quijada, R. Brieva, F. Rebolledo, V. Gotor, Chemoenzymatic synthesis of orthogonally protected (3R,4R)- and (3S,4S)-trans-3-amino-4-hydroxypyrrolidines, Tetrahedron, 69 (2013) 5407–5412.
[103] F. Le Joubioux, Y.B. Henda, N. Bridiau, O. Achour, M. Graber, T. Maugard, The effect of substrate structure on the chemoselectivity of Candida antarctica lipase B-catalyzed acylation of amino-alcohols, J. Mol. Catal. B Enzym., 85–86 (2013) 193–199.
[104] E. Husson, V. Garcia-Matilla, C. Humeau, I. Chevalot, F. Fournier, I. Marc, Enzymatic acylation of a bifunctional molecule in 2-methyl-2-butanol: Kinetic modelling, Enzyme Microb. Technol., 46 (2010) 338–346.
[105] L. Schönstein, E. Forró, F. Fülöp, Continuous-flow enzymatic resolution strategy for the acylation of amino alcohols with a remote stereogenic centre: synthesis of calycotomine enantiomers, Tetrahedron Asymmetry, 24 (2013) 202–206.
[106] K. Lundell, E. Katainen, A. Kiviniemi, L.T. Kanerva, Enantiomers of adrenaline-type amino alcohols by Burkholderia cepacia lipase-catalyzed asymmetric acylation, Tetrahedron Asymmetry, 15 (2004) 3723–3729.
[107] F. Le Joubioux, N. Bridiau, Y. Ben Henda, O. Achour, M. Graber, T. Maugard, The control of Novozym® 435 chemoselectivity and specificity by the solvents in acylation reactions of amino-alcohols, J. Mol. Catal. B Enzym., 95 (2013) 99–110.
[108] M. Fernández-Pérez, C. Otero, Selective enzymatic synthesis of amide surfactants from diethanolamine, Enzyme Microb. Technol., 33 (2003) 650–660.
[109] L.T. Kanerva, M. Kosonen, E. Vänttinen, T.T. Huuhtanen, M. Dahlqvist, M.M. Kady, S.B. Christensen, Studies on the Chemo- and Enantio-selectivity of the Enzymatic Monoacylations of Amino Alcohols, Acta Chem. Scand., 46 (1992) 1101–1105.
[110] T. Furutani, M. Furui, H. Ooshima, J. Kato, n-acylation of β-amino alcohol by acyl migration following enzyme-catalyzed esterification, Enzyme Microb. Technol., 19 (1996) 578–584.
[111] P.-O. Syrén, F. Le Joubioux, Y. Ben Henda, T. Maugard, K. Hult, M. Graber, Proton Shuttle Mechanism in the Transition State of Lipase-Catalyzed N-Acylation of Amino Alcohols, ChemCatChem, 5 (2013) 1842–1853.
[112] P.-O. Syrén, K. Hult, Substrate Conformations Set the Rate of Enzymatic Acrylation by Lipases, ChemBioChem, 11 (2010) 802–810.
[113] E. Husson, C. Humeau, F. Blanchard, X. Framboisier, I. Marc, I. Chevalot, Chemo-selectivity of the N,O-enzymatic acylation in organic media and in ionic liquids, J. Mol. Catal. B Enzym., 55 (2008) 110–117.
[114] D. Yildirim, S.S. Tükel, Immobilized Pseudomonas sp lipase: A powerful biocatalyst for asymmetric acylation of (±)-2-amino-1-phenylethanols with vinyl acetate, Process Biochem., 48 (2013) 819–830.
[115] N. Otte, Combined Quantum Mechanical / Molecular Mechanical Investigation of Enantioselective Reactions in Lipases, Ph.D. thesis, Universität Düsseldorf, Germany, 2006.
[116] D.F. DeTar, Computation of enzyme-substrate specificity, Biochemistry (Mosc.), 20 (1981) 1730–1743.
[117] E. Holmberg, K. Hult, Temperature as an enantioselective parameter in enzymatic resolutions of racemic mixtures, Biotechnol. Lett., 13 (1991) 323–326.
[118] M. Norin, K. Hult, A. Mattson, T. Norin, Molecular Modelling of Chymotrypsin-Substrate Interactions: Calculation of Enantioselectivity, Biocatal. Biotransformation, 7 (1993) 131–147.
[119] R.S. Phillips, Temperature effects on stereochemistry of enzymatic reactions, Enzyme Microb. Technol., 14 (1992) 417–419.
[120] J.-H. Park, H.-J. Ha, W.K. Lee, T. Généreux-Vincent, R.J. Kazlauskas, Molecular Basis for the Stereoselective Ammoniolysis of N-Alkyl Aziridine-2-Carboxylates Catalyzed by Candida antarctica Lipase B, ChemBioChem, 10 (2009) 2213–2222.

[121] M. Cygler, P. Grochulski, R.J. Kazlauskas, J.D. Schrag, F. Bouthillier, B. Rubin, A.N. Serreqi, A.K. Gupta, A Structural Basis for the Chiral Preferences of Lipases, J. Am. Chem. Soc., 116 (1994) 3180–3186.
[122] G. Colombo, S. Toba, K.M. Merz, Rationalization of the Enantioselectivity of Subtilisin in DMF, J. Am. Chem. Soc., 121 (1999) 3486–3493.
[123] G. Colombo, G. Ottolina, G. Carrea, K.M.M. Jr, Modelling the enantioselectivity of subtilisin in water and organic solvents: insights from molecular dynamics and quantum mechanical/molecular mechanical studies, Chem. Commun., (2000) 559–560.
[124] M. Bocola, M.T. Stubbs, C. Sotriffer, B. Hauer, T. Friedrich, K. Dittrich, G. Klebe, Structural and energetic determinants for enantiopreferences in kinetic resolution of lipases, Protein Eng., 16 (2003) 319–322.
[125] T. Schulz, R.D. Schmid, J. Pleiss, Structural basis of stereoselectivity in Candida rugosa lipase-catalyzed hydrolysis of secondary alcohols, Mol. Model. Annu., 7 (2001) 265–270.
[126] F. Hæffner, T. Norin, K. Hult, Molecular Modeling of the Enantioselectivity in Lipase-Catalyzed Transesterification Reactions, Biophys. J., 74 (1998) 1251–1262.
[127] J. Ottosson, J.C. Rotticci-Mulder, D. Rotticci, K. Hult, Rational design of enantioselective enzymes requires considerations of entropy, Protein Sci. Publ. Protein Soc., 10 (2001) 1769–1774.
[128] J. Ottosson, L. Fransson, K. Hult, Substrate entropy in enzyme enantioselectivity: an experimental and molecular modeling study of a lipase, Protein Sci. Publ. Protein Soc., 11 (2002) 1462–1471.
[129] I.-S. Ng, S.-W. Tsai, Partially purified Carica papaya lipase: a versatile biocatalyst for the hydrolytic resolution of (R,S)-2-arylpropionic thioesters in water-saturated organic solvents, Biotechnol. Bioeng., 91 (2005) 106–113.
[130] T. Ema, Mechanism of Enantioselectivity of Lipases and Other Synthetically Useful Hydrolases, Curr. Org. Chem., 8 (2004) 1009–1025.
[131] H. Zhou, J. Chen, L. Ye, H. Lin, Y. Yuan, Enhanced performance of lipase-catalyzed kinetic resolution of secondary alcohols in monoether-functionalized ionic liquids, Bioresour. Technol., 102 (2011) 5562–5566.
[132] R.J. Kazlauskas, U.T. Bornscheuer, Biotransformations with Lipases, in: H.-J. Rehm, G. Reed (Eds.), Biotechnol. Set, Wiley-VCH Verlag GmbH, 2001: pp. 37–191.
[133] D.L. Ollis, E. Cheah, M. Cygler, B. Dijkstra, F. Frolow, S.M. Franken, M. Harel, S.J. Remington, I. Silman, J. Schrag, The alpha/beta hydrolase fold, Protein Eng., 5 (1992) 197–211.
[134] T.B. Nielsen, M. Ishii, O. Kirk, Lipases A and B from the yeast Candida antarctica, in: P.R. Margesin, P.F. Schinner (Eds.), Biotechnol. Appl. Cold-Adapt. Org., Springer Berlin Heidelberg, 1999: pp. 49–61.
[135] Hans Peter Heldt-Hansen, Michiyo Ishii, Shamkant A. Patkar, Tomas T. Hansen, Peter Eigtved, A New Immobilized Positional Nonspecific Lipase for Fat Modification and Ester Synthesis, in: Biocatal. Agric. Biotechnol., American Chemical Society, 1989: pp. 158–172.
[136] J. Uppenberg, M.T. Hansen, S. Patkar, T.A. Jones, The sequence, crystal structure determination and refinement of two crystal forms of lipase B from Candida antarctica, Struct. Lond. Engl. 1993, 2 (1994) 293–308.
[137] J. Uppenberg, N. Oehrner, M. Norin, K. Hult, G.J. Kleywegt, S. Patkar, V. Waagen, T. Anthonsen, T.A. Jones, Crystallographic and molecular-modeling studies of lipase B from Candida antarctica reveal a stereospecificity pocket for secondary alcohols, Biochemistry (Mosc.), 34 (1995) 16838–16851.
[138] M. Svedendahl, P. Carlqvist, C. Branneby, O. Allnér, A. Frise, K. Hult, P. Berglund, T. Brinck, Direct Epoxidation in Candida antarctica Lipase B Studied by Experiment and Theory, ChemBioChem, 9 (2008) 2443–2451.

[139] A. Warshel, COMPUTER SIMULATIONS OF ENZYME CATALYSIS: Methods, Progress, and Insights, Annu. Rev. Biophys. Biomol. Struct., 32 (2003) 425–443.
[140] S. Martí, M. Roca, J. Andrés, V. Moliner, E. Silla, I. Tuñón, J. Bertrán, Theoretical insights in enzyme catalysis, Chem. Soc. Rev., 33 (2004) 98–107.
[141] P. Monecke, R. Friedemann, S. Naumann, R. Csuk, Molecular Modelling Studies on the Catalytic Mechanism of Candida Rugosa Lipase, Mol. Model. Annu., 4 (1998) 395–404.
[142] A. Leach, Molecular Modelling: Principles and Applications, 2 edition, Prentice Hall, Harlow, England ; New York, 2001.
[143] H.M. Senn, J. Kästner, J. Breidung, W. Thiel, Finite-temperature effects in enzymatic reactions — Insights from QM/MM free-energy simulations, Can. J. Chem., 87 (2009) 1322–1337.
[144] H.M. Senn, W. Thiel, QM/MM Methods for Biological Systems, in: M. Reiher (Ed.), At. Approaches Mod. Biol., Springer Berlin Heidelberg, 2007: pp. 173–290.
[145] H.M. Senn, W. Thiel, QM/MM studies of enzymes, Curr. Opin. Chem. Biol., 11 (2007) 182–187.
[146] H. Lin, D.G. Truhlar, QM/MM: what have we learned, where are we, and where do we go from here?, Theor. Chem. Acc., 117 (2007) 185–199.
[147] G. Fernandez-Lorente, Z. Cabrera, C. Godoy, R. Fernandez-Lafuente, J.M. Palomo, J.M. Guisan, Interfacially activated lipases against hydrophobic supports: Effect of the support nature on the biocatalytic properties, Process Biochem., 43 (2008) 1061–1067.
[148] M.M. Bradford, A rapid and sensitive method for the quantitation of microgram quantities of protein utilizing the principle of protein-dye binding, Anal. Biochem., 72 (1976) 248–254.
[149] Gatterman, L., Practices of organic chemistry, 2nd ed., 1961.
[150] M.L. Testa, E. Zaballos, R.J. Zaragozá, Reactivity of β-amino alcohols against dialkyl oxalate: synthesis and mechanism study in the formation of substituted oxalamide and/or morpholine-2,3-dione derivatives, Tetrahedron, 68 (2012) 9583–9591.
[151] J.R. Satam, R.V. Jayaram, Acetylation of alcohols, phenols and amines using ammonium salt of 12-tungstophosphoric acid: Environmentally benign method, Catal. Commun., 9 (2008) 2365–2370.
[152] http://www.poissonboltzmann.org/pdb2pqr/, (n.d.).
[153] T.J. Dolinsky, J.E. Nielsen, J.A. McCammon, N.A. Baker, PDB2PQR: an automated pipeline for the setup of Poisson-Boltzmann electrostatics calculations, Nucleic Acids Res., 32 (2004) W665–W667.
[154] T.J. Dolinsky, P. Czodrowski, H. Li, J.E. Nielsen, J.H. Jensen, G. Klebe, N.A. Baker, PDB2PQR: expanding and upgrading automated preparation of biomolecular structures for molecular simulations, Nucleic Acids Res., 35 (2007) W522–W525.
[155] H. Li, A.D. Robertson, J.H. Jensen, Very fast empirical prediction and rationalization of protein pKa values, Proteins Struct. Funct. Bioinforma., 61 (2005) 704–721.
[156] D.C. Bas, D.M. Rogers, J.H. Jensen, Very fast prediction and rationalization of pKa values for protein-ligand complexes, Proteins, 73 (2008) 765–783.
[157] B.R. Brooks, C.L. Brooks, A.D. Mackerell, L. Nilsson, R.J. Petrella, B. Roux, Y. Won, G. Archontis, C. Bartels, S. Boresch, A. Caflisch, L. Caves, Q. Cui, A.R. Dinner, M. Feig, S. Fischer, J. Gao, M. Hodoscek, W. Im, K. Kuczera, et al., CHARMM: The biomolecular simulation program, J. Comput. Chem., 30 (2009) 1545–1614.
[158] A.D. Mackerell, M. Feig, C.L. Brooks, Extending the treatment of backbone energetics in protein force fields: Limitations of gas-phase quantum mechanics in reproducing protein conformational distributions in molecular dynamics simulations, J. Comput. Chem., 25 (2004) 1400–1415.
[159] A. D. MacKerell, D. Bashford, M. Bellott, R. L. Dunbrack, J.D. Evanseck, M.J. Field, S. Fischer, J. Gao, H. Guo, S. Ha, D. Joseph-McCarthy, L. Kuchnir, K. Kuczera, F.T.K. Lau, C.

Mattos, S. Michnick, T. Ngo, D.T. Nguyen, B. Prodhom, W.E. Reiher, et al., All-Atom Empirical Potential for Molecular Modeling and Dynamics Studies of Proteins†, J. Phys. Chem. B, 102 (1998) 3586–3616.
[160] J.-P. Ryckaert, G. Ciccotti, H.J.. Berendsen, Numerical integration of the cartesian equations of motion of a system with constraints: molecular dynamics of n-alkanes, J. Comput. Phys., 23 (1977) 327–341.
[161] R.H. Stote, D.J. States, M. Karplus, On the treatment of electrostatic interactions in biomolecular simulation, J. Chim. Phys., 88 (1991) 2419–2433.
[162] O. Trott, A.J. Olson, AutoDock Vina: improving the speed and accuracy of docking with a new scoring function, efficient optimization, and multithreading, J. Comput. Chem., 31 (2010) 455–461.
[163] M.W. Chang, C. Ayeni, S. Breuer, B.E. Torbett, Virtual screening for HIV protease inhibitors: a comparison of AutoDock 4 and Vina, PloS One, 5 (2010) e11955.
[164] A.M. Davis, S.J. Teague, Hydrogen Bonding, Hydrophobic Interactions, and Failure of the Rigid Receptor Hypothesis, Angew. Chem. Int. Ed., 38 (1999) 736–749.
[165] M. Elstner, D. Porezag, G. Jungnickel, J. Elsner, M. Haugk, T. Frauenheim, S. Suhai, G. Seifert, Self-consistent-charge density-functional tight-binding method for simulations of complex materials properties, Phys. Rev. B, 58 (1998) 7260–7268.
[166] E.B. De Oliveira, C. Humeau, L. Chebil, E.R. Maia, F. Dehez, B. Maigret, M. Ghoul, J.-M. Engasser, A molecular modelling study to rationalize the regioselectivity in acylation of flavonoid glycosides catalyzed by Candida antarctica lipase B, J. Mol. Catal. B Enzym., 59 (2009) 96–105.
[167] W. Humphrey, A. Dalke, K. Schulten, VMD: Visual molecular dynamics, J. Mol. Graph., 14 (1996) 33–38.
[168] P. Trodler, J. Pleiss, Modeling structure and flexibility of Candida antarctica lipase B in organic solvents, BMC Struct. Biol., 8 (2008) 9.
[169] C. Oger, Z. Marton, Y. Brinkmann, V. Bultel-Poncé, T. Durand, M. Graber, J.-M. Galano, Lipase-Catalyzed Regioselective Monoacetylation of Unsymmetrical 1,5-Primary Diols, J. Org. Chem., 75 (2010) 1892–1897.
[170] I. Vallikivi, L. Fransson, K. Hult, I. Järving, T. Pehk, N. Samel, V. Tõugu, L. Villo, O. Parve, The modelling and kinetic investigation of the lipase-catalysed acetylation of stereoisomeric prostaglandins, J. Mol. Catal. B Enzym., 35 (2005) 62–69.
[171] C. Palocci, M. Falconi, S. Alcaro, A. Tafi, R. Puglisi, F. Ortuso, M. Botta, L. Alberghina, E. Cernia, An approach to address Candida rugosa lipase regioselectivity in the acylation reactions of trytilated glucosides, J. Biotechnol., 128 (2007) 908–918.
[172] H.B. Burgi, J.D. Dunitz, E. Shefter, Geometrical reaction coordinates II Nucleophilic addition to a carbonyl group, J. Am. Chem. Soc., 95 (1973) 5065–5067.
[173] G.A. Worth, F. Nardi, R.C. Wade, Use of Multiple Molecular Dynamics Trajectories To Study Biomolecules in Solution: The YTGP Peptide, J. Phys. Chem. B, 102 (1998) 6260–6272.
[174] L.S.D. Caves, J.D. Evanseck, M. Karplus, Locally accessible conformations of proteins: Multiple molecular dynamics simulations of crambin, Protein Sci., 7 (1998) 649–666.
[175] P. Trodler, R.D. Schmid, J. Pleiss, Modeling of solvent-dependent conformational transitions in Burkholderia cepacia lipase, BMC Struct. Biol., 9 (2009) 38.
[176] T.C. Bruice, A View at the Millennium: the Efficiency of Enzymatic Catalysis, Acc. Chem. Res., 35 (2002) 139–148.
[177] S. Hur, T.C. Bruice, Comparison of Formation of Reactive Conformers (NACs) for the Claisen Rearrangement of Chorismate to Prephenate in Water and in the E coli Mutase: The Efficiency of the Enzyme Catalysis, J. Am. Chem. Soc., 125 (2003) 5964–5972.
[178] Frisch, M. J., Trucks, G. W., Schlegel, H. B., Scuseria, G. E., Robb, M. A., Cheeseman, J. R., Scalmani, G., Barone, V., Mennucci, B., Petersson, G. A., Nakatsuji, H., Caricato, M., Li, X.,

Hratchian, H. P., Izmaylov, A. F., Bloino, J., Zheng, G., Sonnenberg, J. L., Hada, M., Ehara, M., et al., Gaussian09, Revision D01, Gaussian, Inc., Wallingford, CT, 2009.
[179] N. Otte, M. Scholten, W. Thiel, Looking at Self-Consistent-Charge Density Functional Tight Binding from a Semiempirical Perspective†, J. Phys. Chem. A, 111 (2007) 5751–5755.
[180] L. Capoferri, M. Mor, J. Sirirak, E. Chudyk, A.J. Mulholland, A. Lodola, Application of a SCC-DFTB QM/MM approach to the investigation of the catalytic mechanism of fatty acid amide hydrolase, J. Mol. Model., 17 (2011) 2375–2383.
[181] M.R. Ganjalikhany, B. Ranjbar, A.H. Taghavi, T. Tohidi Moghadam, Functional Motions of Candida antarctica Lipase B: A Survey through Open-Close Conformations, PLoS ONE, 7 (2012) e40327.
[182] M. Skjøt, L. De Maria, R. Chatterjee, A. Svendsen, S.A. Patkar, P.R. Østergaard, J. Brask, Understanding the Plasticity of the α/β Hydrolase Fold: Lid Swapping on the Candida antarctica Lipase B Results in Chimeras with Interesting Biocatalytic Properties, ChemBioChem, 10 (2009) 520–527.
[183] M. Nishio, The CH/π hydrogen bond in chemistry Conformation, supramolecules, optical resolution and interactions involving carbohydrates, Phys. Chem. Chem. Phys., 13 (2011) 13873–13900.
[184] T. Ema, Y. Nakano, D. Yoshida, S. Kamata, T. Sakai, Redesign of enzyme for improving catalytic activity and enantioselectivity toward poor substrates: manipulation of the transition state, Org. Biomol. Chem., 10 (2012) 6299–6308.
[185] M. Yamakawa, I. Yamada, R. Noyori, CH/π Attraction: The Origin of Enantioselectivity in Transfer Hydrogenation of Aromatic Carbonyl Compounds Catalyzed by Chiral η6-Arene-Ruthenium(II) Complexes, Angew. Chem. Int. Ed., 40 (2001) 2818–2821.
[186] Y. Zhang, J. Kua, J.A. McCammon, Influence of Structural Fluctuation on Enzyme Reaction Energy Barriers in Combined Quantum Mechanical/Molecular Mechanical Studies, J Phys Chem B, 107 (2003) 4459–4463.
[187] R.S. Mulliken, Electronic Population Analysis on LCAO–MO Molecular Wave Functions I, J. Chem. Phys., 23 (1955) 1833–1840.
[188] R.S. Mulliken, Electronic Population Analysis on LCAO–MO Molecular Wave Functions II Overlap Populations, Bond Orders, and Covalent Bond Energies, J. Chem. Phys., 23 (1955) 1841–1846.
[189] J. Gao, P. Amara, C. Alhambra, M.J. Field, A Generalized Hybrid Orbital (GHO) Method for the Treatment of Boundary Atoms in Combined QM/MM Calculations, J. Phys. Chem. A, 102 (1998) 4714–4721.
[190] A.T. Macias, A.D. MacKerell, CH/π interactions involving aromatic amino acids: Refinement of the CHARMM tryptophan force field, J. Comput. Chem., 26 (2005) 1452–1463.
[191] S. Metz, W. Thiel, A Combined QM/MM Study on the Reductive Half-Reaction of Xanthine Oxidase: Substrate Orientation and Mechanism, J. Am. Chem. Soc., 131 (2009) 14885–14902.
[192] I. Polyak, M.T. Reetz, W. Thiel, Quantum Mechanical/Molecular Mechanical Study on the Mechanism of the Enzymatic Baeyer–Villiger Reaction, J. Am. Chem. Soc., 134 (2012) 2732–2741.
[193] P. Sherwood, A.H. de Vries, M.F. Guest, G. Schreckenbach, C.R.A. Catlow, S.A. French, A.A. Sokol, S.T. Bromley, W. Thiel, A.J. Turner, S. Billeter, F. Terstegen, S. Thiel, J. Kendrick, S.C. Rogers, J. Casci, M. Watson, F. King, E. Karlsen, M. Sjøvoll, et al., QUASI: A general purpose implementation of the QM/MM approach and its application to problems in catalysis, J. Mol. Struct. THEOCHEM, 632 (2003) 1–28.
[194] S.R. Billeter, A.J. Turner, W. Thiel, Linear scaling geometry optimisation and transition state search in hybrid delocalised internal coordinates, Phys. Chem. Chem. Phys., 2 (2000) 2177–2186.
[195] J.C. Slater, A Simplification of the Hartree-Fock Method, Phys. Rev., 81 (1951) 385–390.

[196] S.H. Vosko, L. Wilk, M. Nusair, Accurate spin-dependent electron liquid correlation energies for local spin density calculations: a critical analysis, Can. J. Phys., 58 (1980) 1200–1211.
[197] A.D. Becke, Density-functional exchange-energy approximation with correct asymptotic behavior, Phys. Rev. A, 38 (1988) 3098–3100.
[198] J.P. Perdew, Density-functional approximation for the correlation energy of the inhomogeneous electron gas, Phys. Rev. B, 33 (1986) 8822–8824.
[199] J.P. Perdew, Erratum: Density-functional approximation for the correlation energy of the inhomogeneous electron gas, Phys. Rev. B, 34 (1986) 7406–7406.
[200] A.D. Becke, Density-functional thermochemistry III The role of exact exchange, J. Chem. Phys., 98 (1993) 5648–5652.
[201] Y. Zhao, D.G. Truhlar, The M06 suite of density functionals for main group thermochemistry, thermochemical kinetics, noncovalent interactions, excited states, and transition elements: two new functionals and systematic testing of four M06-class functionals and 12 other functionals, Theor. Chem. Acc., 120 (2008) 215–241.
[202] J.-D. Chai, M. Head-Gordon, Long-range corrected hybrid density functionals with damped atom–atom dispersion corrections, Phys. Chem. Chem. Phys., 10 (2008) 6615–6620.
[203] A. Schäfer, C. Huber, R. Ahlrichs, Fully optimized contracted Gaussian basis sets of triple zeta valence quality for atoms Li to Kr, J. Chem. Phys., 100 (1994) 5829–5835.
[204] M.J.S. Dewar, E.G. Zoebisch, E.F. Healy, J.J.P. Stewart, Development and use of quantum mechanical molecular models 76 AM1: a new general purpose quantum mechanical molecular model, J. Am. Chem. Soc., 107 (1985) 3902–3909.
[205] J.J.P. Stewart, Optimization of parameters for semiempirical methods I Method, J. Comput. Chem., 10 (1989) 209–220.
[206] J.J.P. Stewart, Optimization of parameters for semiempirical methods II Applications, J. Comput. Chem., 10 (1989) 221–264.
[207] M.J.S. Dewar, W. Thiel, Ground states of molecules 38 The MNDO method Approximations and parameters, J. Am. Chem. Soc., 99 (1977) 4899–4907.
[208] W. Wolfgang, PhD thesis, University of Zürich, Zürich, Switzerland, 1996.
[209] W. Weber, W. Thiel, Orthogonalization corrections for semiempirical methods, Theor. Chem. Acc., 103 (2000) 495–506.
[210] S. Mirjam, PhD thesis, University of Düsseldorf, Düsseldorf, Germany, 2003.
[211] R. Ahlrichs, M. Bar, H.-P. Baron, S. Bauernschmitt, S. Bocker, M. Ehrig, K. Eichkorn, S. Elliott, F. Furche, F. Haase, M. Haser, H. Horn, C. Huber, U. Huniar, M. Kattannek, C. Kolmel, M. Kollwitz, K. May, C. Ochsenfeld, H. Ohm, et al., TURBOMOLE, v 63, 2011.
[212] W. Thiel, Program MNDO2005, version 70, Max-Planck-Institüt für Kohlenforschung: Mülheim, 2005.
[213] W. Smith, T.R. Forester, DL_POLY_20: A general-purpose parallel molecular dynamics simulation package, J. Mol. Graph., 14 (1996) 136–141.
[214] D. Bakowies, W. Thiel, Hybrid Models for Combined Quantum Mechanical and Molecular Mechanical Approaches, J. Phys. Chem., 100 (1996) 10580–10594.
[215] A.H. de Vries, P. Sherwood, S.J. Collins, A.M. Rigby, M. Rigutto, G.J. Kramer, Zeolite Structure and Reactivity by Combined Quantum-Chemical−Classical Calculations, J. Phys. Chem. B, 103 (1999) 6133–6141.
[216] P. Sherwood, A.H. de Vries, S.J. Collins, S.P. Greatbanks, N.A. Burton, M.A. Vincent, I.H. Hillier, Computer simulation of zeolite structure and reactivity using embedded cluster methods, Faraday Discuss., 106 (1997) 79–92.
[217] D.C. Liu, J. Nocedal, On the limited memory BFGS method for large scale optimization, Math. Program., 45 (1989) 503–528.

[218] J. Nocedal, Updating quasi-Newton matrices with limited storage, Math. Comput., 35 (1980) 773–782.
[219] J. Baker, An algorithm for the location of transition states, J. Comput. Chem., 7 (1986) 385–395.
[220] A. Banerjee, N. Adams, J. Simons, R. Shepard, Search for stationary points on surfaces, J. Phys. Chem., 89 (1985) 52–57.
[221] K. Eichkorn, O. Treutler, H. Öhm, M. Häser, R. Ahlrichs, Auxiliary basis sets to approximate Coulomb potentials, Chem. Phys. Lett., 240 (1995) 283–290.
[222] K. Eichkorn, F. Weigend, O. Treutler, R. Ahlrichs, Auxiliary basis sets for main row atoms and transition metals and their use to approximate Coulomb potentials, Theor. Chem. Acc., 97 (1997) 119–124.
[223] S. Grimme, Semiempirical GGA-type density functional constructed with a long-range dispersion correction, J. Comput. Chem., 27 (2006) 1787–1799.
[224] K. Yoshimoto, Y. Itatani, Y. Tsuda, ^<13>C-Nuclear Magnetic Resonance (NMR) Spectra of O-Acylglucoses Additivity of Shift Parameters and Its Application to Structure Elucidations, Chem. Pharm. Bull. (Tokyo), 28 (1980) 2065–2076.